# Strål säkerhets myndigheten

Swedish Radiation Safety Authority

Author:  Peter Dillström
Jens Gunnars
Petter von Unge
Daniel Mångård

Kiwa Inspecta Technology AB, Stockholm

Research

# 2018:18

## Procedure for Safety Assessment of Components with Defects

– Handbook Edition 5

## SSM perspective

### Background

SSM and the Swedish nuclear power plant owners have financed Kiwa Inspecta Technology in Sweden to develop a new version of the handbook for assessment of defects. This represents a major update of the former fracture mechanics handbook that was published at SSM as Research 2008:01. The procedure in the handbook is based on the British R6-method where the failure mechanisms fracture and plastic collapse are considered for cracked components of metallic materials by evaluating the stress intensity factor and the plastic limit load. Almost all elements of the handbook are included in a computer based expert code called ISAAC, which also have been revised as part of the project. ISAAC is an acronym for Integrity and SAfety Assessment of Components.

### Results

- The results of the project have meant that a number of new and updated features are now implemented in the handbook. This includes the following:

- Implementation of the R6-procedure, Rev. 4

- Implementation of ASME, section XI, edition 2007.

- A revised system of safety factors to be used with the R6 procedure.

- Revised chapters on defect characterization, stress intensity factor solutions for new crack geometries, weld residual stresses and material data including new data for fatigue crack growth and stress corrosion crack growth for nuclear applications.

### Objective

- The SSM regulations SSMFS 2008:13, containing rules for mechanical components in certain nuclear facilities, allows for further operation of a nuclear power plant if cracks are detected in mechanical components without repair or replacement, when it has been demonstrated that sufficient safety margins exist against fracture. Thus, there is a need for tools that can perform reliable safety assessments of components with defects in order to verify that the regulations are fulfilled. The fracture mechanics handbook satisfies this need. Many applied research projects since 2008, financed by SSM and in some cases together with the Swedish nuclear power plant owners, have been used to generate results, which have been included in the handbook and the computer code ISAAC. This includes the following SSM research reports:

- Research 2009:15, Improvement and Validation of Weld Residual Stress Modelling Procedure.

- Research 2009:16, Influence of Hardening Model on Weld Residual Stress Distribution.

- Research 2009:26, Tillämpning av stabil spricktillväxt vid brottmekanisk bedömning av defekter i sega material.

- Research 2009:27, Analysis Strategy for Fracture Assessment of Defects in Ductile Materials.

- Research 2011:19, Experimental Evaluation of Influence from Residual Stresses on Crack Initiation and Ductile Crack Growth at High Primary Loads.

- Research 2012:07, Implementation of the Master Curve Method in ProSACC.

- Research 2013:01, Validation of Weld Residual Stress Modelling in the NRC International Round Robin Study.

- Research 2015:03, Brottmekaniska K-lösningar för sprickor i massiv stång med icke-linjärt rotationssymmetriskt spänningstillstånd.

- Research 2016:35, Säkerhetsvärdering mot plastisk kollaps vid skade-tålighetsanalyser.

- Research 2016:39, Recommended Residual Stress Profiles for Stainless Steel Pipe Welds.

- Research 2017:03, Inverkan av inre tryck på sprickytan vid gräns-lastanalyser.

- Research 2017:16, Stress Intensity Factor Solutions for Circumferential Cracks in Cylindrical Bars under Axisymmetric Loading and Global Bending.

**Need for further research**
There will be a continuous need for further updates, supported by research, of the fracture mechanics handbook and the associated computer code ISAAC. This includes for example Leak Before Break (LBB) assessments and the influence of Warm Pre-stressing Effect (WPS) on fracture. This ensures that SSM as well as the Swedish nuclear power plant owners will have the best available tools, based on the latest research achievements, to assess the safety of damaged mechanical components.

**Project information**
Contact person SSM: Björn Brickstad
Reference: SSM2010-4481/2030049-09

Author:    Peter Dillström
           Jens Gunnars
           Petter von Unge
           Daniel Mångård

           Kiwa Inspecta Technology AB, Stockholm

# 2018:18

# Procedure for Safety Assessment of Components with Defects
## – Handbook Edition 5

# Summary

This handbook presents a procedure for analyzing the influence of defects and damage in components and structures. Damage tolerance analysis is an approach that assume that defects and flaws exists in a component, and acceptable defect sizes are determined regarding failure and damage growth. This procedure describes steps for assessing the safety margin against failure by both fracture and plastic collapse for a component containing a defect. Recommendations are also given for analyzing crack growth due to fatigue and stress corrosion.

The integrity of a structure is evaluated using a failure assessment diagram (FAD) to evaluate if fracture or plastic collapse occurs for the current loading and defect size. The procedure is based on the R6 method and two variables are used to assess failure; $K_r$ the ratio between the stress intensity factor and the fracture toughness, and $L_r$ the ratio between applied load and the limit load for the component containing a defect. A safety assessment system is included in the procedure with the possibility to specify safety factors. For nuclear applications specific safety factors are recommended to achieve margins corresponding to the requirements of ASME III and ASME XI.

The handbook includes recommendations for defect characterization, material data including values for fracture toughness and crack growth, a probabilistic procedure, as well as stress intensity factor and limit load solutions covering a number of different crack geometries, components and loading conditions.

# Sammanfattning

Denna handbok beskriver en procedur för att analysera betydelsen av defekter och skadetillväxt i komponenter och strukturer. Skadetålighetsanalys antar att defekter förekommer i alla komponenter och används för att analysera vilken storlek på defekter som en komponent kan tolerera avseende fara för haveri och skadetillväxt. Proceduren beskriver stegen för att analysera säkerhetsmarginalen mot brott och plastisk kollaps för en komponent med en defekt. Rekommendationer ges även för analys av spricktillväxt på grund av utmattning och spänningskorrosion.

Proceduren baseras på R6-metoden där påkänningen på en defekt avseende brott eller plastisk kollaps beskrivs med de två variablerna $K_r$ och $L_r$. $K_r$ är kvoten mellan spänningsintensitetsfaktorn och materialets brottseghet, medan $L_r$ är kvoten mellan pålagd last och gränslasten för komponenten med defekt. Värdena plottas i ett diagram (Failure Assessment Diagram, FAD) för att bedöma om haveri genom brott eller plastisk kollaps inträffar för aktuell belastning och defektstorlek.

I proceduren ingår ett säkerhetsvärderingssystem som ger möjligheten att inkludera säkerhetsmarginaler i bedömningen. Specifika säkerhetsfaktorer för nukleära ändamål inkluderas som motsvarar säkerhetsmarginalerna enligt ASME III och ASME XI.

Handboken innehåller rekommendationer för defektkaraktärisering, utvärdering av växelverkan mellan defekter, svetsegenspänningar, material-data inklusive brottseghetsvärden och spricktillväxtdata, en probabilistisk procedur, samt spänningsintensitetsfaktorer och gränslastlösningar för olika sprickgeometrier, komponenter och belastningar.

***Table of Content***             ***Page***

# Nomenclature

| | |
|---|---|
| $a$ | Crack depth for surface cracks |
| $\bar{a}$ | Crack depth with a plastic zone correction |
| $A$ | Geometry evaluation point |
| $2a$ | Crack depth for embedded cracks |
| $\mathrm{d}a/\mathrm{d}N$ | Local crack growth rate for fatigue crack cracking |
| $\mathrm{d}a/\mathrm{d}t$ | Local crack growth rate for stress corrosion cracking |
| $b$ | Geometry parameter to define a crack in a cylindrical bar |
| $B$ | Geometry evaluation point |
| $c$ | Half crack length for embedded cracks; Constant in algorithm to calculate the most probable point of failure (MPP) |
| $c_1, c_2$ | Constants in the distribution function - Probability of Detection |
| $c_i$ | Constants in fitting polynomial |
| $C$ | Constant for fatigue or stress corrosion crack growth |
| $C_0$ | Constant in $J_R$-Curve (kJ/m$^2$) |
| $C_1$ | Exponential constant in $J$R-Curve |
| $cfl$ | Crack front length |
| $C_p$ | Permissible membrane factor |
| $C_T$ | Temperature dependent coefficient |
| $d$ | Distance from the closest free surface to the crack center (for embedded cracks) |
| $d_i$ | Search direction vector to the most probable point of failure (MPP) |
| $D$ | Diameter |
| $D(\ldots)$ | Detection event |
| $E$ | Elastic modulus |
| $e$ | Eccentricity of embedded cracks |
| $f$ | Frequency |
| $f_i$ | Geometry function for stress intensity factor |
| $f(K_I)$ | Weibull probability density function |
| $f_1$ | Permissible global bending factor for $S_m$ |
| $f_2$ | Permissible global bending factor for $\sigma_Y$ |
| $f_2^{cy}$ | R6 revision 4, approximate Option 2 type assessment curve – Continuous Yielding |
| $f_2^{dy}$ | R6 revision 4, approximate Option 2 type assessment curve – Discontinuous Yielding |
| $f_b$ | Geometry function for stress intensity factor, $b \rightarrow$ bending |
| $f_{FAD}$ | Failure assessment curve |

| | |
|---|---|
| $f_m$ | Geometry function for stress intensity factor, $m \rightarrow$ membrane |
| $f_{R6}$ | R6 revision 4, approximate Option 2 type failure assessment curve |
| $f_x(x)$ | Joint probability density function |
| $F_{POD}$ | Distribution function - Probability of Detection |
| $F_x(x)$ | Cumulative distribution function |
| $g(x)$ | Limit state function |
| $g(X)$ | Limit state function |
| $g_f$ | Material function to define the crack growth (fatigue) |
| $g_{FAD}(X)$ | Limit state function - Failure assessment diagram |
| $g_{Linear}(u)$ | Transformed limit state function, using a linear approximation |
| $g_{L_r^{max}}(X)$ | Limit state function - Upper limit of $L_r$ |
| $g_{Quadratic}(u)$ | Transformed limit state function, using a quadratic approximation |
| $g_{SC}$ | Material function to define the crack growth (stress corrosion) |
| $g_U(u)$ | Limit state function in a transformed standard normal space $U$ |
| $G(\ldots)$ | Limit state event |
| $J$ | $J$-integral |
| $J_{Ic}$ | Critical $J$-value according to ASTM E1820 |
| $J_{acc}$ | Acceptable value of the $J$-integral |
| $J_R$ | $J$-resistance (curve) |
| $k$ | Weibull distribution parameter - shape |
| $K_I$ | Stress intensity factor |
| $K_I^{max}$ | Maximum stress intensity factor |
| $K_I^{min}$ | Minimum stress intensity factor |
| $K_I^p$ | Primary stress intensity factor |
| $K_I^s$ | Secondary stress intensity factor |
| $K_{Ic}$ | Fracture toughness according to ASTM E399 |
| $K_1$ | Elastic stress intensity factor (used in the modified version of Budden`s method) |
| $K_2$ | Plastic stress intensity factor (used in the modified version of Budden`s method) |
| $K_{1mm}$ | Critical value of stress intensity factor including 1 mm stable crack growth |
| $K_{2mm}$ | Critical value of stress intensity factor including 2 mm stable crack growth |
| $K_{cr}$ | Critical value of stress intensity factor |
| $K_{cr}^d$ | Critical value of stress intensity factor (used in design) |

| | |
|---|---|
| $K_{JC}$ | Fracture toughness |
| $K_{JC}^{cfl}$ | Fracture toughness corrected for the crack front length |
| $K_{IC}^{1T}$ | Fracture toughness from 1T specimens |
| $K_r$ | Fracture parameter |
| $K_r^{acc}$ | Acceptable fracture parameter |
| $l$ | Crack length |
| $l_m$ | Crack length at the mean radius of a cylinder |
| $L$ | Crack length |
| $L*$ | Length used in calculation for a cylindrical bar with a part circumferential surface crack |
| $L_r$ | Limit load parameter |
| $L_r^m$ | Limit load parameter for membrane stresses only |
| $L_r^b$ | Limit load parameter for global bending stresses only |
| $L_r^{max}\ L_r^{max}$ | Maximum allowed value of the limit load parameter |
| $m(...)$ | Merit function in algorithm to calculate the most probable point of failure (MPP) |
| $M_0$ | Applied bending moment on a cylindrical bar |
| $M_f$ | Limit load in pure bending for a cylindrical bar |
| $M_{limit}$ | Limit load parameter for a cylindrical bar |
| $n$ | Constant for fatigue or stress corrosion crack growth |
| $n_L$ | Normalized limit force |
| $N$ | Number (cycles / simulations / random variables / inspections) |
| $N_{R6}$ | Strain hardening exponent in R6 revision 4, approximate Option 2 |
| $N_0$ | Applied tensile force on a cylindrical bar |
| $N_f$ | Limit load in pure tension for a cylindrical bar |
| $N_F$ | Number of failures during simulation |
| $N_{limit}$ | Limit load parameter for a cylindrical bar |
| $P$ | Primary load |
| $P_F$ | Probability of failure |
| $P_{F,FORM}$ | Probability of failure - using First-Order Reliability Method |
| $P_{F,MCS}$ | Probability of failure - using Simple Monte Carlo Simulation |
| $P_{F,SORM}$ | Probability of failure - using Second-Order Reliability Method |
| $P_L$ | Limit load; Local membrane stress |
| $P_m$ | The primary general membrane stress |
| $POD$ | Probability of detection |

| | |
|---|---|
| $r$ | Coordinate |
| $R$ | Stress intensity factor ratio, $R = K_I^{min} / K_I^{max}$;<br>Radius of a cylindrical bar |
| $R_e$ | Yield strength – standardized value |
| $R_{eL}$ | Lower yield strength |
| $R_i$ | Inner radius |
| $R_m$ | Ultimate tensile strength – standardized value;<br>Mean radius of a cylinder |
| $R_{p0.2}$ | 0.2% elongation stress |
| $R_{p1.0}$ | 1.0% elongation stress |
| $R_{NDT}$ | Nil-ductility transition temperature |
| $s$ | Distance between neighboring defects |
| $s_{bg}$ | Stress parameter, used in the definition of limit loads for circumferential cracks in a cylinder |
| $s'_{bg}$ | Stress parameter, used in the definition of limit loads for circumferential cracks in a cylinder |
| $s_i$ | Step size in algorithm to calculate the most probable point of failure (MPP) |
| $s_m$ | Stress parameter, used in the definition of limit loads for circumferential cracks in a cylinder |
| $s'_m$ | Stress parameter, used in the definition of limit loads for circumferential cracks in a cylinder |
| $SF$ | Safety factor |
| $SF_J$ | Safety factor against fracture described by $J$ |
| $SF_K$ | Safety factor against fracture described by $K_I$, $SF_K = \sqrt{SF_J}$ |
| $SF_K^{Primary}$ | Primary safety factor against fracture described by $K_I$ |
| $SF_K^{Secondary}$ | Secondary safety factor against fracture described by $K_I$ |
| $SF_L$ | Safety factor against plastic collapse |
| $SF_L^m$ | Safety factor against plastic collapse for membrane and local bending stresses |
| $SF_L^b$ | Safety factor against plastic collapse for global bending stresses |
| $S_m$ | Allowable design stress |
| $S_r$ | Magnitude of residual stresses |
| $T$ | Temperature |
| $T_0$ | Fracture toughness testing temperature (Master Curve) |
| $T_{28J}$ | Charpy impact test temperature |
| $T_{41J}$ | Charpy impact test temperature |
| $T_{act}$ | Actual temperature (Master Curve) |
| $T_{app}$ | Applied tearing modulus |
| $T_R$ | Tearing modulus |

| | |
|---|---|
| $t$ | Plate or wall thickness; Time |
| $t_i$ | Inspection time |
| $t_{clad}$ | Cladding thickness |
| $u$ | Coordinate; Random number - between 0 and 1; Transformed random parameter |
| $U$ | Transformed random vector |
| $V$ | Multiplying factor for interaction between primary and secondary stresses |
| $W$ | Width |
| $x$ | Coordinate; Random parameter; Random variable |
| $X$ | Random vector |
| $y_i$ | Approximation to the most probable point of failure (MPP) |
| $z$ | Parameter of the gamma function |
| $\Delta a$ | Stable crack growth |
| $\Delta K_I$ | Stress intensity factor range, $\Delta K_I = K_I^{max} - K_I^{min}$ |
| $\Delta K_I^{eff}$ | Effective stress intensity factor range |
| $\Delta_{total}$ | Total displacement, used in the definition of applied tearing modulus |
| $\nabla g_U$ | Gradient of the limit state function |
| $\alpha$ | Angle parameter - used in the definition of limit loads for circumferential cracks in a cylinder; Confidence level for error estimation - using Simple Monte Carlo Simulation |
| $\beta$ | Angle to the neutral axis of flawed cylinders; Angle to the axis intersecting the deepest crack point of a part circumferential crack in a bar; Parameter used to differentiate between plane stress and plane strain in a plastic zone correction according to Irwin |
| $\beta_{HL}$ | Reliability index |
| $\varepsilon_{MCS}$ | Error estimate - using Simple Monte Carlo Simulation |
| $\Phi$ | Angle parameter, used in the definition of limit loads for surface cracks in a bar |
| $\Phi(u)$ | Cumulative distribution function in standard normal space |
| $\gamma$ | Geometry parameter for embedded cracks |
| $\gamma_m^k$ | Partial coefficient (related to fracture toughness) |
| $\gamma_m^y$ | Partial coefficient (related to yield strength) |
| $\Gamma(z)$ | Gamma function |
| $\kappa_i$ | Principal curvatures of the limit state surface |
| $\lambda$ | Equivalent crack length; Exponential distribution parameter |

| | |
|---|---|
| $\lambda_{R6}$ | Material parameter for R6 revision 4, approximate Option 2 |
| $\mu$ | Material parameter for R6 revision 4, approximate Option 2 |
| $\mu_a$ | Defect size - mean value |
| $\mu_{K_{Ic}}$ | Fracture toughness - mean value |
| $\mu_{LogNor}$ | Log-normal distribution parameter - log-normal mean value |
| $\mu_{\sigma_U}$ | Ultimate tensile strength - mean value |
| $\mu_{\sigma_Y}$ | Yield strength - mean value |
| $v$ | Poisson's ratio |
| $\theta$ | Angle parameter - used in the definition of limit loads for circumferential cracks in a cylinder; Weibull distribution parameter - scale |
| $\rho$ | Additive parameter for interaction between primary and secondary stresses |
| $\sigma$ | Stress |
| $\sigma_0$ | Stress amplitude |
| $\sigma_a$ | Axial stress; Defect size - standard deviation |
| $\sigma_b$ | Through-thickness bending stress |
| $\sigma_{bg}$ | Global bending stress |
| $\sigma_{bg}^{ref}$ | Global bending reference stress |
| $\sigma_f$ | Flow stress |
| $\sigma_h$ | Hoop stress |
| $\sigma_i$ | Stress component |
| $\sigma_{K_{Ic}}$ | Fracture toughness - standard deviation |
| $\sigma_L$ | Longitudinal stress component |
| $\sigma_{LogNor}$ | Log-normal distribution parameter - log-normal standard deviation |
| $\sigma_m$ | Membrane stress |
| $\sigma_m^{ref}$ | Membrane reference stress |
| $\sigma^p$ | Primary stress |
| $\sigma_m^p$ | Primary membrane stress |
| $\sigma^s$ | Secondary stress |
| $\sigma_b^s$ | Secondary bending stress |
| $\sigma_T$ | Transverse stress component |
| $\sigma_Y$ | Yield strength, $R_{eL}$ or $R_{p0.2}$ (used in design) |
| $\sigma_Y^{20°C}$ | Yield strength at room temperature |
| $\sigma_Y^d$ | Yield strength (used in design) |
| $\sigma_Y^T$ | Yield strength at operating temperature |

| | |
|---|---|
| $\sigma_U$ | Ultimate tensile strength, $R_m$ |
| $\sigma_U^{20°C}$ | Ultimate tensile strength at room temperature |
| $\sigma_U^T$ | Ultimate tensile strength at operating temperature |
| $\sigma_{\sigma_U}$ | Ultimate tensile strength - standard deviation |
| $\sigma_{\sigma_Y}$ | Yield strength - standard deviation |
| $\chi$ | Parameter for calculation of interaction parameter $\rho$ between primary and secondary stresses |
| $\zeta$ | Equivalent crack depth over length ratio |
| $\Delta\varepsilon$ | Lüders strain used for R6 revision 4, approximate Option 2 |

# 1. Introduction

## 1.1. Background to Damage Tolerance Analysis

The capacity of a component to tolerate defects and damage is essential for safe and reliable use. Small defects and heterogeneities (such as pores, pits, second phase particles, oxide inclusions, or microcracks) that occur naturally in materials and are in general acceptable. Larger defects of significance may be introduced in components during manufacturing, for example at casting, forging or welding. Defects and damage can also occur and grow during operation and use of components, both due to degradation processes (e.g. fatigue, stress corrosion cracking, or local corrosion), and due to external or unusual events (e.g. collisions, impacts, overloads, cleaning or occasional elevated temperature). As defects grow during operation, or as occasional upset loads occur, a defect can be large enough to cause failure of the component. Failure occur when the component is loaded beyond its maximum load bearing capacity with regard to the mechanisms fracture, plastic collapse or buckling. It is thus important to analyze the influence of defects, to be able to establish appropriate measures that ensure operation and use with high reliability and adequate safety margins.

Damage tolerance analysis (DTA) is the approach that assume that defects and flaws can exist in any component and evaluates their effect. The purpose is to determine limits for defect sizes, and other parameters, that influence failure and damage growth. The size of acceptable defects can be established to ensure adequate safety margins against failure. Procedures as the one described in this handbook have been develop for engineering assessments for various defects in different components, materials, and loadings. Assessment can be made when a defect is detected by non-destructive testing (NDT) to evaluate conditions for continued safe operation. Analysis can also be made for assumed (postulated) defects in order to evaluate the damage tolerance of a new design, or when establishing requirements for an inspection program. It is central to be able to assess the significance of different defects, but also to have knowledge on the ability to detect defects or damage through inspection and testing.

The effect of a defect on the integrity of a component depends on a number of influencing factors within the areas of loads, stresses, material properties and strength, as well as environment and damage that can occur. An initial crack size is normally assumed based on the capability for a particular inspection method to detect a crack. Appropriate safety margins must be applied in the assessments to account for scatter and uncertainties in influencing parameters, and with respect to the consequences of failure of the component or structure.

The effect from the influencing factors has to be analyzed for the specific situation, to determine which defects are harmless and which impose a threat. The factors affect how long the component may operate before inspections are necessary to assure opportunities to discover a damaged state in time for repair or other measures.

Damage tolerance analysis can be used in many situations and for different purposes. Below are some general applications described:

- Damage tolerance analysis can be applied as a basis for planning of in-service inspection (ISI) and maintenance of components in the operational phase. The purpose is to determine inspection intervals and evaluate the required NDT detection capability, to assure that any defects and degradation are found before they become significant for safety and operational reliability. A detectable defect is assumed to exist and any active or potential degradation is considered. Inspection intervals are established to assure that the component will sustain defects safely until further inspection or repair can be effected.

- When defects and damage are found during inspections the procedure can be used for detailed fitness-for-service (FFS) assessment, with the purpose to evaluate whether continued operation of the component with defects and damage is acceptable for a specific period, or if it is necessary to immediately repair or replace the component. A damage tolerant structure and continued safe operation may be ensured by developing an inspection schedule based on the capability for defect detection and sizing of the selected NDT system.

- Damage tolerance analysis can be applied in assessments for life extension of components and equipment, considering unique aspects in design and threats from degradation, ageing and loadings, especially addressing damage not considered during design. For fatigue, crack initiation is commonly neglected and the damage tolerance analysis is based upon fatigue crack growth from an assumed reasonable flaw size that could exist in the structure. The assessment should consider any earlier inspection findings and damages, new recommendations and standards, together with review of historical and expected future operational loads, operating conditions and potential degradation mechanisms. Purposes can be to develop targeted status inspections, verify the structural integrity for the life extension period or remaining design life, identify necessary repairs and replacements, and develop a plan for adapted recurrent inspections and other actions as needed to achieve safety and reliability for an extended operational lifetime.

- Another application area is during the <u>design phase</u>, to consider pre-existing flaws and assure a design that results in sufficient capacity of a component to tolerate surface defects and damage. In contrast to conventional design assessments for pressure equipment made from ductile materials, defects can be assumed to exist or occur at the surface as reasonably for the anticipated operation and environment. This can be especially useful when developing components in new or less common materials with unusual properties (e.g. high strength steels), or for components with less common geometry, loadings or environment. The results can guide adjustments of geometry, material selection, manufacturing and inspections for improved damage tolerance.

- Damage tolerance analysis results can be useful for assessing the requirements for <u>control during manufacturing and installation</u> of a component. This is especially relevant for quality assurance of new applications or when using new materials, where common quality criteria based on experience can be uncertain. Manufacturing errors can be a major source for initiating damage in some applications, and consideration of manufacturing defects is important to ensure safety. Damage tolerance results are also useful for the purpose to avoid unnecessary repairs in complex and expensive components. If a defect has been detected by NDT at the manufacturing control, its relevance can be evaluated in detail for the specific operational loads for the component. Damage tolerance results can be useful if alternative methods for manufacturing control are consider, or for establishing detailed specification of reporting/acceptance levels for defects in a component, considering the anticipated future loading. It can be noted that conventional quality control acceptance levels applied in standards are generally based on experience from use in certain applications and with common materials and loadings. They are very useful and reflect good workmanship. However, it is important that the acceptance level corresponds to a fraction of the acceptable defect size as obtained by damage tolerance analysis. For new materials and applications it can be useful to employ damage tolerance results for verification when establishing criteria.

- Damage tolerance analysis can be used in <u>failure investigations</u> to analyze causes of failure, with the purpose to clarify the influence from different key parameters for failure modes and damage growth, and assess the most likely causes. When the root cause has been determined it is important to consider similar positions and components.

This handbook builds on earlier editions [1.1] and describes a procedure for assessment of the significance of defects in components and

structures, as well as recommendations for evaluation of crack growth due to fatigue and stress corrosion. Other procedures for assessment of defects are given in SINTAP, R6, BS 7910, ASME XI, and API 579, [1.2] – [1.6]. The procedures are based on similar methods and approaches, but this procedure contains particular approaches established by research, development and validation performed in Sweden, including for example a safety assessment procedure, treatment of secondary stresses and specific solutions and recommendations developed for several geometries, welds and materials. Development have been performed continuously with the purpose to reduce conservatism, increase accuracy and introduce new knowledge when important for practical applications.

## 1.2. Overview of the Handbook

The handbook describes in detail the steps for performing a safety assessment of a component considering the effect of defects. A failure assessment diagram (FAD) approach is used for assessment of fracture or plastic collapse at combined primary and secondary loadings. Recommendations and guidance are given in Appendices for flaw combination and evaluation of interaction between defects, weld residual stresses, safety factors, material properties, fracture toughness, embrittlement, crack growth during operation due to fatigue and stress corrosion. Stress intensity factor solutions and limit load solutions are provided for various crack geometries, different component geometries, and different loadings.

The FAD approach utilized for simultaneous assessment of fracture and plastic collapse is based on R6 [1.3]. Initiation of failure from a defect is characterized by two parameters; $K_r$ and $L_r$. $K_r$ is the ratio between the stress intensity factor at the defect and the fracture toughness of the material, and $L_r$ is the ratio between applied load and the plastic limit load of the component with the defect. The values of $K_r$ and $L_r$ are plotted in a failure assessment diagram which is divided into a critical and non-critical region. If the point is situated within the non-critical region, fracture is not predicted to occur. If the point is situated in the critical region however, failure and unstable crack growth may occur by fracture or plastic collapse.

A safety assessment system is included in the procedure with the possibility to include safety margins in the assessment. For nuclear applications, specific safety margins are introduced to achieve the margins corresponding to the requirements of the ASME Boiler and Pressure Vessel Code, Sections III and XI [1.5], [1.7].

The procedure with given solutions of the stress intensity factor and the limit load are validated in [1.8] to confirm conservatism. Predictions by the procedure are compared with the actual outcome of full scale experiments reported in the literature. Some of the new solutions

introduced in the fourth and fifth edition of the handbook are, however, not included in the validation reported [1.8]. However, additional validations have been published in the R6 document [1.3].

The procedure is mainly verified for steel alloys but can be used for other metallic materials. The method is not intended for use in temperature regions where creep deformation is of importance.

## 1.3. Summary of Updates in the Handbook Edition 5

The first edition of this handbook was released in 1990, the second in 1991, the third in 1996 and the fourth in 2008 [1.1]. This fifth edition includes extensive revisions as summarized below.

The standard FAD is changed to the approximate Option 2 FAD according to R6 Revision 4 [1.3]. Procedures based on the ASME Section XI code is revised to the 2007 edition with 2009b addendum [1.5]. This affects several sections including defect characterization and defect interaction, and safety assessment for nuclear applications. Other changes include new and updated geometry solutions, new recommendations for weld residual stresses, updated crack growth laws, recommendations for fracture toughness data using Master Curve, a safety assessment procedure for reducing conservatism for secondary stresses, and probabilistic analysis as an alternative.

## 1.4. The ISAAC Software

The damage tolerance analysis procedures described in this handbook are implemented in the software ISAAC [1.9]. The software has modules for safety assessment of defects in component with respect to fracture and plastic collapse, as well as modules for analysis of crack growth due to fatigue and stress corrosion cracking. Solutions are implemented for different types of cracks, component geometries and loadings, as described in the handbook.

ISAAC (Integrity and SAfety Assessment of Components) has a module for safety assessment of cracks by a procedure with FAD based on the R6-method. It also includes modules for assessment according to the ASME Boiler and Pressure Vessel Code, Section XI, Appendices A and C (defects in ferritic components and in austenitic and ferritic piping). The software provides efficiency at practical analyses, for example by facilitating analysis of limiting defect sizes, assessment of different types of defect in a component, analysis of crack growth, ductile tearing, and sensitivity analyses. The software can reduce input errors and provides automated reporting. The implementation has been validated and verified during a long period since the first revisions of the program.

## 1.5. Acknowledgments

## 1.6. References

[1.1]   SSM 2008:01, (2008), "A combined deterministic and probabilistic procedure for safety assessment of components with cracks – Handbook", SSM Research Report 2008:01, Swedish Radiation Safety Authority.

[1.2]   SINTAP, (1999), "Structural Integrity Assessment Procedures for European Industry", Brite-Euram Project No. BE95-1426, BRPR-CT95-0024, Final Report.

[1.3]   R6, (2015), "Assessment of the Integrity of Structures Containing Defects", R6 –Revision 4, Up to amendment record No.11, EDF Energy Nuclear Generation Ltd.

[1.4]   BS 7910, (2015), "Guide to methods for assessing the acceptability of flaws in metallic structures", BS 7910:2013+A1:2015, The British Standards Institution.

[1.5]   ASME XI, (2007), "ASME Boiler and Pressure Vessel Code: Rules for In-service Inspection of Nuclear Power Plant Component", ASME XI 2007+Addendum 2009b, The American Society of Mechanical Engineers, New York, USA.

[1.6]   API 579, (2016), "API 579-1/ASME FFS-1, Fitness-For-Service", American Petroleum Institute and The American Society of Mechanical Engineers.

[1.7]   ASME III, (2013), "ASME Boiler and Pressure Vessel Code, Section III, Division 1 – Subsection NB Class 1 Components", The American Society of Mechanical Engineers, New York, USA.

[1.8]   SATTARI-FAR, I., and F. NILSSON, (1991), "Validation of a procedure for safety assessment of cracks", SA/FoU-Report 91/19, SAQ Kontroll AB, Stockholm, Sweden.

[1.9]   ISAAC, (2017), User´s Manual, Kiwa Inspecta Technology AB, Stockholm, Sweden.

# 2. Procedure

## 2.1. Overview

Failure assessment according to the procedure includes the following main steps:

1) Characterization of defect (Chapter 2.2 and Appendix A).
2) Choice of geometry (Chapter 2.3 and Appendix G).
3) Determination of stress state (Chapter 2.4).
4) Determination of material data (Chapter 2.5 and Appendix M).
5) Analysis of possible slow crack growth during operation (Chapter 2.6 and Appendix M).
6) Calculation of stress intensity factors $K_I^p$ and $K_I^s$ (Chapter 2.7 and Appendix K).
7) Calculation of limit load $L_r$ (Chapter 2.8 and Appendix L).
8) Evaluation of $K_r$ (Chapter 2.9).
9) Failure assessment (Chapter 2.10).
10) Safety assessment of results (Chapter 2.11).

The non-critical region is limited by (as defined in Chapter 2.10),

$$K_r \leq f_{R6} , \qquad (2.1)$$

$$L_r \leq L_r^{max} , \qquad (2.2)$$

according to Figure 2.1.
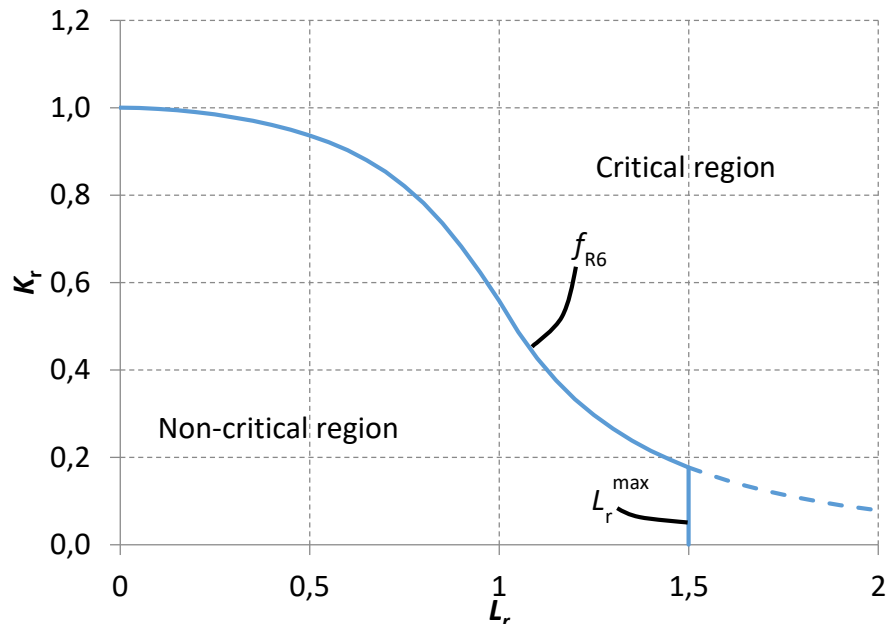


Figure 2.1. Failure Assessment Diagram (FAD).

## 2.2. Characterization of Defect

A fracture mechanics analysis requires that the actual defect geometry is defined. For application to components in nuclear power facilities, methods according to Appendix A are recommended in order to consider interaction effects and characterize the shape and size of a crack.

For assessment of an actual defect it is important to determine whether the defect remains from the manufacturing or has occurred because of service induced processes such as fatigue or stress corrosion cracking.

## 2.3. Choice of Geometry

The geometries available in this procedure are documented in Appendix G. In the idealization process from the real geometry to these cases care should be taken to avoid non-conservatism. In cases when an idealization of the real geometry to one of the cases considered here are not adequate, stress intensity factor and limit load solutions may be found in the literature or be calculated by numerical methods. The use of such solutions should be carefully verified for accuracy.

## 2.4. Stress State

In this procedure it is assumed that the stresses have been obtained under the assumption of linearly elastic material behavior. The term nominal stress denotes the stress state that would act at the plane of the crack in the corresponding crack free component.

The stresses are divided into primary $\sigma^p$ and secondary $\sigma^s$ stresses. Primary stresses are caused by the part of the loading that contributes to plastic collapse e.g. pressure, gravity loading etc. Secondary stresses are caused by the part of the loading that does not contribute to plastic collapse e.g. stresses caused by thermal gradients, weld residual stresses etc. If the component is cladded this should be taken into account when the stresses are determined.

All stresses acting in the component shall be considered. The stresses caused by the service conditions should be calculated according to reliable methods. Some guidance about weld residual stresses is given in Appendix R.

For pressurized components, the pressure acting directly on the crack face should be considered while calculating the stress intensity factor, $K_I$. This can be done by adding the pressure as a membrane stress on the crack face.

## 2.5. Material Data

To perform the assessments, the yield strength, $\sigma_Y$, ultimate tensile strength, $\sigma_U$, and critical stress intensity factor, $K_{cr}$, or $J_r$-curves of the

material must be determined. If possible, data obtained from testing of the actual material of the component should be used. Test data presented in a material certificate is however not sufficient to give reliable values. When actual material properties cannot be obtained, minimum values for $\sigma_Y$ and $\sigma_U$ from codes, standards or material specifications may be used. These data should be determined at the actual temperature.

$\sigma_Y$ is equal to the lower yield strength $R_{eL}$ if this can be determined and in other cases the 0.2% proof stress $R_{p0.2}$. In the cases when $R_{eL}$ can be determined the material is considered to have a yield plateau. This is for instance common for certain low alloy carbon manganese steels at low temperatures.

$\sigma_U$ is the ultimate tensile strength of the material.

The yield strength and ultimate tensile strength of the base material should normally be used even when the crack is situated in a welded joint. The reason for this is that the yield limit of the structure is not a local property but also depends on the strength properties of the material remote from the crack.

$K_{cr}$ is the critical value of the stress intensity factor for the material at the crack front. If possible, $K_{cr}$ should be set equal to the fracture toughness $K_{Ic}$ according to ASTM E399 [2.1]. It is in many cases not possible to obtain a valid $K_{Ic}$-value. $J_{Ic}$-values according to ASTM E1820 [2.2] can instead be used and converted according to Eq. (2.3).

$$K_{cr} = \sqrt{\frac{EJ_{Ic}}{1 - v^2}} \ . \tag{2.3}$$

Here $E$ is the elastic modulus of the material and $v$ is Poisson's ratio.

Ductile materials normally show a significant raise of the $J$-resistance curve after initiation. When taking this into account, $J_r$-data according to ASTM E1820 [2.2] should be used.

For application on nuclear components fracture toughness and $J_r$-curves according to Appendix M can be used if sufficient actual test data for the considered material is not available. Appendix M includes data for irradiation embrittlement.

When not stated otherwise the material data for the actual temperature should be used.

## 2.6. Calculation of Slow Crack Growth

The final fracture assessment as described below should be based on the estimated crack size at the end of the service period. In cases where slow crack growth due to fatigue, stress corrosion cracking or some

other mechanism can occur the possible growth must be accounted for in the determination of the final crack size.

The rate of crack growth due to both fatigue and stress corrosion cracking is assumed to be governed by the stress intensity factor $K_I$. This quantity is calculated according to methods described in Appendix K.

For fatigue crack growth, the rate of growth per loading cycle can be described by an expression of the form

$$\frac{da}{dN} = g_f(\Delta K_I, R).$$ (2.4)

Here

$$\Delta K_I = K_I^{max} - K_I^{min},$$ (2.5)

and

$$R = \frac{K_I^{min}}{K_I^{max}},$$ (2.6)

where $K_I^{max}$ and $K_I^{min}$ are the algebraic maximum and minimum, respectively, of $K_I$ during the load cycle. $g_f$ is a material function that can also depend on environmental factors such as temperature and humidity. For cases when $R < 0$ the influence of the $R$-value on the crack growth rate can be estimated by use of growth data for $R = 0$ and an effective stress intensity factor range according to

$$\Delta K_I^{eff} = K_I^{max}, \text{ if } K_I^{min} < 0.$$ (2.7)

For application on nuclear components fatigue crack growth data according to Appendix M can be used if actual test data for the considered material is not available.

For stress corrosion cracking, the growth rate per time unit can be described by a relation of the form

$$\frac{da}{dt} = g_{sc}(K_I).$$ (2.8)

$g_{sc}$ is a material function which is strongly dependent on environmental factors such as the temperature and the chemical properties of the environment.

For application on nuclear components stress corrosion crack growth data according to Appendix M can be used if actual test data for the material and environment under consideration is not available.

## 2.7.  Calculation of $K_I^p$ and $K_I^s$

The stress intensity factors $K_I^p$ (caused by primary stresses $\sigma^p$) and $K_I^s$ (caused by secondary stresses $\sigma^s$) are calculated with the methods given in Appendix K. For the cases given it is assumed that the nominal stress distribution (i.e. without consideration of the crack) is known.

Limits for the applicability of the solutions are given for the different cases. If results are desired for a situation outside the applicability limits a recharacterization of the crack geometry can sometimes be made. The following recharacterizations are recommended:

a)     A semi-elliptical surface crack with a length/depth ratio which is larger than the applicability limit can instead be treated as an infinitely long two-dimensional crack.

b)     A semi-elliptical surface crack with a depth that exceeds the applicability limit can instead be treated as a through-thickness crack with the same length as the original crack.

c)     A cylinder with a ratio between wall thickness and inner radius which is below the applicability limit can instead be treated as a plate with a corresponding stress state.

In cases when the solutions of Appendix K cannot be applied, stress intensity factors can be obtained either by use of solutions found in the literature, see for example the handbooks [2.3], [2.4], [2.5] and [2.6], or by numerical calculations, e.g. by the finite element method.

## 2.8.  Calculation of $L_r$

$L_r$ is defined as the ratio between the current primary load and the limit load $P_L$ for the component under consideration and with the presence of the crack taken into account. $P_L$ should be calculated under the assumption of a perfectly-plastic material with the yield strength $\sigma_Y$ chosen as discussed in Chapter 2.5. Appendix L contains solutions of $L_r$ for the cases considered in this procedure.

Limits for the applicability of the solutions are given for the different cases. If results are desired for a situation outside the applicability limits a recharacterization of the crack geometry can sometimes be made similarly to what was discussed for the stress intensity factor above.

In cases when the solutions of Appendix L cannot be applied, $L_r$ can be obtained either by use of solutions found in the literature, see for example [2.7], or by numerical calculations, e.g. by the finite element method.

## 2.9. Calculation of $K_r$

The ordinate $K_r$ in the failure assessment diagram (Figure 2.1) is calculated in the following way.

$$K_r = \frac{K_I^p + K_I^s}{K_{cr}} + \rho ,$$  (2.9)

where $\rho$ is a parameter that accounts for plastic effects due to interaction between secondary and primary stresses. $\rho$ is dependent on the $f_{R6}$-curve [2.8] and typical values are illustrated in the diagram in Figure 2.2 where $\rho$ is given as a function of $L_r$ and the parameter $\chi$ defined as

$$\chi = \frac{K_I^s L_r}{K_I^p} .$$  (2.10)

$\chi$ is set to zero if $\chi$ falls below zero. Also, $\rho$ is restricted to non-negative values as defined in Figure 2.2.
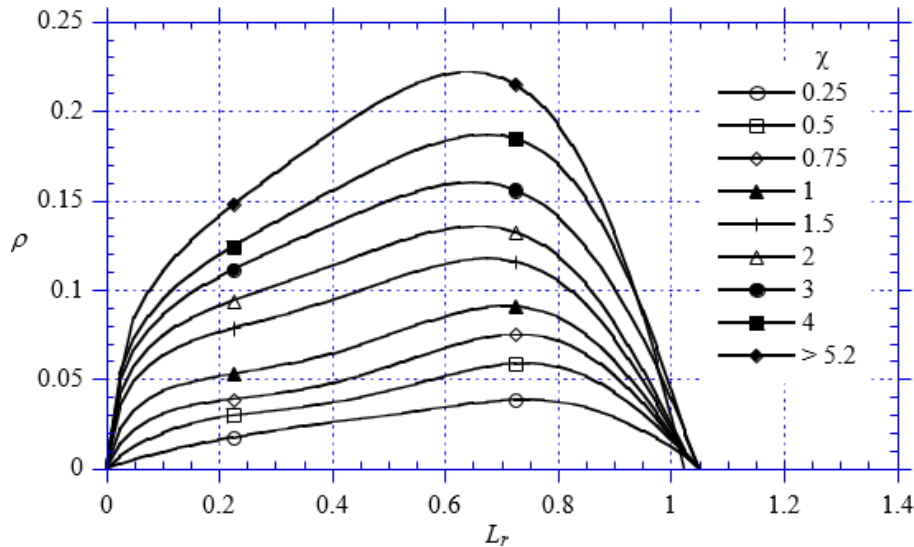


Figure 2.2. Example diagram for $\rho$.

An alternative approach instead of the additive factor $\rho$ is the multiplying factor $V$ which can be used to calculate $K_r$ as

$$K_r = \frac{K_I^p + V K_I^s}{K_{cr}}.$$  (2.11)

The factor $V$ has recently replaced the factor $\rho$ in R6 [2.9].

## 2.10. Failure Assessment

In order to assess the margin to failure for the defect loading, the assessment point $(L_r, K_r)$ is calculated as described above and plotted in the diagram in Figure 2.1. If the point is situated within the non-critical region no initiation of farcture or collapse is predicted to occur. The non-critical region is limited by the R6 approximate Option 2 type failure assessment curve [2.9] according to

23

$$K_r \leq f_{R6}(L_r) = \begin{cases} f_2^{cy}(L_r) & \text{Continuous Yielding} \\ f_2^{dy}(L_r) & \text{Discontinuous Yielding} \end{cases}, \qquad (2.12)$$

$$L_r \leq L_r^{max} = \frac{\sigma_f}{\sigma_Y}, \qquad (2.13)$$

where $f_2^{cy}$ is the approximate Option 2 curve for materials which show a continuous stress-strain curve without any yield plateau and $f_2^{dy}$ is the approximate Option 2 curve for materials with a stress-stain curve that exhibit discontinuous yielding. $L_r^{max}$ is the cut-off value for $L_r$ and the uniaxial flow stress $\sigma_f$ is defined as

$$\sigma_f = \frac{\sigma_Y + \sigma_U}{2}. \qquad (2.14)$$

For materials which show continuous yielding, the failure assessment curve is defined as

$$f_2^{cy}(L_r) = \begin{cases} \dfrac{0.3 + 0.7e^{-\mu L_r^6}}{\sqrt{1 + 0.5L_r^2}} & L_r \leq 1 \\ f_2^{cy}(1)L_r^{\frac{N_{R6}-1}{2N_{R6}}} & 1 < L_r < L_r^{max} \end{cases}, \qquad (2.15)$$

where

$$\mu = \min\left(\frac{0.001E}{\sigma_Y}, 0.6\right), \qquad (2.16)$$

$$N_{R6} = 0.3\left[1 - \frac{\sigma_Y}{\sigma_U}\right]. \qquad (2.17)$$

For materials with discontinuous yielding, the failure assessment curve is defined as

$$f_2^{dy}(L_r) = \begin{cases} \dfrac{1}{\sqrt{1 + 0.5L_r^2}} & L_r < 1 \\ \dfrac{1}{\sqrt{\lambda_{R6} + 1/2\lambda_{R6}}} & L_r = 1 \\ f_2^{dy}(1)L_r^{\frac{N_{R6}-1}{2N_{R6}}} & 1 < L_r < L_r^{max} \end{cases}, \qquad (2.18)$$

where

$$\lambda_{R6} = 1 + \frac{E\Delta\varepsilon}{\sigma_Y}, \qquad (2.19)$$

$$\Delta\varepsilon = 0.0375\left[1 - \frac{\sigma_Y}{1000}\right], \qquad (2.20)$$

where the yield strength, $\sigma_Y$ is in MPa.

When the failure load of a component with a crack is sought, the above described procedure is carried out for different load levels and the crack geometry is kept constant. The critical load is then given by the load level which causes the point $(L_r, K_r)$ to fall on the border to the critical region. Similarly, the limiting crack size is obtained by keeping the loads fixed and calculating the point $(L_r, K_r)$ for different crack sizes until it falls on the border of the critical region.

In order to assess the risk of fracture for materials with high toughness, stable crack growth has to be included in the assessment. The non-critical region is here limited by

$$J = J_R ,$$ (2.21)

$$T_{app} \leq T_R .$$ (2.22)

Where $J$ is the applied $J$, $J_R$ is the resistance curve, $T_{app}$ is the applied tearing modulus and $T_R$ is the tearing modulus of the material. Background to this assessment procedure is given in Appendix B.

## 2.11. Safety Assessment

The following conditions should be fulfilled to determine if a detected crack of a certain size is acceptable, cf. [2.10]:

$$J \leq \frac{J_{Ic}}{SF_J} ,$$ (2.23)

$$P \leq \frac{P_L}{SF_L} .$$ (2.24)

Eqs. (2.23) and (2.24) account for the failure mechanisms fracture and plastic collapse, and $SF_J$ and $SF_L$ are the respective safety factors against these failure mechanisms. Plastic collapse is assumed to occur when the primary load $P$ is equal to the limit load $P_L$. This occurs when the remaining ligament of the cracked section becomes fully plastic and has reached the flow stress $\sigma_f$. $J$ is the path-independent $J$-integral which is meaningful for situations where $J$ completely characterizes the crack-tip conditions. $J$ should be evaluated with all stresses present (including residual stresses) and for the actual material data. $J_{Ic}$ is the value of the $J$-integral at which initiation of crack growth occurs.

In this procedure $J$ is estimated using the approximate Option 2 type R6, Revision 4 failure assessment curve [2.9]. The R6-estimation of $J$ is given by

$$J = \frac{(1 - \nu^2)K_I^2}{E} \frac{1}{[f_{R6}(L_r) - \rho]^2} ,$$ (2.25)

where $f_{R6}$ is defined by Eq. (2.12). The second fraction on the right hand side of Eq. (2.25) can be interpreted as a plasticity correction function, based on the limit load, for the linear elastic value of $J$ determined by the stress intensity factor $K_I$, where $K_I = K_I^p + K_I^s$.

Combining Eqs. (2.3), (2.23) and (2.25) gives the following relation for the acceptance of a crack:

$$\frac{K_I}{K_{cr}} + \frac{\rho}{\sqrt{SF_J}} \leq \frac{f_{R6}(L_r)}{\sqrt{SF_J}}. \qquad (2.26)$$

The left-hand side of Eq. (2.26) represents the parameter $K_r$ used for safety assessment. Eq. (2.26) implies that the assessment point $(L_r, K_r)$ should be located below the R6 failure assessment curve divided by the safety factor $\sqrt{SF_J}$. The maximum acceptable condition is obtained in the limit when the assessment point is located on the reduced failure assessment curve, expressed by Eq. (2.26) with a sign of equality. In addition a safety factor against plastic collapse, corresponding to Eq. (2.24), is introduced as a safety margin against the cut-off of $L_r$ as

$$L_r \leq \frac{L_r^{max}}{SF_L}. \qquad (2.27)$$

Eqs. (2.26) and (2.27) represent the safety assessment procedure used in this handbook and in the calculation software ISAAC [2.13] as well as its predecessor ProSACC [2.12]. In Appendix S, a set of safety factors are defined for different types of load cases, as to be used for nuclear applications, cf. [2.10] and [2.11]. The safety factor $SF_K$ is introduced which is the safety factor on $K_{cr}$ corresponding to the safety factor $SF_J$ on $J_{Ic}$. They are related through $SF_K = \sqrt{SF_J}$. Critical conditions are obtained when all safety factors are set to unity and when the assessment point is located on the failure assessment curve.

This safety evaluation system is may overestimate the contribution from secondary stresses (i.e. welding residual stresses or stresses from a thermal transient) for ductile materials. Therefore, an alternative safety evaluation system has been introduced that quantify the treatment of secondary stresses for high $L_r$-values in a R6 fracture assessment. This recommendation defines alternative safety factors against fracture described by $K_I$ and differentiate between $SF_K^{Primary}$ (relating to primary stresses) and $SF_K^{Secondary}$ (relating to secondary stresses). This safety evaluation system is described in more detail in Appendix B.

Ductile materials normally show a significant raise of the $J$-resistance curve after initiation. In safety assessments including stable crack growth, Eq. (2.23) is no longer valid and the acceptable region is given by

$$J \leq \frac{J_R}{SF_J} \text{ and } T_{app} \leq \frac{T_R}{SF_J}. \tag{2.28}$$

It is generally recommended to performe sensitivity analysis to understand the influence of parameter uncertainties. Such an analysis should consider a systematic variation of the load, crack size and material properties.

## 2.12. References

[2.1]   —, (2012), "Standard Test Method for Linear-Elastic Plane-Strain Fracture Toughness $K_{Ic}$ of Metallic Materials", ASTM E399-12e3, ASTM International, West Conshohocken, PA, U.S.A.

[2.2]   —, (2015), "Standard Test Method for Measurement of Fracture Toughness", ASTM E1820-15, ASTM International, West Conshohocken, PA, U.S.A.

[2.3]   MURAKAMI, Y. (ed.), (1987-1991), *Stress intensity factors handbook*, Vol. 1-3, Pergamon Press, Oxford, U.K.

[2.4]   MURAKAMI, Y. (ed.), (2001), *Stress intensity factors handbook*, Vol. 4-5, Elsevier, Oxford, U.K.

[2.5]   TADA, H., PARIS, P. C., and G. C. IRWIN, (1985), *The stress analysis of cracks handbook*, 2nd edition, Paris Productions Inc., St. Louis, U.S.A.

[2.6]   ROOKE, D. P., and D. J. CARTWRIGHT, (1976), *Compendium of stress intensity factors*, Her Majesty's Stationary Office, London, U.K.

[2.7]   MILLER, A. G., (1988), "Review of limit loads of structures containing defects", *The International Journal of Pressure Vessels and Piping*, Vol. 32, pp. 197-327.

[2.8]   AINSWORTH, R. A., (1988), "The Treatment of Thermal and Residual Stresses in Fracture Assessment", Central Electricity Generating Board, Berkeley Nuclear Laboratories, Berkeley, Gloucestershire, U.K.

[2.9]   —, (2013), "Assessment of the Integrity of Structures Containing Defects", R6 –Revision 4, Up to amendment record No.10, EDF Energy Nuclear Generation Ltd.

[2.10]  BRICKSTAD, B., and M. BERGMAN, (1996), "Development of safety factors to be used for evaluation of cracked nuclear components", SAQ/FoU-Report 96/07, SAQ Kontroll AB, Stockholm, Sweden.

[2.11]  VON UNGE, P., (2016), "Säkerhetsvärdering mot plastisk kollaps vid skadetålighetsanalyser", Research Report 2016:35, Swedish Radiation Safety Authority, Stockholm, Sweden. (Available at: http://www.stralsakerhetsmyndigheten.se).

[2.12]  ProSACC, (2016), User's Manual, Inspecta Technology AB, Stockholm, Sweden.

[2.13]  ISAAC, (2017), User´s Manual, Kiwa Inspecta Technology AB, Stockholm, Sweden.

# APPENDIX A. DEFECT CHARACTERIZATION

A fracture mechanics assessment requires that the current defect geometry is characterized uniquely. In this appendix general rules for this are given. For additional information it is referred to ASME Boiler and Pressure Vessel Code, Sect. XI [A1].

## A1.     Defect geometry

Surface defects are characterized as semi-elliptical cracks. Embedded defects are characterized as elliptical cracks. Through thickness defects are characterized as rectangular cracks. The characterizing parameters of the crack are defined as follows:

a)        The depth of a surface crack $a$ corresponding to half of the minor axis of the ellipse.

b)        The depth of an embedded crack $2a$ corresponding to the minor axis of the ellipse.

c)        The length of a crack $l$ corresponding to the major axis of the ellipse for surface and embedded cracks or the side of the rectangle for through thickness cracks.

In case the plane of the defect does not coincide with a plane normal to a principal stress direction, the defect shall be projected on to normal planes of each principal stress direction. The one of these projections is chosen for the assessment that gives the most conservative result according to this procedure.

## A2.     Interaction between neighboring defects

When a defect is situated near a free surface or is close to other defects the interaction shall be taken into account. Some cases of practical importance are illustrated in Fig. A1. According to the present rules the defects shall be regarded as one compound defect if the distance $s$ satisfies the condition given in the figure. The compound defect size is determined by the length and depth of the geometry described above which circumscribes the defects. The following shall be noted:

a)        The ratio $l/a$ shall be greater than or equal to 2. Using the rules in BS 7910 [A2] it is possible to evaluate defects with a ratio less than 2.

b)        In case of surface cracks in cladded surfaces the crack depth should be measured from the free surface of the cladding. If the defect is wholly contained in the cladding the need of an assessment has to be judged on a case-by-case basis.

c)        Defects in parallel planes should be regarded as situated in a common plane if the distance between their respective planes is less than 12.7 mm (0.5 inch).

| Case | Defect sketches | Criterion |
|------|-----------------|-----------|
| 1 |  | If $s < 0.4a_1$<br>then<br>$a = 2a_1 + s$ |
| 2 |  | If $s < \max(0.5a_1, 0.5a_2)$<br>then<br>$l = l_1 + l_2 + s$<br><br>See note (1). |
| 3 |  | If $s < \max(a_1, a_2)$<br>then<br>$l = l_1 + l_2 + s$ |
| 4 |  | If $s < \max(a_1, a_2)$<br>then<br>$2a = 2a_1 + 2a_2 + s$ |
| 5 |  | If $s < \max(a_1, 0.5a_2)$<br>then<br>$a = 2a_1 + a_2 + s$ |
| 6 |  | If $s_1 < \max(a_1, 0.5a_2)$<br>and $s_2 < \max(a_1, 0.5a_2)$<br>then<br>$a = 2a_1 + a_2 + s_1$<br>$l = l_1 + l_2 + s_2$ |

(1) If $l/a < 2$, the criterion $s < \min(l_1, l_2)$ could be used according to BS 7910 [A2].

Figure A1.  Rules for defect characterization at interaction.

## A3.    References

[A1]    —, (2007), *ASME Boiler and Pressure Vessel Code, Sect. XI, Rules for inservice inspection of nuclear power plant components.* The American Society of Mechanical Engineers, New York, U.S.A.

[A2]    —, (2015), *BS 7910:2013+A1:2015, Guide to methods for assessing the acceptability of flaws in metallic structures*, BSI Standards Publication, BSI Standards Limited.

# APPENDIX R.  RESIDUAL STRESSES

This appendix gives recommendations on weld residual stress distributions for use in fracture mechanical assessment of flaws at welds in pipes and plates.

## Background

The effects of residual stresses should be considered when calculating fracture mechanics stress intensity factors. Residual stresses can be introduced at manufacturing for example by welding, forming, rolling, thermal treatments, shrink fit, and surface treatment such as shot peening. Residual stresses are defined as stresses existing in a component after removal of all external loading, and consequently they are self-balanced within the component. The distribution and magnitude of residual stresses in a component depend on the manufacturing process and is sometimes influenced by operating loads.

It is important to consider residual stresses since they have substantial influence on crack growth by stress corrosion and fatigue, and they can also affect failure by fracture. In addition residual stresses influence crack opening which are important to consider in leak rate assessments and for certain non-destructive testing methods.

Residual stresses can occur in many manufacturing processes but residual stresses from welding are of particular importance. Defects and degradation frequently concentrate to welds due to defects that can occur during the welding process, due to local changes in micro-structure caused by welding, and due to local stress concentrations at welds. In addition to this, welding generate residual stresses of high magnitude. During welding residual stresses are generated as a result of non-uniform plastic deformation caused by rapid local heating and cooling, phase changes, solidification and differences in thermal expansion. The distribution of the weld residual stresses through the thickness of a component is dependent on component geometry, material and welding process. Further, bending and forming, as well as mechanical and thermal loads during operation, may affect the as-welded residual stress field. For example a pressure test may reduce peak stresses in a residual stress distribution.

Weld residual stresses may be approximated by assuming a uniform stress distribution at the level of the yield strength of the material, which generally provide conservatively higher effect from weld residual stress when assessing a flaw at a weld. This assumption may be used for an initial assessment, but if not adequate safety margins are obtained, then more detailed information is needed about the distribution of the residual stresses through the component thickness. This appendix provide recommendations on distributions of residual stress in as-welded butt welds.

Weld residual stresses have large influence on degradation processes resulting in slow crack growth during operation, such as stress corrosion cracking or fatigue. However, the influence from residual stresses to failure by fracture is limited in some situations. There are numerical and experimental investigations showing a declining influence from weld residual stress on the driving force for fracture in ductile materials in situations with high primary loading ($L_r > 0.8$). The effect is due to substantial plasticity at the crack front before initiation of fracture in these cases, and the effect is rapidly decreasing for lower $L_r$. ASME Section XI disregard weld residual stress in all situations for fracture of austenitic stainless steels, but this approximation can be rough for situations dominated by secondary loads (e.g. weld residual stress and a thermal shock) or if the material is not sufficiently ductile. Procedures have been developed for consideration of the contribution from weld residual stresses at high $L_r$-values and the safety assessment procedure is described in Appendix B.

*General recommendations and definitions*

When assessing a flaw at a weld, residual stress can as a first approximation be assumed to be a uniform distribution of tensile stress equal to the yield strength of the material. It is recommended to use typical data for yield strength (not minimum required data) and the yield strength at room temperature. The greater of the yield strength of the weld material and the base material should be assumed. This weld residual stress assumption is recommended for initiall assessments.

If the simplified residual stress assumption does not result in adequate safety margins, then more detailed information is needed about the distribution of the weld residual stresses through the component thickness. It also can be valuable to use more precise assumptions for the reason to achieve more representative and realistic assessment results, in efforts to focus inspection and other preventing measures to important areas. Recommendations for residual stress profiles at welds in pipes and plates are provided in the next sections. The recommendations can be used unless other more precise information is available.

Realistic residual stress distributions have been established for pipe butt weld configurations. These residual stress distributions have been developed by detailed numerical simulations using best-estimate data for material and welding conditions, together with validation to experimental measurements for available cases [R1, R2]. In section R1 recommendations are given for circumferential butt welds in stainless steel pipes and in nickel base dissimilar metal welds for configurations common in Swedish power plants. These results should be considered as representing best-estimate residual stress distributions for these pipe welds in as-welded condition. The recommendations may be subject to future review to take into account any significant new information or new developments. The user should confirm that the welding conditions and materials are representative for the weld being assessed. For other weld configurations, upper bound residual stress distributions may be found in references [R3-R5]. Recommendations for the effect of post-weld heat treatments (PWHT) are given in section R4.

When analyzing stress corrosion crack (SCC) growth in damage tolerance analyses, the applied growth rate data is in general from upper bound relations. If pessimistic upper bound assumptions would be applied also for the residual stress distribution, this can give unrealistic results with very high crack growth rates. This could result in unreasonable and unnecessary efforts. For this reason more realistic residual stress profiles have been establish in [R1] and [R2] for common pipe butt weld configurations. Application of realistic residual stress distributions together with upper bound SCC data is considered to result in more representative assessment results.

The sensitivity of the assessment results to likely variations in input parameters should normally be investigated as part of a damage tolerance assessment, especially where the weld residual stress distribution have large influence. A conservative assumption of a uniform distribution of tensile stress can be necessary in cases with uncertainties regarding e.g. welding conditions or restraints during welding. When detailed information is lacking this could be assessed on a case by case basis to confirm relevant assumptions, for example by simulating the effect of different or changing restraint during welding, or effects from non-symmetric weld application processes.

In the next sections stress distributions are presented for transverse and longitudinal weld residual stress. The transverse stress component, $\sigma_T$, is the stress perpendicular to the weld run, and the longitudinal stress component, $\sigma_L$, is the stress parallel to the direction along the weld run. For pipe circumferential butt welds, the transverse stress is equivalent to axial stress in the pipe, and the longitudinal stress is equivalent to hoop stress in the pipe.

Stress distributions through the component are given as a function of the distance normalized with the plate or pipe thickness. The distance is generally measured from the weld root and for pipe geometries from the inside surface of the pipe.

Weld residual stress distributions are normalized with an amplitude parameter $S_r$ which is defined as the typical 0.2% offset yield strength of the base material at room temperature. (Note that the definition of $S_r$ has changed from previous editions of the handbook.) $S_r$ is independent of temperature and any temperature dependence is described in the equations for the residual stress profile. It is important to not underestimate the weld residual stress. In order to obtain realistic estimates of the residual stresses, minimum required yield strength data cannot be used, and instead typical yield strength data shall be used. Typical data may also be described by other terms, such as best-estimate data or mean value data. In many cases typical yield strength can be estimated from minimum required yield strength by applying a factor of 1.35.

For stainless steel piping in Swedish plants, strength matched filler material has generally been used. Stainless steel filler metal is normally selected with slightly higher alloy content to be overmatched with respect to corrosion resistance. Still, with respect to tensile strength the filler is generally quite well matched (within ±70 MPa as-welded). However, if a strength overmatched filler material is used, the stress profile for the transverse stress at the heat affected zone (HAZ) and at the weld centerline, and the longitudinal stress at HAZ, are relatively well estimated by using $S_r$ based on the yield strength of the base material [R1]. The stresses at the weld centerline for overmatched filler material can be estimated by using $S_r$ based on the approximate yield strength of the *unhardened* weld material (before weld induced deformation). The unhardened yield strength of an overmatched weld material may be estimated from the yield strength of a corresponding base material.

## R1. Pipe butt welds

Realistic residual stress distributions have been established for pipe circumferential butt welds [R1, R2]. New recommendations have been developed to account for progress since [R7-R9] regarding new information and knowledge developed within measurements and numerical simulation. Residual stress distributions are developed by detailed numerical welding simulations using typical data, together with validation to available measurements on mock-ups. The results represent best-estimate residual stress distributions for these pipe welds. The results are for full penetration butt welds in as-welded condition. No post-weld heat treatment is assumed. Note that the stress distributions are not applicable for circumferential pipe welds closer than $2.5\sqrt{Rt}$ from each other, and such situations need to be individually assessed and expert advice should be sought. Stress distributions have been developed for pipe butt welds in stainless steel and in nickel base material.

Figure R1 illustrates a pipe butt weld and a results path at the weld centerline. Below are results given for axial stress $\sigma_a$, and for hoop stress $\sigma_h$ along the centerline.
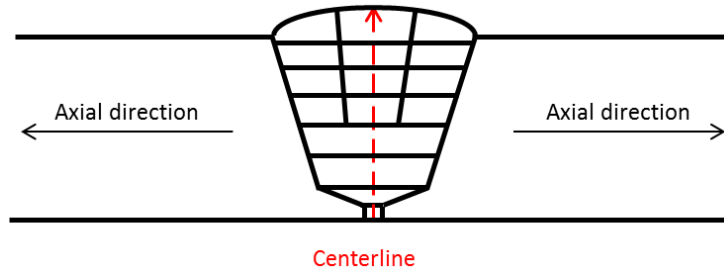


Figure R1. Pipe butt weld with results path along the centerline and definition of axial direction.

### R1.1 Stainless steel pipe butt welds

Recommended through-thickness residual stress distribution for butt welds in austenitic steel pipes can be found in [R1]. Residual stress profiles along the weld centerline are presented below for normal operation temperature. Results for paths in the heat affected zone are available in [R1]. The results are applicable for pipe geometries corresponding to a radius to thickness ratio $R/t$ in the range 5 to 20. The weld residual stress profiles are described by the following 5th order polynomial

$$\sigma\left(\frac{u}{t}\right) = S_r \, C_T \left( c_0 + c_1 \left(\frac{u}{t}\right) + c_2 \left(\frac{u}{t}\right)^2 + c_3 \left(\frac{u}{t}\right)^3 + c_4 \left(\frac{u}{t}\right)^4 + c_5 \left(\frac{u}{t}\right)^5 \right), \tag{R1}$$

where $c_i$ are coefficients and $u/t$ the normalised position along the centerline. The coefficients are presented in Table R1 for different thicknesses. Linear interpolation of stress (or coefficients) is recommended for thicknesses between those available in Table R1. Extrapolation for thicknesses below 6 mm or above 65 mm should be avoided. The temperature dependent coefficient $C_T$ is given by

$$C_T = \frac{269}{266} - \frac{3}{5320} T \quad \text{for } \sigma_h, \text{ and } C_T = 1 \quad \text{for } \sigma_a. \tag{R2}$$

where $T$ in °C is the temperature of the pipe for the loading situation during the assessment.

Profiles for the axial and hoop stresses along the weld centerline according to Table R1 at 286 °C are shown in Figure R2 and Figure R3.

Table R1.  Coefficients for the 5$^{th}$ order polynomial along the weld centreline [R1]

| Thickness [mm] | Inner radius [mm] | Stress component | $c_0$ | $c_1$ | $c_2$ | $c_3$ | $c_4$ | $c_5$ |
|---|---|---|---|---|---|---|---|---|
| 6 | 60 | Axial stress | 1.08 | -2.4157 | 16.907 | -58.2 | 64.605 | -23.274 |
| | | Hoop stress | 0.63983 | -0.5842 | 5.3703 | -8.4527 | -1.4992 | 4.3204 |
| 10 | 100 | Axial stress | 0.45756 | -0.0517 | -2.3712 | 9.0886 | -16.37 | 8.2058 |
| | | Hoop stress | 1.6752 | 0.93035 | -23.766 | 81.924 | -104.33 | 43.827 |
| 12 | 120 | Axial stress | 0.17729 | -0.8621 | 1.6547 | 9.6666 | -23.651 | 12.109 |
| | | Hoop stress | 1.4974 | 1.3405 | -17.974 | 58.279 | -71.413 | 28.589 |
| 15 | 150 | Axial stress | 0.55005 | -5.6076 | -6.0824 | 81.908 | -128.89 | 57.506 |
| | | Hoop stress | 1.0065 | 2.3163 | -19.086 | 66.405 | -84.172 | 34.034 |
| 20 | 200 | Axial stress | 1.0159 | -8.5275 | -16.027 | 117.77 | -155.8 | 61.818 |
| | | Hoop stress | 0.77832 | -5.2064 | 29.019 | -40.918 | 22.702 | -5.3028 |
| 25 | 250 | Axial stress | 1.0336 | -10.661 | -13.038 | 130.6 | -179.36 | 71.16 |
| | | Hoop stress | 0.54484 | -3.1805 | 13.704 | 4.8588 | -30.401 | 15.26 |
| 65 | 650 | Axial stress | 0.93865 | -23.273 | 131.04 | -337.67 | 397.63 | -168.58 |
| | | Hoop stress | 0.16267 | 3.6352 | 20.619 | -111.13 | 173.45 | -86.001 |
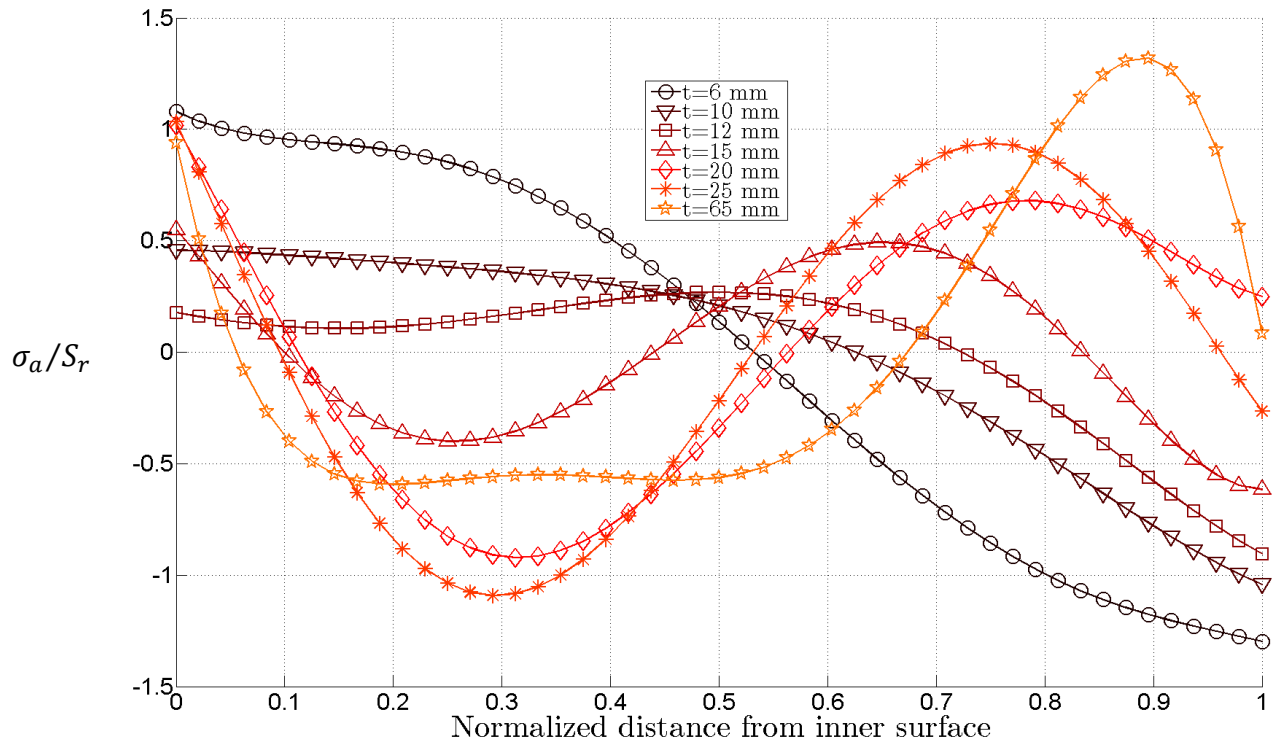
Figure R2. Axial residual stress in austenitic steel pipe butt weld along the weld centerline at 286 °C. The polynomial coefficients are listed in Table R1.
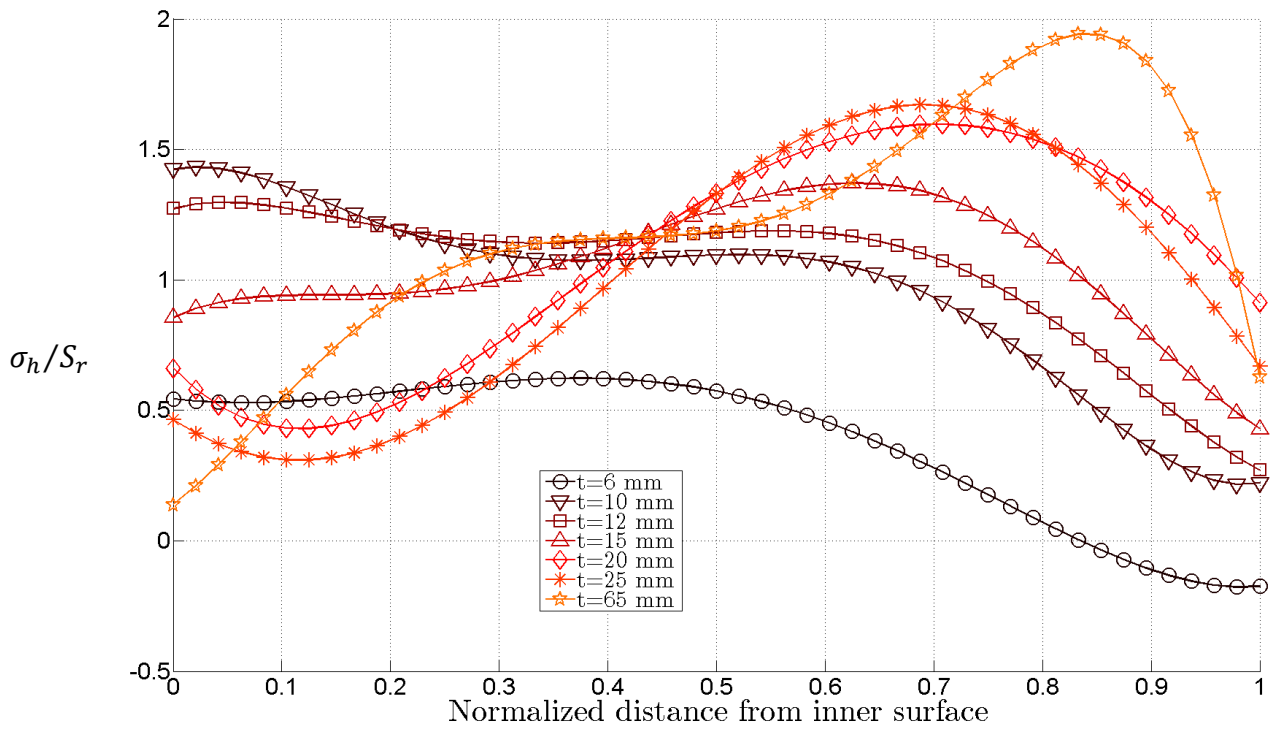


Figure R3. Hoop residual stress in austenitic steel pipe butt weld along the weld centerline at 286 °C. The polynomial coefficients are listed in Table R1.

37

*R1.2      Nickel base dissimilar metal pipe butt welds*

Recommended residual stress profiles for nickel base pipe welds are presented in [R2] for nozzle and primary piping configurations common in Swedish plants.

Nickel base welds are generally used for joining dissimilar metals such as ferritic steel and austenitic stainless steel. Typically the joint is performed by welding nickel base material to the ferritic carbon or low alloy steel component to form a transition section called buttering. The buttering is subjected to post weld heat treatment at a temperature designed to relax residual stresses in the ferritic steel, and the stress in the nickel base material will also be affected. Finally a joint is prepared and the stainless steel component is welded to the buttering by use of a Ni-base weld alloy. In a few cases the joint has been performed without buttering. Manufacturing variables important for the dissimilar metal weld include for example joint design, filler metal, welding process, heat input and design of post weld treatments. Dissimilar metal welds at nozzles, penetrations and attachments are frequently made of Ni-base material Alloy 600 and its compatible weld alloys Alloy 182 (for SMAW) and Alloy 82 (for GTA/TIG and SAW). (Sometimes Alloy 182 and Alloy 82 are also denoted Inconel 182 and Inconel 82.) Alloy 690 and associated weld metals Alloy 152 and Alloy 52 has been used more recently as a replacement materials with higher resistance to SCC.

Nickel base weld material is under certain conditions subjected to hazard of SCC. If upper bound assumptions are used for the residual stress distributions, together with upper bound SCC data, this will result in very high postulated crack growth rates and corresponding short inspection intervals. Experiences of operational damage are not consistent to this, and for this reason efforts have been made to establish more realistic residual stress profiles.

Realistic through-thickness residual stress distributions have been developed for nickel base welds by detailed numerical welding simulation using typical data. Recommended residual stress profiles are presented in [R2] for nickel base pipe butt welds for configurations common in Swedish plants. Validation has been performed for cases were detailed measurements were available for nickel base dissimilar metal welds. The report [R2] summarizes nickel base dissimilar metal butt welds at nozzles and primary piping in Swedish plants. No generalized recommendations for Ni-based pipe welds are given in this section, and it is recommended to apply the detailed residual stress distributions given in [R2] for different weld configurations. Note that when realistic residual stress profiles are used, instead of conservative upper bound stress profiles, it is increasingly important to perform sensitivity studies as part of a defect tolerance assessment.

The residual stress field is sometimes affected by repair welding. Repairs can be performed at the pipe outside surface when removing defects found during manufacturing, and repairs may be performed at the inside surface to remove a defect found at in-service inspection, or as a preventive measure to protect susceptible material. The effect on the residual stress profile due to different types of weld repairs are shown in [R6] for nickel base dissimilar metal welds.

The stress distributions in circumferential pipe butt welds have similar main features for welds in ferritic and stainless steels. If no specific data exists for a ferritic weld, it is a reasonable approximation to apply the distribution of a corresponding stainless steel weld geometry, after adjustment of typical yield properties to the ferritic material. References [R4, R5 and R10] suggest that the same distribution may be used, especially for cases of high heat input.

When welding ferritic steels phase changes will occur and result in local residual strains in a zone around each weld bead. Phase transformations occur when ferritic steel is subjected to sufficiently large temperature ranges. When the temperature is increasing high enough, ferritic/perlitic structures (BCC) will transform to the more close-packed austenitic structure (FCC), which results in rapid volume decrease when the temperature is increasing in this transformation region. When the austenitic structure is cooling it will transform, depending on the cooling rate, to ferrite/perlite (at slow cooling), bainite or martensite (at rapid cooling), and a volume expansion is experienced. The development of residual stresses during welding is influenced by these volume changes, and the largest effect is usually from the volume expansion at the transformation of austenite to martensite during cooling.

The phase transformations results in volume changes in thin regions in the heat affected zone (HAZ) and influence the residual stresses locally. Effects of phase changes on residual stresses have been investigated numerically and experimentally, for example in [R11]. The results support that phase transformations mainly affect the residual stress distribution locally in HAZ. The effect from phase transformations is limited in regions further away from the weld bead, where the residual stresses are mainly caused by inhomogeneous plastic deformation from the rapid heating and cooling from the weld beads. The local variations in the residual stress field due to phase changes in ferritic steels can be important in cases of brittle fracture mechanism or when small defects are governing, and also with respect to any in-service crack growth that would follow this region in HAZ. Contrary, in cases where the governing failure mechanism is ductile fracture, these localized stress variations have decreasing influence on the safety margins as the acceptable crack size increase.

## R2.     Butt welded plates

*R2.1     Thin butt welded plates*

Butt welded plates are defined as thin in relation to the weld bead size, that is plates are thin in this context when the weld consist of only one or a few weld beads. The distribution of longitudinal residual stress at the surface of a thin plate is illustrated in Figure R4. Through the thickness the stress state is usually fairly constant in thin plates. The coordinate $x$ is measured from the weld center line and in the direction perpendicular to the weld run. The width of the zone with tensile stress, $W$, is approximately four to six times the plate thickness. The distribution is usually wider for austenitic steels compared to ferritic steels. The distribution in Figure R4 is relevant away from edges, but as the weld run ends at a free surface the longitudinal stress component tend to zero.
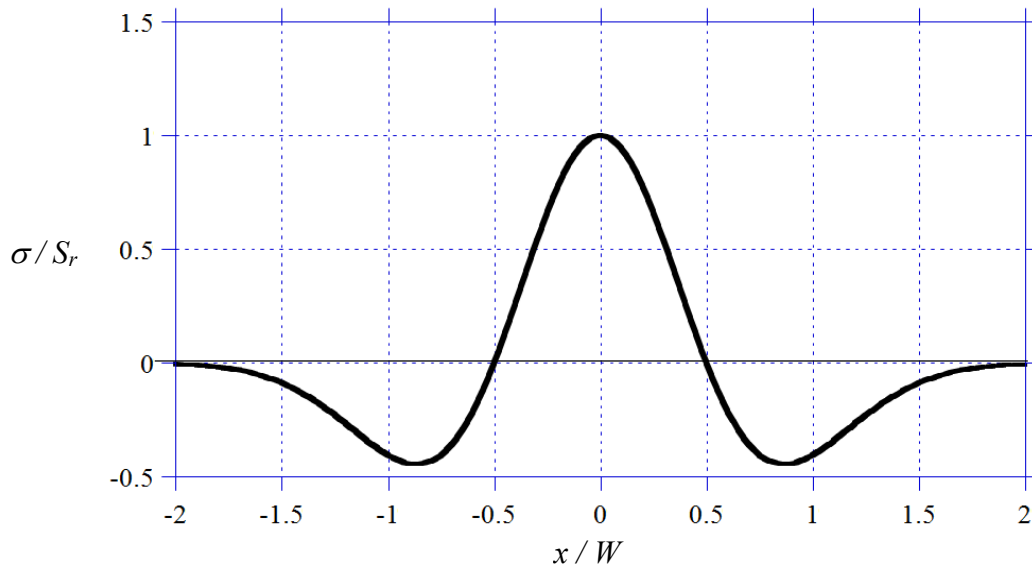
Figure R4. Distribution of the longitudinal stress component in a thin plate, for a section perpendicular to the welding direction.

The magnitude of the transverse stress component in thin plate welds, generally varies along the weld run, due to difference in the restraints during welding and due to welding sequences. Thin plates fixed to each other during welding (by clamping, tack welding or for final parts in a weld sequence) can obtain transverse residual stresses with a magnitude of $S_r$. On the other hand when one of the two plates is free to move during welding the transverse residual stress may become limited to a fraction of the yield stress, e.g. 0.3 $S_r$.

*R2.2    Thick butt welded plates*

Thick plates are defined as plates welded together with joints consisting of many beads. In thick plates the variation of the residual stresses in the thickness direction can be substantial. The residual stress distribution depend on the welding process, joint design and welding conditions, resulting in the more complicated through-thickness stress distribution compared to thin plates. In thick plates the stresses are varying less along the weld direction (especially for the stress component transverse to the welding direction) compared to thin plates, since a lesser part of the residual stress originate from global structural restraints. The transition from thin to thick plate characteristics is dependent of the bead size relative to the plate thickness and heat input, and it is hard to specify a general rule but an estimate is when more than three layers of beads are used.

The residual stresses vary both across the weld and in the thickness direction. It is difficult to give general realistic estimates for weld residual stresses in thick plates. The simplest but in many cases conservative assumption is that the weld residual stress is constant and equal to $S_r$ throughout the entire thickness. More information for upper bound estimates can be found in [R3-R5].

In a symmetric joint with many weld beads, for instance an X-joint or a double U-joint, the residual stress through the thickness $t$ may be approximated as shown in Figure R5. The distribution shown for the transverse stress is valid if any of the plates is free to move during the welding.
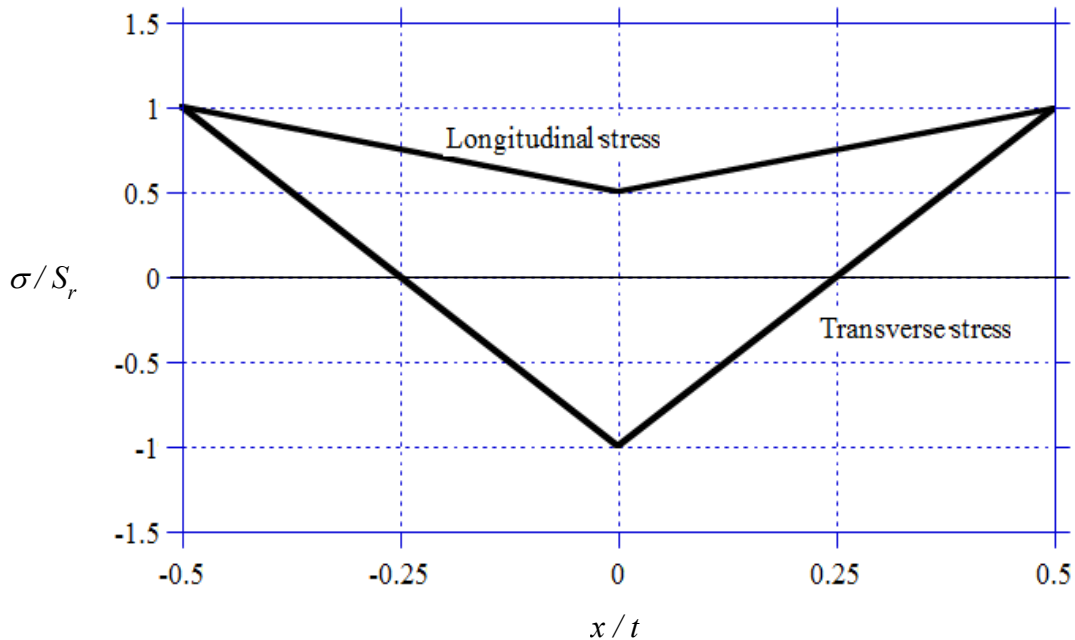


Figure R5. Through-thickness weld residual stress distribution in thick plates for a symmetric joint with many weld beads. The distribution for the transverse stress presuppose one of the plates is free during the welding.

### R3. Pipe seam welds

The residual stresses acting longitudinal and transverse to a pipe seam weld may as an approximation be estimated from the corresponding distribution in a plate, provided that the pipe is not adjusted with respect to roundness after welding. Upper bound residual stress distributions are also found in [R1] and [R2].

### R4. Fillet welds

The residual stresses acting longitudinal and transverse to a fillet weld may be approximated to the as-welded yield stress $S_r$. Upper bound stress distributions are found in [R3-R5].

### R5. Post-Weld Heat Treatment (PWHT) for stress relieved welds

Post-weld heat treatment (PWHT) can reduce weld residual stresses substantially. Accurate selection, specification and control of the PWHT procedure is important in order to assure the effectiveness of PWHT and to avoid undesirable micro structural changes. The main mechanism behind the stress relieve from PWHT is creep.

41

*R5.1     Ferritic steel welds*

The stress relief of ferritic steel components subjected to PWHT is generally high for stress relieving temperatures common for nuclear components. Reference [R12] indicate that a hold temperature of 600 °C in 10 hours may result in a relaxation down to 80 MPa for SA533. For a temperature of 565 °C an initial residual stress of 205 MPa is reduced by approximately 65% for a hold time of 10 hours. In [R13] stress relief from PWHT is studied for seam welds in ferritic pipes and reduction is given as a function of hold time and holding temperature for stress perpendicular to the weld direction. For a hold temperature of 620 °C up to 80% reduction can be achieved.

The relaxation from PWHT can be substantial in ferritic steel but depends on the temperature, hold time and initial level of residual stress. If a weld has been subjected to PWHT according to the requirements specified for stress relief in a design standard, then the following general approximations can be used. The residual stress parallel to the welding direction can be assumed to be 30% of the room temperature yield strength of the material (or of the as-welded residual stress distribution). The residual stress perpendicular to the weld run can be assumed to be 20% of the yield strength of the material (or of the as-welded residual stress distribution). For more accurate residual stresses, the levels can be estimated by use of stress relaxation tests, or by welding simulation based on detailed material data.

*R5.2     Stainless steel welds*

The temperature at which stress relieving of nuclear components is performed is commonly designed for ferritic steels and this temperature is only high enough to remove parts of residual stresses in stainless steel welds. Stainless steels are much more creep resistant than carbon steels and extensive stress relief will not occur for PWHT at 620 °C. Reference [R14] illustrates that an initial residual stress of 230 MPa is reduced by approximately 35% at a temperature of 600 °C and a hold time of 10 hours.

For high stress relief in stainless steels a temperature above about 850 °C would be needed, but this is not recommended for metallurgical reasons that may degrade the corrosion resistance and sensitize the material to stress corrosion cracking. Low temperature stress relief below about 540 °C and hold time of an hour may be used for stainless steel to achieve some stress relief and avoid sensitization, and in such cases a small reduction of about 20% of the as-welded stresses can be expected. Generally PWHT for stress relieving is avoided for austenitic welds.

*R5.3     Nickel base dissimilar metal welds*

There exist few references that verify the relief of residual stresses in nickel base dissimilar metal welds. The use of a PWHT is expected to provide an overall beneficial effect due to relief of residual stresses. Nickel base metals have a high heat resistance compared to carbon steels and the stress relief is moderate at 620 °C.

Reference [R15] illustrates that an as-welded residual stress of approximately 350 MPa in a nickel base buttering is reduced to approximately 230 MPa after PWHT at a temperature of 620 °C and a hold time of 7 hours. Detailed numerical analyses were performed for nickel base Alloy 182 welds, based on creep data measured for the actual hold temperature and time frame. The relief of stresses in the weld was validated by residual stress measurements.

**R6.     References**

[R1]    BONNAUD, E. and GUNNARS, J. (2016), ”Recommended residual stress profiles for stainless steel pipe welds”, SSM Report 2016:39, Strålsäkerhetsmyndigheten. (Available at: http://www.stralsakerhetsmyndigheten.se).

[R2]    BONNAUD, E., BREMBERG, D. and GUNNARS, J. (2018), ”Residual stress profiles for nickel base dissimilar metal pipe welds”, Technical Report No. 50014970-1 Rev. 2, Kiwa Inspecta Technology AB, Stockholm, Sweden. (to appear as a SSM report)

[R3]    R6, ”Assessment of the Integrity of Structures Containing Defects”, Revision 4, 2015.

[R4]    API 579-1/ASME FFS-1, “Fitness-For-Service”, ASME, 2016.

[R5]    BS 7910:2013, “Guide to methods for assessing the acceptability of flaws in metallic structures”, Amendment A1:2015, British Standard, BSI Standards, 2015.

[R6]    BONNAUD, E. and GUNNARS, J. (2017), ”Effects of weld repairs on residual stresses in nickel base dissimilar metal welds”, SSM Report 2017:22, Strålsäkerhetsmyndigheten. (Available at: http://www.stralsakerhetsmyndigheten.se).

[R7]    BRICKSTAD, B. and L. JOSEFSON (1996), ”A parametric study of residual stress in multipass butt-welded stainless steel pipes”, SAQ/FoU-Report 96/01, SAQ Kontroll AB, Stockholm, Sweden.

[R8]    DELFIN, P., B. BRICKSTAD and L. JOSEFSON, (1998), ”Residual stresses in multi-pass butt-welded bimetallic piping, Part I”, SAQ/FoU-Report 98/12, SAQ Kontroll AB, Stockholm, Sweden.

[R9]    DELFIN, P., B. BRICKSTAD and J. GUNNARS, (1999), ”Residual stresses in multi-pass butt-welded bimetallic piping, Part II”, SAQ/FoU-Report 99/06, SAQ Kontroll AB, Stockholm, Sweden.

[R10]   SCARAMANGAS, A., (1984), ”Residual stresses in girth butt weld pipes”, Technical Report No. CUED/D-Struct./TR. 109, Dept. of Engineering, Cambridge University, U.K.

[R11]   KATSUYAMA, J., M. UDAGAWA, H. NISHIKAWA, M. NAKAMURA, and K. ONIZAWA, (2010), "Evaluation of Weld Residual Stress near the Cladding and J-weld in Reactor Pressure Vessel Head for the assessment of PWSCC Behavior," E-Journal of Advanced Maintenance, Vol. 2, pp. 50-64.

[R12]   REDDY, G.B. and AYRES, D.J., (1982), “High-Temperature Elastic-Plastic and Creep Properties for SA-533 Grade B Class 1 and SA-508 Materials”, EPRI-NP-2763.

[R13]   DONG, P. and HONG, J.K., (2008), “Residual Stress Relief in Post-Weld Heat Treatment”, Proceedings of the ASME 2008 Pressure Vessels & Piping Conference, PVP2008-61210.

[R14]   “Practical Guidelines for the Fabrication of High Performance Austenitic Stainless Steels”, Nickel Institute and International Molybdenum Association (IMOA), 2010.

[R15]   BREMBERG, D., GUNNARS, J., BONNAUD, E., EDLING, L.O. and KINGSTON, E., (2014), ”Residual Stresses in Alloy 182 PWHT Buttering and Attachment Weld – Validation by Modeling and Measurements of a Full Scale Mockup”, Proceedings of the ASME 2014 Pressure Vessels & Piping Conference, PVP2014-28965.

# APPENDIX G.  GEOMETRIES TREATED IN THIS HANDBOOK

## G1.  Cracks in a plate

*G1.1     Finite surface crack*
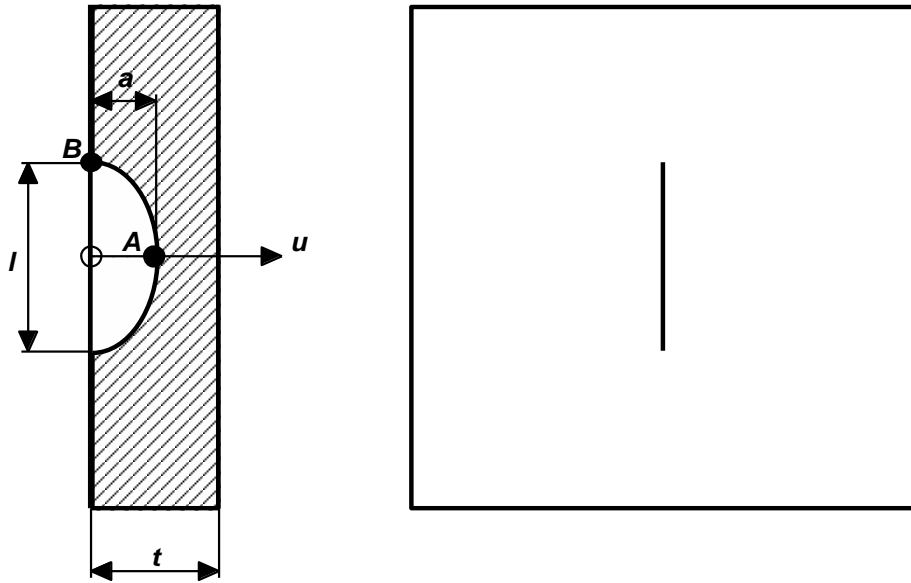


Figure G1.1.  Finite surface crack in a plate.

## G1.2    *Infinite surface crack*
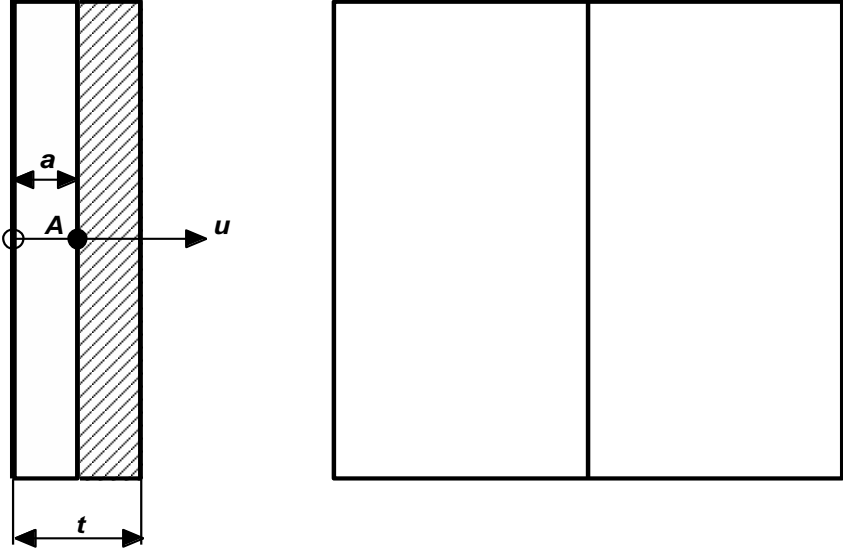


Figure G1.2.  Infinite surface crack in a plate.

*G1.3    Embedded crack*
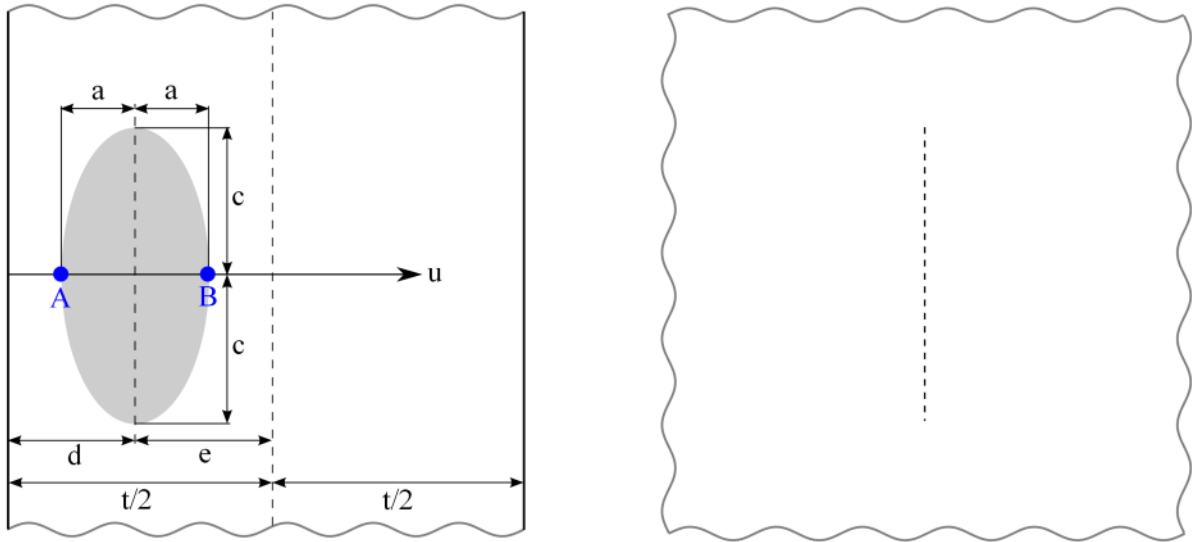


Figure G1.3.  Embedded crack in a plate.

Figure G1.4. Through-thickness crack in a plate.

## G2. Axial cracks in a cylinder

*G2.1     Finite internal surface crack*
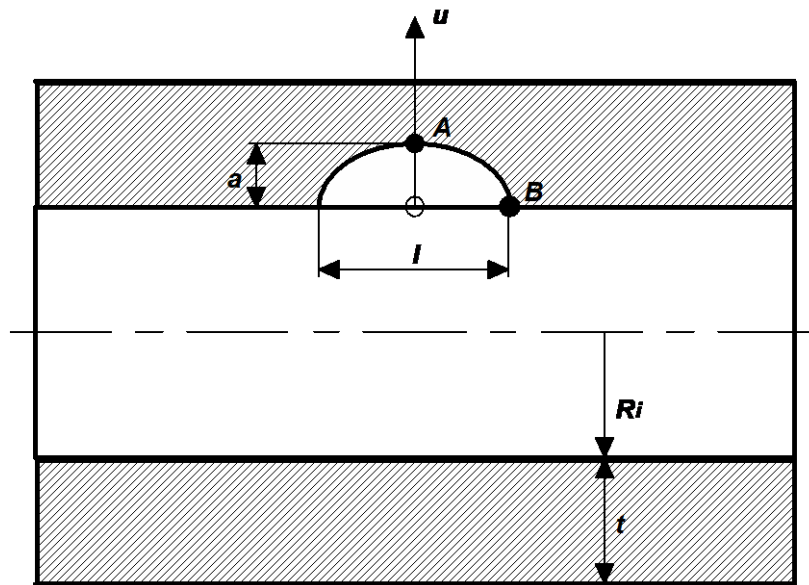


Figure G2.1.  Finite axial internal surface crack in a cylinder.
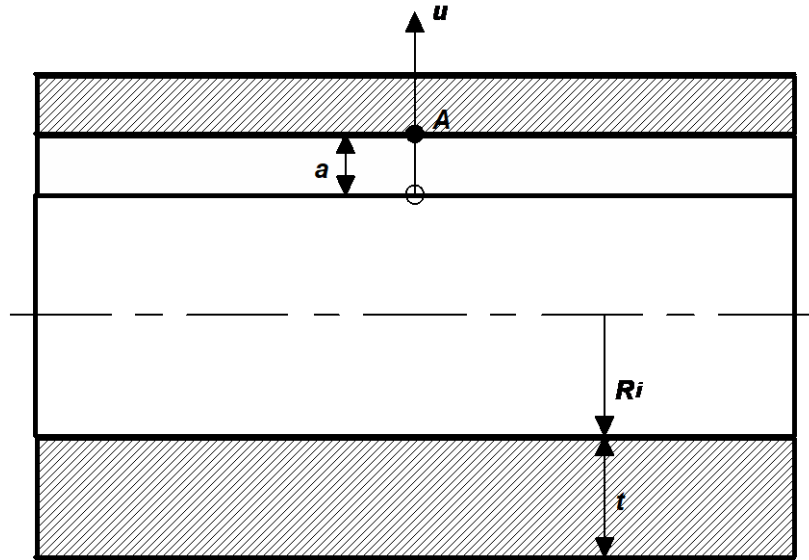
Figure G2.2.  Infinite axial internal surface crack in a cylinder.

Figure G2.3.  Finite axial external surface crack in a cylinder.

*G2.4*     *Infinite external surface crack*
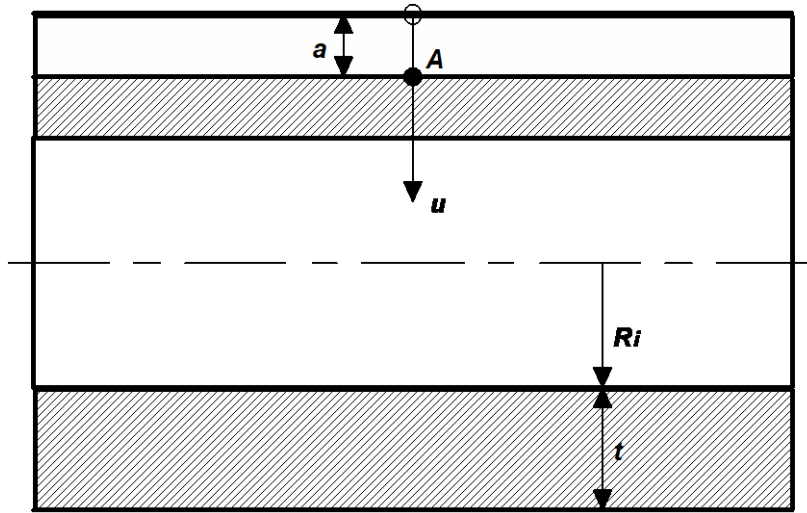


Figure G2.4.  Infinite axial external surface crack in a cylinder.
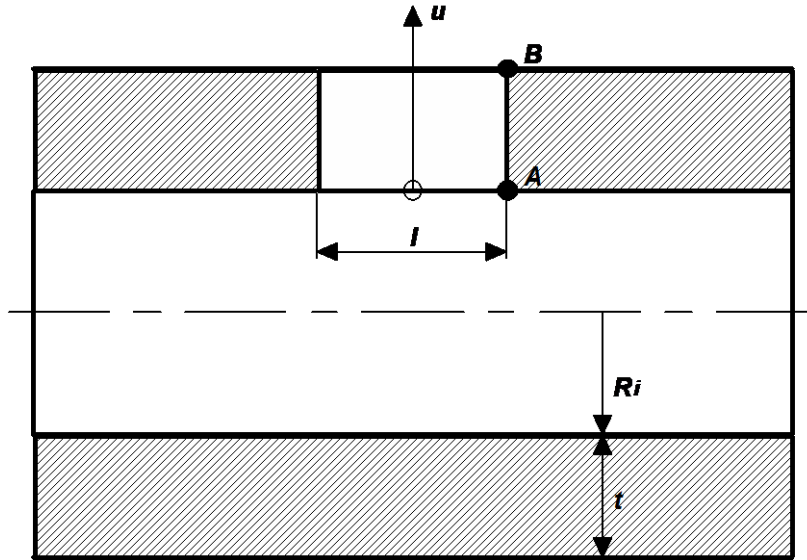
Figure G2.5.  Axial through-thickness crack in a cylinder.

## G3. Circumferential cracks in a cylinder

### G3.1 *Part circumferential internal surface crack*
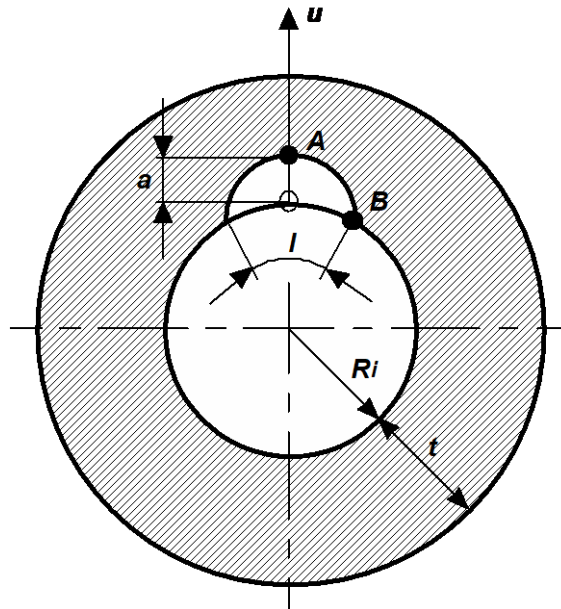


Figure G3.1.  Part circumferential internal surface crack in a cylinder.

*G3.2    Complete circumferential internal surface crack*
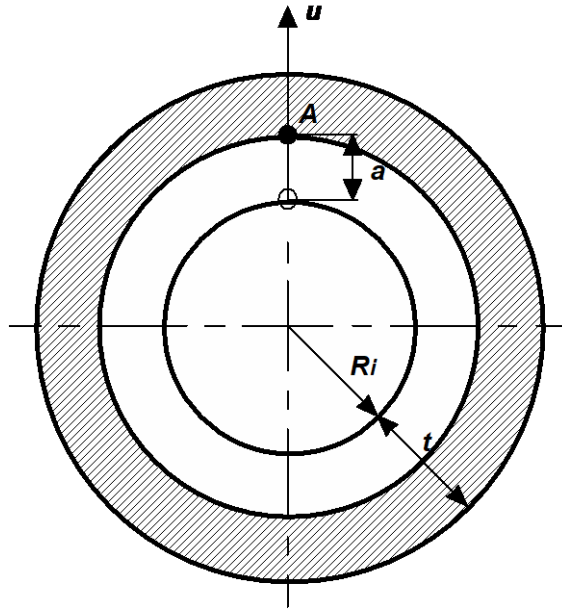


Figure G3.2.  Complete circumferential internal surface crack in a cylinder.

Figure G3.3. Part circumferential external surface crack in a cylinder.

Figure G3.4.  Complete circumferential external surface crack in a cylinder.
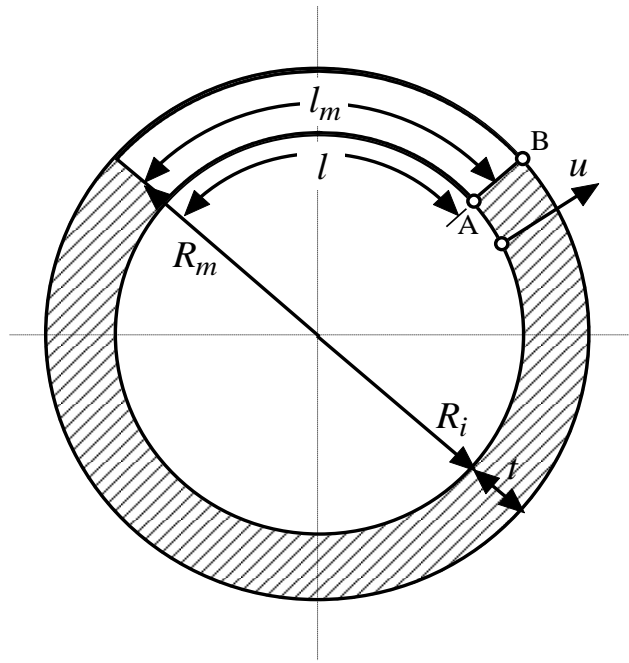
Figure G3.5.  Circumferential through-thickness crack in a cylinder.

# G4.    Cracks in a sphere

## G4.1    *Through-thickness crack*
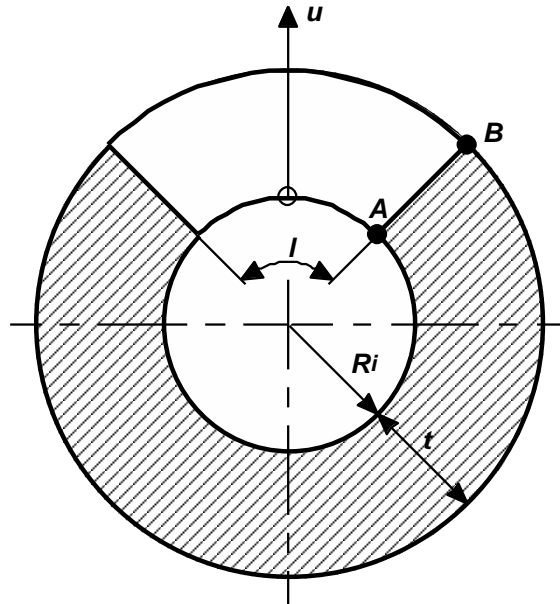


Figure G4.1.  Circumferential through-thickness crack in a sphere.

## G5. Cracks in a bar

*G5.1    Part circumferential surface crack in a bar*
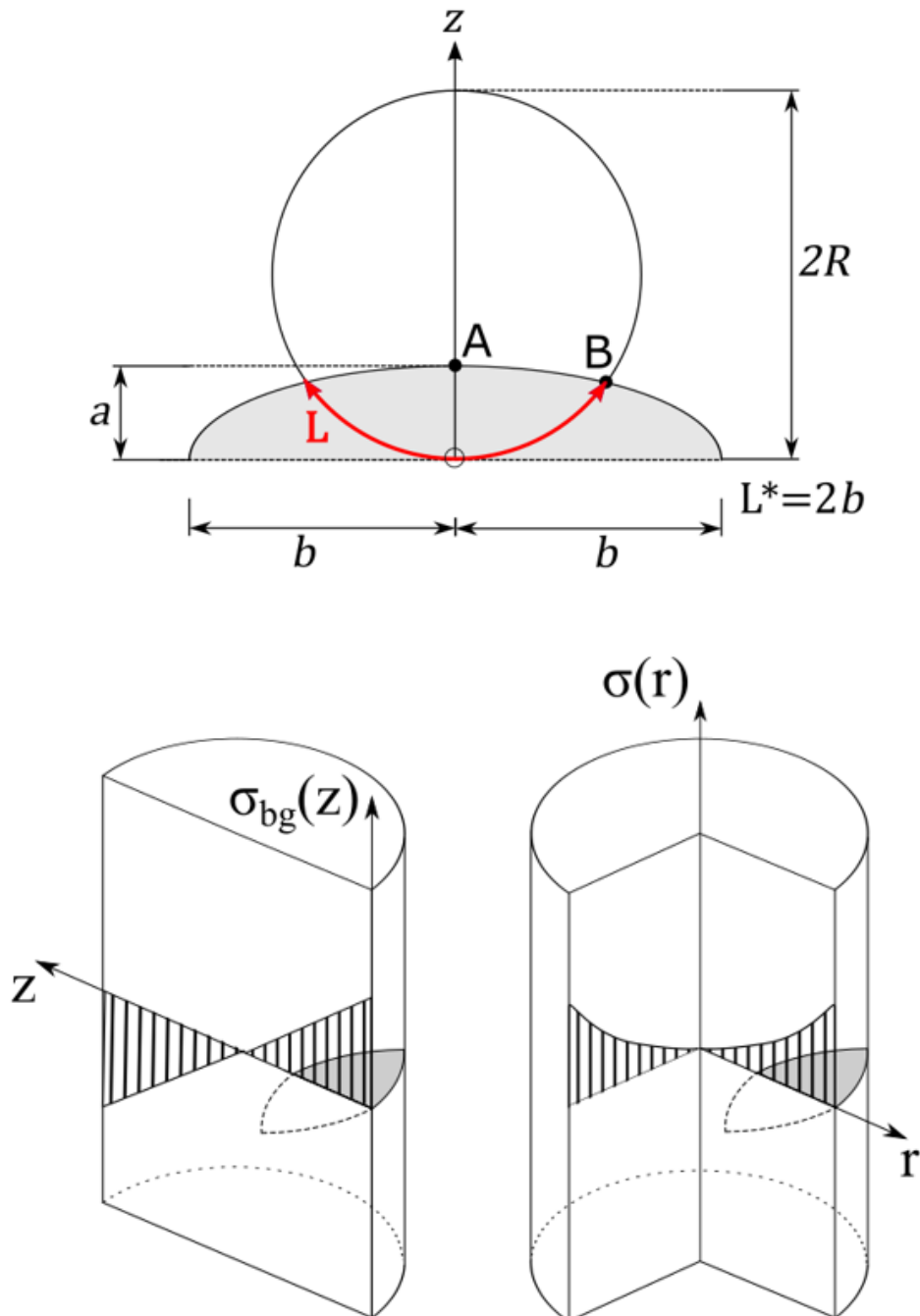


Figure G5.1.  Part circumferential surface crack in a cylindrical bar.

Figure G5.2. Complete circumferential surface crack in a cylindrical bar.

# APPENDIX K.  STRESS INTENSITY FACTOR SOLUTIONS

## K1.      Cracks in a plate

### K1.1      Finite surface crack

$K_I$ is given by

$$K_{\mathrm{I}} = \sqrt{\pi a} \sum_{i=0}^{5} \sigma_i f_i\left(a/t, l/a\right) \quad . \tag{K1}$$

$\sigma_i$ ($i = 0$ to 5) are stress components which define the stress state $\sigma$ according to

$$\sigma = \sigma(u) = \sum_{i=0}^{5} \sigma_i \left(\frac{u}{a}\right)^i \qquad \text{for } 0 \le u \le a . \tag{K2}$$

$\sigma$ is to be taken normal to the prospective crack plane in an uncracked plate. $\sigma_i$ is determined by fitting $\sigma$ to Eq. (K2). The coordinate $u$ is defined in Fig. G1.1.

$f_i$ ($i = 0$ to 5) are geometry functions which are given in Tables K1 and K2 for the deepest point of the crack ($f_i^A$), and at the intersection of the crack with the free surface ($f_i^B$), respectively. See Fig. G1.1.

Remark:    The plate should be large in comparison to the length of the crack so that edge effects do not influence the results.

Ref.:  [K1-K2].

Table K1-1.   Geometry functions for a finite surface crack in a plate — deepest point of the crack
(2 ≤ l / a ≤ 5)

| | $l / a = 2$ | | | | | |
|---|---|---|---|---|---|---|
| $a / t$ | $f_0^A$ | $f_1^A$ | $f_2^A$ | $f_3^A$ | $f_4^A$ | $f_5^A$ |
| 0 | 0.659 | 0.471 | 0.387 | 0.337 | 0.299 | 0.266 |
| 0.2 | 0.663 | 0.473 | 0.388 | 0.337 | 0.299 | 0.269 |
| 0.4 | 0.678 | 0.479 | 0.390 | 0.339 | 0.300 | 0.271 |
| 0.6 | 0.692 | 0.486 | 0.396 | 0.342 | 0.304 | 0.274 |
| 0.8 | 0.697 | 0.497 | 0.405 | 0.349 | 0.309 | 0.278 |
| | $l / a = 5/2$ | | | | | |
| $a / t$ | $f_0^A$ | $f_1^A$ | $f_2^A$ | $f_3^A$ | $f_4^A$ | $f_5^A$ |
| 0 | 0.741 | 0.510 | 0.411 | 0.346 | 0.300 | 0.266 |
| 0.2 | 0.746 | 0.512 | 0.413 | 0.352 | 0.306 | 0.270 |
| 0.4 | 0.771 | 0.519 | 0.416 | 0.356 | 0.309 | 0.278 |
| 0.6 | 0.800 | 0.531 | 0.422 | 0.362 | 0.317 | 0.284 |
| 0.8 | 0.820 | 0.548 | 0.436 | 0.375 | 0.326 | 0.295 |
| | $l / a = 10/3$ | | | | | |
| $a / t$ | $f_0^A$ | $f_1^A$ | $f_2^A$ | $f_3^A$ | $f_4^A$ | $f_5^A$ |
| 0 | 0.833 | 0.549 | 0.425 | 0.351 | 0.301 | 0.267 |
| 0.2 | 0.841 | 0.554 | 0.430 | 0.359 | 0.309 | 0.271 |
| 0.4 | 0.885 | 0.568 | 0.442 | 0.371 | 0.320 | 0.285 |
| 0.6 | 0.930 | 0.587 | 0.454 | 0.381 | 0.331 | 0.295 |
| 0.8 | 0.960 | 0.605 | 0.476 | 0.399 | 0.346 | 0.310 |
| | $l / a = 5$ | | | | | |
| $a / t$ | $f_0^A$ | $f_1^A$ | $f_2^A$ | $f_3^A$ | $f_4^A$ | $f_5^A$ |
| 0 | 0.939 | 0.580 | 0.434 | 0.353 | 0.302 | 0.268 |
| 0.2 | 0.957 | 0.595 | 0.446 | 0.363 | 0.310 | 0.273 |
| 0.4 | 1.057 | 0.631 | 0.475 | 0.389 | 0.332 | 0.292 |
| 0.6 | 1.146 | 0.668 | 0.495 | 0.407 | 0.350 | 0.309 |
| 0.8 | 1.190 | 0.698 | 0.521 | 0.428 | 0.367 | 0.324 |

Table K1-2.  Geometry functions for a finite surface crack in a plate — deepest point of the crack $(10 \leq l / a \leq \infty)$

| | | | $l / a = 10$ | | | |
|---|---|---|---|---|---|---|
| $a / t$ | $f_0^A$ | $f_1^A$ | $f_2^A$ | $f_3^A$ | $f_4^A$ | $f_5^A$ |
| 0 | 1.053 | 0.606 | 0.443 | 0.357 | 0.302 | 0.269 |
| 0.2 | 1.106 | 0.640 | 0.467 | 0.374 | 0.314 | 0.277 |
| 0.4 | 1.306 | 0.724 | 0.525 | 0.420 | 0.348 | 0.304 |
| 0.6 | 1.572 | 0.815 | 0.571 | 0.448 | 0.377 | 0.327 |
| 0.8 | 1.701 | 0.880 | 0.614 | 0.481 | 0.399 | 0.343 |
| | | | $l / a = 32$ | | | |
| $a / t$ | $f_0^A$ | $f_1^A$ | $f_2^A$ | $f_3^A$ | $f_4^A$ | $f_5^A$ |
| 0 | 1.070 | 0.641 | 0.496 | 0.418 | 0.367 | 0.330 |
| 0.2 | 1.240 | 0.716 | 0.541 | 0.451 | 0.394 | 0.353 |
| 0.4 | 1.680 | 0.876 | 0.623 | 0.499 | 0.426 | 0.376 |
| 0.6 | 2.453 | 1.148 | 0.764 | 0.585 | 0.482 | 0.416 |
| 0.8 | 3.316 | 1.453 | 0.924 | 0.685 | 0.552 | 0.467 |
| | | | $l / a = 60$ | | | |
| $a / t$ | $f_0^A$ | $f_1^A$ | $f_2^A$ | $f_3^A$ | $f_4^A$ | $f_5^A$ |
| 0 | 1.076 | 0.646 | 0.499 | 0.421 | 0.369 | 0.332 |
| 0.2 | 1.284 | 0.736 | 0.553 | 0.459 | 0.400 | 0.358 |
| 0.4 | 1.825 | 0.935 | 0.657 | 0.522 | 0.443 | 0.389 |
| 0.6 | 2.896 | 1.316 | 0.856 | 0.645 | 0.525 | 0.448 |
| 0.8 | 4.519 | 1.872 | 1.142 | 0.820 | 0.644 | 0.535 |
| | | | $l / a \rightarrow \infty$ | | | |
| $a / t$ | $f_0^A$ | $f_1^A$ | $f_2^A$ | $f_3^A$ | $f_4^A$ | $f_5^A$ |
| 0 | 1.123 | 0.682 | 0.524 | 0.440 | 0.386 | 0.344 |
| 0.2 | 1.380 | 0.784 | 0.582 | 0.478 | 0.414 | 0.369 |
| 0.4 | 2.106 | 1.059 | 0.735 | 0.578 | 0.485 | 0.423 |
| 0.6 | 4.025 | 1.750 | 1.105 | 0.814 | 0.651 | 0.548 |
| 0.8 | 11.92 | 4.437 | 2.484 | 1.655 | 1.235 | 0.977 |

Table K2-1.    Geometry functions for a finite surface crack in a plate — intersection of crack with free surface $(2 \leq l / a \leq 5)$

| | | | $l / a = 2$ | | | |
|---|---|---|---|---|---|---|
| $a / t$ | $f_0^B$ | $f_1^B$ | $f_2^B$ | $f_3^B$ | $f_4^B$ | $f_5^B$ |
| 0 | 0.716 | 0.118 | 0.041 | 0.022 | 0.014 | 0.010 |
| 0.2 | 0.729 | 0.123 | 0.045 | 0.023 | 0.014 | 0.010 |
| 0.4 | 0.777 | 0.133 | 0.050 | 0.026 | 0.015 | 0.011 |
| 0.6 | 0.839 | 0.148 | 0.058 | 0.029 | 0.018 | 0.012 |
| 0.8 | 0.917 | 0.167 | 0.066 | 0.035 | 0.022 | 0.015 |
| | | | $l / a = 5/2$ | | | |
| $a / t$ | $f_0^B$ | $f_1^B$ | $f_2^B$ | $f_3^B$ | $f_4^B$ | $f_5^B$ |
| 0 | 0.730 | 0.124 | 0.041 | 0.021 | 0.013 | 0.010 |
| 0.2 | 0.749 | 0.126 | 0.046 | 0.023 | 0.014 | 0.010 |
| 0.4 | 0.795 | 0.144 | 0.054 | 0.028 | 0.017 | 0.012 |
| 0.6 | 0.901 | 0.167 | 0.066 | 0.033 | 0.021 | 0.015 |
| 0.8 | 0.995 | 0.193 | 0.076 | 0.042 | 0.026 | 0.017 |
| | | | $l / a = 10/3$ | | | |
| $a / t$ | $f_0^B$ | $f_1^B$ | $f_2^B$ | $f_3^B$ | $f_4^B$ | $f_5^B$ |
| 0 | 0.723 | 0.118 | 0.039 | 0.019 | 0.011 | 0.008 |
| 0.2 | 0.747 | 0.125 | 0.044 | 0.022 | 0.014 | 0.010 |
| 0.4 | 0.803 | 0.145 | 0.056 | 0.029 | 0.018 | 0.012 |
| 0.6 | 0.934 | 0.180 | 0.072 | 0.037 | 0.023 | 0.016 |
| 0.8 | 1.070 | 0.218 | 0.087 | 0.047 | 0.029 | 0.020 |
| | | | $l / a = 5$ | | | |
| $a / t$ | $f_0^B$ | $f_1^B$ | $f_2^B$ | $f_3^B$ | $f_4^B$ | $f_5^B$ |
| 0 | 0.673 | 0.104 | 0.032 | 0.015 | 0.009 | 0.006 |
| 0.2 | 0.704 | 0.114 | 0.038 | 0.018 | 0.011 | 0.007 |
| 0.4 | 0.792 | 0.139 | 0.053 | 0.027 | 0.016 | 0.011 |
| 0.6 | 0.921 | 0.183 | 0.074 | 0.038 | 0.024 | 0.017 |
| 0.8 | 1.147 | 0.244 | 0.097 | 0.052 | 0.032 | 0.021 |

Table K2-2.    Geometry functions for a finite surface crack in a plate — intersection of crack with free
surface ($10 \leq l\,/\,a \leq \infty$)

| | | $l\,/\,a = 10$ | | | | |
|---|---|---|---|---|---|---|
| $a\,/\,t$ | $f_0^{\mathrm{B}}$ | $f_1^{\mathrm{B}}$ | $f_2^{\mathrm{B}}$ | $f_3^{\mathrm{B}}$ | $f_4^{\mathrm{B}}$ | $f_5^{\mathrm{B}}$ |
| 0 | 0.516 | 0.069 | 0.017 | 0.009 | 0.005 | 0.004 |
| 0.2 | 0.554 | 0.076 | 0.022 | 0.011 | 0.007 | 0.005 |
| 0.4 | 0.655 | 0.099 | 0.039 | 0.019 | 0.012 | 0.008 |
| 0.6 | 0.840 | 0.157 | 0.063 | 0.032 | 0.020 | 0.013 |
| 0.8 | 1.143 | 0.243 | 0.099 | 0.055 | 0.034 | 0.023 |
| | | $l\,/\,a = 32$ | | | | |
| $a\,/\,t$ | $f_0^{\mathrm{B}}$ | $f_1^{\mathrm{B}}$ | $f_2^{\mathrm{B}}$ | $f_3^{\mathrm{B}}$ | $f_4^{\mathrm{B}}$ | $f_5^{\mathrm{B}}$ |
| .05 | 0.203 | 0.010 | 0.004 | 0.007 | 0.000 | 0.000 |
| 0.2 | 0.215 | 0.015 | 0.010 | 0.009 | 0.000 | 0.000 |
| 0.4 | 0.273 | 0.021 | 0.016 | 0.010 | 0.000 | 0.000 |
| 0.6 | 0.435 | 0.061 | 0.031 | 0.013 | 0.000 | 0.000 |
| 0.8 | 0.735 | 0.142 | 0.065 | 0.032 | 0.011 | 0.000 |
| | | $l\,/\,a = 60$ | | | | |
| $a\,/\,t$ | $f_0^{\mathrm{B}}$ | $f_1^{\mathrm{B}}$ | $f_2^{\mathrm{B}}$ | $f_3^{\mathrm{B}}$ | $f_4^{\mathrm{B}}$ | $f_5^{\mathrm{B}}$ |
| .05 | 0.121 | 0.017 | 0.005 | 0.001 | 0.000 | 0.000 |
| 0.2 | 0.163 | 0.032 | 0.011 | 0.005 | 0.000 | 0.000 |
| 0.4 | 0.214 | 0.007 | 0.015 | 0.010 | 0.000 | 0.000 |
| 0.6 | 0.355 | 0.089 | 0.020 | 0.015 | 0.000 | 0.000 |
| 0.8 | 0.642 | 0.113 | 0.050 | 0.021 | 0.003 | 0.000 |
| | | $l\,/\,a \rightarrow \infty$ | | | | |
| $a\,/\,t$ | $f_0^{\mathrm{B}}$ | $f_1^{\mathrm{B}}$ | $f_2^{\mathrm{B}}$ | $f_3^{\mathrm{B}}$ | $f_4^{\mathrm{B}}$ | $f_5^{\mathrm{B}}$ |
| 0 | 0.000 | 0.000 | 0.000 | 0.000 | 0.000 | 0.000 |
| 0.2 | 0.000 | 0.000 | 0.000 | 0.000 | 0.000 | 0.000 |
| 0.4 | 0.000 | 0.000 | 0.000 | 0.000 | 0.000 | 0.000 |
| 0.6 | 0.000 | 0.000 | 0.000 | 0.000 | 0.000 | 0.000 |
| 0.8 | 0.000 | 0.000 | 0.000 | 0.000 | 0.000 | 0.000 |

$K_I$ is given by

$$K_I = \frac{1}{\sqrt{2\pi a}} \int_0^a \sigma(u) \sum_{i=1}^5 f_i(a/t) \left(1 - \frac{u}{a}\right)^{i-\frac{3}{2}} du \quad . \tag{K3}$$

The stress state $\sigma = \sigma(u)$ is to be taken normal to the prospective crack plane in an uncracked plate. The coordinate $u$ is defined in Fig. G1.2.

$f_i$ ($i$ = 1 to 5) are geometry functions which are given in Table K3 for the deepest point of the crack ($f_i^A$). See Fig. G1.2.

Remark:    The plate should be large in the transverse direction to the crack so that edge effects do not influence the results.

Ref.: [K3].

Table K3.    Geometry functions for an infinite surface crack in a plate

| $a/t$ | $f_1^A$ | $f_2^A$ | $f_3^A$ | $f_4^A$ | $f_5^A$ |
|-------|---------|---------|---------|---------|---------|
| 0 | 2.000 | 0.977 | 1.142 | -0.350 | -0.091 |
| 0.1 | 2.000 | 1.419 | 1.138 | -0.355 | -0.076 |
| 0.2 | 2.000 | 2.537 | 1.238 | -0.347 | -0.056 |
| 0.3 | 2.000 | 4.238 | 1.680 | -0.410 | -0.019 |
| 0.4 | 2.000 | 6.636 | 2.805 | -0.611 | 0.039 |
| 0.5 | 2.000 | 10.02 | 5.500 | -1.340 | 0.218 |
| 0.6 | 2.000 | 15.04 | 11.88 | -3.607 | 0.786 |
| 0.7 | 2.000 | 23.18 | 28.03 | -10.50 | 2.587 |
| 0.8 | 2.000 | 38.81 | 78.75 | -36.60 | 9.871 |
| 0.9 | 2.000 | 82.70 | 351.0 | -207.1 | 60.86 |

*K1.3    Embedded crack*

$K_I$ is given by

$$K_{\mathrm{I}} = \sqrt{\pi a} \sum_{i=0}^{3} \sigma_i f_i (a,c,d,t) \quad .$$ (K4)

The stress components $\sigma_i$ define the stress state according to

$$\sigma = \sigma \left( \frac{u-d}{a} \right) = \sum_{i=0}^{3} \sigma_i \left( \frac{u-d}{a} \right)^i \qquad \text{for } 0 \leq u \leq t \quad .$$ (K5)

The nominal stress field is assumed to act normal to the prospective crack plane in an uncracked plate. The individual stress components are determined by fitting the active stress field to Eq. (K5). The crack depth $2a$, crack length $l = 2c$, distance from the closest free surface to the crack center $d$, distance from the plate mid plane to the center of the crack $e$, plate thickness $t$ and coordinate $u$ are defined in Fig. G1.3.

The geometry functions $f_i(a, c, d, t)$ are given in Tables K4 and K5 for the points of the crack (A) closest to and (B) furthest from $u = 0$, respectively. See Fig. G1.3.

Remark:    The plate should be large in comparison to the length of the crack so that edge effects do not influence the results.

Ref.:  [K4].

Table K4-1.    Geometry function $f_0$ for an embedded crack in a plate — point closest to $u = 0$

| a/c | 2a/t | a/d=0.05 | a/d=0.1 | a/d=0.2 | a/d=0.3 | a/d=0.4 | a/d=0.5 | a/d=0.6 | a/d=0.7 | a/d=0.8 | a/d=0.85 | a/d=0.9 |
|---|---|---|---|---|---|---|---|---|---|---|---|---|
| 1 | 0.05 | 0.6353 | 0.6354 | 0.6359 | 0.6373 | 0.6404 | 0.6459 | 0.6564 | 0.6757 | 0.7119 | 0.7423 | 0.7921 |
|  | 0.1 |  | 0.6356 | 0.6362 | 0.6377 | 0.6406 | 0.6465 | 0.6572 | 0.6760 | 0.7116 | 0.7427 | 0.7926 |
|  | 0.2 |  |  | 0.6368 | 0.6385 | 0.6418 | 0.6480 | 0.6587 | 0.6787 | 0.7138 | 0.7452 | 0.7963 |
|  | 0.3 |  |  |  | 0.6391 | 0.6422 | 0.6488 | 0.6602 | 0.6795 | 0.7163 | 0.7476 | 0.8005 |
|  | 0.4 |  |  |  |  | 0.6435 | 0.6499 | 0.6623 | 0.6819 | 0.7191 | 0.7508 | 0.8053 |
|  | 0.5 |  |  |  |  |  | 0.6511 | 0.6631 | 0.6841 | 0.7230 | 0.7554 | 0.8119 |
| 0.5 | 0.05 | 0.8245 | 0.8248 | 0.8262 | 0.8303 | 0.8391 | 0.8542 | 0.8807 | 0.9244 | 1.0007 | 1.0616 | 1.1594 |
|  | 0.1 |  | 0.8253 | 0.8269 | 0.8312 | 0.8397 | 0.8554 | 0.8820 | 0.9246 | 1.0005 | 1.0632 | 1.1614 |
|  | 0.2 |  |  | 0.8284 | 0.8327 | 0.8422 | 0.8587 | 0.8853 | 0.9308 | 1.0065 | 1.0692 | 1.1721 |
|  | 0.3 |  |  |  | 0.8352 | 0.8443 | 0.8618 | 0.8906 | 0.9357 | 1.0154 | 1.0786 | 1.1841 |
|  | 0.4 |  |  |  |  | 0.8499 | 0.8665 | 0.8977 | 0.9441 | 1.0248 | 1.0899 | 1.1991 |
|  | 0.5 |  |  |  |  |  | 0.8725 | 0.9018 | 0.9520 | 1.0325 | 1.1031 | 1.2202 |
| 0.25 | 0.05 | 0.9317 | 0.9323 | 0.9357 | 0.9443 | 0.9605 | 0.9872 | 1.0291 | 1.0952 | 1.2067 | 1.2964 | 1.4401 |
|  | 0.1 |  | 0.9331 | 0.9366 | 0.9455 | 0.9618 | 0.9890 | 1.0315 | 1.0954 | 1.2080 | 1.3013 | 1.4447 |
|  | 0.2 |  |  | 0.9402 | 0.9493 | 0.9678 | 0.9970 | 1.0406 | 1.1105 | 1.2202 | 1.3145 | 1.4679 |
|  | 0.3 |  |  |  | 0.9558 | 0.9724 | 1.0045 | 1.0525 | 1.1235 | 1.2444 | 1.3422 | 1.4991 |
|  | 0.4 |  |  |  |  | 0.9830 | 1.0122 | 1.0651 | 1.1400 | 1.2702 | 1.3746 | 1.5414 |
|  | 0.5 |  |  |  |  |  | 1.0257 | 1.0746 | 1.1575 | 1.2951 | 1.4077 | 1.5851 |
| 0.125 | 0.05 | 0.9771 | 0.9781 | 0.9839 | 0.9968 | 1.0189 | 1.0525 | 1.1034 | 1.1829 | 1.3165 | 1.4254 | 1.5996 |
|  | 0.1 |  | 0.9796 | 0.9864 | 1.0004 | 1.0231 | 1.0578 | 1.1101 | 1.1881 | 1.3225 | 1.4348 | 1.6112 |
|  | 0.2 |  |  | 0.9907 | 1.0046 | 1.0307 | 1.0689 | 1.1238 | 1.2098 | 1.3539 | 1.4711 | 1.6589 |
|  | 0.3 |  |  |  | 1.0135 | 1.0375 | 1.0809 | 1.1438 | 1.2346 | 1.4001 | 1.5259 | 1.7280 |
|  | 0.4 |  |  |  |  | 1.0546 | 1.0952 | 1.1674 | 1.2677 | 1.4424 | 1.5808 | 1.8023 |
|  | 0.5 |  |  |  |  |  | 1.1117 | 1.1788 | 1.2919 | 1.4813 | 1.6351 | 1.8780 |
| 0 | 0.05 | 1.0012 | 1.0045 | 1.0152 | 1.0323 | 1.0586 | 1.0979 | 1.1562 | 1.2471 | 1.4009 | 1.5235 | 1.7187 |
|  | 0.1 |  | 1.0059 | 1.0195 | 1.0410 | 1.0708 | 1.1132 | 1.1752 | 1.2694 | 1.4266 | 1.5567 | 1.7592 |
|  | 0.2 |  |  | 1.0245 | 1.0502 | 1.0923 | 1.1478 | 1.2237 | 1.3342 | 1.5157 | 1.6642 | 1.8993 |
|  | 0.3 |  |  |  | 1.0576 | 1.0991 | 1.1689 | 1.2648 | 1.4017 | 1.6210 | 1.7967 | 2.0771 |
|  | 0.4 |  |  |  |  | 1.1092 | 1.1740 | 1.2849 | 1.4495 | 1.7141 | 1.9267 | 2.2674 |
|  | 0.5 |  |  |  |  |  | 1.1864 | 1.2887 | 1.4698 | 1.7747 | 2.0242 | 2.4247 |

Table K4-2.   Geometry function $f_1$ for an embedded crack in a plate — point closest to $u = 0$

| a/c | 2a/t | a/d=0.05 | a/d=0.1 | a/d=0.2 | a/d=0.3 | a/d=0.4 | a/d=0.5 | a/d=0.6 | a/d=0.7 | a/d=0.8 | a/d=0.85 | a/d=0.9 |
|---|---|---|---|---|---|---|---|---|---|---|---|---|
| 1 | 0.05 | -0.4231 | -0.4232 | -0.4232 | -0.4235 | -0.4240 | -0.4248 | -0.4273 | -0.4334 | -0.4482 | -0.4630 | -0.4902 |
|  | 0.1 |  | -0.4232 | -0.4232 | -0.4234 | -0.4238 | -0.4248 | -0.4275 | -0.4334 | -0.4479 | -0.4630 | -0.4903 |
|  | 0.2 |  |  | -0.4232 | -0.4234 | -0.4238 | -0.4249 | -0.4272 | -0.4337 | -0.4480 | -0.4632 | -0.4909 |
|  | 0.3 |  |  |  | -0.4234 | -0.4238 | -0.4249 | -0.4275 | -0.4332 | -0.4483 | -0.4632 | -0.4912 |
|  | 0.4 |  |  |  |  | -0.4238 | -0.4251 | -0.4281 | -0.4334 | -0.4487 | -0.4637 | -0.4920 |
|  | 0.5 |  |  |  |  |  | -0.4251 | -0.4282 | -0.4344 | -0.4494 | -0.4647 | -0.4931 |
| 0.5 | 0.05 | -0.4734 | -0.4734 | -0.4734 | -0.4741 | -0.4753 | -0.4771 | -0.4824 | -0.4937 | -0.5191 | -0.5431 | -0.5860 |
|  | 0.1 |  | -0.4735 | -0.4736 | -0.4739 | -0.4748 | -0.4772 | -0.4826 | -0.4931 | -0.5185 | -0.5431 | -0.5861 |
|  | 0.2 |  |  | -0.4737 | -0.4740 | -0.4750 | -0.4774 | -0.4822 | -0.4941 | -0.5188 | -0.5434 | -0.5879 |
|  | 0.3 |  |  |  | -0.4739 | -0.4752 | -0.4775 | -0.4829 | -0.4937 | -0.5195 | -0.5439 | -0.5886 |
|  | 0.4 |  |  |  |  | -0.4749 | -0.4778 | -0.4839 | -0.4942 | -0.5205 | -0.5453 | -0.5906 |
|  | 0.5 |  |  |  |  |  | -0.4776 | -0.4843 | -0.4963 | -0.5222 | -0.5477 | -0.5935 |
| 0.25 | 0.05 | -0.4918 | -0.4919 | -0.4920 | -0.4926 | -0.4943 | -0.4977 | -0.5052 | -0.5204 | -0.5529 | -0.5838 | -0.6382 |
|  | 0.1 |  | -0.4921 | -0.4922 | -0.4928 | -0.4943 | -0.4979 | -0.5056 | -0.5197 | -0.5523 | -0.5841 | -0.6382 |
|  | 0.2 |  |  | -0.4922 | -0.4928 | -0.4946 | -0.4982 | -0.5053 | -0.5213 | -0.5528 | -0.5846 | -0.6405 |
|  | 0.3 |  |  |  | -0.4927 | -0.4947 | -0.4987 | -0.5064 | -0.5210 | -0.5544 | -0.5862 | -0.6426 |
|  | 0.4 |  |  |  |  | -0.4944 | -0.4992 | -0.5082 | -0.5224 | -0.5570 | -0.5895 | -0.6474 |
|  | 0.5 |  |  |  |  |  | -0.4987 | -0.5088 | -0.5258 | -0.5607 | -0.5945 | -0.6537 |
| 0.125 | 0.05 | -0.4975 | -0.4976 | -0.4978 | -0.4987 | -0.5008 | -0.5049 | -0.5134 | -0.5305 | -0.5670 | -0.6018 | -0.6630 |
|  | 0.1 |  | -0.4976 | -0.4979 | -0.4986 | -0.5006 | -0.5050 | -0.5139 | -0.5299 | -0.5665 | -0.6021 | -0.6634 |
|  | 0.2 |  |  | -0.4978 | -0.4989 | -0.5010 | -0.5054 | -0.5138 | -0.5320 | -0.5679 | -0.6037 | -0.6670 |
|  | 0.3 |  |  |  | -0.4985 | -0.5013 | -0.5063 | -0.5155 | -0.5323 | -0.5710 | -0.6073 | -0.6718 |
|  | 0.4 |  |  |  |  | -0.5009 | -0.5072 | -0.5183 | -0.5352 | -0.5758 | -0.6136 | -0.6807 |
|  | 0.5 |  |  |  |  |  | -0.5066 | -0.5199 | -0.5405 | -0.5825 | -0.6224 | -0.6926 |
| 0 | 0.05 | -0.4998 | -0.4999 | -0.5002 | -0.5011 | -0.5034 | -0.5081 | -0.5174 | -0.5361 | -0.5760 | -0.6129 | -0.6775 |
|  | 0.1 |  | -0.4998 | -0.5003 | -0.5013 | -0.5036 | -0.5085 | -0.5180 | -0.5368 | -0.5764 | -0.6146 | -0.6800 |
|  | 0.2 |  |  | -0.5002 | -0.5020 | -0.5049 | -0.5102 | -0.5204 | -0.5401 | -0.5817 | -0.6217 | -0.6917 |
|  | 0.3 |  |  |  | -0.5015 | -0.5062 | -0.5130 | -0.5246 | -0.5463 | -0.5914 | -0.6340 | -0.7096 |
|  | 0.4 |  |  |  |  | -0.5054 | -0.5153 | -0.5295 | -0.5545 | -0.6048 | -0.6522 | -0.7365 |
|  | 0.5 |  |  |  |  |  | -0.5143 | -0.5334 | -0.5630 | -0.6202 | -0.6737 | -0.7680 |

Table K4-3.   Geometry function $f_2$ for an embedded crack in a plate — point closest to $u = 0$

| a/c | 2a/t | a/d=0.05 | a/d=0.1 | a/d=0.2 | a/d=0.3 | a/d=0.4 | a/d=0.5 | a/d=0.6 | a/d=0.7 | a/d=0.8 | a/d=0.85 | a/d=0.9 |
|---|---|---|---|---|---|---|---|---|---|---|---|---|
| 1 | 0.05 | 0.3805 | 0.3805 | 0.3806 | 0.3810 | 0.3818 | 0.3828 | 0.3854 | 0.3907 | 0.4026 | 0.4142 | 0.4358 |
|  | 0.1 |  | 0.3805 | 0.3807 | 0.3810 | 0.3816 | 0.3829 | 0.3856 | 0.3908 | 0.4024 | 0.4143 | 0.4360 |
|  | 0.2 |  |  | 0.3808 | 0.3812 | 0.3819 | 0.3832 | 0.3858 | 0.3915 | 0.4029 | 0.4148 | 0.4370 |
|  | 0.3 |  |  |  | 0.3813 | 0.3819 | 0.3834 | 0.3861 | 0.3912 | 0.4034 | 0.4152 | 0.4378 |
|  | 0.4 |  |  |  |  | 0.3822 | 0.3836 | 0.3867 | 0.3916 | 0.4039 | 0.4159 | 0.4388 |
|  | 0.5 |  |  |  |  |  | 0.3839 | 0.3869 | 0.3924 | 0.4048 | 0.4169 | 0.4402 |
| 0.5 | 0.05 | 0.4398 | 0.4399 | 0.4402 | 0.4414 | 0.4435 | 0.4463 | 0.4528 | 0.4644 | 0.4875 | 0.5084 | 0.5453 |
|  | 0.1 |  | 0.4401 | 0.4404 | 0.4413 | 0.4431 | 0.4466 | 0.4531 | 0.4642 | 0.4873 | 0.5087 | 0.5458 |
|  | 0.2 |  |  | 0.4407 | 0.4417 | 0.4437 | 0.4473 | 0.4536 | 0.4658 | 0.4885 | 0.5099 | 0.5486 |
|  | 0.3 |  |  |  | 0.4421 | 0.4441 | 0.4479 | 0.4547 | 0.4663 | 0.4903 | 0.5117 | 0.5510 |
|  | 0.4 |  |  |  |  | 0.4452 | 0.4489 | 0.4563 | 0.4678 | 0.4923 | 0.5141 | 0.5542 |
|  | 0.5 |  |  |  |  |  | 0.4501 | 0.4572 | 0.4699 | 0.4940 | 0.5169 | 0.5586 |
| 0.25 | 0.05 | 0.4737 | 0.4739 | 0.4745 | 0.4764 | 0.4800 | 0.4862 | 0.4968 | 0.5145 | 0.5477 | 0.5773 | 0.6281 |
|  | 0.1 |  | 0.4741 | 0.4749 | 0.4768 | 0.4804 | 0.4867 | 0.4974 | 0.5144 | 0.5477 | 0.5782 | 0.6290 |
|  | 0.2 |  |  | 0.4756 | 0.4775 | 0.4816 | 0.4883 | 0.4989 | 0.5178 | 0.5502 | 0.5810 | 0.6343 |
|  | 0.3 |  |  |  | 0.4789 | 0.4825 | 0.4899 | 0.5015 | 0.5198 | 0.5551 | 0.5866 | 0.6407 |
|  | 0.4 |  |  |  |  | 0.4847 | 0.4915 | 0.5044 | 0.5231 | 0.5605 | 0.5934 | 0.6498 |
|  | 0.5 |  |  |  |  |  | 0.4943 | 0.5062 | 0.5273 | 0.5658 | 0.6005 | 0.6592 |
| 0.125 | 0.05 | 0.4899 | 0.4901 | 0.4913 | 0.4943 | 0.4995 | 0.5078 | 0.5209 | 0.5427 | 0.5827 | 0.6183 | 0.6789 |
|  | 0.1 |  | 0.4904 | 0.4918 | 0.4949 | 0.5003 | 0.5089 | 0.5225 | 0.5434 | 0.5837 | 0.6202 | 0.6813 |
|  | 0.2 |  |  | 0.4928 | 0.4958 | 0.5019 | 0.5111 | 0.5249 | 0.5484 | 0.5902 | 0.6277 | 0.6918 |
|  | 0.3 |  |  |  | 0.4978 | 0.5034 | 0.5137 | 0.5293 | 0.5530 | 0.6000 | 0.6393 | 0.7065 |
|  | 0.4 |  |  |  |  | 0.5072 | 0.5168 | 0.5348 | 0.5599 | 0.6092 | 0.6514 | 0.7231 |
|  | 0.5 |  |  |  |  |  | 0.5206 | 0.5373 | 0.5659 | 0.6180 | 0.6637 | 0.7403 |
| 0 | 0.05 | 0.5000 | 0.5008 | 0.5035 | 0.5078 | 0.5145 | 0.5247 | 0.5404 | 0.5660 | 0.6128 | 0.6528 | 0.7207 |
|  | 0.1 |  | 0.5012 | 0.5046 | 0.5100 | 0.5176 | 0.5286 | 0.5451 | 0.5716 | 0.6191 | 0.6614 | 0.7311 |
|  | 0.2 |  |  | 0.5059 | 0.5123 | 0.5230 | 0.5373 | 0.5573 | 0.5879 | 0.6417 | 0.6887 | 0.7675 |
|  | 0.3 |  |  |  | 0.5142 | 0.5247 | 0.5425 | 0.5677 | 0.6049 | 0.6684 | 0.7224 | 0.8132 |
|  | 0.4 |  |  |  |  | 0.5272 | 0.5438 | 0.5727 | 0.6170 | 0.6921 | 0.7558 | 0.8627 |
|  | 0.5 |  |  |  |  |  | 0.5469 | 0.5737 | 0.6221 | 0.7076 | 0.7809 | 0.9037 |

Table K4-4.  Geometry function $f_3$ for an embedded crack in a plate — point closest to $u = 0$

| a/c | 2a/t | a/d=0.05 | a/d=0.1 | a/d=0.2 | a/d=0.3 | a/d=0.4 | a/d=0.5 | a/d=0.6 | a/d=0.7 | a/d=0.8 | a/d=0.85 | a/d=0.9 |
|---|---|---|---|---|---|---|---|---|---|---|---|---|
| 1 | 0.05 | -0.3258 | -0.3258 | -0.3259 | -0.3260 | -0.3262 | -0.3266 | -0.3277 | -0.3307 | -0.3383 | -0.3465 | -0.3627 |
|  | 0.1 |  | -0.3258 | -0.3259 | -0.3259 | -0.3261 | -0.3266 | -0.3278 | -0.3307 | -0.3382 | -0.3465 | -0.3628 |
|  | 0.2 |  |  | -0.3259 | -0.3259 | -0.3261 | -0.3266 | -0.3276 | -0.3308 | -0.3382 | -0.3466 | -0.3631 |
|  | 0.3 |  |  |  | -0.3259 | -0.3261 | -0.3266 | -0.3278 | -0.3304 | -0.3383 | -0.3466 | -0.3633 |
|  | 0.4 |  |  |  |  | -0.3262 | -0.3267 | -0.3282 | -0.3305 | -0.3385 | -0.3468 | -0.3636 |
|  | 0.5 |  |  |  |  |  | -0.3267 | -0.3281 | -0.3310 | -0.3388 | -0.3473 | -0.3640 |
| 0.5 | 0.05 | -0.3565 | -0.3565 | -0.3565 | -0.3568 | -0.3574 | -0.3581 | -0.3607 | -0.3662 | -0.3794 | -0.3925 | -0.4176 |
|  | 0.1 |  | -0.3566 | -0.3566 | -0.3568 | -0.3571 | -0.3582 | -0.3608 | -0.3659 | -0.3791 | -0.3926 | -0.4177 |
|  | 0.2 |  |  | -0.3566 | -0.3568 | -0.3572 | -0.3583 | -0.3606 | -0.3665 | -0.3792 | -0.3927 | -0.4187 |
|  | 0.3 |  |  |  | -0.3567 | -0.3574 | -0.3584 | -0.3609 | -0.3660 | -0.3795 | -0.3929 | -0.4190 |
|  | 0.4 |  |  |  |  | -0.3572 | -0.3585 | -0.3614 | -0.3661 | -0.3799 | -0.3935 | -0.4199 |
|  | 0.5 |  |  |  |  |  | -0.3584 | -0.3615 | -0.3672 | -0.3808 | -0.3946 | -0.4212 |
| 0.25 | 0.05 | -0.3686 | -0.3686 | -0.3686 | -0.3689 | -0.3697 | -0.3713 | -0.3750 | -0.3827 | -0.3998 | -0.4171 | -0.4485 |
|  | 0.1 |  | -0.3687 | -0.3688 | -0.3691 | -0.3698 | -0.3715 | -0.3752 | -0.3823 | -0.3994 | -0.4172 | -0.4485 |
|  | 0.2 |  |  | -0.3688 | -0.3691 | -0.3699 | -0.3716 | -0.3750 | -0.3831 | -0.3997 | -0.4174 | -0.4497 |
|  | 0.3 |  |  |  | -0.3690 | -0.3699 | -0.3718 | -0.3755 | -0.3828 | -0.4003 | -0.4181 | -0.4506 |
|  | 0.4 |  |  |  |  | -0.3698 | -0.3720 | -0.3764 | -0.3833 | -0.4015 | -0.4195 | -0.4506 |
|  | 0.5 |  |  |  |  |  | -0.3718 | -0.3766 | -0.3850 | -0.4031 | -0.4218 | -0.4556 |
| 0.125 | 0.05 | -0.3726 | -0.3726 | -0.3728 | -0.3732 | -0.3742 | -0.3762 | -0.3804 | -0.3892 | -0.4086 | -0.4281 | -0.4616 |
|  | 0.1 |  | -0.3726 | -0.3727 | -0.3731 | -0.3740 | -0.3762 | -0.3808 | -0.3888 | -0.4083 | -0.4283 | -0.4638 |
|  | 0.2 |  |  | -0.3727 | -0.3732 | -0.3742 | -0.3764 | -0.3806 | -0.3899 | -0.4089 | -0.4290 | -0.4655 |
|  | 0.3 |  |  |  | -0.3731 | -0.3743 | -0.3768 | -0.3813 | -0.3897 | -0.4103 | -0.4305 | -0.4676 |
|  | 0.4 |  |  |  |  | -0.3741 | -0.3772 | -0.3827 | -0.3909 | -0.4125 | -0.4334 | -0.4717 |
|  | 0.5 |  |  |  |  |  | -0.3769 | -0.3834 | -0.3936 | -0.4155 | -0.4374 | -0.4772 |
| 0 | 0.05 | -0.3747 | -0.3747 | -0.3749 | -0.3753 | -0.3765 | -0.3788 | -0.3836 | -0.3933 | -0.4148 | -0.4354 | -0.4729 |
|  | 0.1 |  | -0.3747 | -0.3749 | -0.3754 | -0.3766 | -0.3790 | -0.3839 | -0.3937 | -0.4149 | -0.4363 | -0.4742 |
|  | 0.2 |  |  | -0.3749 | -0.3758 | -0.3772 | -0.3799 | -0.3851 | -0.3953 | -0.4176 | -0.4399 | -0.4803 |
|  | 0.3 |  |  |  | -0.3755 | -0.3779 | -0.3813 | -0.3872 | -0.3984 | -0.4225 | -0.4460 | -0.4894 |
|  | 0.4 |  |  |  |  | -0.3775 | -0.3824 | -0.3897 | -0.4025 | -0.4292 | -0.4552 | -0.5031 |
|  | 0.5 |  |  |  |  |  | -0.3820 | -0.3917 | -0.4068 | -0.4370 | -0.4661 | -0.5191 |

Table K5-1.   Geometry function $f_0$ for an embedded crack in a plate — point furthest from $u = 0$

| a/c | 2a/t | a/d=0.05 | a/d=0.1 | a/d=0.2 | a/d=0.3 | a/d=0.4 | a/d=0.5 | a/d=0.6 | a/d=0.7 | a/d=0.8 | a/d=0.85 | a/d=0.9 |
|---|---|---|---|---|---|---|---|---|---|---|---|---|
| 1 | 0.05 | 0.6353 | 0.6354 | 0.6358 | 0.6365 | 0.6376 | 0.6391 | 0.6414 | 0.6443 | 0.6478 | 0.6498 | 0.6528 |
|  | 0.1 |  | 0.6356 | 0.6360 | 0.6368 | 0.6380 | 0.6397 | 0.6418 | 0.6446 | 0.6481 | 0.6501 | 0.6533 |
|  | 0.2 |  |  | 0.6368 | 0.6374 | 0.6389 | 0.6408 | 0.6432 | 0.6461 | 0.6495 | 0.6516 | 0.6548 |
|  | 0.3 |  |  |  | 0.6391 | 0.6394 | 0.6412 | 0.6438 | 0.6470 | 0.6505 | 0.6527 | 0.6566 |
|  | 0.4 |  |  |  |  | 0.6435 | 0.6428 | 0.6449 | 0.6482 | 0.6514 | 0.6535 | 0.6578 |
|  | 0.5 |  |  |  |  |  | 0.6511 | 0.6482 | 0.6497 | 0.6533 | 0.6550 | 0.6597 |
| 0.5 | 0.05 | 0.8245 | 0.8247 | 0.8259 | 0.8283 | 0.8321 | 0.8372 | 0.8450 | 0.8538 | 0.8668 | 0.8739 | 0.8838 |
|  | 0.1 |  | 0.8253 | 0.8264 | 0.8289 | 0.8329 | 0.8385 | 0.8458 | 0.8549 | 0.8675 | 0.8750 | 0.8851 |
|  | 0.2 |  |  | 0.8284 | 0.8302 | 0.8347 | 0.8409 | 0.8489 | 0.8586 | 0.8714 | 0.8787 | 0.8902 |
|  | 0.3 |  |  |  | 0.8352 | 0.8366 | 0.8428 | 0.8514 | 0.8623 | 0.8758 | 0.8835 | 0.8959 |
|  | 0.4 |  |  |  |  | 0.8499 | 0.8491 | 0.8563 | 0.8675 | 0.8795 | 0.8872 | 0.9006 |
|  | 0.5 |  |  |  |  |  | 0.8725 | 0.8666 | 0.8735 | 0.8828 | 0.8916 | 0.9085 |
| 0.25 | 0.05 | 0.9317 | 0.9322 | 0.9348 | 0.9399 | 0.9479 | 0.9593 | 0.9744 | 0.9929 | 1.0162 | 1.0308 | 1.0499 |
|  | 0.1 |  | 0.9331 | 0.9355 | 0.9410 | 0.9495 | 0.9611 | 0.9756 | 0.9933 | 1.0184 | 1.0344 | 1.0532 |
|  | 0.2 |  |  | 0.9402 | 0.9444 | 0.9541 | 0.9671 | 0.9835 | 1.0030 | 1.0261 | 1.0421 | 1.0647 |
|  | 0.3 |  |  |  | 0.9558 | 0.9590 | 0.9721 | 0.9899 | 1.0121 | 1.0391 | 1.0566 | 1.0792 |
|  | 0.4 |  |  |  |  | 0.9830 | 0.9827 | 0.9978 | 1.0209 | 1.0500 | 1.0694 | 1.0943 |
|  | 0.5 |  |  |  |  |  | 1.0257 | 1.0176 | 1.0334 | 1.0614 | 1.0818 | 1.1083 |
| 0.125 | 0.05 | 0.9771 | 0.9779 | 0.9824 | 0.9907 | 1.0028 | 1.0189 | 1.0388 | 1.0637 | 1.0956 | 1.1161 | 1.1428 |
|  | 0.1 |  | 0.9796 | 0.9847 | 0.9940 | 1.0071 | 1.0235 | 1.0436 | 1.0685 | 1.1014 | 1.1228 | 1.1505 |
|  | 0.2 |  |  | 0.9907 | 0.9974 | 1.0123 | 1.0312 | 1.0543 | 1.0815 | 1.1216 | 1.1449 | 1.1751 |
|  | 0.3 |  |  |  | 1.0135 | 1.0189 | 1.0386 | 1.0647 | 1.0970 | 1.1459 | 1.1728 | 1.2075 |
|  | 0.4 |  |  |  |  | 1.0546 | 1.0555 | 1.0790 | 1.1145 | 1.1614 | 1.1922 | 1.2321 |
|  | 0.5 |  |  |  |  |  | 1.1117 | 1.1028 | 1.1286 | 1.1752 | 1.2085 | 1.2523 |
| 0 | 0.05 | 1.0012 | 1.0040 | 1.0128 | 1.0247 | 1.0403 | 1.0599 | 1.0841 | 1.1144 | 1.1549 | 1.1803 | 1.2125 |
|  | 0.1 |  | 1.0059 | 1.0163 | 1.0320 | 1.0505 | 1.0726 | 1.0995 | 1.1326 | 1.1752 | 1.2028 | 1.2379 |
|  | 0.2 |  |  | 1.0245 | 1.0376 | 1.0643 | 1.0957 | 1.1321 | 1.1755 | 1.2312 | 1.2673 | 1.3134 |
|  | 0.3 |  |  |  | 1.0576 | 1.0683 | 1.1037 | 1.1503 | 1.2076 | 1.2815 | 1.3292 | 1.3909 |
|  | 0.4 |  |  |  |  | 1.1092 | 1.1124 | 1.1546 | 1.2193 | 1.3095 | 1.3702 | 1.4507 |
|  | 0.5 |  |  |  |  |  | 1.1864 | 1.1760 | 1.2245 | 1.3161 | 1.3839 | 1.4772 |

Table K5-2.  Geometry function $f_1$ for an embedded crack in a plate — point furthest from $u = 0$

| a/c | 2a/t | a/d=0.05 | a/d=0.1 | a/d=0.2 | a/d=0.3 | a/d=0.4 | a/d=0.5 | a/d=0.6 | a/d=0.7 | a/d=0.8 | a/d=0.85 | a/d=0.9 |
|---|---|---|---|---|---|---|---|---|---|---|---|---|
| 1 | 0.05 | 0.4231 | 0.4232 | 0.4232 | 0.4232 | 0.4231 | 0.4230 | 0.4228 | 0.4225 | 0.4221 | 0.4218 | 0.4215 |
|  | 0.1 |  | 0.4232 | 0.4232 | 0.4231 | 0.4231 | 0.4230 | 0.4227 | 0.4225 | 0.4221 | 0.4218 | 0.4215 |
|  | 0.2 |  |  | 0.4232 | 0.4232 | 0.4231 | 0.4230 | 0.4228 | 0.4224 | 0.4221 | 0.4218 | 0.4215 |
|  | 0.3 |  |  |  | 0.4234 | 0.4231 | 0.4230 | 0.4227 | 0.4224 | 0.4220 | 0.4217 | 0.4214 |
|  | 0.4 |  |  |  |  | 0.4238 | 0.4233 | 0.4229 | 0.4224 | 0.4220 | 0.4217 | 0.4214 |
|  | 0.5 |  |  |  |  |  | 0.4251 | 0.4238 | 0.4231 | 0.4223 | 0.4220 | 0.4217 |
| 0.5 | 0.05 | 0.4734 | 0.4734 | 0.4734 | 0.4733 | 0.4730 | 0.4727 | 0.4722 | 0.4709 | 0.4698 | 0.4689 | 0.4681 |
|  | 0.1 |  | 0.4735 | 0.4735 | 0.4734 | 0.4732 | 0.4728 | 0.4721 | 0.4710 | 0.4697 | 0.4689 | 0.4681 |
|  | 0.2 |  |  | 0.4737 | 0.4736 | 0.4733 | 0.4729 | 0.4722 | 0.4710 | 0.4696 | 0.4687 | 0.4680 |
|  | 0.3 |  |  |  | 0.4739 | 0.4733 | 0.4728 | 0.4720 | 0.4710 | 0.4694 | 0.4684 | 0.4674 |
|  | 0.4 |  |  |  |  | 0.4749 | 0.4734 | 0.4723 | 0.4710 | 0.4693 | 0.4682 | 0.4672 |
|  | 0.5 |  |  |  |  |  | 0.4776 | 0.4743 | 0.4722 | 0.4702 | 0.4688 | 0.4677 |
| 0.25 | 0.05 | 0.4918 | 0.4918 | 0.4918 | 0.4916 | 0.4911 | 0.4903 | 0.4894 | 0.4877 | 0.4849 | 0.4835 | 0.4819 |
|  | 0.1 |  | 0.4921 | 0.4920 | 0.4918 | 0.4914 | 0.4906 | 0.4893 | 0.4873 | 0.4848 | 0.4835 | 0.4819 |
|  | 0.2 |  |  | 0.4922 | 0.4918 | 0.4913 | 0.4905 | 0.4892 | 0.4873 | 0.4845 | 0.4829 | 0.4812 |
|  | 0.3 |  |  |  | 0.4927 | 0.4916 | 0.4905 | 0.4890 | 0.4870 | 0.4838 | 0.4821 | 0.4803 |
|  | 0.4 |  |  |  |  | 0.4944 | 0.4917 | 0.4895 | 0.4870 | 0.4834 | 0.4814 | 0.4791 |
|  | 0.5 |  |  |  |  |  | 0.4987 | 0.4930 | 0.4890 | 0.4844 | 0.4820 | 0.4793 |
| 0.125 | 0.05 | 0.4975 | 0.4975 | 0.4975 | 0.4972 | 0.4966 | 0.4956 | 0.4940 | 0.4917 | 0.4879 | 0.4857 | 0.4830 |
|  | 0.1 |  | 0.4976 | 0.4975 | 0.4971 | 0.4965 | 0.4955 | 0.4939 | 0.4913 | 0.4879 | 0.4855 | 0.4828 |
|  | 0.2 |  |  | 0.4978 | 0.4971 | 0.4964 | 0.4953 | 0.4936 | 0.4910 | 0.4870 | 0.4843 | 0.4811 |
|  | 0.3 |  |  |  | 0.4985 | 0.4968 | 0.4952 | 0.4932 | 0.4904 | 0.4856 | 0.4826 | 0.4789 |
|  | 0.4 |  |  |  |  | 0.5009 | 0.4969 | 0.4937 | 0.4900 | 0.4846 | 0.4811 | 0.4767 |
|  | 0.5 |  |  |  |  |  | 0.5066 | 0.4989 | 0.4930 | 0.4858 | 0.4815 | 0.4762 |
| 0 | 0.05 | 0.4998 | 0.4997 | 0.4996 | 0.4991 | 0.4983 | 0.4971 | 0.4951 | 0.4918 | 0.4866 | 0.4827 | 0.4767 |
|  | 0.1 |  | 0.4998 | 0.4995 | 0.4990 | 0.4981 | 0.4968 | 0.4947 | 0.4915 | 0.4861 | 0.4816 | 0.4753 |
|  | 0.2 |  |  | 0.5002 | 0.4988 | 0.4974 | 0.4957 | 0.4931 | 0.4893 | 0.4829 | 0.4778 | 0.4699 |
|  | 0.3 |  |  |  | 0.5015 | 0.4981 | 0.4951 | 0.4915 | 0.4865 | 0.4784 | 0.4720 | 0.4619 |
|  | 0.4 |  |  |  |  | 0.5054 | 0.4984 | 0.4926 | 0.4856 | 0.4750 | 0.4668 | 0.4542 |
|  | 0.5 |  |  |  |  |  | 0.5143 | 0.5014 | 0.4905 | 0.4765 | 0.4663 | 0.4508 |

Table K5-3. Geometry function $f_2$ for an embedded crack in a plate — point furthest from $u = 0$

| a/c | 2a/t | a/d=0.05 | a/d=0.1 | a/d=0.2 | a/d=0.3 | a/d=0.4 | a/d=0.5 | a/d=0.6 | a/d=0.7 | a/d=0.8 | a/d=0.85 | a/d=0.9 |
|---|---|---|---|---|---|---|---|---|---|---|---|---|
| 1 | 0.05 | 0.3805 | 0.3805 | 0.3806 | 0.3807 | 0.3810 | 0.3813 | 0.3817 | 0.3824 | 0.3831 | 0.3835 | 0.3840 |
| | 0.1 | | 0.3805 | 0.3806 | 0.3808 | 0.3810 | 0.3814 | 0.3818 | 0.3824 | 0.3831 | 0.3836 | 0.3841 |
| | 0.2 | | | 0.3808 | 0.3809 | 0.3812 | 0.3816 | 0.3821 | 0.3827 | 0.3834 | 0.3839 | 0.3845 |
| | 0.3 | | | | 0.3813 | 0.3813 | 0.3817 | 0.3822 | 0.3829 | 0.3836 | 0.3841 | 0.3847 |
| | 0.4 | | | | | 0.3822 | 0.3820 | 0.3824 | 0.3831 | 0.3838 | 0.3843 | 0.3849 |
| | 0.5 | | | | | | 0.3839 | 0.3832 | 0.3835 | 0.3842 | 0.3847 | 0.3853 |
| 0.5 | 0.05 | 0.4398 | 0.4399 | 0.4401 | 0.4406 | 0.4414 | 0.4425 | 0.4442 | 0.4460 | 0.4489 | 0.4504 | 0.4524 |
| | 0.1 | | 0.4401 | 0.4403 | 0.4408 | 0.4416 | 0.4428 | 0.4443 | 0.4461 | 0.4489 | 0.4507 | 0.4526 |
| | 0.2 | | | 0.4407 | 0.4412 | 0.4420 | 0.4433 | 0.4450 | 0.4470 | 0.4498 | 0.4514 | 0.4534 |
| | 0.3 | | | | 0.4421 | 0.4424 | 0.4437 | 0.4455 | 0.4478 | 0.4507 | 0.4524 | 0.4546 |
| | 0.4 | | | | | 0.4452 | 0.4450 | 0.4465 | 0.4488 | 0.4514 | 0.4532 | 0.4554 |
| | 0.5 | | | | | | 0.4501 | 0.4487 | 0.4501 | 0.4523 | 0.4542 | 0.4565 |
| 0.25 | 0.05 | 0.4737 | 0.4738 | 0.4743 | 0.4754 | 0.4771 | 0.4796 | 0.4831 | 0.4872 | 0.4925 | 0.4963 | 0.5015 |
| | 0.1 | | 0.4741 | 0.4746 | 0.4758 | 0.4776 | 0.4801 | 0.4832 | 0.4871 | 0.4928 | 0.4971 | 0.5022 |
| | 0.2 | | | 0.4756 | 0.4765 | 0.4785 | 0.4813 | 0.4849 | 0.4892 | 0.4944 | 0.4985 | 0.5046 |
| | 0.3 | | | | 0.4789 | 0.4796 | 0.4823 | 0.4862 | 0.4911 | 0.4971 | 0.5016 | 0.5076 |
| | 0.4 | | | | | 0.4847 | 0.4846 | 0.4879 | 0.4929 | 0.4994 | 0.5042 | 0.5108 |
| | 0.5 | | | | | | 0.4943 | 0.4923 | 0.4957 | 0.5019 | 0.5070 | 0.5140 |
| 0.125 | 0.05 | 0.4899 | 0.4901 | 0.4910 | 0.4929 | 0.4956 | 0.4994 | 0.5040 | 0.5099 | 0.5176 | 0.5231 | 0.5307 |
| | 0.1 | | 0.4904 | 0.4914 | 0.4934 | 0.4964 | 0.5003 | 0.5050 | 0.5107 | 0.5188 | 0.5245 | 0.5324 |
| | 0.2 | | | 0.4928 | 0.4942 | 0.4976 | 0.5019 | 0.5072 | 0.5135 | 0.5230 | 0.5291 | 0.5374 |
| | 0.3 | | | | 0.4978 | 0.4990 | 0.5034 | 0.5094 | 0.5168 | 0.5281 | 0.5350 | 0.5444 |
| | 0.4 | | | | | 0.5072 | 0.5073 | 0.5126 | 0.5206 | 0.5316 | 0.5393 | 0.5498 |
| | 0.5 | | | | | | 0.5206 | 0.5183 | 0.5241 | 0.5349 | 0.5432 | 0.5546 |
| 0 | 0.05 | 0.5000 | 0.5007 | 0.5029 | 0.5059 | 0.5098 | 0.5147 | 0.5208 | 0.5283 | 0.5388 | 0.5456 | 0.5546 |
| | 0.1 | | 0.5012 | 0.5038 | 0.5077 | 0.5124 | 0.5179 | 0.5247 | 0.5330 | 0.5440 | 0.5513 | 0.5612 |
| | 0.2 | | | 0.5059 | 0.5091 | 0.5158 | 0.5237 | 0.5328 | 0.5438 | 0.5582 | 0.5679 | 0.5807 |
| | 0.3 | | | | 0.5142 | 0.5168 | 0.5257 | 0.5374 | 0.5519 | 0.5710 | 0.5837 | 0.6006 |
| | 0.4 | | | | | 0.5272 | 0.5279 | 0.5385 | 0.5549 | 0.5781 | 0.5942 | 0.6162 |
| | 0.5 | | | | | | 0.5469 | 0.5441 | 0.5562 | 0.5798 | 0.5978 | 0.6231 |

Table K5-4. Geometry function $f_3$ for an embedded crack in a plate — point furthest from $u = 0$

| a/c | 2a/t | a/d=0.05 | a/d=0.1 | a/d=0.2 | a/d=0.3 | a/d=0.4 | a/d=0.5 | a/d=0.6 | a/d=0.7 | a/d=0.8 | a/d=0.85 | a/d=0.9 |
|---|---|---|---|---|---|---|---|---|---|---|---|---|
| 1 | 0.05 | 0.3258 | 0.3258 | 0.3259 | 0.3258 | 0.3258 | 0.3258 | 0.3257 | 0.3256 | 0.3254 | 0.3253 | 0.3252 |
|  | 0.1 |  | 0.3258 | 0.3258 | 0.3259 | 0.3258 | 0.3258 | 0.3257 | 0.3256 | 0.3254 | 0.3253 | 0.3252 |
|  | 0.2 |  |  | 0.3259 | 0.3259 | 0.3258 | 0.3258 | 0.3257 | 0.3255 | 0.3254 | 0.3253 | 0.3252 |
|  | 0.3 |  |  |  | 0.3259 | 0.3259 | 0.3258 | 0.3257 | 0.3255 | 0.3254 | 0.3253 | 0.3252 |
|  | 0.4 |  |  |  |  | 0.3262 | 0.3259 | 0.3258 | 0.3256 | 0.3254 | 0.3253 | 0.3252 |
|  | 0.5 |  |  |  |  |  | 0.3267 | 0.3262 | 0.3258 | 0.3256 | 0.3254 | 0.3254 |
| 0.5 | 0.05 | 0.3565 | 0.3564 | 0.3565 | 0.3564 | 0.3563 | 0.3562 | 0.3560 | 0.3554 | 0.3550 | 0.3546 | 0.3542 |
|  | 0.1 |  | 0.3565 | 0.3565 | 0.3565 | 0.3564 | 0.3563 | 0.3559 | 0.3554 | 0.3549 | 0.3546 | 0.3542 |
|  | 0.2 |  |  | 0.3566 | 0.3566 | 0.3565 | 0.3563 | 0.3560 | 0.3555 | 0.3549 | 0.3545 | 0.3542 |
|  | 0.3 |  |  |  | 0.3568 | 0.3565 | 0.3562 | 0.3559 | 0.3554 | 0.3548 | 0.3544 | 0.3540 |
|  | 0.4 |  |  |  |  | 0.3572 | 0.3565 | 0.3560 | 0.3555 | 0.3548 | 0.3543 | 0.3539 |
|  | 0.5 |  |  |  |  |  | 0.3584 | 0.3570 | 0.3560 | 0.3552 | 0.3546 | 0.3540 |
| 0.25 | 0.05 | 0.3685 | 0.3686 | 0.3686 | 0.3684 | 0.3682 | 0.3679 | 0.3676 | 0.3668 | 0.3655 | 0.3652 | 0.3648 |
|  | 0.1 |  | 0.3687 | 0.3687 | 0.3686 | 0.3684 | 0.3681 | 0.3675 | 0.3666 | 0.3655 | 0.3652 | 0.3648 |
|  | 0.2 |  |  | 0.3688 | 0.3686 | 0.3684 | 0.3680 | 0.3675 | 0.3666 | 0.3653 | 0.3649 | 0.3644 |
|  | 0.3 |  |  |  | 0.3690 | 0.3685 | 0.3680 | 0.3674 | 0.3664 | 0.3650 | 0.3646 | 0.3641 |
|  | 0.4 |  |  |  |  | 0.3698 | 0.3686 | 0.3676 | 0.3665 | 0.3648 | 0.3642 | 0.3636 |
|  | 0.5 |  |  |  |  |  | 0.3718 | 0.3692 | 0.3674 | 0.3653 | 0.3645 | 0.3637 |
| 0.125 | 0.05 | 0.3726 | 0.3726 | 0.3726 | 0.3725 | 0.3722 | 0.3717 | 0.3710 | 0.3699 | 0.3681 | 0.3673 | 0.3665 |
|  | 0.1 |  | 0.3726 | 0.3725 | 0.3724 | 0.3721 | 0.3717 | 0.3709 | 0.3697 | 0.3681 | 0.3672 | 0.3664 |
|  | 0.2 |  |  | 0.3727 | 0.3724 | 0.3721 | 0.3716 | 0.3708 | 0.3696 | 0.3677 | 0.3667 | 0.3655 |
|  | 0.3 |  |  |  | 0.3730 | 0.3723 | 0.3715 | 0.3706 | 0.3693 | 0.3671 | 0.3660 | 0.3645 |
|  | 0.4 |  |  |  |  | 0.3741 | 0.3723 | 0.3709 | 0.3691 | 0.3666 | 0.3653 | 0.3635 |
|  | 0.5 |  |  |  |  |  | 0.3769 | 0.3732 | 0.3705 | 0.3672 | 0.3655 | 0.3633 |
| 0 | 0.05 | 0.3747 | 0.3747 | 0.3746 | 0.3743 | 0.3739 | 0.3733 | 0.3724 | 0.3707 | 0.3681 | 0.3661 | 0.3631 |
|  | 0.1 |  | 0.3747 | 0.3745 | 0.3743 | 0.3738 | 0.3732 | 0.3722 | 0.3706 | 0.3679 | 0.3656 | 0.3624 |
|  | 0.2 |  |  | 0.3749 | 0.3742 | 0.3735 | 0.3726 | 0.3714 | 0.3695 | 0.3663 | 0.3638 | 0.3598 |
|  | 0.3 |  |  |  | 0.3756 | 0.3738 | 0.3723 | 0.3706 | 0.3681 | 0.3641 | 0.3608 | 0.3556 |
|  | 0.4 |  |  |  |  | 0.3775 | 0.3740 | 0.3711 | 0.3676 | 0.3624 | 0.3582 | 0.3518 |
|  | 0.5 |  |  |  |  |  | 0.3820 | 0.3756 | 0.3701 | 0.3631 | 0.3580 | 0.3500 |

*K1.4    Through-thickness crack*

$K_I$ is given by

$$K_I = \sqrt{\pi l / 2}\left(\sigma_m f_m + \sigma_b f_b\right) \quad.$$
(K6)

$\sigma_m$ and $\sigma_b$ are the membrane and bending stress components respectively, which define the stress state $\sigma$ according to

$$\sigma = \sigma(u) = \sigma_m + \sigma_b\left(1 - \frac{2u}{t}\right) \qquad \text{for } 0 \leq u \leq t \quad.$$
(K7)

$\sigma$ is to be taken normal to the prospective crack plane in an uncracked plate. $\sigma_m$ and $\sigma_b$ are determined by fitting $\sigma$ to Eq. (K7). The coordinate $u$ is defined in Fig. G1.4.

$f_m$ and $f_b$ are geometry functions which are given in Table K6 for the intersections of the crack with the free surface at $u = 0$ ($f^A$), and at $u = t$ ($f^B$). See Fig. G1.4.

Remark:    The plate should be large in comparison to the length of the crack so that edge effects do not influence the results.

Ref.:  [K5].

Table K6.    Geometry functions for a through-thickness crack in a plate

| $f_m{}^A$ | $f_b{}^A$ | $f_m{}^B$ | $f_b{}^B$ |
|-----------|-----------|-----------|-----------|
| 1.000 | 1.000 | 1.000 | -1.000 |

## K2.    Axial cracks in a cylinder

### K2.1    Finite internal surface crack

$K_\text{I}$ is given by

$$K_\text{I} = \sqrt{\pi a} \sum_{j=0}^{3} \sigma_j f_j \left( a/t, l/a, R_i/t \right) \quad .$$
(K8)

$\sigma_\text{j}$ ($j = 0$ to 3) are stress components which define the stress state $\sigma$ according to

$$\sigma = \sigma(u) = \sum_{j=0}^{3} \sigma_j \left( \frac{u}{a} \right)^j \qquad \text{for } 0 \leq u \leq a \quad .$$
(K9)

$\sigma$ is to be taken normal to the prospective crack plane in an uncracked cylinder. $\sigma_\text{j}$ is determined by fitting $\sigma$ to Eq. (K9). The coordinate $u$ is defined in Fig. G2.1.

$f_\text{j}$ ($j = 0$ to 3) are geometry functions which are given in Tables K7 and K8 for the deepest point of the crack ($f^A$), and at the intersection of the crack with the free surface ($f^B$), respectively. See Fig. G2.1.

Remarks:    The cylinder should be long in comparison to the length of the crack so that edge effects do not influence the results.

Ref.: [K1] and [K6].

Table K7.     Geometry functions for a finite axial internal surface crack in a cylinder — deepest point of crack

| $a/t$ | $l/a = 2, R_i/t = 4$ | | | | $l/a = 2, R_i/t = 10$ | | | |
|---|---|---|---|---|---|---|---|---|
| | $f_0^A$ | $f_1^A$ | $f_2^A$ | $f_3^A$ | $f_0^A$ | $f_1^A$ | $f_2^A$ | $f_3^A$ |
| 0 | 0.659 | 0.471 | 0.387 | 0.337 | 0.659 | 0.471 | 0.387 | 0.337 |
| 0.2 | 0.643 | 0.454 | 0.375 | 0.326 | 0.647 | 0.456 | 0.375 | 0.326 |
| 0.5 | 0.663 | 0.463 | 0.378 | 0.328 | 0.669 | 0.464 | 0.380 | 0.328 |
| 0.8 | 0.704 | 0.489 | 0.397 | 0.342 | 0.694 | 0.484 | 0.394 | 0.339 |

| $a/t$ | $l/a = 5, R_i/t = 4$ | | | | $l/a = 5, R_i/t = 10$ | | | |
|---|---|---|---|---|---|---|---|---|
| | $f_0^A$ | $f_1^A$ | $f_2^A$ | $f_3^A$ | $f_0^A$ | $f_1^A$ | $f_2^A$ | $f_3^A$ |
| 0 | 0.939 | 0.580 | 0.434 | 0.353 | 0.939 | 0.580 | 0.434 | 0.353 |
| 0.2 | 0.919 | 0.579 | 0.452 | 0.382 | 0.932 | 0.584 | 0.455 | 0.383 |
| 0.5 | 1.037 | 0.622 | 0.474 | 0.395 | 1.058 | 0.629 | 0.477 | 0.397 |
| 0.8 | 1.255 | 0.720 | 0.534 | 0.443 | 1.211 | 0.701 | 0.523 | 0.429 |

| $a/t$ | $l/a = 10, R_i/t = 4$ | | | | $l/a = 10, R_i/t = 10$ | | | |
|---|---|---|---|---|---|---|---|---|
| | $f_0^A$ | $f_1^A$ | $f_2^A$ | $f_3^A$ | $f_0^A$ | $f_1^A$ | $f_2^A$ | $f_3^A$ |
| 0 | 1.053 | 0.606 | 0.443 | 0.357 | 1.053 | 0.606 | 0.443 | 0.357 |
| 0.2 | 1.045 | 0.634 | 0.487 | 0.406 | 1.062 | 0.641 | 0.489 | 0.417 |
| 0.5 | 1.338 | 0.739 | 0.540 | 0.438 | 1.359 | 0.746 | 0.544 | 0.440 |
| 0.8 | 1.865 | 0.948 | 0.659 | 0.516 | 1.783 | 0.914 | 0.639 | 0.504 |

Table K8.    Geometry functions for a finite axial internal surface crack in a cylinder — intersection of crack with free surface

| $a / t$ | $l / a = 2, R_\text{i} / t = 4$ | | | | $l / a = 2, R_\text{i} / t = 10$ | | | |
|---|---|---|---|---|---|---|---|---|
| | $f_0{}^\text{B}$ | $f_1{}^\text{B}$ | $f_2{}^\text{B}$ | $f_3{}^\text{B}$ | $f_0{}^\text{B}$ | $f_1{}^\text{B}$ | $f_2{}^\text{B}$ | $f_3{}^\text{B}$ |
| 0 | 0.716 | 0.118 | 0.041 | 0.022 | 0.716 | 0.118 | 0.041 | 0.022 |
| 0.2 | 0.719 | 0.124 | 0.046 | 0.024 | 0.726 | 0.126 | 0.047 | 0.024 |
| 0.5 | 0.759 | 0.136 | 0.052 | 0.027 | 0.777 | 0.141 | 0.054 | 0.028 |
| 0.8 | 0.867 | 0.158 | 0.062 | 0.032 | 0.859 | 0.163 | 0.063 | 0.033 |
| $a / t$ | $l / a = 5, R_\text{i} / t = 4$ | | | | $l / a = 5, R_\text{i} / t = 10$ | | | |
| | $f_0{}^\text{B}$ | $f_1{}^\text{B}$ | $f_2{}^\text{B}$ | $f_3{}^\text{B}$ | $f_0{}^\text{B}$ | $f_1{}^\text{B}$ | $f_2{}^\text{B}$ | $f_3{}^\text{B}$ |
| 0 | 0.673 | 0.104 | 0.032 | 0.016 | 0.673 | 0.104 | 0.032 | 0.015 |
| 0.2 | 0.670 | 0.107 | 0.037 | 0.018 | 0.676 | 0.109 | 0.037 | 0.018 |
| 0.5 | 0.803 | 0.151 | 0.059 | 0.031 | 0.814 | 0.153 | 0.060 | 0.031 |
| 0.8 | 1.060 | 0.229 | 0.095 | 0.051 | 1.060 | 0.225 | 0.092 | 0.049 |
| $a / t$ | $l / a = 10, R_\text{i} / t = 4$ | | | | $l / a = 10, R_\text{i} / t = 10$ | | | |
| | $f_0{}^\text{B}$ | $f_1{}^\text{B}$ | $f_2{}^\text{B}$ | $f_3{}^\text{B}$ | $f_0{}^\text{B}$ | $f_1{}^\text{B}$ | $f_2{}^\text{B}$ | $f_3{}^\text{B}$ |
| 0 | 0.516 | 0.069 | 0.017 | 0.009 | 0.516 | 0.069 | 0.017 | 0.009 |
| 0.2 | 0.577 | 0.075 | 0.022 | 0.010 | 0.578 | 0.075 | 0.022 | 0.010 |
| 0.5 | 0.759 | 0.134 | 0.051 | 0.027 | 0.753 | 0.131 | 0.050 | 0.026 |
| 0.8 | 1.144 | 0.250 | 0.103 | 0.056 | 1.123 | 0.241 | 0.099 | 0.053 |

## K2.2    *Infinite internal surface crack*

$K_I$ is given by

$$K_{\mathrm{I}} = \frac{1}{\sqrt{2\pi a}} \int_0^a \sigma(u) \sum_{j=1}^{3} f_j\left(a/t, R_i/t\right)\left(1 - \frac{u}{a}\right)^{j-\frac{3}{2}} du \quad . \tag{K10}$$

The stress state $\sigma = \sigma(u)$ is to be taken normal to the prospective crack plane in an uncracked cylinder. The coordinate $u$ is defined in Fig. G2.2.

$f_j$ ($j$ = 1 to 3) are geometry functions which are given in Table K9 for the deepest point of the crack ($f^A$). See Fig. G2.2.

Ref.:  [K3].

Table K9.    Geometry functions for an infinite axial internal surface crack in a cylinder

| $a / t$ | $R_i / t = 0.5$ | | | $R_i / t = 1$ | | |
|---|---|---|---|---|---|---|
| | $f_1^A$ | $f_2^A$ | $f_3^A$ | $f_1^A$ | $f_2^A$ | $f_3^A$ |
| 0 | 2.000 | 1.328 | 0.220 | 2.000 | 1.336 | 0.220 |
| 0.1 | 2.000 | 0.900 | 0.155 | 2.000 | 1.271 | 0.184 |
| 0.2 | 2.000 | 0.895 | 0.193 | 2.000 | 1.566 | 0.237 |
| 0.3 | 2.000 | 1.032 | 0.252 | 2.000 | 1.997 | 0.360 |
| 0.4 | 2.000 | 1.329 | 0.210 | 2.000 | 2.501 | 0.542 |
| 0.5 | 2.000 | 1.796 | 0.093 | 2.000 | 3.072 | 0.762 |
| 0.6 | 2.000 | 2.457 | -0.074 | 2.000 | 3.807 | 0.892 |
| 0.7 | 2.000 | 3.597 | -0.618 | 2.000 | 4.877 | 0.825 |
| 0.75 | 2.000 | 4.571 | -1.272 | 2.000 | 5.552 | 0.786 |
| $a / t$ | $R_i / t = 2$ | | | $R_i / t = 4$ | | |
| | $f_1^A$ | $f_2^A$ | $f_3^A$ | $f_1^A$ | $f_2^A$ | $f_3^A$ |
| 0 | 2.000 | 1.340 | 0.219 | 2.000 | 1.340 | 0.219 |
| 0.1 | 2.000 | 1.519 | 0.212 | 2.000 | 1.659 | 0.217 |
| 0.2 | 2.000 | 2.119 | 0.322 | 2.000 | 2.475 | 0.358 |
| 0.3 | 2.000 | 2.934 | 0.551 | 2.000 | 3.615 | 0.709 |
| 0.4 | 2.000 | 3.820 | 1.066 | 2.000 | 4.982 | 1.499 |
| 0.5 | 2.000 | 4.692 | 1.853 | 2.000 | 6.455 | 2.936 |
| 0.6 | 2.000 | 5.697 | 2.600 | 2.000 | 7.977 | 5.018 |
| 0.7 | 2.000 | 6.995 | 3.224 | 2.000 | 9.513 | 7.637 |
| 0.75 | 2.000 | 7.656 | 3.733 | 2.000 | 10.24 | 9.134 |

*K2.3    Finite external surface crack*

$K_I$ is given by

$$K_I = \sqrt{\pi a} \sum_{j=0}^{3} \sigma_j f_j \left( a/t, l/a, R_i/t \right) \quad .$$

(K11)

$\sigma_j$ ($j = 0$ to $3$) are stress components which define the stress state $\sigma$ according to

$$\sigma = \sigma(u) = \sum_{j=0}^{3} \sigma_j \left( \frac{u}{a} \right)^j \qquad \text{for } 0 \le u \le a \quad .$$

(K12)

$\sigma$ is to be taken normal to the prospective crack plane in an uncracked cylinder. $\sigma_j$ is determined by fitting $\sigma$ to Eq. (K12). The coordinate $u$ is defined in Fig. G2.3.

$f_j$ ($j = 0$ to $3$) are geometry functions which are given in Tables K10 and K11 for the deepest point of the crack ($f^A$), and at the intersection of the crack with the free surface ($f^B$), respectively. See Fig. G2.3.

Remarks:    The cylinder should be long in comparison to the length of the crack so that edge effects do not influence the results.

Ref.:  [K1] and [K6].

Table K10.    Geometry functions for a finite axial external surface crack in a cylinder — deepest point of crack

| $a/t$ | $l/a = 2$, $R_i/t = 4$ | | | | $l/a = 2$, $R_i/t = 10$ | | | |
|---|---|---|---|---|---|---|---|---|
| | $f_0^A$ | $f_1^A$ | $f_2^A$ | $f_3^A$ | $f_0^A$ | $f_1^A$ | $f_2^A$ | $f_3^A$ |
| 0 | 0.659 | 0.471 | 0.387 | 0.337 | 0.659 | 0.471 | 0.387 | 0.337 |
| 0.2 | 0.656 | 0.459 | 0.377 | 0.327 | 0.653 | 0.457 | 0.376 | 0.327 |
| 0.5 | 0.697 | 0.473 | 0.384 | 0.331 | 0.687 | 0.470 | 0.382 | 0.330 |
| 0.8 | 0.736 | 0.495 | 0.398 | 0.342 | 0.712 | 0.487 | 0.394 | 0.340 |
| $a/t$ | $l/a = 5$, $R_i/t = 4$ | | | | $l/a = 5$, $R_i/t = 10$ | | | |
| | $f_0^A$ | $f_1^A$ | $f_2^A$ | $f_3^A$ | $f_0^A$ | $f_1^A$ | $f_2^A$ | $f_3^A$ |
| 0 | 0.939 | 0.580 | 0.434 | 0.353 | 0.939 | 0.580 | 0.434 | 0.353 |
| 0.2 | 0.964 | 0.596 | 0.461 | 0.387 | 0.953 | 0.591 | 0.459 | 0.386 |
| 0.5 | 1.183 | 0.672 | 0.500 | 0.410 | 1.139 | 0.656 | 0.491 | 0.405 |
| 0.8 | 1.502 | 0.795 | 0.568 | 0.455 | 1.361 | 0.746 | 0.543 | 0.439 |
| $a/t$ | $l/a = 10$, $R_i/t = 4$ | | | | $l/a = 10$, $R_i/t = 10$ | | | |
| | $f_0^A$ | $f_1^A$ | $f_2^A$ | $f_3^A$ | $f_0^A$ | $f_1^A$ | $f_2^A$ | $f_3^A$ |
| 0 | 1.053 | 0.606 | 0.443 | 0.357 | 1.053 | 0.606 | 0.443 | 0.357 |
| 0.2 | 1.107 | 0.658 | 0.499 | 0.413 | 1.092 | 0.652 | 0.496 | 0.411 |
| 0.5 | 1.562 | 0.820 | 0.584 | 0.465 | 1.508 | 0.799 | 0.571 | 0.457 |
| 0.8 | 2.390 | 1.122 | 0.745 | 0.568 | 2.188 | 1.047 | 0.704 | 0.541 |

Table K11. Geometry functions for a finite axial external surface crack in a cylinder — intersection of crack with free surface

| $a/t$ | $l/a = 2, R_i/t = 4$ | | | | $l/a = 2, R_i/t = 10$ | | | |
|---|---|---|---|---|---|---|---|---|
| | $f_0^B$ | $f_1^B$ | $f_2^B$ | $f_3^B$ | $f_0^B$ | $f_1^B$ | $f_2^B$ | $f_3^B$ |
| 0 | 0.716 | 0.118 | 0.041 | 0.022 | 0.716 | 0.118 | 0.041 | 0.022 |
| 0.2 | 0.741 | 0.130 | 0.049 | 0.026 | 0.736 | 0.129 | 0.048 | 0.025 |
| 0.5 | 0.819 | 0.155 | 0.061 | 0.033 | 0.807 | 0.150 | 0.059 | 0.031 |
| 0.8 | 0.954 | 0.192 | 0.078 | 0.041 | 0.926 | 0.182 | 0.072 | 0.038 |
| $a/t$ | $l/a = 5, R_i/t = 4$ | | | | $l/a = 5, R_i/t = 10$ | | | |
| | $f_0^B$ | $f_1^B$ | $f_2^B$ | $f_3^B$ | $f_0^B$ | $f_1^B$ | $f_2^B$ | $f_3^B$ |
| 0 | 0.673 | 0.104 | 0.032 | 0.015 | 0.673 | 0.104 | 0.032 | 0.015 |
| 0.2 | 0.690 | 0.113 | 0.039 | 0.019 | 0.685 | 0.111 | 0.039 | 0.019 |
| 0.5 | 0.864 | 0.170 | 0.068 | 0.036 | 0.856 | 0.167 | 0.066 | 0.035 |
| 0.8 | 1.217 | 0.277 | 0.117 | 0.064 | 1.198 | 0.269 | 0.112 | 0.061 |
| $a/t$ | $l/a = 10, R_i/t = 4$ | | | | $l/a = 10, R_i/t = 10$ | | | |
| | $f_0^B$ | $f_1^B$ | $f_2^B$ | $f_3^B$ | $f_0^B$ | $f_1^B$ | $f_2^B$ | $f_3^B$ |
| 0 | 0.516 | 0.069 | 0.017 | 0.009 | 0.516 | 0.069 | 0.017 | 0.009 |
| 0.2 | 0.583 | 0.076 | 0.022 | 0.010 | 0.583 | 0.076 | 0.022 | 0.010 |
| 0.5 | 0.748 | 0.128 | 0.047 | 0.024 | 0.768 | 0.135 | 0.051 | 0.027 |
| 0.8 | 1.105 | 0.230 | 0.092 | 0.049 | 1.202 | 0.264 | 0.109 | 0.059 |

## K2.4    *Infinite external surface crack*

$K_I$ is given by

$$K_{\mathrm{I}} = \frac{1}{\sqrt{2\pi a}} \int_0^a \sigma(u) \sum_{j=1}^4 f_j\left(a/t, R_i/t\right)\left(1-\frac{u}{a}\right)^{j-\frac{3}{2}} du \quad .$$

(K13)

The stress state $\sigma = \sigma(u)$ is to be taken normal to the prospective crack plane in an uncracked cylinder. The coordinate $u$ is defined in Fig. G2.4.

$f_j$ ($j$ = 1 to 4) are geometry functions which are given in Table K12 for the deepest point of the crack ($f^A$). See Fig. G2.4.

Ref.:  [K3].

Table K12.    Geometry functions for an infinite axial external surface crack in a cylinder

| $a/t$ | $R_i/t = 0.5$ | | | | $R_i/t = 1$ | | | |
|---|---|---|---|---|---|---|---|---|
| | $f_1^A$ | $f_2^A$ | $f_3^A$ | $f_4^A$ | $f_1^A$ | $f_2^A$ | $f_3^A$ | $f_4^A$ |
| 0 | 2.000 | 0.901 | 1.401 | -0.620 | 2.000 | 0.901 | 1.401 | -0.620 |
| 0.1 | 2.000 | 1.359 | 1.376 | -0.585 | 2.000 | 1.331 | 1.365 | -0.584 |
| 0.2 | 2.000 | 1.933 | 1.387 | -0.549 | 2.000 | 1.967 | 1.369 | -0.543 |
| 0.3 | 2.000 | 2.614 | 1.422 | -0.510 | 2.000 | 2.766 | 1.484 | -0.512 |
| 0.4 | 2.000 | 3.408 | 1.541 | -0.481 | 2.000 | 3.708 | 1.759 | -0.505 |
| 0.5 | 2.000 | 4.321 | 1.799 | -0.472 | 2.000 | 4.787 | 2.238 | -0.528 |
| 0.6 | 2.000 | 5.459 | 2.101 | -0.456 | 2.000 | 6.055 | 2.904 | -0.577 |
| 0.7 | 2.000 | 7.145 | 2.187 | -0.361 | 2.000 | 7.726 | 3.601 | -0.605 |
| 0.75 | 2.000 | 8.355 | 2.112 | -0.265 | 2.000 | 8.853 | 3.901 | -0.590 |
| $a/t$ | $R_i/t = 2$ | | | | $R_i/t = 4$ | | | |
| | $f_1^A$ | $f_2^A$ | $f_3^A$ | $f_4^A$ | $f_1^A$ | $f_2^A$ | $f_3^A$ | $f_4^A$ |
| 0 | 2.000 | 0.901 | 1.401 | -0.620 | 2.000 | 0.900 | 1.400 | -0.620 |
| 0.1 | 2.000 | 1.330 | 1.370 | -0.585 | 2.000 | 1.335 | 1.382 | -0.587 |
| 0.2 | 2.000 | 2.086 | 1.403 | -0.542 | 2.000 | 2.219 | 1.416 | -0.535 |
| 0.3 | 2.000 | 3.095 | 1.580 | -0.510 | 2.000 | 3.464 | 1.658 | -0.501 |
| 0.4 | 2.000 | 4.307 | 2.054 | -0.524 | 2.000 | 4.993 | 2.412 | -0.549 |
| 0.5 | 2.000 | 5.643 | 3.004 | -0.625 | 2.000 | 6.823 | 3.794 | -0.704 |
| 0.6 | 2.000 | 7.103 | 4.376 | -0.802 | 2.000 | 8.984 | 6.051 | -1.011 |
| 0.7 | 2.000 | 8.976 | 5.735 | -0.949 | 2.000 | 11.10 | 10.07 | -1.674 |
| 0.75 | 2.000 | 10.28 | 6.243 | -0.963 | 2.000 | 11.80 | 13.08 | -2.229 |

*K2.5    Through-thickness crack*

$K_I$ is given by

$$K_I = \sqrt{\pi l / 2} \left( \sum_{j=0}^{4} \sigma_j f_j (l/t, R_i/t) \right) \quad , \tag{K14}$$

where $\sigma_j$ ($j = 0$ to 4) are stress components which define the stress state $\sigma$ according to

$$\sigma = \sigma(u) = \sum_{j=0}^{4} \sigma_j \left( \frac{u}{t} \right)^j \qquad \text{for } 0 \le u \le t \quad . \tag{K15}$$

$\sigma$ is to be taken normal to the prospective crack plane in an uncracked cylinder. $\sigma_j$ is determined by fitting $\sigma$ to Eq. (K15). The coordinate $u$ is defined in Fig. G2.5.

$f_j$ ($j = 0$ to 4) are geometry functions which are given in Tables K13 and K14 for the intersections of the crack with the free surface at $u = 0$ ($f^A$), and at $u = t$ ($f^B$). See Fig. G2.5.

Remarks:   The cylinder should be long in comparison to the length of the crack so that edge effects do not influence. The small negative values given in Table K13-1 to K13-3 are the result of the fitting procedure in [K7].

Ref.:  [K7].

Table K13-1.  Geometry functions for an axial through-thickness crack in a cylinder — the intersection of the crack with the free surface at $u = 0$

| $l/t$ | $f_0^A$ | $f_1^A$ | $f_2^A$ | $f_3^A$ | $f_4^A$ |
|---|---|---|---|---|---|
| | | $R_i/t = 5$ | | | |
| $l/t$ | $f_0^A$ | $f_1^A$ | $f_2^A$ | $f_3^A$ | $f_4^A$ |
| 1 | 1.003 | 0.099 | 0.004 | -0.022 | -0.022 |
| 2 | 1.017 | 0.155 | 0.036 | -0.001 | -0.016 |
| 4 | 1.233 | 0.316 | 0.146 | 0.082 | 0.051 |
| 6 | 1.569 | 0.520 | 0.288 | 0.190 | 0.139 |
| 8 | 1.966 | 0.747 | 0.445 | 0.311 | 0.236 |
| 10 | 2.396 | 0.987 | 0.610 | 0.437 | 0.338 |
| 15 | 3.538 | 1.605 | 1.033 | 0.759 | 0.599 |
| 20 | 4.700 | 2.221 | 1.454 | 1.079 | 0.857 |
| 25 | 5.826 | 2.812 | 1.856 | 1.384 | 1.103 |
| 30 | 6.873 | 3.360 | 2.227 | 1.665 | 1.330 |
| 50 | 9.656 | 4.812 | 3.213 | 2.412 | 1.931 |
| | | $R_i/t = 10$ | | | |
| $l/t$ | $f_0^A$ | $f_1^A$ | $f_2^A$ | $f_3^A$ | $f_4^A$ |
| 1 | 1.017 | 0.095 | -0.001 | -0.028 | -0.038 |
| 2 | 0.999 | 0.132 | 0.016 | -0.019 | -0.033 |
| 4 | 1.097 | 0.225 | 0.077 | 0.026 | 0.005 |
| 6 | 1.284 | 0.347 | 0.161 | 0.091 | 0.057 |
| 8 | 1.525 | 0.491 | 0.261 | 0.168 | 0.119 |
| 10 | 1.801 | 0.649 | 0.370 | 0.251 | 0.187 |
| 15 | 2.578 | 1.076 | 0.665 | 0.476 | 0.368 |
| 20 | 3.421 | 1.528 | 0.973 | 0.710 | 0.558 |
| 25 | 4.294 | 1.988 | 1.286 | 0.948 | 0.749 |
| 30 | 5.175 | 2.448 | 1.599 | 1.185 | 0.940 |
| 50 | 8.584 | 4.209 | 2.788 | 2.083 | 1.663 |

Table K13-2. Geometry functions for an axial through-thickness crack in a cylinder — the intersection of the crack with the free surface at $u = 0$

| $R_i / t = 20$ | | | | | |
|---|---|---|---|---|---|
| $l / t$ | $f_0^A$ | $f_1^A$ | $f_2^A$ | $f_3^A$ | $f_4^A$ |
| 1 | 1.025 | 0.094 | -0.003 | -0.029 | -0.038 |
| 2 | 0.997 | 0.121 | 0.006 | -0.041 | -0.037 |
| 4 | 1.029 | 0.175 | 0.038 | -0.005 | -0.022 |
| 6 | 1.120 | 0.244 | 0.085 | 0.031 | 0.007 |
| 8 | 1.251 | 0.328 | 0.144 | 0.076 | 0.043 |
| 10 | 1.412 | 0.424 | 0.211 | 0.127 | 0.085 |
| 15 | 1.895 | 0.699 | 0.401 | 0.272 | 0.203 |
| 20 | 2.448 | 1.001 | 0.609 | 0.431 | 0.331 |
| 25 | 3.040 | 1.319 | 0.826 | 0.596 | 0.465 |
| 30 | 3.656 | 1.645 | 1.048 | 0.765 | 0.601 |
| 50 | 6.203 | 2.971 | 1.947 | 1.445 | 1.148 |
| $R_i / t = 50$ | | | | | |
| $l / t$ | $f_0^A$ | $f_1^A$ | $f_2^A$ | $f_3^A$ | $f_4^A$ |
| 1 | 1.020 | 0.093 | -0.003 | -0.029 | -0.037 |
| 2 | 0.999 | 0.116 | 0.001 | -0.035 | -0.047 |
| 4 | 0.997 | 0.147 | 0.016 | -0.024 | -0.038 |
| 6 | 1.023 | 0.179 | 0.036 | -0.009 | -0.027 |
| 8 | 1.071 | 0.217 | 0.063 | 0.011 | -0.010 |
| 10 | 1.138 | 0.262 | 0.094 | 0.036 | 0.010 |
| 15 | 1.366 | 0.401 | 0.191 | 0.110 | 0.070 |
| 20 | 1.652 | 0.565 | 0.305 | 0.197 | 0.141 |
| 25 | 1.975 | 0.744 | 0.429 | 0.292 | 0.218 |
| 30 | 2.323 | 0.934 | 0.559 | 0.392 | 0.298 |
| 50 | 3.852 | 1.746 | 1.114 | 0.813 | 0.639 |

Table K13-3. Geometry functions for an axial through-thickness crack in a cylinder — the intersection of the crack with the free surface at $u = 0$

| $R_i / t = 100$ | | | | | |
|---|---|---|---|---|---|
| $l / t$ | $f_0^A$ | $f_1^A$ | $f_2^A$ | $f_3^A$ | $f_4^A$ |
| 1 | 0.989 | 0.089 | -0.002 | -0.026 | -0.034 |
| 2 | 0.990 | 0.114 | 0.000 | -0.034 | -0.045 |
| 4 | 0.990 | 0.140 | 0.009 | -0.030 | -0.037 |
| 6 | 0.995 | 0.158 | 0.020 | -0.022 | -0.039 |
| 8 | 1.013 | 0.178 | 0.034 | -0.012 | -0.041 |
| 10 | 1.042 | 0.202 | 0.050 | 0.001 | -0.019 |
| 15 | 1.156 | 0.278 | 0.103 | 0.041 | 0.014 |
| 20 | 1.313 | 0.373 | 0.170 | 0.092 | 0.055 |
| 25 | 1.501 | 0.482 | 0.245 | 0.151 | 0.103 |
| 30 | 1.711 | 0.600 | 0.328 | 0.214 | 0.154 |
| 50 | 2.681 | 1.129 | 0.692 | 0.492 | 0.380 |

Table K14-1.  Geometry functions for an axial through-thickness crack in a cylinder — the intersection of the crack with the free surface at $u = t$

| | $R_i / t = 5$ | | | | |
|---|---|---|---|---|---|
| $l / t$ | $f_0^B$ | $f_1^B$ | $f_2^B$ | $f_3^B$ | $f_4^B$ |
| 1 | 1.159 | 1.022 | 0.911 | 0.835 | 0.783 |
| 2 | 1.276 | 1.043 | 0.890 | 0.790 | 0.720 |
| 4 | 1.595 | 1.168 | 0.945 | 0.808 | 0.716 |
| 6 | 1.919 | 1.309 | 1.024 | 0.856 | 0.746 |
| 8 | 2.211 | 1.439 | 1.100 | 0.906 | 0.780 |
| 10 | 2.464 | 1.551 | 1.167 | 0.951 | 0.812 |
| 15 | 2.938 | 1.758 | 1.290 | 1.033 | 0.870 |
| 20 | 3.251 | 1.890 | 1.367 | 1.084 | 0.907 |
| 25 | 3.479 | 1.984 | 1.421 | 1.120 | 0.932 |
| 30 | 3.670 | 2.063 | 1.467 | 1.151 | 0.954 |
| 50 | 4.272 | 2.327 | 1.627 | 1.262 | 1.036 |
| | $R_i / t = 10$ | | | | |
| $l / t$ | $f_0^B$ | $f_1^B$ | $f_2^B$ | $f_3^B$ | $f_4^B$ |
| 1 | 1.111 | 0.994 | 0.891 | 0.818 | 0.766 |
| 2 | 1.176 | 0.992 | 0.854 | 0.763 | 0.697 |
| 4 | 1.397 | 1.075 | 0.884 | 0.764 | 0.682 |
| 6 | 1.649 | 1.185 | 0.945 | 0.799 | 0.701 |
| 8 | 1.900 | 1.299 | 1.012 | 0.843 | 0.731 |
| 10 | 2.138 | 1.408 | 1.078 | 0.888 | 0.763 |
| 15 | 2.647 | 1.641 | 1.222 | 0.987 | 0.836 |
| 20 | 3.035 | 1.817 | 1.330 | 1.063 | 0.893 |
| 25 | 3.323 | 1.945 | 1.408 | 1.117 | 0.933 |
| 30 | 3.530 | 2.034 | 1.462 | 1.153 | 0.959 |
| 50 | 3.848 | 2.149 | 1.519 | 1.186 | 0.979 |

Table K14-2. Geometry functions for an axial through-thickness crack in a cylinder — the intersection of the crack with the free surface at $u = t$

| $R_i / t = 20$ | | | | | |
|---|---|---|---|---|---|
| $l / t$ | $f_0^B$ | $f_1^B$ | $f_2^B$ | $f_3^B$ | $f_4^B$ |
| 1 | 1.080 | 0.976 | 0.877 | 0.807 | 0.757 |
| 2 | 1.110 | 0.957 | 0.830 | 0.740 | 0.683 |
| 4 | 1.250 | 1.002 | 0.836 | 0.728 | 0.653 |
| 6 | 1.425 | 1.077 | 0.874 | 0.747 | 0.660 |
| 8 | 1.612 | 1.162 | 0.923 | 0.777 | 0.679 |
| 10 | 1.801 | 1.250 | 0.976 | 0.813 | 0.704 |
| 15 | 2.249 | 1.459 | 1.106 | 0.903 | 0.770 |
| 20 | 2.637 | 1.640 | 1.219 | 0.983 | 0.830 |
| 25 | 2.963 | 1.791 | 1.314 | 1.050 | 0.881 |
| 30 | 3.231 | 1.914 | 1.391 | 1.104 | 0.922 |
| 50 | 3.872 | 2.198 | 1.565 | 1.226 | 1.013 |
| $R_i / t = 50$ | | | | | |
| $l / t$ | $f_0^B$ | $f_1^B$ | $f_2^B$ | $f_3^B$ | $f_4^B$ |
| 1 | 1.045 | 0.951 | 0.858 | 0.792 | 0.744 |
| 2 | 1.057 | 0.927 | 0.810 | 0.727 | 0.669 |
| 4 | 1.128 | 0.940 | 0.794 | 0.696 | 0.627 |
| 6 | 1.224 | 0.977 | 0.808 | 0.697 | 0.619 |
| 8 | 1.335 | 1.026 | 0.833 | 0.710 | 0.625 |
| 10 | 1.453 | 1.080 | 0.864 | 0.729 | 0.638 |
| 15 | 1.762 | 1.224 | 0.952 | 0.789 | 0.680 |
| 20 | 2.066 | 1.368 | 1.043 | 0.852 | 0.727 |
| 25 | 2.350 | 1.502 | 1.128 | 0.913 | 0.773 |
| 30 | 2.608 | 1.624 | 1.205 | 0.968 | 0.815 |
| 50 | 3.392 | 1.990 | 1.437 | 1.135 | 0.943 |

Table K14-3. Geometry functions for an axial through-thickness crack in a cylinder — the intersection of the crack with the free surface at $u = t$

| $R_i / t = 100$ | | | | | |
|---|---|---|---|---|---|
| $l / t$ | $f_0^B$ | $f_1^B$ | $f_2^B$ | $f_3^B$ | $f_4^B$ |
| 1 | 1.003 | 0.916 | 0.830 | 0.768 | 0.724 |
| 2 | 1.024 | 0.905 | 0.792 | 0.713 | 0.658 |
| 4 | 1.073 | 0.910 | 0.773 | 0.679 | 0.615 |
| 6 | 1.131 | 0.928 | 0.774 | 0.671 | 0.598 |
| 8 | 1.200 | 0.956 | 0.786 | 0.674 | 0.593 |
| 10 | 1.276 | 0.990 | 0.804 | 0.684 | 0.601 |
| 15 | 1.486 | 1.088 | 0.862 | 0.721 | 0.625 |
| 20 | 1.706 | 1.192 | 0.927 | 0.766 | 0.658 |
| 25 | 1.925 | 1.297 | 0.993 | 0.812 | 0.693 |
| 30 | 2.137 | 1.397 | 1.057 | 0.858 | 0.728 |
| 50 | 2.855 | 1.736 | 1.272 | 1.013 | 0.847 |

## K3. Circumferential cracks in a cylinder

### K3.1 Part circumferential internal surface crack

$K_I$ is given by

$$K_I = \sqrt{\pi a}\left(\sum_{j=0}^{3}\sigma_j f_j\left(a/t, l/a, R_i/t\right) + \sigma_{bg} f_{bg}\left(a/t, l/a, R_i/t\right)\right) \quad . \tag{K16}$$

where $\sigma_j$ ($j = 0$ to 3) are stress components which define the stress state $\sigma$ according to

$$\sigma = \sigma(u) = \sum_{j=0}^{3}\sigma_j\left(\frac{u}{a}\right)^j \qquad \text{for } 0 \le u \le a \quad , \tag{K17}$$

and $\sigma_{bg}$ is the global bending stress. $\sigma$ and $\sigma_{bg}$ are to be taken normal to the prospective crack plane in an uncracked cylinder. $\sigma_j$ is determined by fitting $\sigma$ to Eq. (K17). The coordinate $u$ is defined in Fig. G3.1.

$f_j$ ($j = 0$ to 3) and $f_{bg}$ are geometry functions which are given in Tables K15 and K16 for the deepest point of the crack ($f^A$), and at the intersection of the crack with the free surface ($f^B$), respectively. See Fig. G3.1.

Remark: The cylinder should be long in the transverse direction to the crack so that edge effects do not influence.

Ref.: [K2].

Table K15-1. Geometry functions for a part circumferential internal surface crack in a cylinder — deepest point of crack ($l / a = 2$)

| $a / t$ | $l / a = 2, R_i / t = 1$ | | | | | $l / a = 2, R_i / t = 2$ | | | | |
|---|---|---|---|---|---|---|---|---|---|---|
| | $f_0^A$ | $f_1^A$ | $f_2^A$ | $f_3^A$ | $f_{bg}^A$ | $f_0^A$ | $f_1^A$ | $f_2^A$ | $f_3^A$ | $f_{bg}^A$ |
| 0 | 0.657 | 0.465 | 0.385 | 0.338 | 0.329 | 0.657 | 0.465 | 0.385 | 0.338 | 0.438 |
| 0.1 | 0.661 | 0.468 | 0.387 | 0.339 | 0.355 | 0.659 | 0.466 | 0.385 | 0.337 | 0.456 |
| 0.2 | 0.667 | 0.473 | 0.391 | 0.342 | 0.381 | 0.664 | 0.469 | 0.387 | 0.339 | 0.475 |
| 0.4 | 0.685 | 0.485 | 0.399 | 0.348 | 0.385 | 0.681 | 0.478 | 0.393 | 0.343 | 0.517 |
| 0.6 | 0.723 | 0.505 | 0.413 | 0.359 | 0.484 | 0.707 | 0.492 | 0.403 | 0.350 | 0.567 |
| 0.8 | 0.831 | 0.565 | 0.453 | 0.388 | 0.602 | 0.769 | 0.530 | 0.430 | 0.371 | 0.651 |

| $a / t$ | $l / a = 2, R_i / t = 5$ | | | | | $l / a = 2, R_i / t = 10$ | | | | |
|---|---|---|---|---|---|---|---|---|---|---|
| | $f_0^A$ | $f_1^A$ | $f_2^A$ | $f_3^A$ | $f_{bg}^A$ | $f_0^A$ | $f_1^A$ | $f_2^A$ | $f_3^A$ | $f_{bg}^A$ |
| 0 | 0.657 | 0.465 | 0.385 | 0.338 | 0.548 | 0.657 | 0.465 | 0.385 | 0.338 | 0.597 |
| 0.1 | 0.658 | 0.464 | 0.383 | 0.336 | 0.556 | 0.657 | 0.464 | 0.383 | 0.335 | 0.602 |
| 0.2 | 0.662 | 0.466 | 0.385 | 0.337 | 0.567 | 0.661 | 0.465 | 0.384 | 0.336 | 0.610 |
| 0.4 | 0.677 | 0.472 | 0.388 | 0.339 | 0.596 | 0.676 | 0.470 | 0.387 | 0.337 | 0.632 |
| 0.6 | 0.697 | 0.482 | 0.395 | 0.344 | 0.627 | 0.693 | 0.479 | 0.392 | 0.341 | 0.656 |
| 0.8 | 0.727 | 0.507 | 0.413 | 0.358 | 0.671 | 0.712 | 0.498 | 0.407 | 0.353 | 0.683 |

| $a / t$ | $l / a = 2, R_i / t = 20$ | | | | | $l / a = 2, R_i / t = 40$ | | | | |
|---|---|---|---|---|---|---|---|---|---|---|
| | $f_0^A$ | $f_1^A$ | $f_2^A$ | $f_3^A$ | $f_{bg}^A$ | $f_0^A$ | $f_1^A$ | $f_2^A$ | $f_3^A$ | $f_{bg}^A$ |
| 0 | 0.657 | 0.465 | 0.385 | 0.338 | 0.626 | 0.657 | 0.465 | 0.385 | 0.338 | 0.641 |
| 0.1 | 0.657 | 0.463 | 0.383 | 0.335 | 0.628 | 0.657 | 0.463 | 0.383 | 0.335 | 0.642 |
| 0.2 | 0.661 | 0.465 | 0.383 | 0.335 | 0.634 | 0.660 | 0.464 | 0.383 | 0.335 | 0.647 |
| 0.4 | 0.675 | 0.469 | 0.386 | 0.336 | 0.652 | 0.675 | 0.469 | 0.385 | 0.336 | 0.663 |
| 0.6 | 0.691 | 0.477 | 0.390 | 0.340 | 0.672 | 0.690 | 0.476 | 0.390 | 0.339 | 0.680 |
| 0.8 | 0.703 | 0.493 | 0.403 | 0.350 | 0.689 | 0.699 | 0.490 | 0.402 | 0.349 | 0.692 |

| $a / t$ | $l / a = 2, R_i / t = 80$ | | | | | $l / a = 2, R_i / t \rightarrow \infty$ | | | | |
|---|---|---|---|---|---|---|---|---|---|---|
| | $f_0^A$ | $f_1^A$ | $f_2^A$ | $f_3^A$ | $f_{bg}^A$ | $f_0^A$ | $f_1^A$ | $f_2^A$ | $f_3^A$ | $f_{bg}^A$ |
| 0 | 0.657 | 0.465 | 0.385 | 0.338 | 0.649 | 0.657 | 0.465 | 0.385 | 0.338 | 0.657 |
| 0.1 | 0.657 | 0.463 | 0.382 | 0.335 | 0.649 | 0.657 | 0.463 | 0.382 | 0.335 | 0.657 |
| 0.2 | 0.660 | 0.464 | 0.383 | 0.335 | 0.653 | 0.660 | 0.464 | 0.383 | 0.335 | 0.660 |
| 0.4 | 0.674 | 0.468 | 0.385 | 0.336 | 0.668 | 0.675 | 0.469 | 0.385 | 0.336 | 0.675 |
| 0.6 | 0.688 | 0.475 | 0.389 | 0.339 | 0.683 | 0.691 | 0.475 | 0.389 | 0.339 | 0.691 |
| 0.8 | 0.696 | 0.488 | 0.400 | 0.348 | 0.692 | 0.697 | 0.489 | 0.400 | 0.348 | 0.697 |

Table K15-2. Geometry functions for a part circumferential internal surface crack in a cylinder — deepest point of crack ($l/a = 4$)

| $a/t$ | $l/a = 4$, $R_i/t = 1$ | | | | | $l/a = 4$, $R_i/t = 2$ | | | | |
|---|---|---|---|---|---|---|---|---|---|---|
| | $f_0^A$ | $f_1^A$ | $f_2^A$ | $f_3^A$ | $f_{bg}^A$ | $f_0^A$ | $f_1^A$ | $f_2^A$ | $f_3^A$ | $f_{bg}^A$ |
| 0 | 0.883 | 0.569 | 0.451 | 0.386 | 0.442 | 0.883 | 0.569 | 0.451 | 0.386 | 0.589 |
| 0.1 | 0.863 | 0.562 | 0.447 | 0.382 | 0.461 | 0.874 | 0.565 | 0.448 | 0.382 | 0.602 |
| 0.2 | 0.855 | 0.561 | 0.447 | 0.382 | 0.483 | 0.874 | 0.566 | 0.449 | 0.383 | 0.621 |
| 0.4 | 0.866 | 0.567 | 0.451 | 0.385 | 0.538 | 0.900 | 0.576 | 0.454 | 0.387 | 0.674 |
| 0.6 | 0.932 | 0.599 | 0.471 | 0.400 | 0.628 | 0.956 | 0.601 | 0.470 | 0.398 | 0.753 |
| 0.8 | 1.166 | 0.715 | 0.545 | 0.452 | 0.803 | 1.102 | 0.677 | 0.519 | 0.434 | 0.896 |

| $a/t$ | $l/a = 4$, $R_i/t = 5$ | | | | | $l/a = 4$, $R_i/t = 10$ | | | | |
|---|---|---|---|---|---|---|---|---|---|---|
| | $f_0^A$ | $f_1^A$ | $f_2^A$ | $f_3^A$ | $f_{bg}^A$ | $f_0^A$ | $f_1^A$ | $f_2^A$ | $f_3^A$ | $f_{bg}^A$ |
| 0 | 0.883 | 0.569 | 0.451 | 0.386 | 0.736 | 0.883 | 0.569 | 0.451 | 0.386 | 0.803 |
| 0.1 | 0.880 | 0.566 | 0.448 | 0.382 | 0.743 | 0.882 | 0.567 | 0.448 | 0.382 | 0.807 |
| 0.2 | 0.888 | 0.569 | 0.450 | 0.384 | 0.759 | 0.893 | 0.571 | 0.450 | 0.384 | 0.822 |
| 0.4 | 0.930 | 0.584 | 0.457 | 0.388 | 0.814 | 0.943 | 0.588 | 0.459 | 0.388 | 0.878 |
| 0.6 | 0.988 | 0.607 | 0.471 | 0.397 | 0.882 | 1.005 | 0.611 | 0.472 | 0.397 | 0.946 |
| 0.8 | 1.069 | 0.656 | 0.505 | 0.422 | 0.972 | 1.061 | 0.650 | 0.500 | 0.419 | 1.010 |

| $a/t$ | $l/a = 4$, $R_i/t = 20$ | | | | | $l/a = 4$, $R_i/t = 40$ | | | | |
|---|---|---|---|---|---|---|---|---|---|---|
| | $f_0^A$ | $f_1^A$ | $f_2^A$ | $f_3^A$ | $f_{bg}^A$ | $f_0^A$ | $f_1^A$ | $f_2^A$ | $f_3^A$ | $f_{bg}^A$ |
| 0 | 0.883 | 0.569 | 0.451 | 0.386 | 0.841 | 0.883 | 0.569 | 0.451 | 0.386 | 0.861 |
| 0.1 | 0.883 | 0.567 | 0.448 | 0.382 | 0.844 | 0.884 | 0.567 | 0.448 | 0.382 | 0.864 |
| 0.2 | 0.895 | 0.571 | 0.451 | 0.384 | 0.858 | 0.896 | 0.572 | 0.451 | 0.384 | 0.878 |
| 0.4 | 0.951 | 0.590 | 0.459 | 0.389 | 0.917 | 0.954 | 0.591 | 0.460 | 0.389 | 0.937 |
| 0.6 | 1.016 | 0.614 | 0.473 | 0.398 | 0.985 | 1.022 | 0.615 | 0.473 | 0.398 | 1.006 |
| 0.8 | 1.059 | 0.648 | 0.498 | 0.417 | 1.033 | 1.059 | 0.646 | 0.497 | 0.416 | 1.046 |

| $a/t$ | $l/a = 4$, $R_i/t = 80$ | | | | | $l/a = 4$, $R_i/t \rightarrow \infty$ | | | | |
|---|---|---|---|---|---|---|---|---|---|---|
| | $f_0^A$ | $f_1^A$ | $f_2^A$ | $f_3^A$ | $f_{bg}^A$ | $f_0^A$ | $f_1^A$ | $f_2^A$ | $f_3^A$ | $f_{bg}^A$ |
| 0 | 0.883 | 0.569 | 0.451 | 0.386 | 0.872 | 0.883 | 0.569 | 0.451 | 0.386 | 0.883 |
| 0.1 | 0.884 | 0.567 | 0.448 | 0.382 | 0.874 | 0.884 | 0.567 | 0.449 | 0.383 | 0.884 |
| 0.2 | 0.896 | 0.572 | 0.451 | 0.384 | 0.887 | 0.898 | 0.572 | 0.451 | 0.384 | 0.898 |
| 0.4 | 0.955 | 0.591 | 0.460 | 0.389 | 0.946 | 0.962 | 0.593 | 0.461 | 0.390 | 0.962 |
| 0.6 | 1.023 | 0.615 | 0.473 | 0.398 | 1.015 | 1.038 | 0.620 | 0.476 | 0.399 | 1.038 |
| 0.8 | 1.058 | 0.645 | 0.496 | 0.416 | 1.052 | 1.070 | 0.649 | 0.498 | 0.416 | 1.070 |

Table K15-3. Geometry functions for a part circumferential internal surface crack in a cylinder — deepest point of crack ($l / a = 8$)

| $a / t$ | $l / a = 8, R_i / t = 1$ | | | | | $l / a = 8, R_i / t = 2$ | | | | |
|---|---|---|---|---|---|---|---|---|---|---|
| | $f_0^A$ | $f_1^A$ | $f_2^A$ | $f_3^A$ | $f_{bg}^A$ | $f_0^A$ | $f_1^A$ | $f_2^A$ | $f_3^A$ | $f_{bg}^A$ |
| 0 | 1.022 | 0.632 | 0.491 | 0.415 | 0.511 | 1.022 | 0.632 | 0.491 | 0.415 | 0.681 |
| 0.1 | 0.982 | 0.617 | 0.482 | 0.407 | 0.523 | 1.004 | 0.624 | 0.485 | 0.409 | 0.691 |
| 0.2 | 0.966 | 0.612 | 0.479 | 0.406 | 0.566 | 1.008 | 0.626 | 0.486 | 0.410 | 0.712 |
| 0.4 | 0.992 | 0.624 | 0.486 | 0.410 | 0.593 | 1.062 | 0.646 | 0.497 | 0.416 | 0.784 |
| 0.6 | 1.106 | 0.676 | 0.518 | 0.432 | 0.678 | 1.179 | 0.695 | 0.525 | 0.436 | 0.892 |
| 0.8 | 1.549 | 0.904 | 0.669 | 0.545 | 0.892 | 1.484 | 0.837 | 0.613 | 0.498 | 1.125 |

| $a / t$ | $l / a = 8, R_i / t = 5$ | | | | | $l / a = 8, R_i / t = 10$ | | | | |
|---|---|---|---|---|---|---|---|---|---|---|
| | $f_0^A$ | $f_1^A$ | $f_2^A$ | $f_3^A$ | $f_{bg}^A$ | $f_0^A$ | $f_1^A$ | $f_2^A$ | $f_3^A$ | $f_{bg}^A$ |
| 0 | 1.022 | 0.632 | 0.491 | 0.415 | 0.852 | 1.022 | 0.632 | 0.491 | 0.415 | 0.929 |
| 0.1 | 1.018 | 0.629 | 0.487 | 0.411 | 0.859 | 1.022 | 0.630 | 0.488 | 0.411 | 0.935 |
| 0.2 | 1.039 | 0.636 | 0.491 | 0.413 | 0.885 | 1.051 | 0.640 | 0.493 | 0.414 | 0.966 |
| 0.4 | 1.139 | 0.671 | 0.509 | 0.424 | 0.989 | 1.176 | 0.684 | 0.515 | 0.427 | 1.094 |
| 0.6 | 1.274 | 0.723 | 0.538 | 0.442 | 1.124 | 1.333 | 0.740 | 0.546 | 0.447 | 1.248 |
| 0.8 | 1.479 | 0.821 | 0.600 | 0.487 | 1.314 | 1.487 | 0.819 | 0.597 | 0.484 | 1.402 |

| $a / t$ | $l / a = 8, R_i / t = 20$ | | | | | $l / a = 8, R_i / t = 40$ | | | | |
|---|---|---|---|---|---|---|---|---|---|---|
| | $f_0^A$ | $f_1^A$ | $f_2^A$ | $f_3^A$ | $f_{bg}^A$ | $f_0^A$ | $f_1^A$ | $f_2^A$ | $f_3^A$ | $f_{bg}^A$ |
| 0 | 1.022 | 0.632 | 0.491 | 0.415 | 0.973 | 1.022 | 0.632 | 0.491 | 0.415 | 0.997 |
| 0.1 | 1.025 | 0.631 | 0.489 | 0.411 | 0.979 | 1.026 | 0.632 | 0.489 | 0.411 | 1.003 |
| 0.2 | 1.057 | 0.643 | 0.494 | 0.415 | 1.013 | 1.061 | 0.644 | 0.495 | 0.415 | 1.038 |
| 0.4 | 1.200 | 0.691 | 0.519 | 0.429 | 1.156 | 1.212 | 0.695 | 0.521 | 0.430 | 1.190 |
| 0.6 | 1.376 | 0.754 | 0.552 | 0.450 | 1.332 | 1.403 | 0.762 | 0.556 | 0.453 | 1.380 |
| 0.8 | 1.505 | 0.821 | 0.597 | 0.483 | 1.464 | 1.523 | 0.826 | 0.598 | 0.484 | 1.501 |

| $a / t$ | $l / a = 8, R_i / t = 80$ | | | | | $l / a = 8, R_i / t \to \infty$ | | | | |
|---|---|---|---|---|---|---|---|---|---|---|
| | $f_0^A$ | $f_1^A$ | $f_2^A$ | $f_3^A$ | $f_{bg}^A$ | $f_0^A$ | $f_1^A$ | $f_2^A$ | $f_3^A$ | $f_{bg}^A$ |
| 0 | 1.022 | 0.632 | 0.491 | 0.415 | 1.009 | 1.022 | 0.632 | 0.491 | 0.415 | 1.022 |
| 0.1 | 1.023 | 0.632 | 0.489 | 0.411 | 1.015 | 1.027 | 0.632 | 0.489 | 0.412 | 1.027 |
| 0.2 | 1.061 | 0.644 | 0.495 | 0.415 | 1.050 | 1.066 | 0.645 | 0.496 | 0.416 | 1.066 |
| 0.4 | 1.216 | 0.696 | 0.521 | 0.431 | 1.205 | 1.234 | 0.703 | 0.525 | 0.433 | 1.234 |
| 0.6 | 1.415 | 0.766 | 0.558 | 0.453 | 1.404 | 1.452 | 0.778 | 0.563 | 0.457 | 1.452 |
| 0.8 | 1.534 | 0.828 | 0.599 | 0.484 | 1.523 | 1.573 | 0.840 | 0.604 | 0.487 | 1.573 |

Table K15-4. Geometry functions for a part circumferential internal surface crack in a cylinder — deepest point of crack ($l / a = 16$)

| $a / t$ | $l / a = 16, R_i / t = 1$ | | | | | $l / a = 16, R_i / t = 2$ | | | | |
|---|---|---|---|---|---|---|---|---|---|---|
| | $f_0^A$ | $f_1^A$ | $f_2^A$ | $f_3^A$ | $f_{bg}^A$ | $f_0^A$ | $f_1^A$ | $f_2^A$ | $f_3^A$ | $f_{bg}^A$ |
| 0 | 1.088 | 0.664 | 0.512 | 0.431 | 0.544 | 1.088 | 0.664 | 0.512 | 0.431 | 0.725 |
| 0.1 | 1.035 | 0.643 | 0.499 | 0.420 | 0.581 | 1.064 | 0.653 | 0.504 | 0.424 | 0.731 |
| 0.2 | 1.021 | 0.638 | 0.497 | 0.419 | 0.562 | 1.077 | 0.658 | 0.507 | 0.425 | 0.758 |
| 0.4 | 1.079 | 0.672 | 0.520 | 0.438 | 0.594 | 1.163 | 0.692 | 0.525 | 0.436 | 0.840 |
| 0.6 | 1.200 | 0.730 | 0.557 | 0.464 | 0.675 | 1.353 | 0.771 | 0.572 | 0.468 | 0.966 |
| 0.8 | 1.549 | 0.904 | 0.669 | 0.545 | 0.892 | 1.829 | 1.003 | 0.721 | 0.577 | 1.247 |

| $a / t$ | $l / a = 16, R_i / t = 5$ | | | | | $l / a = 16, R_i / t = 10$ | | | | |
|---|---|---|---|---|---|---|---|---|---|---|
| | $f_0^A$ | $f_1^A$ | $f_2^A$ | $f_3^A$ | $f_{bg}^A$ | $f_0^A$ | $f_1^A$ | $f_2^A$ | $f_3^A$ | $f_{bg}^A$ |
| 0 | 1.088 | 0.664 | 0.512 | 0.431 | 0.907 | 1.088 | 0.664 | 0.512 | 0.431 | 0.989 |
| 0.1 | 1.083 | 0.660 | 0.508 | 0.426 | 0.912 | 1.090 | 0.663 | 0.509 | 0.427 | 0.996 |
| 0.2 | 1.126 | 0.676 | 0.516 | 0.431 | 0.958 | 1.146 | 0.683 | 0.520 | 0.433 | 1.054 |
| 0.4 | 1.291 | 0.736 | 0.547 | 0.450 | 1.112 | 1.361 | 0.760 | 0.560 | 0.458 | 1.258 |
| 0.6 | 1.522 | 0.824 | 0.596 | 0.482 | 1.323 | 1.640 | 0.861 | 0.615 | 0.493 | 1.522 |
| 0.8 | 1.921 | 0.996 | 0.699 | 0.552 | 1.653 | 1.984 | 1.008 | 0.701 | 0.552 | 1.844 |

| $a / t$ | $l / a = 16, R_i / t = 20$ | | | | | $l / a = 16, R_i / t = 40$ | | | | |
|---|---|---|---|---|---|---|---|---|---|---|
| | $f_0^A$ | $f_1^A$ | $f_2^A$ | $f_3^A$ | $f_{bg}^A$ | $f_0^A$ | $f_1^A$ | $f_2^A$ | $f_3^A$ | $f_{bg}^A$ |
| 0 | 1.088 | 0.664 | 0.512 | 0.431 | 1.036 | 1.088 | 0.664 | 0.512 | 0.431 | 1.061 |
| 0.1 | 1.094 | 0.664 | 0.510 | 0.427 | 1.045 | 1.096 | 0.665 | 0.510 | 0.427 | 1.071 |
| 0.2 | 1.157 | 0.687 | 0.522 | 0.434 | 1.109 | 1.163 | 0.689 | 0.523 | 0.435 | 1.139 |
| 0.4 | 1.410 | 0.776 | 0.568 | 0.463 | 1.357 | 1.439 | 0.786 | 0.573 | 0.466 | 1.412 |
| 0.6 | 1.737 | 0.893 | 0.630 | 0.502 | 1.678 | 1.809 | 0.916 | 0.641 | 0.509 | 1.778 |
| 0.8 | 2.043 | 1.022 | 0.706 | 0.554 | 1.979 | 2.106 | 1.039 | 0.714 | 0.558 | 2.073 |

| $a / t$ | $l / a = 16, R_i / t = 80$ | | | | | $l / a = 16, R_i / t \rightarrow \infty$ | | | | |
|---|---|---|---|---|---|---|---|---|---|---|
| | $f_0^A$ | $f_1^A$ | $f_2^A$ | $f_3^A$ | $f_{bg}^A$ | $f_0^A$ | $f_1^A$ | $f_2^A$ | $f_3^A$ | $f_{bg}^A$ |
| 0 | 1.088 | 0.664 | 0.512 | 0.431 | 1.075 | 1.088 | 0.664 | 0.512 | 0.431 | 1.088 |
| 0.1 | 1.095 | 0.665 | 0.510 | 0.427 | 1.084 | 1.095 | 0.664 | 0.510 | 0.427 | 1.095 |
| 0.2 | 1.165 | 0.689 | 0.523 | 0.435 | 1.153 | 1.172 | 0.692 | 0.524 | 0.436 | 1.172 |
| 0.4 | 1.454 | 0.791 | 0.575 | 0.467 | 1.440 | 1.482 | 0.801 | 0.580 | 0.470 | 1.482 |
| 0.6 | 1.854 | 0.931 | 0.648 | 0.513 | 1.838 | 1.943 | 0.960 | 0.663 | 0.521 | 1.943 |
| 0.8 | 2.159 | 1.055 | 0.720 | 0.561 | 2.142 | 2.300 | 1.098 | 0.741 | 0.573 | 2.300 |

Table K15-5.  Geometry functions for a part circumferential internal surface crack in a cylinder — deepest point of crack ($l/a = 32$)

| $a/t$ | $l/a = 32, R_i/t = 1$ | | | | | $l/a = 32, R_i/t = 2$ | | | | |
|---|---|---|---|---|---|---|---|---|---|---|
| | $f_0^A$ | $f_1^A$ | $f_2^A$ | $f_3^A$ | $f_{bg}^A$ | $f_0^A$ | $f_1^A$ | $f_2^A$ | $f_3^A$ | $f_{bg}^A$ |
| 0 | 1.105 | 0.673 | 0.518 | 0.435 | 0.553 | 1.105 | 0.673 | 0.518 | 0.435 | 0.737 |
| 0.1 | 1.054 | 0.653 | 0.505 | 0.425 | 0.562 | 1.086 | 0.665 | 0.512 | 0.430 | 0.746 |
| 0.2 | 1.050 | 0.656 | 0.510 | 0.430 | 0.564 | 1.108 | 0.674 | 0.517 | 0.433 | 0.778 |
| 0.4 | 1.079 | 0.672 | 0.520 | 0.438 | 0.594 | 1.234 | 0.730 | 0.553 | 0.459 | 0.853 |
| 0.6 | 1.200 | 0.730 | 0.557 | 0.464 | 0.675 | 1.421 | 0.811 | 0.601 | 0.492 | 0.973 |
| 0.8 | 1.549 | 0.904 | 0.669 | 0.545 | 0.892 | 1.829 | 1.003 | 0.721 | 0.577 | 1.247 |

| $a/t$ | $l/a = 32, R_i/t = 5$ | | | | | $l/a = 32, R_i/t = 10$ | | | | |
|---|---|---|---|---|---|---|---|---|---|---|
| | $f_0^A$ | $f_1^A$ | $f_2^A$ | $f_3^A$ | $f_{bg}^A$ | $f_0^A$ | $f_1^A$ | $f_2^A$ | $f_3^A$ | $f_{bg}^A$ |
| 0 | 1.105 | 0.673 | 0.518 | 0.435 | 0.921 | 1.105 | 0.673 | 0.518 | 0.435 | 1.005 |
| 0.1 | 1.111 | 0.674 | 0.517 | 0.433 | 0.937 | 1.120 | 0.677 | 0.519 | 0.434 | 1.025 |
| 0.2 | 1.173 | 0.697 | 0.530 | 0.441 | 0.996 | 1.202 | 0.708 | 0.535 | 0.444 | 1.102 |
| 0.4 | 1.377 | 0.774 | 0.572 | 0.467 | 1.181 | 1.479 | 0.810 | 0.590 | 0.479 | 1.361 |
| 0.6 | 1.690 | 0.896 | 0.639 | 0.512 | 1.428 | 1.881 | 0.959 | 0.671 | 0.531 | 1.734 |
| 0.8 | 2.193 | 1.113 | 0.769 | 0.601 | 1.809 | 2.446 | 1.188 | 0.802 | 0.619 | 2.226 |

| $a/t$ | $l/a = 32, R_i/t = 20$ | | | | | $l/a = 32, R_i/t = 40$ | | | | |
|---|---|---|---|---|---|---|---|---|---|---|
| | $f_0^A$ | $f_1^A$ | $f_2^A$ | $f_3^A$ | $f_{bg}^A$ | $f_0^A$ | $f_1^A$ | $f_2^A$ | $f_3^A$ | $f_{bg}^A$ |
| 0 | 1.105 | 0.673 | 0.518 | 0.435 | 1.052 | 1.105 | 0.673 | 0.518 | 0.435 | 1.078 |
| 0.1 | 1.125 | 0.679 | 0.519 | 0.434 | 1.075 | 1.127 | 0.679 | 0.520 | 0.435 | 1.102 |
| 0.2 | 1.220 | 0.714 | 0.539 | 0.447 | 1.169 | 1.231 | 0.718 | 0.541 | 0.448 | 1.204 |
| 0.4 | 1.556 | 0.837 | 0.604 | 0.488 | 1.496 | 1.609 | 0.856 | 0.614 | 0.494 | 1.577 |
| 0.6 | 2.042 | 1.013 | 0.698 | 0.547 | 1.966 | 2.175 | 1.058 | 0.721 | 0.561 | 2.135 |
| 0.8 | 2.627 | 1.240 | 0.826 | 0.630 | 2.571 | 2.776 | 1.284 | 0.845 | 0.641 | 2.726 |

| $a/t$ | $l/a = 32, R_i/t = 80$ | | | | | $l/a = 32, R_i/t \to \infty$ | | | | |
|---|---|---|---|---|---|---|---|---|---|---|
| | $f_0^A$ | $f_1^A$ | $f_2^A$ | $f_3^A$ | $f_{bg}^A$ | $f_0^A$ | $f_1^A$ | $f_2^A$ | $f_3^A$ | $f_{bg}^A$ |
| 0 | 1.105 | 0.673 | 0.518 | 0.435 | 1.091 | 1.105 | 0.673 | 0.518 | 0.435 | 1.105 |
| 0.1 | 1.128 | 0.680 | 0.520 | 0.435 | 1.115 | 1.129 | 0.680 | 0.520 | 0.435 | 1.129 |
| 0.2 | 1.235 | 0.719 | 0.541 | 0.448 | 1.222 | 1.243 | 0.722 | 0.543 | 0.449 | 1.243 |
| 0.4 | 1.641 | 0.867 | 0.620 | 0.497 | 1.625 | 1.693 | 0.885 | 0.629 | 0.503 | 1.693 |
| 0.6 | 2.275 | 1.091 | 0.737 | 0.571 | 2.255 | 2.470 | 1.157 | 0.770 | 0.591 | 2.470 |
| 0.8 | 2.913 | 1.326 | 0.864 | 0.652 | 2.888 | 3.331 | 1.458 | 0.927 | 0.689 | 3.331 |

Table K15-6. Geometry functions for a part circumferential internal surface crack in a cylinder — deepest point of crack ($l/a \to \infty$)

| $a/t$ | $l/a \to \infty$, $R_i/t = 1$ | | | | | $l/a \to \infty$, $R_i/t = 2$ | | | | |
|---|---|---|---|---|---|---|---|---|---|---|
| | $f_0^A$ | $f_1^A$ | $f_2^A$ | $f_3^A$ | $f_{bg}^A$ | $f_0^A$ | $f_1^A$ | $f_2^A$ | $f_3^A$ | $f_{bg}^A$ |
| 0 | 1.122 | 0.683 | 0.526 | 0.441 | 0.561 | 1.122 | 0.683 | 0.526 | 0.441 | 0.748 |
| 0.1 | 1.067 | 0.660 | 0.511 | 0.431 | 0.555 | 1.107 | 0.676 | 0.520 | 0.436 | 0.751 |
| 0.2 | 1.050 | 0.656 | 0.510 | 0.430 | 0.564 | 1.130 | 0.686 | 0.527 | 0.441 | 0.777 |
| 0.4 | 1.079 | 0.672 | 0.520 | 0.438 | 0.594 | 1.234 | 0.730 | 0.553 | 0.459 | 0.853 |
| 0.6 | 1.200 | 0.730 | 0.557 | 0.464 | 0.675 | 1.421 | 0.811 | 0.601 | 0.492 | 0.973 |
| 0.8 | 1.549 | 0.904 | 0.669 | 0.545 | 0.892 | 1.829 | 1.003 | 0.721 | 0.577 | 1.247 |

| $a/t$ | $l/a \to \infty$, $R_i/t = 5$ | | | | | $l/a \to \infty$, $R_i/t = 10$ | | | | |
|---|---|---|---|---|---|---|---|---|---|---|
| | $f_0^A$ | $f_1^A$ | $f_2^A$ | $f_3^A$ | $f_{bg}^A$ | $f_0^A$ | $f_1^A$ | $f_2^A$ | $f_3^A$ | $f_{bg}^A$ |
| 0 | 1.122 | 0.683 | 0.526 | 0.441 | 0.935 | 1.122 | 0.683 | 0.526 | 0.441 | 1.020 |
| 0.1 | 1.140 | 0.688 | 0.527 | 0.441 | 0.954 | 1.155 | 0.694 | 0.530 | 0.443 | 1.049 |
| 0.2 | 1.211 | 0.718 | 0.544 | 0.453 | 1.019 | 1.255 | 0.735 | 0.554 | 0.459 | 1.144 |
| 0.4 | 1.440 | 0.808 | 0.595 | 0.487 | 1.207 | 1.583 | 0.861 | 0.625 | 0.506 | 1.436 |
| 0.6 | 1.768 | 0.937 | 0.669 | 0.535 | 1.462 | 2.060 | 1.046 | 0.726 | 0.572 | 1.848 |
| 0.8 | 2.281 | 1.161 | 0.804 | 0.629 | 1.867 | 2.700 | 1.307 | 0.880 | 0.676 | 2.410 |

| $a/t$ | $l/a \to \infty$, $R_i/t = 20$ | | | | | $l/a \to \infty$, $R_i/t = 40$ | | | | |
|---|---|---|---|---|---|---|---|---|---|---|
| | $f_0^A$ | $f_1^A$ | $f_2^A$ | $f_3^A$ | $f_{bg}^A$ | $f_0^A$ | $f_1^A$ | $f_2^A$ | $f_3^A$ | $f_{bg}^A$ |
| 0 | 1.122 | 0.683 | 0.526 | 0.441 | 1.069 | 1.122 | 0.683 | 0.526 | 0.441 | 1.095 |
| 0.1 | 1.165 | 0.699 | 0.532 | 0.444 | 1.106 | 1.171 | 0.700 | 0.534 | 0.445 | 1.138 |
| 0.2 | 1.287 | 0.747 | 0.561 | 0.464 | 1.224 | 1.310 | 0.756 | 0.566 | 0.467 | 1.273 |
| 0.4 | 1.706 | 0.908 | 0.651 | 0.523 | 1.614 | 1.807 | 0.946 | 0.672 | 0.537 | 1.746 |
| 0.6 | 2.362 | 1.153 | 0.785 | 0.610 | 2.217 | 2.660 | 1.262 | 0.844 | 0.647 | 2.551 |
| 0.8 | 3.212 | 1.485 | 0.973 | 0.734 | 3.015 | 3.834 | 1.702 | 1.086 | 0.805 | 3.695 |

| $a/t$ | $l/a \to \infty$, $R_i/t = 80$ | | | | | $l/a \to \infty$, $R_i/t \to \infty$ | | | | |
|---|---|---|---|---|---|---|---|---|---|---|
| | $f_0^A$ | $f_1^A$ | $f_2^A$ | $f_3^A$ | $f_{bg}^A$ | $f_0^A$ | $f_1^A$ | $f_2^A$ | $f_3^A$ | $f_{bg}^A$ |
| 0 | 1.122 | 0.683 | 0.526 | 0.441 | 1.108 | 1.122 | 0.683 | 0.526 | 0.441 | 1.122 |
| 0.1 | 1.175 | 0.702 | 0.535 | 0.446 | 1.155 | 1.185 | 0.706 | 0.537 | 0.447 | 1.185 |
| 0.2 | 1.326 | 0.762 | 0.569 | 0.469 | 1.303 | 1.364 | 0.777 | 0.578 | 0.475 | 1.364 |
| 0.4 | 1.886 | 0.976 | 0.688 | 0.547 | 1.842 | 2.109 | 1.061 | 0.736 | 0.584 | 2.109 |
| 0.6 | 2.935 | 1.362 | 0.898 | 0.682 | 2.844 | 4.030 | 1.764 | 1.115 | 0.822 | 4.030 |
| 0.8 | 4.570 | 1.960 | 1.221 | 0.889 | 4.460 | 11.949 | 4.546 | 2.573 | 1.734 | 11.949 |

Table K16-1. Geometry functions for a part circumferential internal surface crack in a cylinder — intersection of crack with free surface ($l / a = 2$)

| $a / t$ | $l / a = 2, R_i / t = 1$ | | | | | $l / a = 2, R_i / t = 2$ | | | | |
|---|---|---|---|---|---|---|---|---|---|---|
| | $f_0^B$ | $f_1^B$ | $f_2^B$ | $f_3^B$ | $f_{bg}^B$ | $f_0^B$ | $f_1^B$ | $f_2^B$ | $f_3^B$ | $f_{bg}^B$ |
| 0 | 0.744 | 0.129 | 0.048 | 0.025 | 0.372 | 0.744 | 0.129 | 0.048 | 0.025 | 0.496 |
| 0.1 | 0.721 | 0.121 | 0.045 | 0.024 | 0.367 | 0.731 | 0.122 | 0.046 | 0.024 | 0.492 |
| 0.2 | 0.711 | 0.120 | 0.046 | 0.024 | 0.364 | 0.727 | 0.122 | 0.046 | 0.024 | 0.492 |
| 0.4 | 0.696 | 0.123 | 0.048 | 0.026 | 0.317 | 0.726 | 0.127 | 0.049 | 0.026 | 0.495 |
| 0.6 | 0.730 | 0.136 | 0.055 | 0.030 | 0.381 | 0.769 | 0.141 | 0.056 | 0.030 | 0.527 |
| 0.8 | 0.807 | 0.163 | 0.070 | 0.040 | 0.432 | 0.837 | 0.161 | 0.066 | 0.036 | 0.577 |

| $a / t$ | $l / a = 2, R_i / t = 5$ | | | | | $l / a = 2, R_i / t = 10$ | | | | |
|---|---|---|---|---|---|---|---|---|---|---|
| | $f_0^B$ | $f_1^B$ | $f_2^B$ | $f_3^B$ | $f_{bg}^B$ | $f_0^B$ | $f_1^B$ | $f_2^B$ | $f_3^B$ | $f_{bg}^B$ |
| 0 | 0.744 | 0.129 | 0.048 | 0.025 | 0.620 | 0.744 | 0.129 | 0.048 | 0.025 | 0.676 |
| 0.1 | 0.737 | 0.122 | 0.046 | 0.024 | 0.616 | 0.739 | 0.125 | 0.046 | 0.024 | 0.673 |
| 0.2 | 0.738 | 0.124 | 0.047 | 0.024 | 0.619 | 0.742 | 0.124 | 0.047 | 0.024 | 0.677 |
| 0.4 | 0.753 | 0.131 | 0.051 | 0.027 | 0.635 | 0.765 | 0.133 | 0.051 | 0.027 | 0.699 |
| 0.6 | 0.805 | 0.147 | 0.058 | 0.031 | 0.681 | 0.821 | 0.150 | 0.059 | 0.031 | 0.753 |
| 0.8 | 0.870 | 0.164 | 0.065 | 0.034 | 0.741 | 0.888 | 0.166 | 0.065 | 0.034 | 0.817 |

| $a / t$ | $l / a = 2, R_i / t = 20$ | | | | | $l / a = 2, R_i / t = 40$ | | | | |
|---|---|---|---|---|---|---|---|---|---|---|
| | $f_0^B$ | $f_1^B$ | $f_2^B$ | $f_3^B$ | $f_{bg}^B$ | $f_0^B$ | $f_1^B$ | $f_2^B$ | $f_3^B$ | $f_{bg}^B$ |
| 0 | 0.744 | 0.129 | 0.048 | 0.025 | 0.709 | 0.744 | 0.129 | 0.048 | 0.025 | 0.726 |
| 0.1 | 0.740 | 0.123 | 0.046 | 0.024 | 0.705 | 0.740 | 0.123 | 0.046 | 0.024 | 0.723 |
| 0.2 | 0.744 | 0.124 | 0.047 | 0.024 | 0.710 | 0.745 | 0.124 | 0.047 | 0.024 | 0.727 |
| 0.4 | 0.772 | 0.134 | 0.052 | 0.027 | 0.738 | 0.776 | 0.135 | 0.052 | 0.027 | 0.758 |
| 0.6 | 0.830 | 0.151 | 0.060 | 0.032 | 0.795 | 0.835 | 0.152 | 0.060 | 0.032 | 0.817 |
| 0.8 | 0.899 | 0.168 | 0.065 | 0.034 | 0.862 | 0.904 | 0.169 | 0.066 | 0.034 | 0.886 |

| $a / t$ | $l / a = 2, R_i / t = 80$ | | | | | $l / a = 2, R_i / t \rightarrow \infty$ | | | | |
|---|---|---|---|---|---|---|---|---|---|---|
| | $f_0^B$ | $f_1^B$ | $f_2^B$ | $f_3^B$ | $f_{bg}^B$ | $f_0^B$ | $f_1^B$ | $f_2^B$ | $f_3^B$ | $f_{bg}^B$ |
| 0 | 0.744 | 0.129 | 0.048 | 0.025 | 0.735 | 0.744 | 0.129 | 0.048 | 0.025 | 0.744 |
| 0.1 | 0.740 | 0.123 | 0.046 | 0.024 | 0.732 | 0.740 | 0.123 | 0.046 | 0.024 | 0.740 |
| 0.2 | 0.745 | 0.124 | 0.047 | 0.024 | 0.736 | 0.746 | 0.125 | 0.047 | 0.024 | 0.746 |
| 0.4 | 0.776 | 0.135 | 0.052 | 0.027 | 0.768 | 0.781 | 0.136 | 0.052 | 0.028 | 0.781 |
| 0.6 | 0.835 | 0.152 | 0.060 | 0.032 | 0.826 | 0.844 | 0.155 | 0.061 | 0.032 | 0.844 |
| 0.8 | 0.903 | 0.168 | 0.065 | 0.034 | 0.894 | 0.920 | 0.173 | 0.067 | 0.035 | 0.920 |

Table K16-2. Geometry functions for a part circumferential internal surface crack in a cylinder — intersection of crack with free surface ($l / a = 4$)

| $a / t$ | $l / a = 4, R_i / t = 1$ | | | | | $l / a = 4, R_i / t = 2$ | | | | |
|---|---|---|---|---|---|---|---|---|---|---|
| | $f_0^B$ | $f_1^B$ | $f_2^B$ | $f_3^B$ | $f_{bg}^B$ | $f_0^B$ | $f_1^B$ | $f_2^B$ | $f_3^B$ | $f_{bg}^B$ |
| 0 | 0.704 | 0.119 | 0.041 | 0.020 | 0.352 | 0.704 | 0.119 | 0.041 | 0.020 | 0.469 |
| 0.1 | 0.689 | 0.107 | 0.038 | 0.019 | 0.347 | 0.698 | 0.109 | 0.039 | 0.020 | 0.468 |
| 0.2 | 0.682 | 0.106 | 0.038 | 0.019 | 0.334 | 0.700 | 0.110 | 0.040 | 0.020 | 0.468 |
| 0.4 | 0.677 | 0.110 | 0.041 | 0.021 | 0.287 | 0.723 | 0.121 | 0.046 | 0.024 | 0.473 |
| 0.6 | 0.712 | 0.124 | 0.049 | 0.026 | 0.236 | 0.778 | 0.140 | 0.056 | 0.030 | 0.493 |
| 0.8 | 0.804 | 0.158 | 0.068 | 0.038 | 0.171 | 0.865 | 0.169 | 0.071 | 0.039 | 0.512 |

| $a / t$ | $l / a = 4, R_i / t = 5$ | | | | | $l / a = 4, R_i / t = 10$ | | | | |
|---|---|---|---|---|---|---|---|---|---|---|
| | $f_0^B$ | $f_1^B$ | $f_2^B$ | $f_3^B$ | $f_{bg}^B$ | $f_0^B$ | $f_1^B$ | $f_2^B$ | $f_3^B$ | $f_{bg}^B$ |
| 0 | 0.704 | 0.119 | 0.041 | 0.020 | 0.587 | 0.704 | 0.119 | 0.041 | 0.020 | 0.640 |
| 0.1 | 0.703 | 0.110 | 0.040 | 0.020 | 0.588 | 0.705 | 0.110 | 0.040 | 0.020 | 0.642 |
| 0.2 | 0.712 | 0.113 | 0.041 | 0.021 | 0.596 | 0.716 | 0.114 | 0.042 | 0.021 | 0.652 |
| 0.4 | 0.761 | 0.131 | 0.050 | 0.026 | 0.637 | 0.777 | 0.135 | 0.052 | 0.028 | 0.709 |
| 0.6 | 0.846 | 0.158 | 0.063 | 0.034 | 0.708 | 0.880 | 0.167 | 0.067 | 0.036 | 0.806 |
| 0.8 | 0.949 | 0.187 | 0.077 | 0.041 | 0.791 | 1.001 | 0.199 | 0.081 | 0.044 | 0.918 |

| $a / t$ | $l / a = 4, R_i / t = 20$ | | | | | $l / a = 4, R_i / t = 40$ | | | | |
|---|---|---|---|---|---|---|---|---|---|---|
| | $f_0^B$ | $f_1^B$ | $f_2^B$ | $f_3^B$ | $f_{bg}^B$ | $f_0^B$ | $f_1^B$ | $f_2^B$ | $f_3^B$ | $f_{bg}^B$ |
| 0 | 0.704 | 0.119 | 0.041 | 0.020 | 0.670 | 0.704 | 0.119 | 0.041 | 0.020 | 0.687 |
| 0.1 | 0.705 | 0.110 | 0.040 | 0.020 | 0.673 | 0.706 | 0.110 | 0.040 | 0.020 | 0.689 |
| 0.2 | 0.718 | 0.115 | 0.042 | 0.022 | 0.685 | 0.719 | 0.115 | 0.042 | 0.022 | 0.702 |
| 0.4 | 0.786 | 0.138 | 0.053 | 0.028 | 0.751 | 0.791 | 0.139 | 0.054 | 0.029 | 0.773 |
| 0.6 | 0.902 | 0.173 | 0.070 | 0.038 | 0.864 | 0.915 | 0.177 | 0.072 | 0.039 | 0.895 |
| 0.8 | 1.038 | 0.208 | 0.085 | 0.046 | 0.995 | 1.061 | 0.215 | 0.088 | 0.047 | 1.039 |

| $a / t$ | $l / a = 4, R_i / t = 80$ | | | | | $l / a = 4, R_i / t \to \infty$ | | | | |
|---|---|---|---|---|---|---|---|---|---|---|
| | $f_0^B$ | $f_1^B$ | $f_2^B$ | $f_3^B$ | $f_{bg}^B$ | $f_0^B$ | $f_1^B$ | $f_2^B$ | $f_3^B$ | $f_{bg}^B$ |
| 0 | 0.704 | 0.119 | 0.041 | 0.020 | 0.695 | 0.704 | 0.119 | 0.041 | 0.020 | 0.704 |
| 0.1 | 0.706 | 0.110 | 0.040 | 0.020 | 0.698 | 0.706 | 0.101 | 0.040 | 0.020 | 0.706 |
| 0.2 | 0.719 | 0.115 | 0.042 | 0.022 | 0.711 | 0.720 | 0.116 | 0.042 | 0.022 | 0.720 |
| 0.4 | 0.792 | 0.139 | 0.054 | 0.029 | 0.783 | 0.800 | 0.142 | 0.055 | 0.029 | 0.800 |
| 0.6 | 0.918 | 0.178 | 0.072 | 0.039 | 0.909 | 0.940 | 0.185 | 0.075 | 0.041 | 0.940 |
| 0.8 | 1.069 | 0.217 | 0.089 | 0.047 | 1.059 | 1.110 | 0.229 | 0.094 | 0.050 | 1.110 |

Table K16-3. Geometry functions for a part circumferential internal surface crack in a cylinder — intersection of crack with free surface ($l / a = 8$)

| $a / t$ | $l / a = 8, R_i / t = 1$ | | | | | $l / a = 8, R_i / t = 2$ | | | | |
|---|---|---|---|---|---|---|---|---|---|---|
| | $f_0^B$ | $f_1^B$ | $f_2^B$ | $f_3^B$ | $f_{bg}^B$ | $f_0^B$ | $f_1^B$ | $f_2^B$ | $f_3^B$ | $f_{bg}^B$ |
| 0 | 0.568 | 0.074 | 0.022 | 0.010 | 0.284 | 0.568 | 0.074 | 0.022 | 0.010 | 0.379 |
| 0.1 | 0.566 | 0.068 | 0.002 | 0.009 | 0.269 | 0.573 | 0.069 | 0.021 | 0.009 | 0.379 |
| 0.2 | 0.561 | 0.067 | 0.020 | 0.009 | 0.254 | 0.579 | 0.072 | 0.022 | 0.010 | 0.366 |
| 0.4 | 0.565 | 0.072 | 0.023 | 0.011 | 0.047 | 0.603 | 0.082 | 0.027 | 0.013 | 0.315 |
| 0.6 | 0.585 | 0.080 | 0.027 | 0.013 | 0.000 | 0.650 | 0.098 | 0.035 | 0.018 | 0.237 |
| 0.8 | 0.685 | 0.090 | 0.030 | 0.015 | 0.000 | 0.727 | 0.122 | 0.049 | 0.027 | 0.145 |
| $a / t$ | $l / a = 8, R_i / t = 5$ | | | | | $l / a = 8, R_i / t = 10$ | | | | |
| | $f_0^B$ | $f_1^B$ | $f_2^B$ | $f_3^B$ | $f_{bg}^B$ | $f_0^B$ | $f_1^B$ | $f_2^B$ | $f_3^B$ | $f_{bg}^B$ |
| 0 | 0.568 | 0.074 | 0.022 | 0.010 | 0.473 | 0.568 | 0.074 | 0.022 | 0.010 | 0.516 |
| 0.1 | 0.578 | 0.071 | 0.021 | 0.010 | 0.482 | 0.579 | 0.071 | 0.021 | 0.010 | 0.527 |
| 0.2 | 0.592 | 0.076 | 0.024 | 0.011 | 0.490 | 0.597 | 0.077 | 0.025 | 0.012 | 0.543 |
| 0.4 | 0.648 | 0.095 | 0.033 | 0.017 | 0.525 | 0.671 | 0.102 | 0.037 | 0.019 | 0.608 |
| 0.6 | 0.731 | 0.121 | 0.046 | 0.024 | 0.572 | 0.784 | 0.136 | 0.053 | 0.028 | 0.705 |
| 0.8 | 0.850 | 0.155 | 0.063 | 0.034 | 0.639 | 0.931 | 0.176 | 0.072 | 0.038 | 0.831 |
| $a / t$ | $l / a = 8, R_i / t = 20$ | | | | | $l / a = 8, R_i / t = 40$ | | | | |
| | $f_0^B$ | $f_1^B$ | $f_2^B$ | $f_3^B$ | $f_{bg}^B$ | $f_0^B$ | $f_1^B$ | $f_2^B$ | $f_3^B$ | $f_{bg}^B$ |
| 0 | 0.568 | 0.074 | 0.022 | 0.010 | 0.541 | 0.568 | 0.074 | 0.022 | 0.010 | 0.554 |
| 0.1 | 0.580 | 0.071 | 0.022 | 0.010 | 0.553 | 0.581 | 0.071 | 0.022 | 0.010 | 0.567 |
| 0.2 | 0.600 | 0.078 | 0.025 | 0.012 | 0.572 | 0.602 | 0.079 | 0.025 | 0.012 | 0.587 |
| 0.4 | 0.686 | 0.106 | 0.039 | 0.020 | 0.654 | 0.694 | 0.109 | 0.040 | 0.021 | 0.678 |
| 0.6 | 0.823 | 0.148 | 0.059 | 0.031 | 0.785 | 0.849 | 0.156 | 0.062 | 0.034 | 0.830 |
| 0.8 | 1.001 | 0.196 | 0.080 | 0.043 | 0.954 | 1.055 | 0.211 | 0.087 | 0.047 | 1.032 |
| $a / t$ | $l / a = 8, R_i / t = 80$ | | | | | $l / a = 8, R_i / t \rightarrow \infty$ | | | | |
| | $f_0^B$ | $f_1^B$ | $f_2^B$ | $f_3^B$ | $f_{bg}^B$ | $f_0^B$ | $f_1^B$ | $f_2^B$ | $f_3^B$ | $f_{bg}^B$ |
| 0 | 0.568 | 0.074 | 0.022 | 0.010 | 0.561 | 0.568 | 0.074 | 0.022 | 0.010 | 0.568 |
| 0.1 | 0.581 | 0.071 | 0.022 | 0.010 | 0.574 | 0.580 | 0.071 | 0.022 | 0.010 | 0.580 |
| 0.2 | 0.602 | 0.079 | 0.025 | 0.012 | 0.595 | 0.603 | 0.079 | 0.026 | 0.012 | 0.603 |
| 0.4 | 0.698 | 0.110 | 0.041 | 0.021 | 0.690 | 0.708 | 0.114 | 0.043 | 0.022 | 0.708 |
| 0.6 | 0.864 | 0.161 | 0.065 | 0.035 | 0.854 | 0.894 | 0.171 | 0.069 | 0.038 | 0.894 |
| 0.8 | 1.088 | 0.221 | 0.091 | 0.049 | 1.076 | 1.160 | 0.242 | 0.101 | 0.055 | 1.160 |

Table K16-4. Geometry functions for a part circumferential internal surface crack in a cylinder — intersection of crack with free surface ($l / a = 16$)

| $a / t$ | $l / a = 16, R_i / t = 1$ | | | | | $l / a = 16, R_i / t = 2$ | | | | |
|---|---|---|---|---|---|---|---|---|---|---|
| | $f_0^B$ | $f_1^B$ | $f_2^B$ | $f_3^B$ | $f_{bg}^B$ | $f_0^B$ | $f_1^B$ | $f_2^B$ | $f_3^B$ | $f_{bg}^B$ |
| 0 | 0.432 | 0.039 | 0.008 | 0.003 | 0.216 | 0.432 | 0.039 | 0.008 | 0.003 | 0.288 |
| 0.1 | 0.432 | 0.034 | 0.007 | 0.003 | 0.185 | 0.437 | 0.035 | 0.008 | 0.003 | 0.272 |
| 0.2 | 0.529 | 0.034 | 0.007 | 0.003 | 0.011 | 0.441 | 0.036 | 0.009 | 0.004 | 0.215 |
| 0.4 | 0.629 | 0.033 | 0.006 | 0.003 | 0.000 | 0.455 | 0.042 | 0.011 | 0.005 | 0.000 |
| 0.6 | 0.629 | 0.032 | 0.005 | 0.003 | 0.000 | 0.478 | 0.047 | 0.014 | 0.006 | 0.000 |
| 0.8 | 0.629 | 0.030 | 0.004 | 0.003 | 0.000 | 0.510 | 0.050 | 0.016 | 0.007 | 0.000 |

| $a / t$ | $l / a = 16, R_i / t = 5$ | | | | | $l / a = 16, R_i / t = 10$ | | | | |
|---|---|---|---|---|---|---|---|---|---|---|
| | $f_0^B$ | $f_1^B$ | $f_2^B$ | $f_3^B$ | $f_{bg}^B$ | $f_0^B$ | $f_1^B$ | $f_2^B$ | $f_3^B$ | $f_{bg}^B$ |
| 0 | 0.432 | 0.039 | 0.008 | 0.003 | 0.360 | 0.432 | 0.039 | 0.008 | 0.003 | 0.393 |
| 0.1 | 0.441 | 0.036 | 0.008 | 0.003 | 0.363 | 0.442 | 0.036 | 0.008 | 0.003 | 0.401 |
| 0.2 | 0.452 | 0.040 | 0.010 | 0.004 | 0.360 | 0.457 | 0.041 | 0.011 | 0.005 | 0.412 |
| 0.4 | 0.488 | 0.051 | 0.015 | 0.007 | 0.344 | 0.509 | 0.058 | 0.018 | 0.009 | 0.444 |
| 0.6 | 0.540 | 0.065 | 0.022 | 0.011 | 0.298 | 0.585 | 0.078 | 0.028 | 0.014 | 0.489 |
| 0.8 | 0.612 | 0.086 | 0.032 | 0.017 | 0.236 | 0.696 | 0.111 | 0.043 | 0.023 | 0.552 |

| $a / t$ | $l / a = 16, R_i / t = 20$ | | | | | $l / a = 16, R_i / t = 40$ | | | | |
|---|---|---|---|---|---|---|---|---|---|---|
| | $f_0^B$ | $f_1^B$ | $f_2^B$ | $f_3^B$ | $f_{bg}^B$ | $f_0^B$ | $f_1^B$ | $f_2^B$ | $f_3^B$ | $f_{bg}^B$ |
| 0 | 0.432 | 0.039 | 0.008 | 0.003 | 0.411 | 0.432 | 0.039 | 0.008 | 0.003 | 0.421 |
| 0.1 | 0.443 | 0.036 | 0.008 | 0.003 | 0.422 | 0.443 | 0.036 | 0.008 | 0.003 | 0.433 |
| 0.2 | 0.461 | 0.042 | 0.012 | 0.005 | 0.438 | 0.463 | 0.043 | 0.012 | 0.005 | 0.451 |
| 0.4 | 0.525 | 0.063 | 0.021 | 0.010 | 0.496 | 0.536 | 0.066 | 0.023 | 0.012 | 0.522 |
| 0.6 | 0.624 | 0.090 | 0.034 | 0.018 | 0.585 | 0.657 | 0.100 | 0.038 | 0.020 | 0.639 |
| 0.8 | 0.768 | 0.131 | 0.052 | 0.027 | 0.712 | 0.833 | 0.150 | 0.060 | 0.032 | 0.809 |

| $a / t$ | $l / a = 16, R_i / t = 80$ | | | | | $l / a = 16, R_i / t \rightarrow \infty$ | | | | |
|---|---|---|---|---|---|---|---|---|---|---|
| | $f_0^B$ | $f_1^B$ | $f_2^B$ | $f_3^B$ | $f_{bg}^B$ | $f_0^B$ | $f_1^B$ | $f_2^B$ | $f_3^B$ | $f_{bg}^B$ |
| 0 | 0.432 | 0.039 | 0.008 | 0.003 | 0.427 | 0.432 | 0.039 | 0.008 | 0.003 | 0.432 |
| 0.1 | 0.443 | 0.036 | 0.008 | 0.003 | 0.438 | 0.441 | 0.036 | 0.009 | 0.003 | 0.441 |
| 0.2 | 0.463 | 0.043 | 0.012 | 0.005 | 0.458 | 0.465 | 0.044 | 0.012 | 0.006 | 0.465 |
| 0.4 | 0.543 | 0.069 | 0.024 | 0.012 | 0.536 | 0.554 | 0.072 | 0.026 | 0.013 | 0.554 |
| 0.6 | 0.680 | 0.108 | 0.042 | 0.023 | 0.672 | 0.720 | 0.121 | 0.048 | 0.026 | 0.720 |
| 0.8 | 0.887 | 0.166 | 0.067 | 0.036 | 0.876 | 1.000 | 0.200 | 0.083 | 0.045 | 1.000 |

Table K16-5. Geometry functions for a part circumferential internal surface crack in a cylinder — intersection of crack with free surface ($l / a = 32$)

| $a / t$ | $l / a = 32, R_i / t = 1$ | | | | | $l / a = 32, R_i / t = 2$ | | | | |
|---|---|---|---|---|---|---|---|---|---|---|
| | $f_0^B$ | $f_1^B$ | $f_2^B$ | $f_3^B$ | $f_{bg}^B$ | $f_0^B$ | $f_1^B$ | $f_2^B$ | $f_3^B$ | $f_{bg}^B$ |
| 0 | 0.282 | 0.020 | 0.003 | 0.001 | 0.141 | 0.282 | 0.020 | 0.003 | 0.001 | 0.188 |
| 0.1 | 0.326 | 0.015 | 0.002 | 0.001 | 0.002 | 0.329 | 0.016 | 0.002 | 0.001 | 0.155 |
| 0.2 | 0.426 | 0.012 | 0.001 | 0.000 | 0.000 | 0.331 | 0.016 | 0.001 | 0.001 | 0.002 |
| 0.4 | 0.456 | 0.010 | 0.000 | 0.000 | 0.000 | 0.350 | 0.014 | 0.000 | 0.000 | 0.000 |
| 0.6 | 0.506 | 0.008 | 0.000 | 0.000 | 0.000 | 0.365 | 0.012 | 0.000 | 0.000 | 0.000 |
| 0.8 | 0.526 | 0.006 | 0.000 | 0.000 | 0.000 | 0.375 | 0.010 | 0.000 | 0.000 | 0.000 |
| $a / t$ | $l / a = 32, R_i / t = 5$ | | | | | $l / a = 32, R_i / t = 10$ | | | | |
| | $f_0^B$ | $f_1^B$ | $f_2^B$ | $f_3^B$ | $f_{bg}^B$ | $f_0^B$ | $f_1^B$ | $f_2^B$ | $f_3^B$ | $f_{bg}^B$ |
| 0 | 0.282 | 0.020 | 0.003 | 0.001 | 0.235 | 0.282 | 0.020 | 0.003 | 0.001 | 0.256 |
| 0.1 | 0.331 | 0.016 | 0.003 | 0.001 | 0.263 | 0.332 | 0.017 | 0.003 | 0.001 | 0.299 |
| 0.2 | 0.338 | 0.018 | 0.004 | 0.001 | 0.231 | 0.342 | 0.019 | 0.004 | 0.002 | 0.296 |
| 0.4 | 0.356 | 0.022 | 0.005 | 0.002 | 0.098 | 0.368 | 0.026 | 0.007 | 0.003 | 0.276 |
| 0.6 | 0.373 | 0.026 | 0.007 | 0.003 | 0.000 | 0.400 | 0.034 | 0.010 | 0.005 | 0.227 |
| 0.8 | 0.391 | 0.030 | 0.007 | 0.003 | 0.000 | 0.439 | 0.044 | 0.014 | 0.007 | 0.156 |
| $a / t$ | $l / a = 32, R_i / t = 20$ | | | | | $l / a = 32, R_i / t = 40$ | | | | |
| | $f_0^B$ | $f_1^B$ | $f_2^B$ | $f_3^B$ | $f_{bg}^B$ | $f_0^B$ | $f_1^B$ | $f_2^B$ | $f_3^B$ | $f_{bg}^B$ |
| 0 | 0.282 | 0.020 | 0.003 | 0.001 | 0.269 | 0.282 | 0.020 | 0.003 | 0.001 | 0.275 |
| 0.1 | 0.333 | 0.017 | 0.003 | 0.001 | 0.316 | 0.333 | 0.017 | 0.003 | 0.001 | 0.325 |
| 0.2 | 0.345 | 0.020 | 0.005 | 0.002 | 0.325 | 0.347 | 0.021 | 0.005 | 0.002 | 0.338 |
| 0.4 | 0.379 | 0.029 | 0.008 | 0.004 | 0.345 | 0.388 | 0.032 | 0.010 | 0.005 | 0.375 |
| 0.6 | 0.426 | 0.042 | 0.014 | 0.007 | 0.367 | 0.448 | 0.048 | 0.017 | 0.008 | 0.428 |
| 0.8 | 0.498 | 0.061 | 0.022 | 0.011 | 0.402 | 0.548 | 0.076 | 0.029 | 0.015 | 0.516 |
| $a / t$ | $l / a = 32, R_i / t = 80$ | | | | | $l / a = 32, R_i / t \to \infty$ | | | | |
| | $f_0^B$ | $f_1^B$ | $f_2^B$ | $f_3^B$ | $f_{bg}^B$ | $f_0^B$ | $f_1^B$ | $f_2^B$ | $f_3^B$ | $f_{bg}^B$ |
| 0 | 0.282 | 0.020 | 0.003 | 0.001 | 0.279 | 0.282 | 0.020 | 0.003 | 0.001 | 0.282 |
| 0.1 | 0.334 | 0.017 | 0.003 | 0.001 | 0.400 | 0.333 | 0.017 | 0.003 | 0.001 | 0.333 |
| 0.2 | 0.348 | 0.021 | 0.005 | 0.002 | 0.344 | 0.349 | 0.022 | 0.005 | 0.003 | 0.349 |
| 0.4 | 0.395 | 0.034 | 0.011 | 0.005 | 0.389 | 0.406 | 0.038 | 0.013 | 0.007 | 0.406 |
| 0.6 | 0.468 | 0.054 | 0.020 | 0.010 | 0.460 | 0.511 | 0.069 | 0.026 | 0.014 | 0.511 |
| 0.8 | 0.592 | 0.089 | 0.034 | 0.018 | 0.580 | 0.723 | 0.129 | 0.053 | 0.029 | 0.723 |

Table K16-6. Geometry functions for a part circumferential internal surface crack in a cylinder — intersection of crack with free surface ($l / a \rightarrow \infty$)

| $a / t$ | $l / a \rightarrow \infty, R_i / t = 1$ | | | | | $l / a \rightarrow \infty, R_i / t = 2$ | | | | |
|---|---|---|---|---|---|---|---|---|---|---|
| | $f_0{}^B$ | $f_1{}^B$ | $f_2{}^B$ | $f_3{}^B$ | $f_{bg}{}^B$ | $f_0{}^B$ | $f_1{}^B$ | $f_2{}^B$ | $f_3{}^B$ | $f_{bg}{}^B$ |
| 0 | 0.000 | 0.000 | 0.000 | 0.000 | 0.000 | 0.000 | 0.000 | 0.000 | 0.000 | 0.000 |
| 0.1 | 0.000 | 0.000 | 0.000 | 0.000 | 0.000 | 0.000 | 0.000 | 0.000 | 0.000 | 0.000 |
| 0.2 | 0.000 | 0.000 | 0.000 | 0.000 | 0.000 | 0.000 | 0.000 | 0.000 | 0.000 | 0.000 |
| 0.4 | 0.000 | 0.000 | 0.000 | 0.000 | 0.000 | 0.000 | 0.000 | 0.000 | 0.000 | 0.000 |
| 0.6 | 0.000 | 0.000 | 0.000 | 0.000 | 0.000 | 0.000 | 0.000 | 0.000 | 0.000 | 0.000 |
| 0.8 | 0.000 | 0.000 | 0.000 | 0.000 | 0.000 | 0.000 | 0.000 | 0.000 | 0.000 | 0.000 |

| $a / t$ | $l / a \rightarrow \infty, R_i / t = 5$ | | | | | $l / a \rightarrow \infty, R_i / t = 10$ | | | | |
|---|---|---|---|---|---|---|---|---|---|---|
| | $f_0{}^B$ | $f_1{}^B$ | $f_2{}^B$ | $f_3{}^B$ | $f_{bg}{}^B$ | $f_0{}^B$ | $f_1{}^B$ | $f_2{}^B$ | $f_3{}^B$ | $f_{bg}{}^B$ |
| 0 | 0.000 | 0.000 | 0.000 | 0.000 | 0.000 | 0.000 | 0.000 | 0.000 | 0.000 | 0.000 |
| 0.1 | 0.000 | 0.000 | 0.000 | 0.000 | 0.000 | 0.000 | 0.000 | 0.000 | 0.000 | 0.000 |
| 0.2 | 0.000 | 0.000 | 0.000 | 0.000 | 0.000 | 0.000 | 0.000 | 0.000 | 0.000 | 0.000 |
| 0.4 | 0.000 | 0.000 | 0.000 | 0.000 | 0.000 | 0.000 | 0.000 | 0.000 | 0.000 | 0.000 |
| 0.6 | 0.000 | 0.000 | 0.000 | 0.000 | 0.000 | 0.000 | 0.000 | 0.000 | 0.000 | 0.000 |
| 0.8 | 0.000 | 0.000 | 0.000 | 0.000 | 0.000 | 0.000 | 0.000 | 0.000 | 0.000 | 0.000 |

| $a / t$ | $l / a \rightarrow \infty, R_i / t = 20$ | | | | | $l / a \rightarrow \infty, R_i / t = 40$ | | | | |
|---|---|---|---|---|---|---|---|---|---|---|
| | $f_0{}^B$ | $f_1{}^B$ | $f_2{}^B$ | $f_3{}^B$ | $f_{bg}{}^B$ | $f_0{}^B$ | $f_1{}^B$ | $f_2{}^B$ | $f_3{}^B$ | $f_{bg}{}^B$ |
| 0 | 0.000 | 0.000 | 0.000 | 0.000 | 0.000 | 0.000 | 0.000 | 0.000 | 0.000 | 0.000 |
| 0.1 | 0.000 | 0.000 | 0.000 | 0.000 | 0.000 | 0.000 | 0.000 | 0.000 | 0.000 | 0.000 |
| 0.2 | 0.000 | 0.000 | 0.000 | 0.000 | 0.000 | 0.000 | 0.000 | 0.000 | 0.000 | 0.000 |
| 0.4 | 0.000 | 0.000 | 0.000 | 0.000 | 0.000 | 0.000 | 0.000 | 0.000 | 0.000 | 0.000 |
| 0.6 | 0.000 | 0.000 | 0.000 | 0.000 | 0.000 | 0.000 | 0.000 | 0.000 | 0.000 | 0.000 |
| 0.8 | 0.000 | 0.000 | 0.000 | 0.000 | 0.000 | 0.000 | 0.000 | 0.000 | 0.000 | 0.000 |

| $a / t$ | $l / a \rightarrow \infty, R_i / t = 80$ | | | | | $l / a \rightarrow \infty, R_i / t \rightarrow \infty$ | | | | |
|---|---|---|---|---|---|---|---|---|---|---|
| | $f_0{}^B$ | $f_1{}^B$ | $f_2{}^B$ | $f_3{}^B$ | $f_{bg}{}^B$ | $f_0{}^B$ | $f_1{}^B$ | $f_2{}^B$ | $f_3{}^B$ | $f_{bg}{}^B$ |
| 0 | 0.000 | 0.000 | 0.000 | 0.000 | 0.000 | 0.000 | 0.000 | 0.000 | 0.000 | 0.000 |
| 0.1 | 0.000 | 0.000 | 0.000 | 0.000 | 0.000 | 0.000 | 0.000 | 0.000 | 0.000 | 0.000 |
| 0.2 | 0.000 | 0.000 | 0.000 | 0.000 | 0.000 | 0.000 | 0.000 | 0.000 | 0.000 | 0.000 |
| 0.4 | 0.000 | 0.000 | 0.000 | 0.000 | 0.000 | 0.000 | 0.000 | 0.000 | 0.000 | 0.000 |
| 0.6 | 0.000 | 0.000 | 0.000 | 0.000 | 0.000 | 0.000 | 0.000 | 0.000 | 0.000 | 0.000 |
| 0.8 | 0.000 | 0.000 | 0.000 | 0.000 | 0.000 | 0.000 | 0.000 | 0.000 | 0.000 | 0.000 |

*K3.2      Complete circumferential internal surface crack*

$K_\mathrm{I}$ is given by

$$K_\mathrm{I} = \frac{1}{\sqrt{2\pi a}} \int_0^a \sigma(u) \sum_{j=1}^{3} f_j\left(a/t, R_i/t\right)\left(1 - \frac{u}{a}\right)^{j-\frac{3}{2}} du \quad .$$  (K18)

The stress state $\sigma = \sigma(u)$ is to be taken normal to the prospective crack plane in an uncracked cylinder. The coordinate $u$ is defined in Fig. G3.2.

$f_j$ ($j = 1$ to 3) are geometry functions which are given in Table K17 for the deepest point of the crack ($f^A$). See Fig. G3.2.

Remark:   The cylinder should be long in the transverse direction to the crack so that edge effects do not influence the results.

Ref.:  [K3].

Table K17.  Geometry functions for a complete circumferential internal surface crack in a cylinder.

| $a/t$ | $R_i/t = 7/3$ | | |
|---|---|---|---|
| | $f_1^A$ | $f_2^A$ | $f_3^A$ |
| 0 | 2.000 | 1.327 | 0.218 |
| 0.1 | 2.000 | 1.337 | 0.200 |
| 0.2 | 2.000 | 1.543 | 0.201 |
| 0.3 | 2.000 | 1.880 | 0.228 |
| 0.4 | 2.000 | 2.321 | 0.293 |
| 0.5 | 2.000 | 2.879 | 0.373 |
| 0.6 | 2.000 | 3.720 | 0.282 |
| $a/t$ | $R_i/t = 4$ | | |
| | $f_1^A$ | $f_2^A$ | $f_3^A$ |
| 0 | 2.000 | 1.336 | 0.218 |
| 0.1 | 2.000 | 1.460 | 0.206 |
| 0.2 | 2.000 | 1.839 | 0.241 |
| 0.3 | 2.000 | 2.359 | 0.353 |
| 0.4 | 2.000 | 2.976 | 0.556 |
| 0.5 | 2.000 | 3.688 | 0.837 |
| 0.6 | 2.000 | 4.598 | 1.086 |
| $a/t$ | $R_i/t = 9$ | | |
| | $f_1^A$ | $f_2^A$ | $f_3^A$ |
| 0 | 2.000 | 1.346 | 0.219 |
| 0.1 | 2.000 | 1.591 | 0.211 |
| 0.2 | 2.000 | 2.183 | 0.279 |
| 0.3 | 2.000 | 2.966 | 0.518 |
| 0.4 | 2.000 | 3.876 | 0.956 |
| 0.5 | 2.000 | 4.888 | 1.614 |
| 0.6 | 2.000 | 5.970 | 2.543 |

*K3.3    Part circumferential external surface crack*

$K_I$ is given by

$$K_{\mathrm{I}} = \sqrt{\pi a} \left( \sum_{j=0}^{3} \sigma_j f_j \left( a/t, l/a, R_i/t \right) + \sigma_{bg} f_{bg} \left( a/t, l/a, R_i/t \right) \right) \quad . \tag{K19}$$

where $\sigma_j$ ($j = 0$ to 3) are stress components which define the stress state $\sigma$ according to

$$\sigma = \sigma(u) = \sum_{j=0}^{3} \sigma_j \left( \frac{u}{a} \right)^j \qquad \text{for } 0 \leq u \leq a \quad , \tag{K20}$$

and $\sigma_{bg}$ is the global bending stress. $\sigma$ and $\sigma_{bg}$ are to be taken normal to the prospective crack plane in an uncracked cylinder. $\sigma_j$ is determined by fitting $\sigma$ to Eq. (K20). The coordinate $u$ is defined in Fig. G3.3.

$f_j$ ($j = 0$ to 3) and $f_{bg}$ are geometry functions which are given in Tables K18 and K19 for the deepest point of the crack ($f^A$), and at the intersection of the crack with the free surface ($f^B$), respectively. See Fig. G3.3.

Remark:    The cylinder should be long in the transverse direction to the crack so that edge effects do not influence.

Ref.:  [K1] and [K8].

Table K18.    Geometry functions for a part circumferential external surface crack in a cylinder — deepest point of crack

| $a/t$ | $l/a = 2$, $R_i/t = 5$ | | | | | $l/a = 2$, $R_i/t = 10$ | | | | |
|---|---|---|---|---|---|---|---|---|---|---|
| | $f_0^A$ | $f_1^A$ | $f_2^A$ | $f_3^A$ | $f_{bg}^A$ | $f_0^A$ | $f_1^A$ | $f_2^A$ | $f_3^A$ | $f_{bg}^A$ |
| 0 | 0.659 | 0.471 | 0.387 | 0.337 | 0.659 | 0.659 | 0.471 | 0.387 | 0.337 | 0.659 |
| 0.2 | 0.661 | 0.455 | 0.367 | 0.313 | 0.645 | 0.662 | 0.456 | 0.368 | 0.313 | 0.653 |
| 0.4 | 0.673 | 0.462 | 0.374 | 0.321 | 0.642 | 0.676 | 0.464 | 0.376 | 0.322 | 0.659 |
| 0.6 | 0.686 | 0.467 | 0.378 | 0.325 | 0.638 | 0.690 | 0.470 | 0.381 | 0.328 | 0.664 |
| 0.8 | 0.690 | 0.477 | 0.387 | 0.333 | 0.626 | 0.695 | 0.482 | 0.392 | 0.337 | 0.660 |

| $a/t$ | $l/a = 4$, $R_i/t = 5$ | | | | | $l/a = 4$, $R_i/t = 10$ | | | | |
|---|---|---|---|---|---|---|---|---|---|---|
| | $f_0^A$ | $f_1^A$ | $f_2^A$ | $f_3^A$ | $f_{bg}^A$ | $f_0^A$ | $f_1^A$ | $f_2^A$ | $f_3^A$ | $f_{bg}^A$ |
| 0 | 0.886 | 0.565 | 0.430 | 0.352 | 0.886 | 0.886 | 0.565 | 0.430 | 0.352 | 0.886 |
| 0.2 | 0.905 | 0.560 | 0.425 | 0.347 | 0.885 | 0.903 | 0.559 | 0.425 | 0.347 | 0.891 |
| 0.4 | 0.972 | 0.586 | 0.443 | 0.363 | 0.932 | 0.969 | 0.586 | 0.443 | 0.363 | 0.947 |
| 0.6 | 1.060 | 0.618 | 0.462 | 0.378 | 0.995 | 1.051 | 0.616 | 0.462 | 0.378 | 1.016 |
| 0.8 | 1.133 | 0.659 | 0.493 | 0.403 | 1.041 | 1.108 | 0.654 | 0.491 | 0.403 | 1.059 |

| $a/t$ | $l/a = 8$, $R_i/t = 5$ | | | | | $l/a = 8$, $R_i/t = 10$ | | | | |
|---|---|---|---|---|---|---|---|---|---|---|
| | $f_0^A$ | $f_1^A$ | $f_2^A$ | $f_3^A$ | $f_{bg}^A$ | $f_0^A$ | $f_1^A$ | $f_2^A$ | $f_3^A$ | $f_{bg}^A$ |
| 0 | 1.025 | 0.600 | 0.441 | 0.356 | 1.025 | 1.025 | 0.600 | 0.441 | 0.356 | 1.025 |
| 0.2 | 1.078 | 0.638 | 0.476 | 0.386 | 1.055 | 1.073 | 0.637 | 0.475 | 0.386 | 1.060 |
| 0.4 | 1.253 | 0.702 | 0.513 | 0.413 | 1.202 | 1.246 | 0.700 | 0.512 | 0.413 | 1.219 |
| 0.6 | 1.502 | 0.790 | 0.561 | 0.446 | 1.413 | 1.489 | 0.786 | 0.559 | 0.445 | 1.443 |
| 0.8 | 1.773 | 0.900 | 0.625 | 0.490 | 1.631 | 1.711 | 0.880 | 0.616 | 0.484 | 1.640 |

| $a/t$ | $l/a = 16$, $R_i/t = 5$ | | | | | $l/a = 16$, $R_i/t = 10$ | | | | |
|---|---|---|---|---|---|---|---|---|---|---|
| | $f_0^A$ | $f_1^A$ | $f_2^A$ | $f_3^A$ | $f_{bg}^A$ | $f_0^A$ | $f_1^A$ | $f_2^A$ | $f_3^A$ | $f_{bg}^A$ |
| 0 | 1.079 | 0.635 | 0.473 | 0.388 | 1.079 | 1.079 | 0.635 | 0.473 | 0.388 | 1.079 |
| 0.2 | 1.186 | 0.685 | 0.504 | 0.406 | 1.162 | 1.182 | 0.684 | 0.504 | 0.405 | 1.168 |
| 0.4 | 1.482 | 0.797 | 0.570 | 0.454 | 1.419 | 1.491 | 0.800 | 0.571 | 0.454 | 1.458 |
| 0.6 | 1.907 | 0.951 | 0.654 | 0.508 | 1.779 | 1.949 | 0.962 | 0.658 | 0.511 | 1.883 |
| 0.8 | 2.461 | 1.166 | 0.776 | 0.591 | 2.220 | 2.479 | 1.165 | 0.772 | 0.587 | 2.363 |

| $a/t$ | $l/a = 32$, $R_i/t = 5$ | | | | | $l/a = 32$, $R_i/t = 10$ | | | | |
|---|---|---|---|---|---|---|---|---|---|---|
| | $f_0^A$ | $f_1^A$ | $f_2^A$ | $f_3^A$ | $f_{bg}^A$ | $f_0^A$ | $f_1^A$ | $f_2^A$ | $f_3^A$ | $f_{bg}^A$ |
| 0 | 1.101 | 0.658 | 0.499 | 0.413 | 1.101 | 1.101 | 0.658 | 0.499 | 0.413 | 1.101 |
| 0.2 | 1.252 | 0.716 | 0.525 | 0.422 | 1.225 | 1.252 | 0.716 | 0.525 | 0.421 | 1.237 |
| 0.4 | 1.599 | 0.854 | 0.607 | 0.482 | 1.525 | 1.651 | 0.869 | 0.614 | 0.485 | 1.611 |
| 0.6 | 2.067 | 1.036 | 0.713 | 0.555 | 1.926 | 2.243 | 1.089 | 0.736 | 0.566 | 2.157 |
| 0.8 | 2.740 | 1.313 | 0.875 | 0.666 | 2.491 | 3.011 | 1.387 | 0.904 | 0.678 | 2.845 |

Table K19. Geometry functions for a part circumferential external surface crack in a cylinder — intersection of crack with free surface

| $a/t$ | $l/a=2, R_i/t=5$ | | | | | $l/a=2, R_i/t=10$ | | | | |
|---|---|---|---|---|---|---|---|---|---|---|
| | $f_0^B$ | $f_1^B$ | $f_2^B$ | $f_3^B$ | $f_{bg}^B$ | $f_0^B$ | $f_1^B$ | $f_2^B$ | $f_3^B$ | $f_{bg}^B$ |
| 0 | 0.715 | 0.117 | 0.040 | 0.020 | 0.717 | 0.713 | 0.117 | 0.041 | 0.020 | 0.713 |
| 0.2 | 0.748 | 0.125 | 0.045 | 0.023 | 0.744 | 0.748 | 0.125 | 0.046 | 0.023 | 0.745 |
| 0.4 | 0.781 | 0.133 | 0.050 | 0.026 | 0.771 | 0.783 | 0.133 | 0.051 | 0.026 | 0.777 |
| 0.6 | 0.837 | 0.147 | 0.057 | 0.030 | 0.821 | 0.841 | 0.149 | 0.058 | 0.030 | 0.832 |
| 0.8 | 0.905 | 0.163 | 0.063 | 0.033 | 0.880 | 0.912 | 0.166 | 0.064 | 0.033 | 0.898 |
| $a/t$ | $l/a=4, R_i/t=5$ | | | | | $l/a=4, R_i/t=10$ | | | | |
| | $f_0^B$ | $f_1^B$ | $f_2^B$ | $f_3^B$ | $f_{bg}^B$ | $f_0^B$ | $f_1^B$ | $f_2^B$ | $f_3^B$ | $f_{bg}^B$ |
| 0 | 0.654 | 0.088 | 0.028 | 0.013 | 0.657 | 0.649 | 0.087 | 0.028 | 0.013 | 0.649 |
| 0.2 | 0.724 | 0.110 | 0.040 | 0.020 | 0.719 | 0.723 | 0.110 | 0.040 | 0.020 | 0.720 |
| 0.4 | 0.794 | 0.132 | 0.052 | 0.027 | 0.781 | 0.797 | 0.133 | 0.052 | 0.027 | 0.791 |
| 0.6 | 0.915 | 0.168 | 0.069 | 0.037 | 0.888 | 0.925 | 0.172 | 0.071 | 0.038 | 0.912 |
| 0.8 | 1.059 | 0.208 | 0.087 | 0.046 | 1.012 | 1.081 | 0.215 | 0.089 | 0.048 | 1.058 |
| $a/t$ | $l/a=8, R_i/t=5$ | | | | | $l/a=8, R_i/t=10$ | | | | |
| | $f_0^B$ | $f_1^B$ | $f_2^B$ | $f_3^B$ | $f_{bg}^B$ | $f_0^B$ | $f_1^B$ | $f_2^B$ | $f_3^B$ | $f_{bg}^B$ |
| 0 | 0.527 | 0.047 | 0.010 | 0.003 | 0.537 | 0.518 | 0.043 | 0.009 | 0.002 | 0.521 |
| 0.2 | 0.610 | 0.074 | 0.024 | 0.011 | 0.603 | 0.610 | 0.074 | 0.024 | 0.011 | 0.607 |
| 0.4 | 0.693 | 0.101 | 0.038 | 0.019 | 0.669 | 0.702 | 0.105 | 0.039 | 0.020 | 0.693 |
| 0.6 | 0.818 | 0.139 | 0.055 | 0.029 | 0.762 | 0.856 | 0.152 | 0.062 | 0.033 | 0.834 |
| 0.8 | 0.972 | 0.185 | 0.077 | 0.041 | 0.868 | 1.060 | 0.211 | 0.088 | 0.047 | 1.019 |
| $a/t$ | $l/a=16, R_i/t=5$ | | | | | $l/a=16, R_i/t=10$ | | | | |
| | $f_0^B$ | $f_1^B$ | $f_2^B$ | $f_3^B$ | $f_{bg}^B$ | $f_0^B$ | $f_1^B$ | $f_2^B$ | $f_3^B$ | $f_{bg}^B$ |
| 0 | 0.425 | 0.029 | 0.004 | 0.001 | 0.454 | 0.409 | 0.023 | 0.003 | 0.000 | 0.417 |
| 0.2 | 0.459 | 0.040 | 0.010 | 0.004 | 0.443 | 0.461 | 0.040 | 0.011 | 0.004 | 0.455 |
| 0.4 | 0.493 | 0.050 | 0.016 | 0.007 | 0.432 | 0.513 | 0.057 | 0.019 | 0.009 | 0.493 |
| 0.6 | 0.529 | 0.058 | 0.018 | 0.008 | 0.390 | 0.589 | 0.078 | 0.028 | 0.014 | 0.542 |
| 0.8 | 0.542 | 0.057 | 0.016 | 0.006 | 0.294 | 0.671 | 0.099 | 0.037 | 0.018 | 0.582 |
| $a/t$ | $l/a=32, R_i/t=5$ | | | | | $l/a=32, R_i/t=10$ | | | | |
| | $f_0^B$ | $f_1^B$ | $f_2^B$ | $f_3^B$ | $f_{bg}^B$ | $f_0^B$ | $f_1^B$ | $f_2^B$ | $f_3^B$ | $f_{bg}^B$ |
| 0 | 0.307 | 0.017 | 0.005 | 0.000 | 0.379 | 0.299 | 0.021 | 0.002 | 0.000 | 0.323 |
| 0.2 | 0.306 | 0.016 | 0.003 | 0.000 | 0.265 | 0.309 | 0.020 | 0.003 | 0.000 | 0.296 |
| 0.4 | 0.305 | 0.014 | 0.001 | 0.000 | 0.151 | 0.319 | 0.019 | 0.004 | 0.000 | 0.269 |
| 0.6 | 0.299 | 0.008 | 0.000 | 0.000 | 0.024 | 0.322 | 0.016 | 0.002 | 0.000 | 0.208 |
| 0.8 | 0.292 | 0.003 | 0.000 | 0.000 | 0.255 | 0.305 | 0.005 | 0.000 | 0.000 | 0.103 |

*K3.4      Complete circumferential external surface crack*

$K_I$ is given by

$$K_{\mathrm{I}} = \frac{1}{\sqrt{2\pi a}} \int_0^a \sigma(u) \sum_{j=1}^{3} f_j\left(a/t, R_i/t\right)\left(1 - \frac{u}{a}\right)^{j-\frac{3}{2}} du \quad .$$  (K21)

The stress state $\sigma = \sigma(u)$ is to be taken normal to the prospective crack plane in an uncracked cylinder. The coordinate $u$ is defined in Fig. G3.4.

$f_j$ ($j$ = 1 to 3) are geometry functions which are given in Table K20 for the deepest point of the crack ($f^A$). See Fig. G3.4.

Remark:     The cylinder should be long in the transverse direction to the crack so that edge effects do not influence the results.

Ref.:  [K3].

Table K20.  Geometry functions for a complete circumferential external surface crack in a cylinder

| $a/t$ | $R_i/t = 7/3$ | | |
|---|---|---|---|
| | $f_1^A$ | $f_2^A$ | $f_3^A$ |
| 0 | 2.000 | 1.359 | 0.220 |
| 0.1 | 2.000 | 1.642 | 0.236 |
| 0.2 | 2.000 | 2.127 | 0.307 |
| 0.3 | 2.000 | 2.727 | 0.447 |
| 0.4 | 2.000 | 3.431 | 0.668 |
| 0.5 | 2.000 | 4.271 | 0.951 |
| 0.6 | 2.000 | 5.406 | 1.183 |
| $a/t$ | $R_i/t = 4$ | | |
| | $f_1^A$ | $f_2^A$ | $f_3^A$ |
| 0 | 2.000 | 1.362 | 0.221 |
| 0.1 | 2.000 | 1.659 | 0.221 |
| 0.2 | 2.000 | 2.220 | 0.303 |
| 0.3 | 2.000 | 2.904 | 0.535 |
| 0.4 | 2.000 | 3.701 | 0.857 |
| 0.5 | 2.000 | 4.603 | 1.311 |
| 0.6 | 2.000 | 5.671 | 1.851 |
| $a/t$ | $R_i/t = 9$ | | |
| | $f_1^A$ | $f_2^A$ | $f_3^A$ |
| 0 | 2.000 | 1.364 | 0.220 |
| 0.1 | 2.000 | 1.694 | 0.211 |
| 0.2 | 2.000 | 2.375 | 0.310 |
| 0.3 | 2.000 | 3.236 | 0.630 |
| 0.4 | 2.000 | 4.252 | 1.136 |
| 0.5 | 2.000 | 5.334 | 1.972 |
| 0.6 | 2.000 | 6.606 | 2.902 |

*K3.5      Through-thickness crack*

$K_I$ is given by

$$K_I = \sqrt{\pi l_m / 2}\left( \sum_{j=0}^{4} \sigma_j f_j (l_m / R_m,\, R_i / t) + \sigma_{bg} f_{bg} (l_m / R_m,\, R_i / t) \right) \quad , \qquad (K22)$$

where $\sigma_j$ ($j = 0$ to 4) are stress components according to

$$\sigma = \sigma(u) = \sum_{j=0}^{4} \sigma_j \left( \frac{u}{t} \right)^j \qquad \text{for } 0 \le u \le t \quad , \qquad (K23)$$

and $\sigma_{bg}$ are global bending stress. The parameters $l_m$, $R_i$ and $R_m$ and the coordinate $u$ is defined in Fig. G3.5.

The geometry functions $f_j$ and $f_{bg}$ are given in Tables K21 and K22 for the intersections of the crack with the free surface at $u = 0$ ($f^A$) and at $u = t$ ($f^B$), respectively. See Fig. G3.5.

Remarks:   The cylinder should be long in the transverse direction to the crack so that edge effects do not influence the results. The small negative values given in Table K21-1 to K21-3 are the result of the fitting procedure in [K7].

Ref.:  [K7].

Table K21-1. Geometry functions for a circumferential through-thickness crack in a cylinder — intersection of crack with free surface at $u = 0$ ($R_i / t = 5$, 10)

| $l_m / \pi R_m$ | $f_0^A$ | $f_1^A$ | $f_2^A$ | $f_3^A$ | $f_4^A$ | $f_{bg}^A$ |
|---|---|---|---|---|---|---|
| $R_i / t = 5$ | | | | | | |
| 0.06 | 0.991 | 0.098 | 0.002 | -0.025 | -0.022 | 0.839 |
| 0.10 | 0.967 | 0.131 | 0.022 | -0.011 | -0.024 | 0.820 |
| 0.20 | 1.001 | 0.227 | 0.096 | 0.049 | 0.027 | 0.849 |
| 0.30 | 1.136 | 0.352 | 0.192 | 0.127 | 0.092 | 0.954 |
| 0.40 | 1.354 | 0.503 | 0.304 | 0.215 | 0.165 | 1.114 |
| 0.50 | 1.644 | 0.681 | 0.430 | 0.313 | 0.245 | 1.315 |
| 0.60 | 2.009 | 0.889 | 0.575 | 0.425 | 0.336 | 1.553 |
| 0.70 | 2.461 | 1.137 | 0.747 | 0.556 | 0.443 | 1.830 |
| 0.80 | 3.028 | 1.442 | 0.956 | 0.715 | 0.571 | 2.156 |
| 0.90 | 3.757 | 1.828 | 1.219 | 0.916 | 0.733 | 2.554 |
| 1.00 | 4.719 | 2.334 | 1.564 | 1.177 | 0.944 | 3.055 |
| $R_i / t = 10$ | | | | | | |
| 0.03 | 1.013 | 0.096 | -0.002 | -0.030 | -0.038 | 0.930 |
| 0.06 | 0.972 | 0.128 | 0.013 | -0.021 | -0.036 | 0.891 |
| 0.10 | 0.958 | 0.167 | 0.043 | 0.003 | -0.014 | 0.877 |
| 0.20 | 1.052 | 0.295 | 0.145 | 0.087 | 0.058 | 0.957 |
| 0.30 | 1.276 | 0.461 | 0.269 | 0.186 | 0.140 | 1.143 |
| 0.40 | 1.583 | 0.649 | 0.403 | 0.290 | 0.226 | 1.384 |
| 0.50 | 1.953 | 0.858 | 0.548 | 0.402 | 0.316 | 1.657 |
| 0.60 | 2.385 | 1.091 | 0.708 | 0.523 | 0.415 | 1.952 |
| 0.70 | 2.900 | 1.363 | 0.894 | 0.664 | 0.528 | 2.278 |
| 0.80 | 3.527 | 1.690 | 1.115 | 0.832 | 0.663 | 2.648 |
| 0.90 | 4.328 | 2.105 | 1.396 | 1.044 | 0.834 | 3.094 |
| 1.00 | 5.377 | 2.644 | 1.760 | 1.319 | 1.055 | 3.650 |

Table K21-2. Geometry functions for a circumferential through-thickness crack in a cylinder — intersection of crack with free surface at $u = 0$ ($R_i / t = 20, 50$)

| $l_m / \pi R_m$ | $f_0^A$ | $f_1^A$ | $f_2^A$ | $f_3^A$ | $f_4^A$ | $f_{bg}^A$ |
|---|---|---|---|---|---|---|
| | | | $R_i / t = 20$ | | | |
| 0.015 | 1.026 | 0.095 | -0.003 | -0.028 | -0.038 | 0.984 |
| 0.03 | 0.986 | 0.121 | 0.005 | -0.037 | -0.033 | 0.944 |
| 0.06 | 0.952 | 0.155 | 0.027 | -0.013 | -0.024 | 0.907 |
| 0.10 | 0.958 | 0.206 | 0.069 | 0.022 | 0.001 | 0.912 |
| 0.20 | 1.159 | 0.390 | 0.213 | 0.140 | 0.101 | 1.095 |
| 0.30 | 1.503 | 0.607 | 0.370 | 0.263 | 0.203 | 1.394 |
| 0.40 | 1.900 | 0.831 | 0.526 | 0.383 | 0.300 | 1.720 |
| 0.50 | 2.332 | 1.063 | 0.685 | 0.504 | 0.398 | 2.047 |
| 0.60 | 2.805 | 1.312 | 0.854 | 0.632 | 0.501 | 2.372 |
| 0.70 | 3.369 | 1.605 | 1.052 | 0.782 | 0.622 | 2.730 |
| 0.80 | 4.052 | 1.955 | 1.289 | 0.960 | 0.765 | 3.131 |
| 0.90 | 4.944 | 2.411 | 1.595 | 1.191 | 0.950 | 3.631 |
| 1.00 | 6.104 | 3.000 | 1.990 | 1.489 | 1.189 | 4.250 |
| | | | $R_i / t = 50$ | | | |
| $l_m / \pi R_m$ | $f_0^A$ | $f_1^A$ | $f_2^A$ | $f_3^A$ | $f_4^A$ | $f_{bg}^A$ |
| 0.010 | 1.006 | 0.113 | -0.000 | -0.036 | -0.044 | 0.991 |
| 0.025 | 1.046 | 0.165 | 0.019 | -0.033 | -0.056 | 1.026 |
| 0.05 | 0.944 | 0.178 | 0.037 | -0.013 | -0.018 | 0.922 |
| 0.10 | 1.018 | 0.280 | 0.119 | 0.057 | 0.019 | 0.991 |
| 0.20 | 1.465 | 0.586 | 0.349 | 0.242 | 0.183 | 1.415 |
| 0.30 | 1.983 | 0.880 | 0.556 | 0.404 | 0.316 | 1.883 |
| 0.40 | 2.452 | 1.131 | 0.729 | 0.536 | 0.423 | 2.271 |
| 0.50 | 2.926 | 1.380 | 0.898 | 0.665 | 0.527 | 2.622 |
| 0.60 | 3.435 | 1.643 | 1.076 | 0.799 | 0.635 | 2.959 |
| 0.70 | 4.079 | 1.973 | 1.298 | 0.966 | 0.769 | 3.359 |
| 0.80 | 4.856 | 2.367 | 1.562 | 1.165 | 0.928 | 3.805 |
| 0.90 | 5.910 | 2.899 | 1.919 | 1.433 | 1.143 | 4.394 |
| 1.00 | 7.270 | 3.582 | 2.375 | 1.775 | 1.416 | 5.120 |

Table K21-3. Geometry functions for a circumferential through-thickness crack in a cylinder — intersection of crack with free surface at $u = 0$ ($R_i / t = 100$)

| $l_m / \pi R_m$ | $f_0^A$ | $f_1^A$ | $f_2^A$ | $f_3^A$ | $f_4^A$ | $f_{bg}^A$ |
|---|---|---|---|---|---|---|
| | | | $R_i / t = 100$ | | | |
| 0.006 | 0.933 | 0.107 | 0.004 | -0.032 | -0.040 | 0.928 |
| 0.015 | 0.949 | 0.147 | 0.020 | -0.018 | -0.036 | 0.944 |
| 0.03 | 0.932 | 0.193 | 0.060 | 0.015 | -0.004 | 0.925 |
| 0.06 | 0.967 | 0.278 | 0.133 | 0.077 | 0.049 | 0.959 |
| 0.10 | 1.159 | 0.427 | 0.247 | 0.168 | 0.126 | 1.146 |
| 0.20 | 1.827 | 0.814 | 0.518 | 0.378 | 0.297 | 1.785 |
| 0.30 | 2.348 | 1.099 | 0.715 | 0.529 | 0.419 | 2.252 |
| 0.40 | 2.788 | 1.328 | 0.870 | 0.646 | 0.513 | 2.603 |
| 0.50 | 3.291 | 1.587 | 1.045 | 0.778 | 0.619 | 2.968 |
| 0.60 | 3.833 | 1.862 | 1.229 | 0.916 | 0.729 | 3.316 |
| 0.70 | 4.548 | 2.224 | 1.471 | 1.098 | 0.875 | 3.755 |
| 0.80 | 5.390 | 2.645 | 1.751 | 1.308 | 1.042 | 4.228 |
| 0.90 | 6.620 | 3.262 | 2.163 | 1.616 | 1.289 | 4.922 |
| 1.00 | 8.185 | 4.037 | 2.677 | 2.000 | 1.594 | 5.762 |

Table K22-1. Geometry functions for a circumferential through-thickness crack in a cylinder — intersection of crack with free surface at $u = t$ ($R_i / t$ = 5, 10)

| $l_m / \pi R_m$ | $f_0^B$ | $f_1^B$ | $f_2^B$ | $f_3^B$ | $f_4^B$ | $f_{bg}^B$ |
|---|---|---|---|---|---|---|
| $R_i / t = 5$ |
| 0.06 | 1.108 | 0.984 | 0.883 | 0.813 | 0.767 | 1.085 |
| 0.10 | 1.130 | 0.956 | 0.834 | 0.752 | 0.695 | 1.095 |
| 0.20 | 1.239 | 0.950 | 0.791 | 0.692 | 0.624 | 1.163 |
| 0.30 | 1.351 | 0.962 | 0.776 | 0.665 | 0.591 | 1.222 |
| 0.40 | 1.459 | 0.984 | 0.774 | 0.653 | 0.574 | 1.262 |
| 0.50 | 1.573 | 1.017 | 0.785 | 0.654 | 0.570 | 1.291 |
| 0.60 | 1.705 | 1.066 | 0.810 | 0.668 | 0.577 | 1.317 |
| 0.70 | 1.867 | 1.136 | 0.850 | 0.694 | 0.596 | 1.349 |
| 0.80 | 2.074 | 1.232 | 0.911 | 0.737 | 0.627 | 1.393 |
| 0.90 | 2.341 | 1.362 | 0.994 | 0.798 | 0.675 | 1.458 |
| 1.00 | 2.690 | 1.536 | 1.109 | 0.882 | 0.741 | 1.555 |
| $R_i / t = 10$ |
| $l_m / \pi R_m$ | $f_0^B$ | $f_1^B$ | $f_2^B$ | $f_3^B$ | $f_4^B$ | $f_{bg}^B$ |
| 0.03 | 1.080 | 0.974 | 0.878 | 0.810 | 0.763 | 1.068 |
| 0.06 | 1.091 | 0.934 | 0.813 | 0.732 | 0.673 | 1.075 |
| 0.10 | 1.144 | 0.924 | 0.781 | 0.689 | 0.625 | 1.120 |
| 0.20 | 1.288 | 0.929 | 0.749 | 0.640 | 0.568 | 1.229 |
| 0.30 | 1.404 | 0.941 | 0.735 | 0.616 | 0.539 | 1.298 |
| 0.40 | 1.508 | 0.961 | 0.734 | 0.607 | 0.526 | 1.338 |
| 0.50 | 1.620 | 0.996 | 0.748 | 0.612 | 0.525 | 1.368 |
| 0.60 | 1.759 | 1.052 | 0.778 | 0.631 | 0.538 | 1.401 |
| 0.70 | 1.937 | 1.131 | 0.827 | 0.664 | 0.562 | 1.446 |
| 0.80 | 2.171 | 1.241 | 0.897 | 0.714 | 0.601 | 1.513 |
| 0.90 | 2.473 | 1.387 | 0.992 | 0.784 | 0.655 | 1.606 |
| 1.00 | 2.868 | 1.582 | 1.120 | 0.879 | 0.730 | 1.738 |

Table K22-2. Geometry functions for a circumferential through-thickness crack in a cylinder — intersection of crack with free surface at $u = t$ ($R_i / t = 20, 50$)

| $l_m / \pi R_m$ | $f_0^B$ | $f_1^B$ | $f_2^B$ | $f_3^B$ | $f_4^B$ | $f_{bg}^B$ |
|---|---|---|---|---|---|---|
| $R_i / t = 20$ | | | | | | |
| 0.015 | 1.063 | 0.967 | 0.874 | 0.809 | 0.762 | 1.056 |
| 0.03 | 1.059 | 0.924 | 0.808 | 0.727 | 0.675 | 1.051 |
| 0.06 | 1.101 | 0.903 | 0.763 | 0.672 | 0.610 | 1.093 |
| 0.10 | 1.180 | 0.904 | 0.742 | 0.640 | 0.571 | 1.165 |
| 0.20 | 1.344 | 0.913 | 0.714 | 0.598 | 0.522 | 1.298 |
| 0.30 | 1.456 | 0.924 | 0.702 | 0.577 | 0.498 | 1.365 |
| 0.40 | 1.558 | 0.948 | 0.707 | 0.574 | 0.491 | 1.404 |
| 0.50 | 1.681 | 0.993 | 0.729 | 0.587 | 0.498 | 1.444 |
| 0.60 | 1.847 | 1.065 | 0.771 | 0.615 | 0.518 | 1.500 |
| 0.70 | 2.063 | 1.164 | 0.834 | 0.660 | 0.552 | 1.576 |
| 0.80 | 2.346 | 1.299 | 0.921 | 0.723 | 0.602 | 1.681 |
| 0.90 | 2.707 | 1.475 | 1.036 | 0.808 | 0.668 | 1.818 |
| 1.00 | 3.180 | 1.708 | 1.189 | 0.922 | 0.759 | 2.004 |
| $R_i / t = 50$ | | | | | | |
| 0.010 | 1.035 | 0.924 | 0.818 | 0.743 | 0.691 | 1.030 |
| 0.025 | 1.165 | 0.967 | 0.816 | 0.713 | 0.642 | 1.163 |
| 0.05 | 1.126 | 0.885 | 0.727 | 0.625 | 0.558 | 1.126 |
| 0.10 | 1.273 | 0.898 | 0.707 | 0.593 | 0.516 | 1.265 |
| 0.20 | 1.434 | 0.907 | 0.685 | 0.560 | 0.480 | 1.397 |
| 0.30 | 1.529 | 0.920 | 0.679 | 0.547 | 0.464 | 1.448 |
| 0.40 | 1.641 | 0.956 | 0.694 | 0.554 | 0.466 | 1.495 |
| 0.50 | 1.795 | 1.020 | 0.731 | 0.579 | 0.484 | 1.559 |
| 0.60 | 2.002 | 1.114 | 0.790 | 0.620 | 0.516 | 1.649 |
| 0.70 | 2.261 | 1.236 | 0.869 | 0.677 | 0.560 | 1.757 |
| 0.80 | 2.601 | 1.400 | 0.975 | 0.756 | 0.622 | 1.903 |
| 0.90 | 3.031 | 1.611 | 1.114 | 0.859 | 0.703 | 2.084 |
| 1.00 | 3.604 | 1.893 | 1.300 | 0.997 | 0.813 | 2.334 |

Table K22-3. Geometry functions for a circumferential through-thickness crack in a cylinder — intersection of crack with free surface at $u = t$ ($R_i / t = 100$)

| | | | $R_i / t = 100$ | | | |
|---|---|---|---|---|---|---|
| $l_m / \pi R_m$ | $f_0^B$ | $f_1^B$ | $f_2^B$ | $f_3^B$ | $f_4^B$ | $f_{bg}^B$ |
| 0.006 | 0.951 | 0.845 | 0.746 | 0.675 | 0.628 | 0.947 |
| 0.015 | 1.015 | 0.851 | 0.720 | 0.632 | 0.569 | 1.011 |
| 0.03 | 1.082 | 0.837 | 0.684 | 0.586 | 0.519 | 1.077 |
| 0.06 | 1.219 | 0.850 | 0.667 | 0.556 | 0.483 | 1.211 |
| 0.10 | 1.327 | 0.855 | 0.649 | 0.531 | 0.454 | 1.314 |
| 0.20 | 1.407 | 0.833 | 0.610 | 0.488 | 0.411 | 1.370 |
| 0.30 | 1.457 | 0.828 | 0.593 | 0.469 | 0.391 | 1.378 |
| 0.40 | 1.608 | 0.891 | 0.631 | 0.494 | 0.409 | 1.464 |
| 0.50 | 1.767 | 0.962 | 0.674 | 0.524 | 0.432 | 1.537 |
| 0.60 | 1.997 | 1.070 | 0.744 | 0.575 | 0.471 | 1.650 |
| 0.70 | 2.261 | 1.197 | 0.825 | 0.635 | 0.518 | 1.764 |
| 0.80 | 2.613 | 1.368 | 0.937 | 0.717 | 0.583 | 1.924 |
| 0.90 | 3.082 | 1.598 | 1.089 | 0.830 | 0.673 | 2.139 |
| 1.00 | 3.714 | 1.908 | 1.293 | 0.982 | 0.793 | 2.434 |

## K4. Cracks in a sphere

*K4.1    Through-thickness crack*

$K_I$ is given by

$$K_I = \sqrt{\pi l / 2}\left[\sigma_m f_m\left(l/t, R_i/t\right) + \sigma_b f_b\left(l/t, R_i/t\right)\right] \quad ,$$

(K24)

where $\sigma_m$ and $\sigma_b$ are the membrane and through-thickness bending stress components, respectively, which define the axisymmetrical stress state $\sigma$ according to

$$\sigma = \sigma(u) = \sigma_m + \sigma_b\left(1 - \frac{2u}{t}\right) \qquad \text{for } 0 \le u \le t \quad .$$

(K25)

$\sigma$ is to be taken normal to the prospective crack plane in an uncracked sphere. $\sigma_m$ and $\sigma_b$ are determined by fitting $\sigma$ to Eq. (K25). The coordinate $u$ is defined in Fig. G4.1.

The geometry functions $f_m$ and $f_b$ are given in Table K23 for the intersections of the crack with the free surface at $u = 0$ ($f^A$) and at $u = t$ ($f^B$), respectively. See Fig. G4.1.

Ref.: [K9].

Table K23.    Geometry functions for a through-thickness crack in a sphere.

| $l / t$ | $R_i = 10$ | | | | $R_i = 20$ | | | |
|---|---|---|---|---|---|---|---|---|
| | $f_m{}^A$ | $f_b{}^A$ | $f_m{}^B$ | $f_b{}^B$ | $f_m{}^A$ | $f_b{}^A$ | $f_m{}^B$ | $f_b{}^B$ |
| 0 | 1.000 | 1.000 | 1.000 | -1.000 | 1.000 | 1.000 | 1.000 | -1.000 |
| 2 | 0.919 | 0.993 | 1.240 | -1.031 | 0.941 | 0.995 | 1.144 | -1.020 |
| 4 | 0.894 | 0.993 | 1.637 | -1.074 | 0.897 | 0.992 | 1.401 | -1.050 |
| 6 | 0.944 | 0.997 | 2.083 | -1.111 | 0.895 | 0.993 | 1.700 | -1.080 |
| 8 | 1.059 | 1.003 | 2.549 | -1.143 | 0.932 | 0.996 | 2.020 | -1.106 |
| 10 | 1.231 | 1.011 | 3.016 | -1.170 | 1.003 | 1.001 | 2.351 | -1.130 |
| 15 | 1.915 | 1.031 | 4.124 | -1.226 | 1.309 | 1.014 | 3.186 | -1.180 |
| 20 | 2.968 | 1.050 | 5.084 | -1.272 | 1.799 | 1.028 | 3.981 | -1.219 |

## K5.    Cracks in a bar

### *K5.1    Part circumferential surface crack*

$K_I$ is given by

$$K_I = \sqrt{\pi a} \left[ \sum_{i=0}^{5} \sigma_i f_i \left( \frac{a}{R}, \frac{a}{b} \right) + \sigma_{bg} f_{bg} \left( \frac{a}{R}, \frac{a}{b} \right) \right].$$    (K26)

$\sigma_i$ ($i = 0$ to 5) are stress components which define the stress state $\sigma$ according to

$$\sigma = \sigma(r) = \sum_{i=0}^{5} \sigma_i \left( \frac{r}{R} \right)^i \quad \text{for } 0 \le r \le R,$$    (K27)

and $\sigma_{bg}$ is the global bending stress. $\sigma$ and $\sigma_{bg}$ are to be taken normal to the prospective crack plane in an uncracked bar. The individual stress components are determined by fitting the active stress field to Eq. (K27). The crack depth $a$, crack length $2b$ (not the physical crack length), coordinate $u$ and coordinate $r$ are defined in Fig. G5.1.

The geometry functions $f_i$ and $f_{bg}$ are given in Tables K24-K25 for the deepest point ($f^A$) and the intersections of the crack with the free surface ($f^B$), respectively. See Fig. G5.1.

Ref.:   [K10].

122

Table K24-1.  Geometry function $f_{bg}{}^A$ for a part circumferential surface crack in a round bar at the deepest point

| a/b | a/R=0.0 | a/R=0.1 | a/R=0.2 | a/R=0.3 | a/R=0.4 | a/R=0.5 | a/R=0.6 | a/R=0.7 | a/R=0.8 | a/R=0.9 | a/R=1.0 |
|-----|---------|---------|---------|---------|---------|---------|---------|---------|---------|---------|---------|
| 0.0 | 1.0497 | 0.9711 | 0.9138 | 0.8769 | 0.8597 | 0.8612 | 0.8804 | 0.9177 | 0.9772 | 1.0641 | 1.1839 |
| 0.1 | 1.0427 | 0.9665 | 0.9111 | 0.8758 | 0.8597 | 0.8618 | 0.8812 | 0.9182 | 0.9770 | 1.0628 | 1.1810 |
| 0.2 | 1.0188 | 0.9467 | 0.8943 | 0.8610 | 0.8459 | 0.8484 | 0.8677 | 0.9039 | 0.9614 | 1.0453 | 1.1608 |
| 0.3 | 0.9822 | 0.9152 | 0.8663 | 0.8351 | 0.8210 | 0.8234 | 0.8418 | 0.8766 | 0.9319 | 1.0128 | 1.1243 |
| 0.4 | 0.9367 | 0.8753 | 0.8300 | 0.8008 | 0.7871 | 0.7889 | 0.8057 | 0.8382 | 0.8903 | 0.9669 | 1.0726 |
| 0.5 | 0.8865 | 0.8304 | 0.7884 | 0.7606 | 0.7469 | 0.7472 | 0.7616 | 0.7907 | 0.8382 | 0.9087 | 1.0067 |
| 0.6 | 0.8355 | 0.7839 | 0.7445 | 0.7173 | 0.7026 | 0.7006 | 0.7113 | 0.7358 | 0.7772 | 0.8398 | 0.9276 |
| 0.7 | 0.7871 | 0.7387 | 0.7007 | 0.6732 | 0.6567 | 0.6513 | 0.6573 | 0.6757 | 0.7095 | 0.7621 | 0.8371 |
| 0.8 | 0.7419 | 0.6959 | 0.6585 | 0.6301 | 0.6111 | 0.6017 | 0.6024 | 0.6138 | 0.6386 | 0.6797 | 0.7401 |
| 0.9 | 0.7001 | 0.6558 | 0.6188 | 0.5894 | 0.5678 | 0.5544 | 0.5495 | 0.5536 | 0.5689 | 0.5976 | 0.6421 |
| 1.0 | 0.6614 | 0.6190 | 0.5826 | 0.5525 | 0.5288 | 0.5118 | 0.5016 | 0.4987 | 0.5045 | 0.5206 | 0.5488 |

Table K24-2.  Geometry function $f_0{}^A$ for a part circumferential surface crack in a round bar at the deepest point

| a/b | a/R=0.0 | a/R=0.1 | a/R=0.2 | a/R=0.3 | a/R=0.4 | a/R=0.5 | a/R=0.6 | a/R=0.7 | a/R=0.8 | a/R=0.9 | a/R=1.0 |
|-----|---------|---------|---------|---------|---------|---------|---------|---------|---------|---------|---------|
| 0.0 | 1.0457 | 1.0375 | 1.0500 | 1.0872 | 1.1530 | 1.2515 | 1.3867 | 1.5652 | 1.8046 | 2.1249 | 2.5462 |
| 0.1 | 1.0377 | 1.0316 | 1.0460 | 1.0849 | 1.1522 | 1.2519 | 1.3878 | 1.5665 | 1.8054 | 2.1244 | 2.5434 |
| 0.2 | 1.0132 | 1.0100 | 1.0263 | 1.0662 | 1.1334 | 1.2320 | 1.3659 | 1.5417 | 1.7763 | 2.0893 | 2.5002 |
| 0.3 | 0.9761 | 0.9762 | 0.9943 | 1.0341 | 1.0999 | 1.1955 | 1.3249 | 1.4947 | 1.7213 | 2.0235 | 2.4205 |
| 0.4 | 0.9305 | 0.9339 | 0.9531 | 0.9921 | 1.0550 | 1.1458 | 1.2684 | 1.4294 | 1.6443 | 1.9313 | 2.3083 |
| 0.5 | 0.8803 | 0.8865 | 0.9062 | 0.9435 | 1.0022 | 1.0865 | 1.2003 | 1.3497 | 1.5496 | 1.8166 | 2.1677 |
| 0.6 | 0.8296 | 0.8376 | 0.8569 | 0.8914 | 0.9449 | 1.0212 | 1.1242 | 1.2597 | 1.4410 | 1.6834 | 2.0024 |
| 0.7 | 0.7816 | 0.7902 | 0.8081 | 0.8390 | 0.8862 | 0.9534 | 1.0440 | 1.1633 | 1.3231 | 1.5368 | 1.8179 |
| 0.8 | 0.7372 | 0.7453 | 0.7612 | 0.7880 | 0.8286 | 0.8862 | 0.9638 | 1.0659 | 1.2025 | 1.3849 | 1.6244 |
| 0.9 | 0.6962 | 0.7034 | 0.7171 | 0.7399 | 0.7743 | 0.8227 | 0.8877 | 0.9729 | 1.0862 | 1.2367 | 1.4336 |
| 1.0 | 0.6586 | 0.6649 | 0.6769 | 0.6965 | 0.7255 | 0.7659 | 0.8197 | 0.8895 | 0.9812 | 1.1015 | 1.2572 |

Table K24-3. Geometry function $f_1^A$ for a part circumferential surface crack in a round bar at the deepest point

| a/b | a/R=0.0 | a/R=0.1 | a/R=0.2 | a/R=0.3 | a/R=0.4 | a/R=0.5 | a/R=0.6 | a/R=0.7 | a/R=0.8 | a/R=0.9 | a/R=1.0 |
|-----|---------|---------|---------|---------|---------|---------|---------|---------|---------|---------|---------|
| 0.0 | 1.0409 | 0.9708 | 0.9218 | 0.8949 | 0.8915 | 0.9125 | 0.9592 | 1.0349 | 1.1516 | 1.3237 | 1.5651 |
| 0.1 | 1.0368 | 0.9670 | 0.9187 | 0.8929 | 0.8906 | 0.9127 | 0.9602 | 1.0362 | 1.1527 | 1.3237 | 1.5633 |
| 0.2 | 1.0148 | 0.9476 | 0.9012 | 0.8766 | 0.8747 | 0.8965 | 0.9430 | 1.0173 | 1.1312 | 1.2983 | 1.5325 |
| 0.3 | 0.9791 | 0.9161 | 0.8723 | 0.8487 | 0.8464 | 0.8667 | 0.9106 | 0.9812 | 1.0901 | 1.2504 | 1.4756 |
| 0.4 | 0.9340 | 0.8760 | 0.8349 | 0.8121 | 0.8088 | 0.8263 | 0.8660 | 0.9311 | 1.0326 | 1.1831 | 1.3955 |
| 0.5 | 0.8839 | 0.8309 | 0.7923 | 0.7697 | 0.7645 | 0.7782 | 0.8123 | 0.8701 | 0.9618 | 1.0994 | 1.2950 |
| 0.6 | 0.8331 | 0.7841 | 0.7474 | 0.7243 | 0.7165 | 0.7254 | 0.7526 | 0.8013 | 0.8808 | 1.0024 | 1.1770 |
| 0.7 | 0.7851 | 0.7389 | 0.7029 | 0.6786 | 0.6674 | 0.6707 | 0.6899 | 0.7279 | 0.7932 | 0.8957 | 1.0454 |
| 0.8 | 0.7406 | 0.6961 | 0.6602 | 0.6342 | 0.6193 | 0.6166 | 0.6274 | 0.6540 | 0.7039 | 0.7856 | 0.9077 |
| 0.9 | 0.6995 | 0.6561 | 0.6201 | 0.5925 | 0.5741 | 0.5657 | 0.5684 | 0.5839 | 0.6184 | 0.6789 | 0.7725 |
| 1.0 | 0.6615 | 0.6194 | 0.5836 | 0.5549 | 0.5337 | 0.5206 | 0.5161 | 0.5217 | 0.5420 | 0.5824 | 0.6484 |

Table K24-4. Geometry function $f_2^A$ for a part circumferential surface crack in a round bar at the deepest point.

| a/b | a/R=0.0 | a/R=0.1 | a/R=0.2 | a/R=0.3 | a/R=0.4 | a/R=0.5 | a/R=0.6 | a/R=0.7 | a/R=0.8 | a/R=0.9 | a/R=1.0 |
|-----|---------|---------|---------|---------|---------|---------|---------|---------|---------|---------|---------|
| 0.0 | 1.0308 | 0.9082 | 0.8139 | 0.7481 | 0.7108 | 0.7021 | 0.7221 | 0.7724 | 0.8609 | 0.9971 | 1.1905 |
| 0.1 | 1.0290 | 0.9058 | 0.8117 | 0.7465 | 0.7101 | 0.7023 | 0.7230 | 0.7736 | 0.8619 | 0.9973 | 1.1891 |
| 0.2 | 1.0087 | 0.8882 | 0.7961 | 0.7322 | 0.6964 | 0.6887 | 0.7088 | 0.7584 | 0.8448 | 0.9774 | 1.1652 |
| 0.3 | 0.9743 | 0.8587 | 0.7698 | 0.7076 | 0.6722 | 0.6638 | 0.6822 | 0.7292 | 0.8121 | 0.9397 | 1.1208 |
| 0.4 | 0.9302 | 0.8208 | 0.7357 | 0.6753 | 0.6400 | 0.6300 | 0.6457 | 0.6888 | 0.7663 | 0.8867 | 1.0583 |
| 0.5 | 0.8808 | 0.7778 | 0.6967 | 0.6379 | 0.6021 | 0.5898 | 0.6016 | 0.6395 | 0.7099 | 0.8207 | 0.9798 |
| 0.6 | 0.8303 | 0.7333 | 0.6555 | 0.5978 | 0.5609 | 0.5456 | 0.5526 | 0.5839 | 0.6454 | 0.7443 | 0.8877 |
| 0.7 | 0.7824 | 0.6901 | 0.6148 | 0.5575 | 0.5189 | 0.4999 | 0.5012 | 0.5247 | 0.5756 | 0.6603 | 0.7850 |
| 0.8 | 0.7378 | 0.6491 | 0.5757 | 0.5184 | 0.4778 | 0.4548 | 0.4501 | 0.4652 | 0.5046 | 0.5736 | 0.6776 |
| 0.9 | 0.6966 | 0.6109 | 0.5391 | 0.4817 | 0.4393 | 0.4125 | 0.4020 | 0.4088 | 0.4367 | 0.4898 | 0.5723 |
| 1.0 | 0.6587 | 0.5760 | 0.5059 | 0.4488 | 0.4051 | 0.3753 | 0.3597 | 0.3591 | 0.3763 | 0.4142 | 0.4759 |

Table K24-5.  Geometry function $f_3^A$ for a part circumferential surface crack in a round bar at the deepest point

| a/b | a/R=0.0 | a/R=0.1 | a/R=0.2 | a/R=0.3 | a/R=0.4 | a/R=0.5 | a/R=0.6 | a/R=0.7 | a/R=0.8 | a/R=0.9 | a/R=1.0 |
|-----|---------|---------|---------|---------|---------|---------|---------|---------|---------|---------|---------|
| 0.0 | 1.0219 | 0.8510 | 0.7229 | 0.6346 | 0.5833 | 0.5658 | 0.5794 | 0.6223 | 0.6986 | 0.8134 | 0.9723 |
| 0.1 | 1.0214 | 0.8497 | 0.7214 | 0.6335 | 0.5828 | 0.5660 | 0.5801 | 0.6233 | 0.6994 | 0.8137 | 0.9714 |
| 0.2 | 1.0025 | 0.8335 | 0.7074 | 0.6209 | 0.5709 | 0.5544 | 0.5682 | 0.6106 | 0.6852 | 0.7973 | 0.9518 |
| 0.3 | 0.9694 | 0.8059 | 0.6834 | 0.5990 | 0.5499 | 0.5331 | 0.5457 | 0.5862 | 0.6580 | 0.7661 | 0.9154 |
| 0.4 | 0.9265 | 0.7700 | 0.6521 | 0.5702 | 0.5218 | 0.5041 | 0.5148 | 0.5522 | 0.6199 | 0.7223 | 0.8640 |
| 0.5 | 0.8780 | 0.7292 | 0.6162 | 0.5368 | 0.4887 | 0.4697 | 0.4774 | 0.5109 | 0.5729 | 0.6678 | 0.7995 |
| 0.6 | 0.8282 | 0.6867 | 0.5783 | 0.5010 | 0.4528 | 0.4317 | 0.4359 | 0.4641 | 0.5192 | 0.6045 | 0.7236 |
| 0.7 | 0.7807 | 0.6455 | 0.5408 | 0.4650 | 0.4161 | 0.3924 | 0.3922 | 0.4143 | 0.4609 | 0.5349 | 0.6390 |
| 0.8 | 0.7362 | 0.6064 | 0.5049 | 0.4301 | 0.3802 | 0.3537 | 0.3487 | 0.3642 | 0.4017 | 0.4630 | 0.5504 |
| 0.9 | 0.6951 | 0.5699 | 0.4713 | 0.3975 | 0.3468 | 0.3175 | 0.3080 | 0.3169 | 0.3450 | 0.3935 | 0.4636 |
| 1.0 | 0.6575 | 0.5366 | 0.4408 | 0.3683 | 0.3173 | 0.2859 | 0.2723 | 0.2752 | 0.2946 | 0.3307 | 0.3840 |

Table K24-6.  Geometry function $f_4^A$ for a part circumferential surface crack in a round bar at the deepest point

| a/b | a/R=0.0 | a/R=0.1 | a/R=0.2 | a/R=0.3 | a/R=0.4 | a/R=0.5 | a/R=0.6 | a/R=0.7 | a/R=0.8 | a/R=0.9 | a/R=1.0 |
|-----|---------|---------|---------|---------|---------|---------|---------|---------|---------|---------|---------|
| 0.0 | 1.0028 | 0.7958 | 0.6458 | 0.5464 | 0.4910 | 0.4731 | 0.4860 | 0.5250 | 0.5918 | 0.6901 | 0.8235 |
| 0.1 | 1.0030 | 0.7951 | 0.6450 | 0.5458 | 0.4908 | 0.4734 | 0.4867 | 0.5259 | 0.5926 | 0.6904 | 0.8228 |
| 0.2 | 0.9851 | 0.7802 | 0.6323 | 0.5346 | 0.4805 | 0.4633 | 0.4765 | 0.5149 | 0.5804 | 0.6764 | 0.8063 |
| 0.3 | 0.9533 | 0.7543 | 0.6103 | 0.5150 | 0.4619 | 0.4447 | 0.4570 | 0.4939 | 0.5571 | 0.6499 | 0.7754 |
| 0.4 | 0.9117 | 0.7203 | 0.5814 | 0.4890 | 0.4370 | 0.4194 | 0.4301 | 0.4646 | 0.5244 | 0.6125 | 0.7318 |
| 0.5 | 0.8645 | 0.6816 | 0.5482 | 0.4588 | 0.4076 | 0.3892 | 0.3977 | 0.4289 | 0.4841 | 0.5659 | 0.6769 |
| 0.6 | 0.8158 | 0.6412 | 0.5131 | 0.4264 | 0.3758 | 0.3559 | 0.3615 | 0.3885 | 0.4379 | 0.5118 | 0.6123 |
| 0.7 | 0.7690 | 0.6018 | 0.4785 | 0.3939 | 0.3432 | 0.3213 | 0.3233 | 0.3453 | 0.3878 | 0.4522 | 0.5401 |
| 0.8 | 0.7251 | 0.5646 | 0.4453 | 0.3625 | 0.3114 | 0.2873 | 0.2854 | 0.3019 | 0.3367 | 0.3906 | 0.4646 |
| 0.9 | 0.6845 | 0.5298 | 0.4143 | 0.3332 | 0.2818 | 0.2557 | 0.2500 | 0.2609 | 0.2878 | 0.3310 | 0.3904 |
| 1.0 | 0.6473 | 0.4982 | 0.3863 | 0.3071 | 0.2559 | 0.2281 | 0.2191 | 0.2249 | 0.2444 | 0.2770 | 0.3224 |

Table K24-7.  Geometry function $f_5^A$ for a part circumferential surface crack in a round bar at the deepest point

| a/b | a/R=0.0 | a/R=0.1 | a/R=0.2 | a/R=0.3 | a/R=0.4 | a/R=0.5 | a/R=0.6 | a/R=0.7 | a/R=0.8 | a/R=0.9 | a/R=1.0 |
|-----|---------|---------|---------|---------|---------|---------|---------|---------|---------|---------|---------|
| 0.0 | 0.9690 | 0.7411 | 0.5803 | 0.4773 | 0.4226 | 0.4067 | 0.4202 | 0.4557 | 0.5144 | 0.5994 | 0.7140 |
| 0.1 | 0.9695 | 0.7409 | 0.5800 | 0.4771 | 0.4227 | 0.4072 | 0.4209 | 0.4565 | 0.5150 | 0.5996 | 0.7136 |
| 0.2 | 0.9525 | 0.7271 | 0.5685 | 0.4672 | 0.4136 | 0.3983 | 0.4119 | 0.4469 | 0.5044 | 0.5875 | 0.6993 |
| 0.3 | 0.9219 | 0.7026 | 0.5482 | 0.4494 | 0.3970 | 0.3818 | 0.3947 | 0.4284 | 0.4840 | 0.5643 | 0.6725 |
| 0.4 | 0.8819 | 0.6705 | 0.5214 | 0.4257 | 0.3746 | 0.3593 | 0.3710 | 0.4027 | 0.4553 | 0.5317 | 0.6345 |
| 0.5 | 0.8362 | 0.6337 | 0.4905 | 0.3981 | 0.3482 | 0.3324 | 0.3422 | 0.3712 | 0.4200 | 0.4910 | 0.5867 |
| 0.6 | 0.7889 | 0.5954 | 0.4579 | 0.3686 | 0.3195 | 0.3027 | 0.3101 | 0.3356 | 0.3794 | 0.4437 | 0.5304 |
| 0.7 | 0.7433 | 0.5580 | 0.4257 | 0.3390 | 0.2902 | 0.2718 | 0.2762 | 0.2974 | 0.3354 | 0.3916 | 0.4674 |
| 0.8 | 0.7004 | 0.5225 | 0.3949 | 0.3104 | 0.2616 | 0.2414 | 0.2425 | 0.2590 | 0.2905 | 0.3377 | 0.4015 |
| 0.9 | 0.6606 | 0.4895 | 0.3663 | 0.2838 | 0.2351 | 0.2132 | 0.2110 | 0.2227 | 0.2474 | 0.2854 | 0.3368 |
| 1.0 | 0.6242 | 0.4595 | 0.3404 | 0.2603 | 0.2120 | 0.1888 | 0.1838 | 0.1910 | 0.2092 | 0.2380 | 0.2774 |

Table K25-1.  Geometry function $f_{\mathrm{bg}}^{\mathrm{B}}$ for a part circumferential surface crack in a round bar at the intersections of the crack with the free surface

| $a/b$ | $a/R$=0.0 | $a/R$=0.1 | $a/R$=0.2 | $a/R$=0.3 | $a/R$=0.4 | $a/R$=0.5 | $a/R$=0.6 | $a/R$=0.7 | $a/R$=0.8 | $a/R$=0.9 | $a/R$=1.0 |
|---|---|---|---|---|---|---|---|---|---|---|---|
| 0.0 | 0.1696 | 0.3057 | 0.4110 | 0.4931 | 0.5595 | 0.6177 | 0.6753 | 0.7397 | 0.8180 | 0.9175 | 1.0450 |
| 0.1 | 0.4108 | 0.4634 | 0.5071 | 0.5457 | 0.5833 | 0.6237 | 0.6710 | 0.7293 | 0.8039 | 0.9001 | 1.0234 |
| 0.2 | 0.5654 | 0.5710 | 0.5799 | 0.5940 | 0.6153 | 0.6456 | 0.6870 | 0.7418 | 0.8143 | 0.9091 | 1.0310 |
| 0.3 | 0.6520 | 0.6378 | 0.6321 | 0.6359 | 0.6503 | 0.6765 | 0.7154 | 0.7688 | 0.8406 | 0.9355 | 1.0579 |
| 0.4 | 0.6892 | 0.6734 | 0.6665 | 0.6696 | 0.6835 | 0.7095 | 0.7483 | 0.8018 | 0.8740 | 0.9699 | 1.0943 |
| 0.5 | 0.6957 | 0.6874 | 0.6861 | 0.6931 | 0.7098 | 0.7376 | 0.7778 | 0.8323 | 0.9058 | 1.0034 | 1.1303 |
| 0.6 | 0.6901 | 0.6892 | 0.6934 | 0.7046 | 0.7242 | 0.7541 | 0.7959 | 0.8519 | 0.9270 | 1.0265 | 1.1560 |
| 0.7 | 0.6873 | 0.6869 | 0.6916 | 0.7033 | 0.7236 | 0.7542 | 0.7970 | 0.8543 | 0.9308 | 1.0318 | 1.1628 |
| 0.8 | 0.6877 | 0.6830 | 0.6845 | 0.6937 | 0.7123 | 0.7418 | 0.7839 | 0.8408 | 0.9170 | 1.0174 | 1.1472 |
| 0.9 | 0.6878 | 0.6785 | 0.6759 | 0.6815 | 0.6967 | 0.7229 | 0.7618 | 0.8152 | 0.8874 | 0.9831 | 1.1071 |
| 1.0 | 0.6841 | 0.6744 | 0.6700 | 0.6723 | 0.6831 | 0.7036 | 0.7356 | 0.7809 | 0.8438 | 0.9286 | 1.0400 |

Table K25-2.  Geometry function $f_0^{\mathrm{B}}$ for a part circumferential surface crack in a round bar at the intersections of the crack with the free surface

| $a/b$ | $a/R$=0.0 | $a/R$=0.1 | $a/R$=0.2 | $a/R$=0.3 | $a/R$=0.4 | $a/R$=0.5 | $a/R$=0.6 | $a/R$=0.7 | $a/R$=0.8 | $a/R$=0.9 | $a/R$=1.0 |
|---|---|---|---|---|---|---|---|---|---|---|---|
| 0.0 | 0.2311 | 0.4109 | 0.5589 | 0.6893 | 0.8158 | 0.9524 | 1.1130 | 1.3126 | 1.5697 | 1.9039 | 2.3350 |
| 0.1 | 0.4115 | 0.5240 | 0.6258 | 0.7266 | 0.8358 | 0.9630 | 1.1178 | 1.3113 | 1.5611 | 1.8859 | 2.3049 |
| 0.2 | 0.5369 | 0.6047 | 0.6756 | 0.7566 | 0.8544 | 0.9757 | 1.1276 | 1.3187 | 1.5658 | 1.8879 | 2.3037 |
| 0.3 | 0.6172 | 0.6583 | 0.7104 | 0.7791 | 0.8697 | 0.9874 | 1.1377 | 1.3282 | 1.5756 | 1.8987 | 2.3167 |
| 0.4 | 0.6625 | 0.6901 | 0.7323 | 0.7939 | 0.8798 | 0.9947 | 1.1436 | 1.3337 | 1.5819 | 1.9075 | 2.3296 |
| 0.5 | 0.6824 | 0.7056 | 0.7434 | 0.8007 | 0.8827 | 0.9943 | 1.1405 | 1.3289 | 1.5765 | 1.9029 | 2.3276 |
| 0.6 | 0.6870 | 0.7101 | 0.7457 | 0.7993 | 0.8765 | 0.9829 | 1.1239 | 1.3075 | 1.5510 | 1.8740 | 2.2963 |
| 0.7 | 0.6850 | 0.7084 | 0.7414 | 0.7901 | 0.8606 | 0.9588 | 1.0911 | 1.2656 | 1.4996 | 1.8127 | 2.2244 |
| 0.8 | 0.6806 | 0.7037 | 0.7335 | 0.7764 | 0.8387 | 0.9269 | 1.0473 | 1.2085 | 1.4273 | 1.7227 | 2.1135 |
| 0.9 | 0.6769 | 0.6987 | 0.7250 | 0.7620 | 0.8161 | 0.8933 | 0.9999 | 1.1441 | 1.3417 | 1.6107 | 1.9689 |
| 1.0 | 0.6770 | 0.6958 | 0.7187 | 0.7510 | 0.7978 | 0.8645 | 0.9562 | 1.0801 | 1.2505 | 1.4835 | 1.7954 |

Table K25-3. Geometry function $f_1^B$ for a part circumferential surface crack in a round bar at the intersections of the crack with the free surface

| a/b | a/R=0.0 | a/R=0.1 | a/R=0.2 | a/R=0.3 | a/R=0.4 | a/R=0.5 | a/R=0.6 | a/R=0.7 | a/R=0.8 | a/R=0.9 | a/R=1.0 |
|-----|---------|---------|---------|---------|---------|---------|---------|---------|---------|---------|---------|
| 0.0 | 0.2671 | 0.4276 | 0.5627 | 0.6815 | 0.7929 | 0.9057 | 1.0291 | 1.1722 | 1.3465 | 1.5634 | 1.8347 |
| 0.1 | 0.4316 | 0.5365 | 0.6316 | 0.7230 | 0.8166 | 0.9184 | 1.0345 | 1.1716 | 1.3395 | 1.5489 | 1.8105 |
| 0.2 | 0.5447 | 0.6112 | 0.6790 | 0.7521 | 0.8344 | 0.9297 | 1.0422 | 1.1766 | 1.3422 | 1.5492 | 1.8078 |
| 0.3 | 0.6162 | 0.6579 | 0.7082 | 0.7698 | 0.8452 | 0.9372 | 1.0481 | 1.1821 | 1.3478 | 1.5555 | 1.8153 |
| 0.4 | 0.6563 | 0.6830 | 0.7226 | 0.7771 | 0.8483 | 0.9382 | 1.0485 | 1.1826 | 1.3493 | 1.5590 | 1.8220 |
| 0.5 | 0.6749 | 0.6928 | 0.7256 | 0.7751 | 0.8428 | 0.9303 | 1.0393 | 1.1728 | 1.3400 | 1.5511 | 1.8168 |
| 0.6 | 0.6822 | 0.6937 | 0.7207 | 0.7647 | 0.8277 | 0.9111 | 1.0166 | 1.1475 | 1.3128 | 1.5230 | 1.7885 |
| 0.7 | 0.6863 | 0.6911 | 0.7109 | 0.7476 | 0.8031 | 0.8794 | 0.9784 | 1.1034 | 1.2633 | 1.4682 | 1.7285 |
| 0.8 | 0.6884 | 0.6868 | 0.6990 | 0.7272 | 0.7736 | 0.8404 | 0.9299 | 1.0455 | 1.1956 | 1.3900 | 1.6381 |
| 0.9 | 0.6879 | 0.6816 | 0.6874 | 0.7075 | 0.7444 | 0.8006 | 0.8782 | 0.9810 | 1.1165 | 1.2937 | 1.5213 |
| 1.0 | 0.6842 | 0.6766 | 0.6786 | 0.6927 | 0.7211 | 0.7663 | 0.8304 | 0.9169 | 1.0325 | 1.1849 | 1.3819 |

Table K25-4. Geometry function $f_2^B$ for a part circumferential surface crack in a round bar at the intersections of the crack with the free surface

| a/b | a/R=0.0 | a/R=0.1 | a/R=0.2 | a/R=0.3 | a/R=0.4 | a/R=0.5 | a/R=0.6 | a/R=0.7 | a/R=0.8 | a/R=0.9 | a/R=1.0 |
|-----|---------|---------|---------|---------|---------|---------|---------|---------|---------|---------|---------|
| 0.0 | 0.2965 | 0.4420 | 0.5624 | 0.6648 | 0.7565 | 0.8446 | 0.9363 | 1.0393 | 1.1642 | 1.3221 | 1.5240 |
| 0.1 | 0.4447 | 0.5459 | 0.6325 | 0.7100 | 0.7838 | 0.8595 | 0.9425 | 1.0390 | 1.1581 | 1.3097 | 1.5037 |
| 0.2 | 0.5453 | 0.6143 | 0.6773 | 0.7382 | 0.8011 | 0.8700 | 0.9488 | 1.0424 | 1.1593 | 1.3088 | 1.5003 |
| 0.3 | 0.6081 | 0.6543 | 0.7013 | 0.7518 | 0.8085 | 0.8742 | 0.9517 | 1.0449 | 1.1619 | 1.3121 | 1.5048 |
| 0.4 | 0.6428 | 0.6730 | 0.7091 | 0.7528 | 0.8059 | 0.8704 | 0.9480 | 1.0418 | 1.1600 | 1.3122 | 1.5077 |
| 0.5 | 0.6593 | 0.6774 | 0.7051 | 0.7434 | 0.7936 | 0.8568 | 0.9342 | 1.0284 | 1.1476 | 1.3016 | 1.5000 |
| 0.6 | 0.6672 | 0.6746 | 0.6938 | 0.7258 | 0.7715 | 0.8315 | 0.9069 | 1.0000 | 1.1188 | 1.2731 | 1.4723 |
| 0.7 | 0.6743 | 0.6703 | 0.6794 | 0.7025 | 0.7405 | 0.7943 | 0.8646 | 0.9538 | 1.0696 | 1.2211 | 1.4176 |
| 0.8 | 0.6804 | 0.6656 | 0.6642 | 0.6771 | 0.7055 | 0.7503 | 0.8127 | 0.8949 | 1.0040 | 1.1486 | 1.3369 |
| 0.9 | 0.6831 | 0.6604 | 0.6501 | 0.6536 | 0.6719 | 0.7065 | 0.7585 | 0.8302 | 0.9282 | 1.0601 | 1.2335 |
| 1.0 | 0.6803 | 0.6546 | 0.6393 | 0.6359 | 0.6455 | 0.6694 | 0.7091 | 0.7666 | 0.8481 | 0.9605 | 1.1107 |

Table K25-5. Geometry function $f_3^B$ for a part circumferential surface crack in a round bar at the intersections of the crack with the free surface

| a/b | a/R=0.0 | a/R=0.1 | a/R=0.2 | a/R=0.3 | a/R=0.4 | a/R=0.5 | a/R=0.6 | a/R=0.7 | a/R=0.8 | a/R=0.9 | a/R=1.0 |
|-----|---------|---------|---------|---------|---------|---------|---------|---------|---------|---------|---------|
| 0.0 | 0.3287 | 0.4565 | 0.5588 | 0.6421 | 0.7128 | 0.7774 | 0.8425 | 0.9149 | 1.0044 | 1.1209 | 1.2747 |
| 0.1 | 0.4614 | 0.5550 | 0.6293 | 0.6900 | 0.7431 | 0.7942 | 0.8493 | 0.9148 | 0.9988 | 1.1105 | 1.2585 |
| 0.2 | 0.5500 | 0.6173 | 0.6715 | 0.7174 | 0.7600 | 0.8042 | 0.8547 | 0.9170 | 0.9991 | 1.1091 | 1.2557 |
| 0.3 | 0.6041 | 0.6509 | 0.6908 | 0.7274 | 0.7646 | 0.8061 | 0.8556 | 0.9176 | 0.9998 | 1.1107 | 1.2586 |
| 0.4 | 0.6330 | 0.6635 | 0.6926 | 0.7232 | 0.7577 | 0.7988 | 0.8491 | 0.9122 | 0.9958 | 1.1087 | 1.2595 |
| 0.5 | 0.6463 | 0.6626 | 0.6825 | 0.7078 | 0.7401 | 0.7811 | 0.8323 | 0.8967 | 0.9819 | 1.0968 | 1.2505 |
| 0.6 | 0.6535 | 0.6559 | 0.6659 | 0.6846 | 0.7128 | 0.7517 | 0.8023 | 0.8668 | 0.9527 | 1.0688 | 1.2238 |
| 0.7 | 0.6619 | 0.6496 | 0.6476 | 0.6566 | 0.6774 | 0.7109 | 0.7578 | 0.8202 | 0.9050 | 1.0201 | 1.1736 |
| 0.8 | 0.6703 | 0.6442 | 0.6297 | 0.6276 | 0.6387 | 0.6641 | 0.7046 | 0.7620 | 0.8425 | 0.9531 | 1.1009 |
| 0.9 | 0.6755 | 0.6388 | 0.6138 | 0.6013 | 0.6025 | 0.6184 | 0.6499 | 0.6990 | 0.7710 | 0.8721 | 1.0085 |
| 1.0 | 0.6742 | 0.6325 | 0.6013 | 0.5816 | 0.5744 | 0.5806 | 0.6012 | 0.6380 | 0.6960 | 0.7812 | 0.8994 |

Table K25-6. Geometry function $f_4^B$ for a part circumferential surface crack in a round bar at the intersections of the crack with the free surface

| a/b | a/R=0.0 | a/R=0.1 | a/R=0.2 | a/R=0.3 | a/R=0.4 | a/R=0.5 | a/R=0.6 | a/R=0.7 | a/R=0.8 | a/R=0.9 | a/R=1.0 |
|-----|---------|---------|---------|---------|---------|---------|---------|---------|---------|---------|---------|
| 0.0 | 0.3653 | 0.4711 | 0.5525 | 0.6154 | 0.6658 | 0.7099 | 0.7535 | 0.8034 | 0.8681 | 0.9566 | 1.0783 |
| 0.1 | 0.4840 | 0.5645 | 0.6228 | 0.6653 | 0.6983 | 0.7281 | 0.7610 | 0.8034 | 0.8631 | 0.9479 | 1.0655 |
| 0.2 | 0.5614 | 0.6208 | 0.6624 | 0.6919 | 0.7151 | 0.7378 | 0.7657 | 0.8050 | 0.8627 | 0.9464 | 1.0635 |
| 0.3 | 0.6067 | 0.6482 | 0.6773 | 0.6989 | 0.7175 | 0.7380 | 0.7652 | 0.8043 | 0.8623 | 0.9469 | 1.0656 |
| 0.4 | 0.6293 | 0.6549 | 0.6740 | 0.6903 | 0.7073 | 0.7283 | 0.7570 | 0.7975 | 0.8572 | 0.9438 | 1.0653 |
| 0.5 | 0.6387 | 0.6489 | 0.6587 | 0.6702 | 0.6859 | 0.7079 | 0.7385 | 0.7811 | 0.8427 | 0.9316 | 1.0559 |
| 0.6 | 0.6441 | 0.6386 | 0.6376 | 0.6425 | 0.6549 | 0.6760 | 0.7072 | 0.7511 | 0.8144 | 0.9050 | 1.0308 |
| 0.7 | 0.6528 | 0.6302 | 0.6160 | 0.6112 | 0.6166 | 0.6333 | 0.6624 | 0.7056 | 0.7692 | 0.8600 | 0.9850 |
| 0.8 | 0.6627 | 0.6240 | 0.5960 | 0.5797 | 0.5759 | 0.5856 | 0.6096 | 0.6496 | 0.7107 | 0.7988 | 0.9195 |
| 0.9 | 0.6698 | 0.6182 | 0.5786 | 0.5517 | 0.5384 | 0.5397 | 0.5563 | 0.5898 | 0.6445 | 0.7252 | 0.8371 |
| 1.0 | 0.6699 | 0.6114 | 0.5648 | 0.5307 | 0.5098 | 0.5026 | 0.5098 | 0.5328 | 0.5756 | 0.6432 | 0.7402 |

Table K25-7. Geometry function $f_5^B$ for a part circumferential surface crack in a round bar at the intersections of the crack with the free surface

| a/b | a/R=0.0 | a/R=0.1 | a/R=0.2 | a/R=0.3 | a/R=0.4 | a/R=0.5 | a/R=0.6 | a/R=0.7 | a/R=0.8 | a/R=0.9 | a/R=1.0 |
|-----|---------|---------|---------|---------|---------|---------|---------|---------|---------|---------|---------|
| 0.0 | 0.4056 | 0.4857 | 0.5441 | 0.5865 | 0.6184 | 0.6453 | 0.6727 | 0.7066 | 0.7546 | 0.8246 | 0.9247 |
| 0.1 | 0.5121 | 0.5740 | 0.6138 | 0.6378 | 0.6525 | 0.6646 | 0.6806 | 0.7069 | 0.7503 | 0.8172 | 0.9145 |
| 0.2 | 0.5788 | 0.6246 | 0.6507 | 0.6633 | 0.6690 | 0.6740 | 0.6849 | 0.7080 | 0.7496 | 0.8158 | 0.9131 |
| 0.3 | 0.6155 | 0.6461 | 0.6618 | 0.6678 | 0.6698 | 0.6732 | 0.6835 | 0.7065 | 0.7484 | 0.8157 | 0.9148 |
| 0.4 | 0.6314 | 0.6472 | 0.6539 | 0.6558 | 0.6571 | 0.6618 | 0.6743 | 0.6991 | 0.7428 | 0.8120 | 0.9138 |
| 0.5 | 0.6361 | 0.6364 | 0.6341 | 0.6320 | 0.6330 | 0.6397 | 0.6551 | 0.6825 | 0.7285 | 0.8001 | 0.9046 |
| 0.6 | 0.6390 | 0.6224 | 0.6092 | 0.6011 | 0.5997 | 0.6067 | 0.6237 | 0.6534 | 0.7016 | 0.7752 | 0.8813 |
| 0.7 | 0.6472 | 0.6120 | 0.5850 | 0.5673 | 0.5598 | 0.5636 | 0.5797 | 0.6099 | 0.6594 | 0.7340 | 0.8396 |
| 0.8 | 0.6580 | 0.6049 | 0.5634 | 0.5343 | 0.5183 | 0.5161 | 0.5286 | 0.5571 | 0.6055 | 0.6785 | 0.7807 |
| 0.9 | 0.6665 | 0.5987 | 0.5448 | 0.5053 | 0.4805 | 0.4712 | 0.4778 | 0.5012 | 0.5448 | 0.6122 | 0.7071 |
| 1.0 | 0.6674 | 0.5913 | 0.5300 | 0.4836 | 0.4521 | 0.4357 | 0.4344 | 0.4489 | 0.4824 | 0.5386 | 0.6211 |

### K5.2    *Complete circumferential surface crack*

$K_\text{I}$ is given by

$$K_\text{I} = \sqrt{\pi a}\left(\sum_{i=0}^{5} \sigma_i f_i + \sigma_\text{bg} f_\text{bg}\right),\qquad\qquad\text{(K28)}$$

where $\sigma_i$ ($i = 0$ to $5$) are stress components which define the stress state $\sigma$ according to

$$\sigma = \sigma(r) = \sum_{i=0}^{5} \sigma_i \left(\frac{r}{R}\right)^i \quad \text{for } 0 \leq r \leq R,\qquad\qquad\text{(K29)}$$

and $\sigma_\text{bg}$ is the global bending stress. $\sigma$ and $\sigma_\text{bg}$ are to be taken normal to the prospective crack plane in an uncracked bar. $\sigma_i$ is determined by fitting $\sigma$ to Eq. (K29). The radius $R$ and the coordinate $r$ are defined in Fig. G5.2.

The geometry functions $f_\text{bg}$ and $f_i$ are given in Table K26 for the point A according to Fig. G5.2.

Remarks:    The bar should be long in the transverse direction to the crack so that edge effects do not influence the results.

Ref: [K11].

Table K26.    Geometry functions for a complete circumferential surface crack in a round bar

| $a/R$ | $f_\text{bg}$ | $f_0$ | $f_1$ | $f_2$ | $f_3$ | $f_4$ | $f_5$ |
|-------|-------|-------|-------|-------|-------|-------|-------|
| 0.0 | 1.1242 | 1.1215 | 1.1215 | 1.1215 | 1.1215 | 1.1215 | 1.1215 |
| 0.1 | 1.1665 | 1.1808 | 1.1104 | 1.0452 | 0.9850 | 0.9294 | 0.8778 |
| 0.2 | 1.3161 | 1.2619 | 1.1147 | 0.9897 | 0.8832 | 0.7922 | 0.7142 |
| 0.3 | 1.5968 | 1.3927 | 1.1568 | 0.9734 | 0.8295 | 0.7156 | 0.6246 |
| 0.4 | 2.0876 | 1.6014 | 1.2550 | 1.0090 | 0.8308 | 0.6992 | 0.5999 |
| 0.5 | 2.9793 | 1.9385 | 1.4420 | 1.1199 | 0.9029 | 0.7512 | 0.6411 |
| 0.6 | 4.7728 | 2.5139 | 1.7904 | 1.3597 | 1.0861 | 0.9014 | 0.7698 |
| 0.7 | 9.0842 | 3.6150 | 2.4913 | 1.8712 | 1.4923 | 1.2403 | 1.0614 |
| 0.8 | 23.421 | 6.2377 | 4.2087 | 3.1520 | 2.5175 | 2.0961 | 1.7959 |

## K6. References

[K1]   FETT T., MUNZ D., and J. NEUMANN, (1990), "Local stress intensity factors for surface cracks in plates under power-shaped stress distributions", *Engineering Fracture Mechanics*, Vol. 36, No. 4, pp 647-651.

[K2]   CHAPULIOT, S., LACIRE,. M. H., and DELLIOU, P. Le., (1998), "Stress intensity factors for internal circumferential cracks in tubes over a wide range of radius over thickness ratio", *ASME PVP*, Vol. 365, pp 95-106.

[K3]   WU X. R., and A. J. CARLSSON, (1991), *Weight functions and stress intensity factor solutions*, Pergamon Press, Oxford, U.K.

[K4]   LE DELLIOU, P., and B. BARTHELET, (2007), "New stress intensity factor solutions for an elliptical crack in a plate", *Nuclear Engineering and Design*, Vol. 237, pp. 1395-1405.

[K5]   SIH, G. C., PARIS, P. F., and F. ERDOGAN, (1962), "Stress intensity factors for plane extension and plate bending problems", *Journal of Applied Mechanics*, Vol. 29, pp. 306-312.

[K6]   RAJU, I. S., and J. C. NEWMAN, (1978), "Stress intensity factor influence coefficients for internal and external surface cracks in cylindrical vessels", *ASME PVP*, Vol. 58, pp. 37-48.

[K7]   ZANG, W., (1997), "Stress intensity factor solutions for axial and circumferential trough-wall cracks in cylinders", SINTAP/SAQ/02, SAQ Control AB, Stockholm, Sweden.

[K8]   BERGMAN, M., (1995), "Stress intensity factors for circumferential surface cracks in pipes", *Fatigue & Fracture of Engineering Materials & Structures*, Vol. 18, No. 10, pp. 1155-1172.

[K9]   ERDOGAN, F., and J. J. KIBLER, (1969), "Cylindrical and spherical shells with cracks", *International Journal of Fracture Mechanics*, Vol. 5, pp.229-237.

[K10]  BREMBERG, D., (2015), " Brottmekaniska K-lösningar för sprickor i massiv stång med icke-linjärt rotationssymmetriskt spänningstillstånd", Research Report 2015:03, Swedish Radiation Safety Authority. Stockholm, Sweden. (Available at: http://www.stralsakerhetsmyndigheten.se)

[K11]  MÅNGÅRD, D., (2017), " Stress intensity factor solutions for circumferential cracks in cylindrical bars under axisymmetric loading and global bending", Research Report 2017:16, Swedish Radiation Safety Authority. Stockholm, Sweden. (Available at: http://www.stralsakerhetsmyndigheten.se)

# APPENDIX L.  LIMIT LOAD SOLUTIONS

## L1.    Cracks in a plate

*L1.1    Finite surface crack*

$L_r$ is given by

$$L_r = \frac{(1-\zeta)^{1.58}\dfrac{\sigma_b}{3} + \sqrt{(1-\zeta)^{3.16}\dfrac{\sigma_b^2}{9} + (1-\zeta)^{3.14}\sigma_m^2}}{(1-\zeta)^2\sigma_Y} \quad , \tag{L1}$$

where

$$\zeta = \frac{al}{t(l+2t)} \tag{L2}$$

See Fig. G1.1. $\sigma_m$ and $\sigma_b$ are the membrane and bending stress components, respectively, which define the stress state $\sigma$ according to

$$\sigma = \sigma(u) = \sigma_m + \sigma_b\left(1 - \frac{2u}{t}\right) \quad \text{for } 0 \le u \le t. \tag{L3}$$

$\sigma$ is to be taken normal to the prospective crack plane in an uncracked plate. $\sigma_m$ and $\sigma_b$ are determined by fitting $\sigma$ to Eq. (L3). The coordinate $u$ is defined in Fig. G1.1.

Remarks:  The solution is limited to $a / t \le 0.8$. Also, the plate should be large in comparison to the length of the crack so that edge effects do not influence.

Ref:  [L1].

## L1.2    *Infinite surface crack*

$L_r$ is given by

$$L_r = \frac{\zeta\sigma_m + \dfrac{\sigma_b}{3} + \sqrt{\left(\zeta\sigma_m + \dfrac{\sigma_b}{3}\right)^2 + (1-\zeta)^2\sigma_m^2}}{(1-\zeta)^2\sigma_Y} \quad , \tag{L4}$$

where

$$\zeta = \frac{a}{t} . \tag{L5}$$

See Fig. G1.2. $\sigma_m$ and $\sigma_b$ are the membrane and bending stress components, respectively, which define the stress state $\sigma$ according to

$$\sigma = \sigma(u) = \sigma_m + \sigma_b\left(1 - \frac{2u}{t}\right) \quad \text{for } 0 \le u \le t. \tag{L6}$$

$\sigma$ is to be taken normal to the prospective crack plane in an uncracked plate. $\sigma_m$ and $\sigma_b$ are determined by fitting $\sigma$ to Eq. (L6). The coordinate u is defined in Fig. G1.2.

Remarks:  The solution is limited to $a / t \le 0.8$. Also, the plate should be large in the transverse direction to the crack so that edge effects do not influence.

Ref:  [L2].

*L1.3     Embedded crack*

$L_r$ is given by

$$L_r = \frac{\zeta\sigma_m + \dfrac{\sigma_b}{3} + \sqrt{\left(\zeta\sigma_m + \dfrac{\sigma_b}{3}\right)^2 + \left[(1-\zeta)^2 + 4\zeta\gamma\right]\sigma_m^2}}{\left[(1-\zeta)^2 + 4\zeta\gamma\right]\sigma_Y} \quad , \tag{L7}$$

where

$$\zeta = \frac{2al}{t(l+2t)} \quad , \tag{L8}$$

$$\gamma = \frac{1}{2} - \frac{a}{t} - \frac{e}{t} . \tag{L9}$$

See Fig. G1.3. $\sigma_m$ and $\sigma_b$ are the membrane and bending stress components, respectively, which define the stress state $\sigma$ according to

$$\sigma = \sigma(u) = \sigma_m + \sigma_b\left(1 - \frac{2u}{t}\right) \quad \text{for } 0 \le u \le t . \tag{L10}$$

$\sigma$ is to be taken normal to the prospective crack plane in an uncracked plate. $\sigma_m$ and $\sigma_b$ are determined by fitting $\sigma$ to Eq. (L10). The coordinate u is defined in Fig. G1.3.

Remarks:   The solution is limited to $a/t \le 0.8$ and $e/t \ge 0$. Also, the plate should be large in comparison to the length of the crack so that edge effects do not influence.

Ref:  [L2].

*L1.4      Through-thickness crack*

$L_r$ is given by

$$L_r = \frac{\dfrac{\sigma_b}{3} + \sqrt{\dfrac{\sigma_b^2}{9} + \sigma_m^2}}{\sigma_Y} .$$  (L11)

See Fig. G1.4. $\sigma_m$ and $\sigma_b$ are the membrane and bending stress components, respectively, which define the stress state $\sigma$ according to

$$\sigma = \sigma(u) = \sigma_m + \sigma_b\left(1 - \frac{2u}{t}\right) \quad \text{for } 0 \le u \le t .$$  (L12)

$\sigma$ is to be taken normal to the prospective crack plane in an uncracked plate. $\sigma_m$ and $\sigma_b$ are determined by fitting $\sigma$ to Eq. (L12). The coordinate u is defined in Fig. G1.4.

Remark:     The plate should be large in comparison to the length of the crack so that edge effects do not influence.

## L2. Axial cracks in a cylinder

### L2.1 Finite internal surface crack

$L_r$ is given by

$$L_r = \frac{1}{\sqrt{\left(1-\zeta^{3.11}\right)^{1.9}}} \frac{\sigma_m}{\sigma_Y} \qquad \text{(L13)}$$

where

$$\zeta = \frac{al}{t(l+2t)}. \qquad \text{(L14)}$$

See Fig. G2.1. $\sigma_m$ is the membrane stress component, which define the stress state $\sigma$ according to

$$\sigma = \sigma(u) = \sigma_m \qquad \text{for } 0 \leq u \leq t. \qquad \text{(L15)}$$

$\sigma$ is to be taken normal to the prospective crack plane in an uncracked cylinder. $\sigma_m$ is determined by fitting $\sigma$ to Eq. (L15). The coordinate u is defined in Fig. G2.1.

Remarks:  The solution is limited to $a/t \leq 0.8$. Also, the cylinder should be long in comparison to the length of the crack so that edge effects do not influence.

Ref:  [L1].

## L2.2    *Infinite internal surface crack*

$L_r$ is given by

$$L_r = \frac{\zeta\sigma_m + \dfrac{\sigma_b}{3} + \sqrt{\left(\zeta\sigma_m + \dfrac{\sigma_b}{3}\right)^2 + (1-\zeta)^2\sigma_m^2}}{(1-\zeta)^2\sigma_Y} \quad , \tag{L16}$$

where

$$\zeta = \frac{a}{t} . \tag{L17}$$

See Fig. G2.2. $\sigma_m$ and $\sigma_b$ are the membrane and bending stress components, respectively, which define the stress state $\sigma$ according to

$$\sigma = \sigma(u) = \sigma_m + \sigma_b\left(1 - \frac{2u}{t}\right) \quad \text{for } 0 \le u \le t . \tag{L18}$$

$\sigma$ is to be taken normal to the prospective crack plane in an uncracked cylinder. $\sigma_m$ and $\sigma_b$ are determined by fitting $\sigma$ to Eq. (L18). The coordinate u is defined in Fig. G2.2.

Remark:    The solution is limited to $a/t \le 0.8$.

Ref:  [L2].

## L2.3    Finite external surface crack

$L_r$ is given by

$$L_r = \frac{1}{\sqrt{\left(1-\zeta^{3.11}\right)^{1.9}}} \frac{\sigma_m}{\sigma_Y} \qquad\qquad\qquad (L19)$$

where

$$\zeta = \frac{al}{t(l+2t)}. \qquad\qquad\qquad (L20)$$

See Fig. G2.3. $\sigma_m$ is the membrane stress component, which define the stress state $\sigma$ according to

$$\sigma = \sigma(u) = \sigma_m \qquad \text{for } 0 \leq u \leq t. \qquad\qquad\qquad (L21)$$

$\sigma$ is to be taken normal to the prospective crack plane in an uncracked cylinder. $\sigma_m$ is determined by fitting $\sigma$ to Eq. (L21). The coordinate u is defined in Fig. G2.3.

Remarks:    The solution is limited to $a/t \leq 0.8$. Also, the cylinder should be long in comparison to the length of the crack so that edge effects do not influence.

Ref: [L1].

## L2.4    *Infinite external surface crack*

$L_r$ is given by

$$L_r = \frac{\zeta\sigma_m + \dfrac{\sigma_b}{3} + \sqrt{\left(\zeta\sigma_m + \dfrac{\sigma_b}{3}\right)^2 + (1-\zeta)^2\sigma_m^2}}{(1-\zeta)^2\sigma_Y} \quad , \tag{L22}$$

where

$$\zeta = \frac{a}{t}. \tag{L23}$$

See Fig. G2.4. $\sigma_m$ and $\sigma_b$ are the membrane and bending stress components, respectively, which define the stress state $\sigma$ according to

$$\sigma = \sigma(u) = \sigma_m + \sigma_b\left(1 - \frac{2u}{t}\right) \quad \text{for } 0 \leq u \leq t. \tag{L24}$$

$\sigma$ is to be taken normal to the prospective crack plane in an uncracked cylinder. $\sigma_m$ and $\sigma_b$ are determined by fitting $\sigma$ to Eq. (L24). The coordinate u is defined in Fig. G2.4.

Remark:    The solution is limited to $a / t \leq 0.8$.

Ref:  [L2].

*L2.5     Through-thickness crack*

$L_r$ is given by

$$L_r = \frac{\sigma_m}{\sigma_Y}\sqrt{1+1.05\lambda^2} \quad , \tag{L25}$$

where

$$\lambda = \frac{l}{2\sqrt{R_i t}} \ . \tag{L26}$$

See Fig. G2.5. $\sigma_m$ is the membrane stress component, which defines the stress state $\sigma$ according to

$$\sigma = \sigma(u) = \sigma_m \qquad \text{for } 0 \leq u \leq t \ . \tag{L27}$$

$\sigma$ is to be taken normal to the prospective crack plane in an uncracked cylinder. $\sigma_m$ is determined by fitting $\sigma$ to Eq. (L27). The coordinate $u$ is defined in Fig. G2.5.

Remarks:    The cylinder should be long in comparison to the length of the crack so that edge effects do not influence.

Ref:  [L3].

# L3. Circumferential cracks in a cylinder

## L3.1    *Part circumferential internal surface crack*

$L_r$ is given by

$$L_r = \sqrt{\frac{\left(\dfrac{\sigma_m}{s'_m}\right)^2 + \left(\dfrac{\sigma_{bg}}{s'_{bg}}\right)^2}{\left(\dfrac{s_m}{s'_m}\right)^2 + \left(\dfrac{s_{bg}}{s'_{bg}}\right)^2}} \quad , \tag{L28}$$

where the parameters $s_m$, $s_m{}'$, $s_{bg}$ and $s_{bg}{}'$ are obtained by solving the equation system

$$\left|\begin{array}{ll}
\dfrac{s_m}{\sigma_Y} = 1 - 2\dfrac{\beta}{\pi} - \dfrac{a}{t}\dfrac{\alpha}{\pi} & \\[3mm]
\dfrac{s_{bg}}{\sigma_Y} = \dfrac{4}{\pi}\sin\beta - \dfrac{2}{\pi}\dfrac{a}{t}\sin\alpha & \\[3mm]
\theta = \dfrac{l}{2R_i} & \\[3mm]
\alpha = \begin{cases} \theta & \text{if } \theta \leq \pi - \beta \\ \pi - \beta & \text{if } \theta > \pi - \beta \end{cases} & \\[3mm]
\sigma_m s_{bg} - \sigma_{bg} s_m = 0 & \\[2mm]
s'_m = s_m & \text{for } s_{bg} = 0 \\[2mm]
s'_{bg} = s_{bg} & \text{for } s_m = 0
\end{array}\right. \tag{L29}$$

See Fig. G3.1. $\sigma_m$ and $\sigma_{bg}$ are the membrane and global bending stress components, respectively. $\sigma_m$ defines the axisymmetrical stress state $\sigma$ according to

$$\sigma = \sigma(u) = \sigma_m \qquad \text{for } 0 \leq u \leq t. \tag{L30}$$

$\sigma$ is to be taken normal to the prospective crack plane in an uncracked cylinder. $\sigma_m$ is determined by fitting $\sigma$ to Eq. (L30). The coordinate $u$ is defined in Fig. G3.1.

Remarks:  The cylinder should be thin-walled. Also, the cylinder should be long in the transverse direction to the crack so that edge effects do not influence.

Ref:  [L4].

*L3.2     Complete circumferential internal surface crack*

$L_r$ is given by

$$L_r = \sqrt{\dfrac{\left(\dfrac{\sigma_m}{s_m'}\right)^2 + \left(\dfrac{\sigma_{bg}}{s_{bg}'}\right)^2}{\left(\dfrac{s_m}{s_m'}\right)^2 + \left(\dfrac{s_{bg}}{s_{bg}'}\right)^2}} \quad , \tag{L31}$$

where the parameters $s_m$, $s_m'$, $s_{bg}$ and $s_{bg}'$ are obtained by solving the equation system

$$\left| \begin{aligned} & \frac{s_m}{\sigma_Y} = 1 - 2\frac{\beta}{\pi} - \frac{a}{t}\frac{\pi - \beta}{\pi} \\ & \frac{s_{bg}}{\sigma_Y} = \frac{2}{\pi}\frac{2t - a}{t}\sin\beta \\ & \sigma_m s_{bg} - \sigma_{bg} s_m = 0 \\ & s_m' = s_m \qquad \text{for } s_{bg} = 0 \\ & s_{bg}' = s_{bg} \qquad \text{for } s_m = 0 \end{aligned} \right. \tag{L32}$$

See Fig. G3.2. $\sigma_m$ and $\sigma_{bg}$ are the membrane and global bending stress components, respectively. $\sigma_m$ defines the axisymmetrical stress state $\sigma$ according to

$$\sigma = \sigma(u) = \sigma_m \qquad \text{for } 0 \leq u \leq t . \tag{L33}$$

$\sigma$ is to be taken normal to the prospective crack plane in an uncracked cylinder. $\sigma_m$ is determined by fitting $\sigma$ to Eq. (L33). The coordinate $u$ is defined in Fig. G3.2.

Remarks:   The cylinder should be thin-walled. Also, the cylinder should be long in the transverse direction to the crack so that edge effects do not influence.

Ref:  [L4].

*L3.3     Part circumferential external surface crack*

$L_r$ is given by

$$L_r = \sqrt{\frac{\left(\dfrac{\sigma_m}{s_m'}\right)^2 + \left(\dfrac{\sigma_{bg}}{s_{bg}'}\right)^2}{\left(\dfrac{s_m}{s_m'}\right)^2 + \left(\dfrac{s_{bg}}{s_{bg}'}\right)^2}} \quad , \tag{L34}$$

where the parameters $s_m$, $s_m'$, $s_{bg}$ and $s_{bg}'$ are obtained by solving the equation system

$$\left|\begin{array}{l} \dfrac{s_m}{\sigma_Y} = 1 - 2\dfrac{\beta}{\pi} - \dfrac{a}{t}\dfrac{\alpha}{\pi} \\[2mm] \dfrac{s_{bg}}{\sigma_Y} = \dfrac{4}{\pi}\sin\beta - \dfrac{2}{\pi}\dfrac{a}{t}\sin\alpha \\[2mm] \theta = \dfrac{l}{2(R_i + t)} \\[2mm] \alpha = \begin{cases} \theta & \text{if } \theta \leq \pi - \beta \\ \pi - \beta & \text{if } \theta > \pi - \beta \end{cases} \\[3mm] \sigma_m s_{bg} - \sigma_{bg} s_m = 0 \\[1mm] s_m' = s_m \qquad \text{for } s_{bg} = 0 \\[1mm] s_{bg}' = s_{bg} \qquad \text{for } s_m = 0 \end{array}\right. \qquad . \tag{L35}$$

See Fig. G3.3. $\sigma_m$ and $\sigma_{bg}$ are the membrane and global bending stress components, respectively. $\sigma_m$ defines the axisymmetrical stress state $\sigma$ according to

$$\sigma = \sigma(u) = \sigma_m \qquad \text{for } 0 \leq u \leq t . \tag{L36}$$

$\sigma$ is to be taken normal to the prospective crack plane in an uncracked cylinder. $\sigma_m$ is determined by fitting $\sigma$ to Eq. (L36). The coordinate $u$ is defined in Fig. G3.3.

Remarks:   The cylinder should be thin-walled. Also, the cylinder should be long in the transverse direction to the crack so that edge effects do not influence.

Ref:  [L4].

145

*L3.4     Complete circumferential external surface crack*

$L_r$ is given by

$$L_r = \sqrt{\frac{\left(\dfrac{\sigma_m}{s'_m}\right)^2 + \left(\dfrac{\sigma_{bg}}{s'_{bg}}\right)^2}{\left(\dfrac{s_m}{s'_m}\right)^2 + \left(\dfrac{s_{bg}}{s'_{bg}}\right)^2}} \quad , \tag{L37}$$

where the parameters $s_m$, $s_m{'}$, $s_{bg}$ and $s_{bg}{'}$ are obtained by solving the equation system

$$\left|
\begin{aligned}
&\frac{s_m}{\sigma_Y} = 1 - 2\frac{\beta}{\pi} - \frac{a}{t}\frac{\pi - \beta}{\pi} \\[2mm]
&\frac{s_{bg}}{\sigma_Y} = \frac{2}{\pi}\frac{2t - a}{t}\sin\beta \\[2mm]
&\sigma_m s_{bg} - \sigma_{bg} s_m = 0 \\[2mm]
&s'_m = s_m \qquad \text{for } s_{bg} = 0 \\[2mm]
&s'_{bg} = s_{bg} \qquad \text{for } s_m = 0
\end{aligned}
\right.
\tag{L38}$$

See Fig. G3.4. $\sigma_m$ and $\sigma_{bg}$ are the membrane and global bending stress components, respectively. $\sigma_m$ defines the axisymmetrical stress state $\sigma$ according to

$$\sigma = \sigma(u) = \sigma_m \qquad \text{for } 0 \leq u \leq t. \tag{L39}$$

$\sigma$ is to be taken normal to the prospective crack plane in an uncracked cylinder. $\sigma_m$ is determined by fitting $\sigma$ to Eq. (L39). The coordinate $u$ is defined in Fig. G3.4.

Remarks:   The cylinder should be thin-walled. Also, the cylinder should be long in the transverse direction to the crack so that edge effects do not influence.

Ref:  [L4].

*L3.5     Through-thickness crack*

$L_r$ is given by

$$L_r = \sqrt{\dfrac{\left(\dfrac{\sigma_m}{s'_m}\right)^2 + \left(\dfrac{\sigma_{bg}}{s'_{bg}}\right)^2}{\left(\dfrac{s_m}{s'_m}\right)^2 + \left(\dfrac{s_{bg}}{s'_{bg}}\right)^2}} \quad , \tag{L40}$$

where the parameters $s_m$, $s_m{'}$, $s_{bg}$ and $s_{bg}{'}$ are obtained by solving the equation system

$$\left| \begin{array}{l} \dfrac{s_m}{\sigma_Y} = 1 - 2\dfrac{\beta}{\pi} - \dfrac{\theta}{\pi} \\[2ex] \dfrac{s_{bg}}{\sigma_Y} = \dfrac{4}{\pi}\sin\beta - \dfrac{2}{\pi}\sin\theta \\[2ex] \theta = \dfrac{l}{2R_i} \\[2ex] \sigma_m s_{bg} - \sigma_{bg} s_m = 0 \\[1ex] s'_m = s_m \qquad \text{for } s_{bg} = 0 \\[1ex] s'_{bg} = s_{bg} \qquad \text{for } s_m = 0 \end{array} \right. \qquad . \tag{L41}$$

See Fig. G3.5. $\sigma_m$ and $\sigma_{bg}$ are the membrane and global bending stress components, respectively. $\sigma_m$ defines the axisymmetrical stress state $\sigma$ according to

$$\sigma = \sigma(u) = \sigma_m \qquad \text{for } 0 \le u \le t. \tag{L42}$$

$\sigma$ is to be taken normal to the prospective crack plane in an uncracked cylinder. $\sigma_m$ is determined by fitting $\sigma$ to Eq. (L42). The coordinate $u$ is defined in Fig. G3.5.

Remarks:   The cylinder should be thin-walled. Also, the cylinder should be long in the transverse direction to the crack so that edge effects do not influence.

Ref:  [L4].

## L4.    Cracks in a sphere

*L4.1    Through-thickness crack*

$L_r$ is given by

$$L_r = \frac{\sigma_m}{\sigma_Y} \frac{1 + \sqrt{1 + 8(\lambda / \cos\theta)^2}}{2} \quad , \tag{L43}$$

where

$$\lambda = \frac{l}{2\sqrt{R_i t}} \quad , \tag{L44}$$

$$\theta = \frac{l}{2R_i} . \tag{L45}$$

See Fig. G4.1. $\sigma_m$ is the membrane stress component. $\sigma_m$ defines the axisymmetrical stress state $\sigma$ according to

$$\sigma = \sigma(u) = \sigma_m \qquad \text{for } 0 \leq u \leq t . \tag{L46}$$

$\sigma$ is to be taken normal to the prospective crack plane in an uncracked sphere. $\sigma_m$ is determined by fitting $\sigma$ to Eq. (L46). The coordinate $u$ is defined in Fig. G4.1.

Remark:    The sphere should be thin-walled.

Ref:  [L5].

## L5. Cracks in a bar

### L5.1 Part circumferential surface crack

$L_r$ is given by

$$L_r = \frac{M_0}{M_{limit}} \quad ,$$
(L47)

Where $M_0$ is the applied bending moment on the bar and $M_{limit}$ is obtained by solving the equation system

$$\begin{cases} N_{limit} = \sigma_Y R^2 \left( 2 \cdot \phi + 2\cos(\phi)\sin(\phi) + \cos(\beta)\sin(\beta) + \beta - \frac{1}{2} \cdot \pi \right) \\ M_{limit} = \sigma_Y R^3 \left( \frac{4}{3}\cos(\phi)^3 - \frac{2}{3}\cos(\beta)^3 \right) \\ \frac{M_{limit}}{M_f} = \frac{M_0 / M_f}{N_0 / N_f} \cdot \frac{N_{limit}}{N_f} \end{cases}$$
(L48)

See Fig. G5.1. $N_0$ and $M_0$ are the applied tensile force and the applied bending moment on the bar, $N_f$ is the pure tensile limit load and $M_f$ is the pure bending limit load.

Ref.: [L6].

## L5.2 *Complete circumferential surface crack*

$L_r$ is according to [L7] given by

$$L_r = \frac{\frac{\sigma_{bg}^{ref}}{2} + \sqrt{\left(\sigma_m^{ref}\right)^2 + \frac{\left(\sigma_{bg}^{ref}\right)^2}{4}}}{\sigma_Y}.$$  (L49)

The membrane reference stress, $\sigma_m{}^{ref}$, is calculated in accordance with [L8] as

$$\sigma_m^{ref} = \frac{\sigma_m}{n_L},$$  (L50)

where $\sigma_m$ is the membrane stress and the normalized limit force, $n_L$, is defined as

$$n_L = \begin{cases} 1 - 0.0077\beta - 1.5287\beta^2 & \text{for } 0 \le \beta \le 0.65 \\ 2.85(1 - \beta)^2 & \text{for } 0.65 < \beta < 1 \end{cases}.$$  (L51)

The global bending reference stress, $\sigma_{bg}{}^{ref}$, is calculated in accordance with [L7] as

$$\sigma_{bg}^{ref} = \sigma_{bg} \frac{3\pi}{16} \left[ \frac{R^4}{R(R - a)^3} \right],$$  (L52)

See Fig. G5.2. $\sigma_{bg}$, is the global bending stress, $R$ is the bar radius and $a$ is the crack depth.

Ref: [L7-L8].

## L6. References

[L1]   DILLSTRÖM, P., and I. SATTARI-FAR., (2002), "Limit load solutions for surface cracks in plates and cylinders", RSE R&D Report No. 2002/01, Det Norske Veritas AB.

[L2]   WILLOUGHBY, A. A., and T. G. DAVEY., (1989), "Plastic collapse in part-wall flaws in plates", *ASTM STP 1020*, American Society for Testing and Materials, Philadelphia, U.S.A., pp. 390-409.

[L3]   KIEFNER, J. F., MAXEY, W. A., EIBER, R. J., and A. R. DUFFY, (1973), "Failure stress levels of flaws in pressurized cylinders", *ASTM STP 536*, American Society for Testing and Materials, Philadelphia, U.S.A., pp. 461-481.

[L4]   DELFIN, P., (1996), "Limit load solutions for cylinders with circumferential cracks subjected to tension and bending", SAQ/FoU-Report 96/05, SAQ Kontroll AB, Stockholm, Sweden.

[L5]   BURDEKIN, F. M., and T. E. TAYLOR, (1969), "Fracture in spherical vessels", *Journal of Mechanical Engineering and Science*, Vol. 11, pp. 486-497.

[L6]   KLASÉN, B., DILLSTRÖM, P., and W. ZANG., (2003), "Stress Intensity Factor and Limit Load Solutions for Surface Cracks in Round Bars", RSE R&D Report No. 2001/04, Rev. 1, Det Norske Veritas AB.

[L7]   —, (2007), "API 579-1/ASME FFS-1 2007 Fitness-For-Service", American Petroleum Institute and The American Society of Mechanical Engineers, Washington, D.C., U.S.A.

[L8]   —, (2013), "Assessment of the Integrity of Structures Containing Defects", R6 –Revision 4, Up to amendment record No.10, EDF Energy Nuclear Generation Ltd.

# APPENDIX M. MATERIAL DATA FOR NUCLEAR APPLICATIONS

In order to perform fracture mechanics assessments according to this handbook knowledge about yield strength $\sigma_Y$, ultimate tensile strength $\sigma_U$, critical stress intensity factor $K_{cr}$ and $J_R$-curves is needed. In addition, crack growth calculations require knowledge about the growth rate per load cycle or per time unit for fatigue cracking and stress corrosion cracking, respectively. All material data should preferably be determined by testing of the material of the considered component in the environment and at the temperature for which the fracture assessment is to be performed. The number of tests should be large enough to assure characteristic values with consideration of scatter. Below, some recommendations are given for steels and nickel base alloys common in nuclear applications. The data is intended for use in cases when test data for the actual materials are lacking. In many cases the data given below are conservative estimates.

## M1. Yield strength, ultimate tensile strength

For many steels used in nuclear applications information about minimum levels of $\sigma_Y$ and $\sigma_U$ as functions of the temperature can be found in ASME Sect. III, Appendices. For other materials minimum levels are in general specified by the respective manufacturer. In cases where higher values than the specified can be verified, actual data may be used. Test data presented in a material certificate may be insufficient to estimate reliable values, since they normally do not provide enough data for calculation of the mean value and standard deviation with high confidence, which could provide beneficial values. In some cases, as for fracture assessments according to ASME 2007 Sect. XI, Appendix C [M1] only minimum yield stress data are allowed.

## M2. Fracture toughness and $J_R$-curves

In cases when the fracture toughness could not be directly determined, $J_{Ic}$–data converted according to Eq. (2.3), section 2.5 has been used. In this case an elastic modulus of 180 000 MPa for stainless steels at 288°C has been used and 195 000 MPa for ferritic steels in materials on the upper shelf region. Poisson's ratio has been set to 0.3 in all cases except for nickel base alloys, where the Poisson's ratio was set to 0.29.

### M2.1 Ferritic steel, plates, pressure vessels

For the materials SA-533 Grad B Class 1, SA-508 Class 2 and SA-508 Class 3 the fracture toughness $K_{Ic}$ in the transition region is given as a function of the difference between actual temperature $T$ and the nil ductility transition temperature $RT_{NDT}$ in ASME 2007, Sect. XI, Appendix A, Fig. A-4200-1M [M1]. This corresponds to the analytic expression ($T$ in °C)

$$K_{Ic} = 36.5 + 22.783\exp[0.036(T - RT_{NDT})]. \tag{M1}$$

For temperatures above the transition region, values higher than 220 MPa$\sqrt{\text{m}}$ are usually not assumed. The value of 220 MPa$\sqrt{\text{m}}$ is generally accepted as a good estimate for the so called upper-shelf region. It is noted that recent work [M32] indicate that the above values may be non-conservative in some situations, and this may be considered in future editions of ASME Sect. XI. Temperature dependence of the upper-shelf value is not entirely insignificant as described in [M33]. Note that neutron irradiation can decrease this level and also increase $RT_{\text{NDT}}$.

Fracture toughness data can also be calculated through the Master Curve method, see Appendix B.

## M2.2 Ferritic steel, pipes

The following data are taken from [M2]. They can be used in the absence of specific measured data. They are also referenced by ASME 2007, sect. XI, Appendix C [M1] and are intended for the following material categories:

Category 1: Seamless or welded carbon steel piping with a minimum yield strength lower than or equal to 276 MPa (base material) and welds with electrodes of type E7015, E7016 or E7018 (basic electrodes with a yield strength of the order of 500 MPa, Charpy-V toughness 27 J at –29°C).

Category 2: All other welded ferritic piping with shielded metal arc welds (SMAW) or submerged arc welds (SAW) with minimum ultimate tensile strength lower than or equal to 522 MPa.

Table M1 differentiates between temperatures above or below the upper-shelf region. In addition, in [M2] and [M1] it is distinguished between circumferential and axial cracks. The fracture properties are often worse for cracks oriented along the texture direction (axial cracks) than for cracks oriented across the texture direction (circumferential cracks). In the absence of specific measured data, the upper shelf temperature for class 1 ferritic piping steels can be taken as 93°C.

Table M1.   Fracture toughness data for carbon steel base metals and weldments, ref. [M2]

| Material category | Temperature interval | Crack orientation | $J_{\text{Ic}}$ (kJ/m$^2$) | $K_{\text{cr}}$ (MPa$\sqrt{\text{m}}$) |
|---|---|---|---|---|
| 1 | $T \geq$ upper shelf | Circumferential | 105 | 150 |
| 1 | $T <$ upper shelf | Circumferential | 7.9 | 42 |
| 2 | $T \geq$ upper shelf | Circumferential | 61.3 | 115 |
| 2 | $T <$ upper shelf | Circumferential | 7.9 | 42 |
| 1, 2 | $T \geq$ upper shelf | Axial | 52.5 | 106 |
| 1, 2 | $T <$ upper shelf | Axial | 7.9 | 42 |

*M2.3 Austenitic stainless steel, pipes*

The following data are mainly taken from ref. [M3], [M4] and [M5] at room temperature and 288°C. Stainless steels base material is of type 304 or type 316, and the welding material is type 308. The different welding performances are shielded metal arc welds (SMAW), submerged arc welds (SAW) or gas tungsten arc welds (GTAW) which are the same as TIG-welding. The data are given in Table M2.

Table M2.   Fracture toughness data, $J_{Ic}$, for austenitic stainless steel 304, ref, [M3], [M4] and [M5]. The welding methods are shielded metal arc welds (SMAW), submerged arc welds (SAW) or gas tungsten arc welds (GTAW) which are same as TIG-welding

| Material type | Temperature °C | $J_{Ic}$ (kJ/m$^2$) | $K_{cr}$ (MPa$\sqrt{\text{m}}$) |
|---|---|---|---|
| Base material | 25 | 1000 | 480 |
| Base material | 288 | > 620 | > 350 |
| SMAW | 25 | 259 | 239 |
| SMAW | 288 | 168 | 182 |
| SAW | 25 | 99 | 148 |
| SAW | 288 | 76 | 122 |
| GTAW | 25 | 500 | 339 |
| GTAW | 288 | 355 | 286 |

In general the fracture toughness for welded stainless steel, type 304, is depending on the welding performance method. The fracture toughness data for GTAW are better than for SMAW, and SMAW are better than for SAW. The high fracture toughness of GTAW welding material is due to advantageous microstructure during cooling after welding. In SAW welding silicon takes up from the fluxing material, forming equality inclusions distributed in the material, which acts as crack initiations points. In GTAW welding the material takes up only a small amount of silicon.

Fracture toughness data for GTAW-welds at 288°C are only slightly below those of the base material. The heat affected zone (HAZ) and the base material have the same toughness. HAZ shows better properties than the weld material. The fracture toughness decreases with increasing temperature.

The standard test method ASTM E1820-01 [M6] is used to qualify the experimental data. A large number of experimental data points have been carried out for the tests, and the mean, lower and upper limits of $J_{Ic}$ can be calculated. For gas tungsten arc welds (GTAW) and heat affected zone (HAZ), the experimental data show a large scatter and only a few results were available. Thus the $J_R$-curve which forms the lowest experimental limit was provided. The $J_R$-curve can be written as

$$J_R = C_0(\Delta a)^{C_1}, \tag{M2}$$

where $C_0$ and $C_1$ are material specific constants and is for different welding performances given in Figures M1-M6.

The experimental $J_R$-curves for SAW welding performance are given in Figure M1 and M2. The statistical mean, lower and upper limits are also presented in the figures.
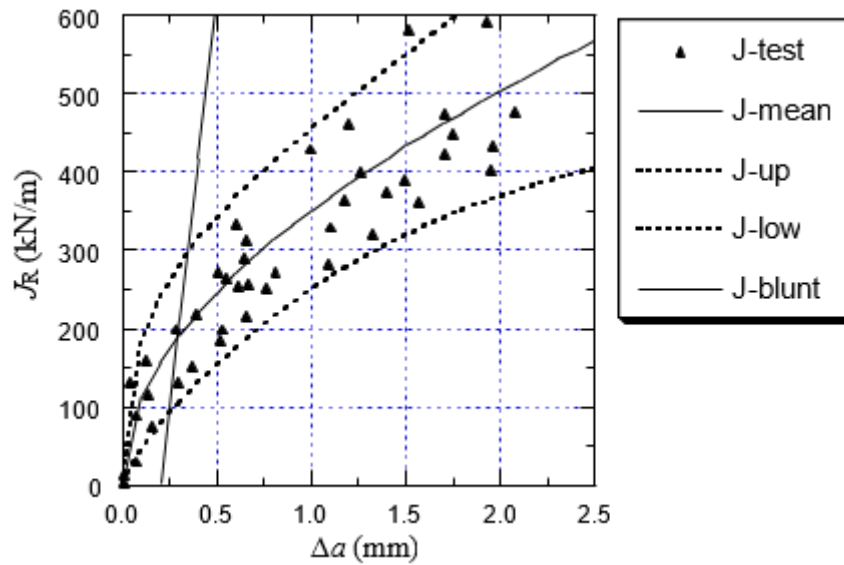


Figure M1.   $J_R$-curves for SAW welding (304) at room temperature, ref. [M3]. The equation for $J$-mean is $J_R = 352.69(\Delta a)^{0.5086}$, $J$-upper is $J_R = 466.36(\Delta a)^{0.4361}$ and $J$-lower is $J_R = 235.49(\Delta a)^{0.6820}$.
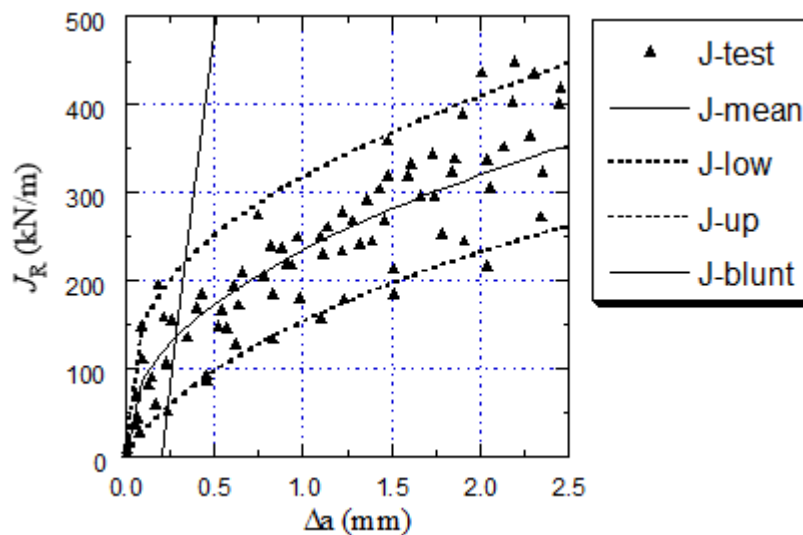


Figure M2.   $J_R$-curves for SAW welding (304) at 288°C, ref. [M3]. The equation for $J$-mean is $J_R = 235.65(\Delta a)^{0.4378}$, $J$-upper is $J_R = 320.07(\Delta a)^{0.3452}$ and $J$-lower is $J_R = 147.39(\Delta a)^{0.6838}$.

The experimental $J_R$-curves for SMAW welding at room temperature and at 288°C are shown in Figure M3 and M4 respectively. The statistical mean, lower and upper limits are also presented in the figures. In lower limit 5 % of the data points are under the curve, and for upper limit 95 % of the data points are under the curve.
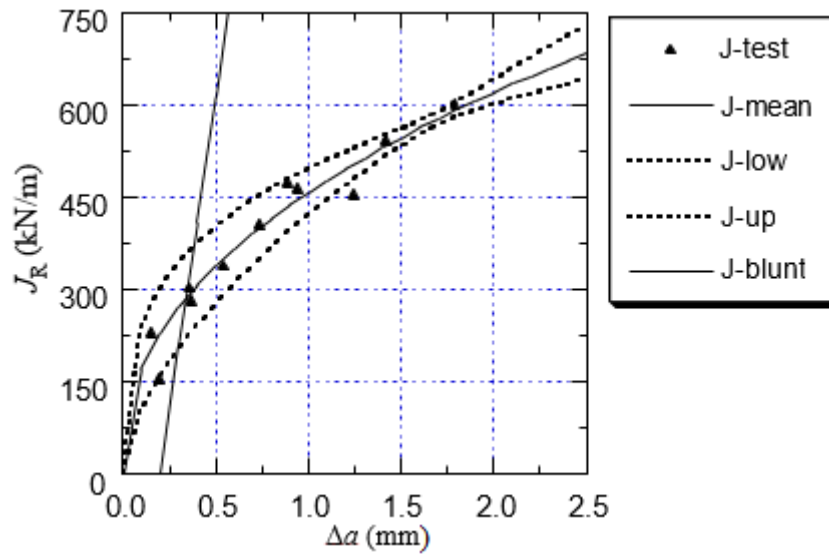
Figure M3. $J_R$-curves for SMAW welding (304) at room temperature, ref. [M3]. The equation for $J$-mean is $J_R = 458.87(\Delta a)^{0.4357}$, $J$-upper is $J_R = 504.91(\Delta a)^{0.3365}$ and $J$-lower is $J_R = 407.90(\Delta a)^{0.5794}$.
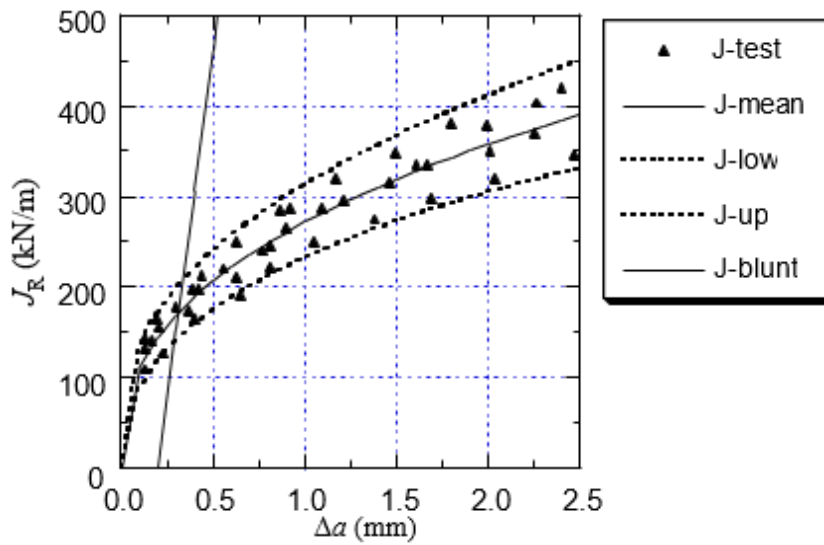


Figure M4. $J_R$-curves for SMAW welding (304) at 288°C, ref. [M3]. The equation for $J$-mean is $J_R = 272.02(\Delta a)^{0.3939}$, $J$-upper is $J_R = 313.96(\Delta a)^{0.3824}$ and $J$-lower is $J_R = 230.03(\Delta a)^{0.4102}$.

The experimental $J_R$-curves for GTAW at room temperature and at 288°C is shown in Figure M5 and M6 respectively. The statistical mean, lower and upper limits are also presented in the figures. It is noticed that the experimental data show a large scatter and only a few results are available. The results by the statistical analysis are therefore not very good. The application of the statistical lower limit may be too conservative. Thus the $J_R$-curve which forms the lowest experimental limit is also provided. This experimental lowest $J_R$-curve is denoted as $J$-lowest in Figure M5 and M6.
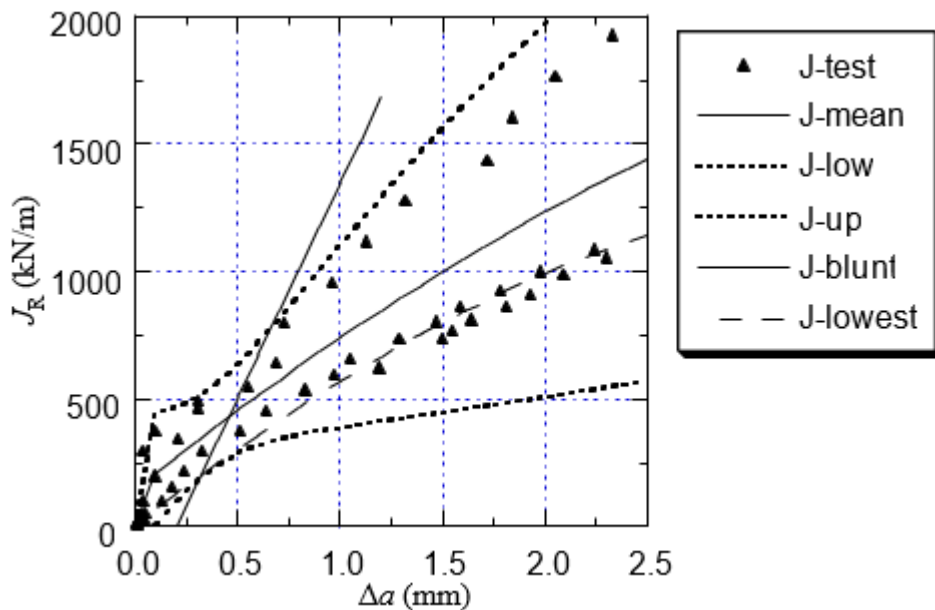


Figure M5.   $J_R$-curves for GTAW welding (304) at room temperature, ref. [M3]. The equation for $J$-mean is $J_R = 765.47(\Delta a)^{0.6454}$, $J$-upper is $J_R = 1183.70(\Delta a)^{0.6273}$ and $J$-lowest is $J_R = 545.76(\Delta a)^{0.8908}$.
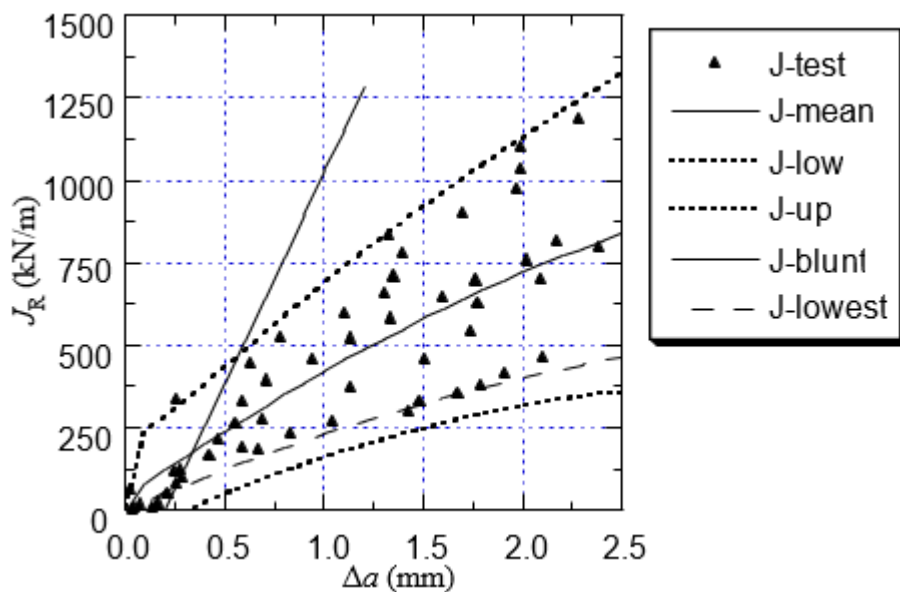


Figure M6.   $J_R$-curves for GTAW welding (304) at 288°C, ref. [M3]. The equation for $J$-mean is $J_R = 418.45(\Delta a)^{0.7740}$, $J$-upper is $J_R = 717.44(\Delta a)^{0.5949}$ and $J$-lowest is $J_R = 220.13(\Delta a)^{0.8911}$.

*M2.4  Irradiated austenitic stainless steel, pipes*

In this section, fracture toughness data from irradiated austenitic stainless steels are presented. It is known that the fracture toughness will vary with the degree of irradiation. Neutron fluence (integrated damage) is reported in $n/cm^2$ or dpa (displacement per atom). For stainless steel, 1dpa $\approx 7 \cdot 10^{20}$ $n/cm^2$ for $E > 1$ MeV. In Sweden, the neutron fluence for a moderator tank in a BWR station is about 0.3 dpa $\approx 2 \cdot 10^{20}$ $n/cm^2$. In addition to the references [M3] and [M4], fracture toughness data for irradiated stainless steel for base material, weld material and HAZ can be found in [M34] and [M35], see also [M19]. The effect of the irradiation can be divided in three domains:

*i)          For low irradiation, the effect on fracture toughness is marginal.*
At a low neutron fluence level, about 0.3 dpa, it is shown by experiments that the irradiation has only a marginal effect on the fracture toughness for base materials. Experiments show that the neutron fluence has some negative effects on the fracture toughness for base materials subjected to moderate neutron fluence level about 1 dpa. In this study, only specimens fabricated from materials removed from service were used. Fracture toughness data are listed in Table M3 for austenitic base materials.

Table M3.     Fracture toughness data for irradiated austenitic base material, ref [M3]

| Material type | Temperature °C | Dose (dpa) | $J_{Ic}$ (kN/m) | Crack growth |
|---|---|---|---|---|
| 304 | 20 | 0.8 | 596 | Stable |
| 304 | 199 | 0.9 | 395 | Stable |
| 304 | 249 | 0.9 | 297 | Stable |

*ii)          For irradiation between 1-10 dpa, the toughness decrease with the time of irradiation.*
At 2 dpa for base stainless steel type 304 the fracture toughness is about 200 kN/m at 125°C. However, no experiments have been performed for materials subjected a neutron fluence of about 3-5 dpa. In this neutron fluence there is lack of data.

*iii)          For irradiation over 10 dpa, the toughness is independent of the irradiation time.*
Comparison between fracture toughness for unirradiated and irradiated material indicates radiated base material 304 in the range 10 till 19 dpa, have a decrease in the fracture toughness with a factor of 10, Ref [M4]. The fracture toughness for radiated stainless steel is in the range 25–35 kN/m.

*M2.5 Irradiated austenitic stainless steel, welding components*

Unirradiated welded austenitic stainless steels, type 308, have better fracture toughness than irradiated welded stainless steels. Fracture toughness for typical irradiated austenitic welding material, 308 L, at different irradiation levels, is given in Table M4.

Table M4. Fracture toughness data for irradiated austenitic welds, ref [M3] and [M4]. The welding methods are shielded metal arc welds (SMAW)

| Material type | Temperature °C | Dose (dpa) | $J_{Ic}$ (kN/m) |
|---|---|---|---|
| 308L / SMAW | 25 | 0,7 | 143 |
| 308L / SMAW | 199 | 0,6 | 125 |
| 308L / SMAW | 25 | 11 | 10-15 |
| 308L / SMAW | 150 | 11 | 10-15 |
| 308L / SMAW | 259 | 11 | 10-15 |

*M2.6 Cast stainless steel*

Cast stainless steels are normally ductile and have a fracture toughness of the same level as the stainless steel base material in Table M2. However, cast duplex stainless steels are subjected to thermal ageing which causes an embrittlement of the ferritic phase. The degree of embrittlement is determined mainly by the ferritic content, ageing time and exposure temperature. For a ferritic content of less than 10%, the risk of embrittlement should be small for component aged at about 300°C. A lower bound value for $J_{Ic}$ of 100 kJ/m$^2$ has been measured for highly embrittled materials. Fracture toughness data are reported in [M7], [M8] and [M9]. In addition to these references, fracture toughness data for thermal aged cast stainless steel can be found in [M36], see also [M19].

*M2.7 Stainless steel cladding*

Many ferritic pressure vessels and piping used for nuclear applications are cladded with a stainless steel layer. Fracture properties for these materials are scarce. $J_R$-curves for three-wire series-arc weld overlay cladding with combinations of type 304, 308 and 309 stainless steel are reported in [M10], [M11] and [M12]. Unirradiated fracture toughness data (mean values of three tests) are given in Table M5. Fracture toughness data for cladding are also reported in [M12] and [M13], which is of the same order as those of [M10]. In [M10], [M12] and [M13], the influence from neutron irradiation on the fracture toughness properties of the cladding is also quantified. At 2 mm of stable crack growth, $J_R$-values are given in Table M6 as reported in [M12] in the unirradiated condition, which also agrees well with the data presented in [M11].

Table M5. Fracture toughness data for unirradiated stainless steel cladding, ref. [M10]

| Temperature °C | $J_{Ic}$ (kJ/m$^2$) | $K_{cr}$ (MPa$\sqrt{m}$) |
|---|---|---|
| 20 | 157 | 186 |
| 120 | 132 | 167 |
| 288 | 75 | 122 |

Table M6.    Fracture toughness data at 2 mm of stable crack growth for unirradiated stainless steel cladding, ref. [M12]

| Temperature °C | $J_{2mm}$ (kJ/m$^2$) |
|---|---|
| 20 | 591 |
| 150 | 502 |
| 300 | 414 |

## M2.8  Nickel base alloys

Very few fracture toughness data for nickel base alloys are found in the literature. Alloy 600 is normally very ductile and should have a fracture toughness of the same level as the stainless steel base material in Table M2. For the weld material alloy 182, room temperature data and high temperature data are published in [M14], [M15], [M16], [M17] and [M18]. Table M7 summarizes the results. It should be noted that formally the thickness requirement according to ASTM E-813 was not fulfilled in the testing in [M15] and [M16], and new testing data have been performed at room and high temperatures for alloy 182 according to ASTM E-1820, ref [M17] and [M18]. Data including a small amount of stable crack growth ($\Delta a = 1 - 2$ mm) is also included in Table M7 [M18].

Table M7.    Fracture toughness data for alloy 182, ref [M17] and [M18]

| Temperature °C | $J_{Ic}$ (kJ/m$^2$) | $K_{cr}$ (MPa $\sqrt{m}$) | $K_{1mm}$ (MPa $\sqrt{m}$) | $K_{2mm}$ (MPa $\sqrt{m}$) |
|---|---|---|---|---|
| 20 | 182 | 205 | — | — |
| $\geq 190$ | 377 | 285 | 335 | 411 |

Typical experimental $J_R$-curves for SMAW for alloy 182 at room temperature and at 288°C is shown in figure M7 and figure M8 respectively. In this case the fracture toughness increase with the testing temperature. A comparison between the tests at 50°C and 288°C shows that the toughness increase with the testing temperature, and that the $J_R$-curve is steeper at high temperatures. Alloy 182 is a tough material compared to austenitic welding stainless steel (SAW and SMAW), which have lower toughness at high temperatures. For alloy 182 the yield stress is rather independent of the temperature, but for stainless steels the yield stress decrease with increasing temperature.
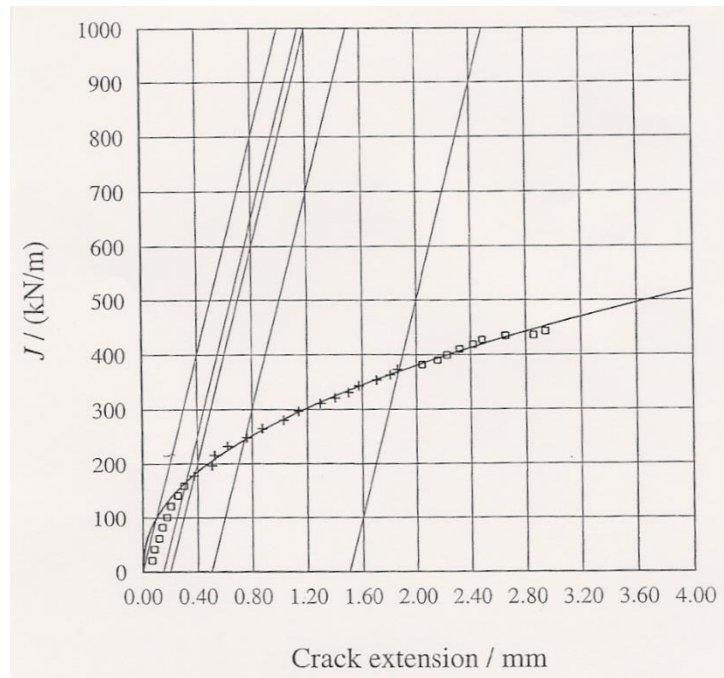
Figure M7. Typical $J_R$-curve for alloy 182 (SMAW-welding) at 50°C, ref. [M17].
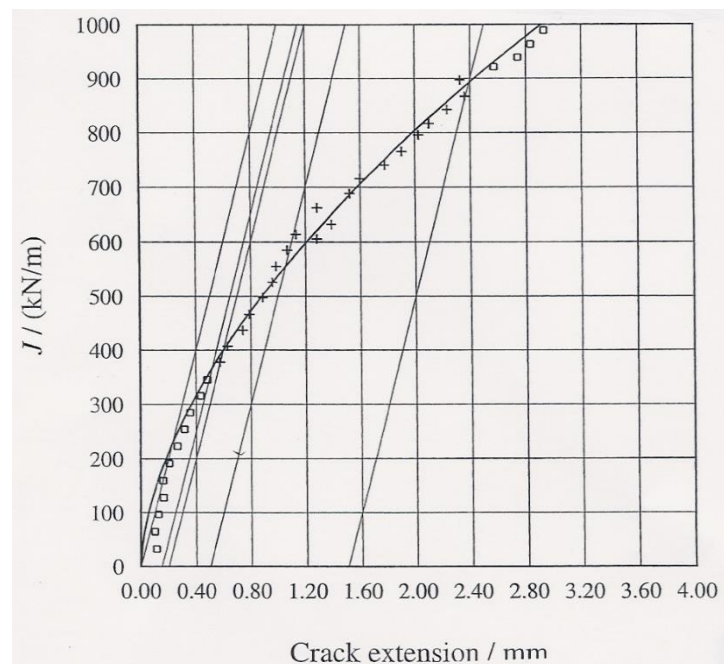


Figure M8. Typical $J_R$-curve for alloy 182 (SMAW-welding) at 190°C (similar at 288°C), ref. [M17]. The equation for $J$-mean, with 90% confidence, is $J_R = 519.70(\Delta a)^{0.5956}$ [M18].

## M3. Crack growth data, fatigue

Recommended fatigue crack growth data are described in this section. For nuclear applications in Sweden, the recommendations in the latest edition of [M19] shall also be observed. At the time of

publication for this edition of the handbook, an evaluation of different crack growth data is being undertaken. The results of which will be presented in [M19], expected during 2018. Generally the fatigue crack growth rate is written as

$$\frac{da}{dN} = C\left(\Delta K_{\mathrm{I}}\right)^n \quad \text{mm/cycle.} \tag{M3}$$

$C$ and $n$ are constants, and $\Delta K_{\mathrm{I}}$ is the range of applied stress intensity factor during the load cycle, i.e.

$$\Delta K_{\mathrm{I}} = K_{\mathrm{I}}^{max} - K_{\mathrm{I}}^{min} \quad . \tag{M4}$$

Beside the environment, $C$ and $n$ may also depend on the so-called $R$-value defined as

$$R = \frac{K_{\mathrm{I}}^{min}}{K_{\mathrm{I}}^{max}} \quad . \tag{M5}$$

Both $R$ and $\Delta K_{\mathrm{I}}$ may be corrected with respect to a compressive phase during a load cycle. For cases when $R < 0$ the influence of the $R$-value on the crack growth rate can be estimated by use of growth data for $R = 0$. If $K_{\mathrm{I}}^{min}$ is negative, an effective stress intensity factor range can be estimated as $\Delta K_{\mathrm{I}}^{eff} = K_{\mathrm{I}}^{max}$. Note that the equations in Table M8 – Table M12 results in growth rates as mm/cycle provided that $K_{\mathrm{I}}$ is given in MPa $\sqrt{\mathrm{m}}$.

References to fatigue data for different materials in nuclear applications are presented below. Data for other materials and environments can for example be found in ref. [M20].

## M3.1 Ferritic steel, plates, pressure vessels

Fatigue crack growth data for the material SA-533 Grade B Class 1, SA-508 Class 2 and SA-508 Class 3 can be found in ASME 2007 Sect. XI, appendix A-4300 [M1] for cracks both in air and reactor water environment.

## M3.2 Austenitic stainless steel, pipes

Fatigue crack growth data for austenitic stainless steel, 304, in air environment can be found in ASME 2007 Sect. XI, appendix C-8410 [M1].

In MD-02 [M20], fatigue crack growth data for austenitic stainless steel, 304, are evaluated for typical BWR reactor water environment. Similar crack growth data were concluded for NWC and HWC environments. The results are specified to be applicable for both BWR and PWR environments. Fatigue crack growth data for different frequencies are presented in Table M8 ($f \geq 0.1$ Hz), Table M9 ($0.1$ Hz $\leq f < 1$ Hz) and Table M10 ($f < 0.1$ Hz).

Table M8. Crack growth data for fatigue of stainless steel, 304, in reactor water environment, $f \geq 1$ Hz [M20]

| Environment | $\Delta K_I$ [MPa $\sqrt{m}$] | $da/dN$ [mm/cycle] |
|---|---|---|
| BWR + PWR | > 5 | $6.41 \cdot 10^{-9}(1+1.8R)\Delta K_I^{3.30}$ |
| BWR + PWR | ≤ 5 | $3.10 \cdot 10^{-23}\Delta K_I^{24.75}$ |

Threshold definition at $f \geq 1$ Hz; the $\Delta K_I$ where the crack growth rate is $10^{-9}$ mm/cycle, which gives the value 3.5 MPa $\sqrt{m}$.

Table M9. Crack growth data for fatigue of stainless steel, 304, in reactor water environment, $0.1$ Hz $\leq f < 1$ Hz [M20]

| Environment | $\Delta K_I$ [MPa $\sqrt{m}$] | $da/dN$ [mm/cycle] |
|---|---|---|
| BWR + PWR | ≥ 0 | $6.41 \cdot 10^{-9}(1+1.8R)\Delta K_I^{3.30}$ |

Table M10. Crack growth data for fatigue of stainless steel, 304, in reactor water environment, $f < 0.1$ Hz [M20]

| Environment | $\Delta K_I$ [MPa $\sqrt{m}$] | $da/dN$ [mm/cycle] |
|---|---|---|
| BWR + PWR | ≥ 0 | $4.55 \cdot 10^{-8}\Delta K_I^{3.35}$ |

For pressurized water reactor environments fatigue crack growth data for austenitic stainless steels, 304, 316, 304L and 316L are presented in ASME Code Case N-809 [M31]. Note that the recommendations in the latest edition of [M19] shall be observed for nuclear applications in Sweden.

*M3.3 Alloy 600*

Fatigue crack growth data for alloy 600, can be found in ASME 2007 Sect. XI, appendix C-8411 [M1] for cracks both in air and reactor water environment.

*M3.4 Alloy 182*

Fatigue crack growth data for alloy 182, at different frequencies are given in Table M11 ($f \geq 0.1$ Hz) and Table M12 ($f < 0.1$ Hz).

Table M11. Crack growth data for fatigue of Alloy 182, in reactor water environment, $f \geq 0.1$ Hz [M20]

| Environment | $\Delta K_I$ [MPa $\sqrt{m}$] | $da/dN$ [mm/cycle] |
|---|---|---|
| BWR + PWR | > 5.45 | $6.41 \cdot 10^{-9}\Delta K_I^{3.30}$ |
| BWR + PWR | ≤ 5.45 | $5.63 \cdot 10^{-20}\Delta K_I^{18.31}$ |

Threshold definition; the $\Delta K_I$ where the crack growth rate is $10^{-9}$ mm/cycle, which gives the value 3.6 MPa$\sqrt{m}$.

Table M12. Crack growth data for fatigue of Alloy 182, in reactor water environment, $f < 0.1$ Hz [M20]

| Environment | $\Delta K_I$ [MPa $\sqrt{m}$ ] | d$a$/d$N$ [mm/cycle] |
|---|---|---|
| BWR + PWR | $\geq 0$ | $1.55 \cdot 10^{-8} \Delta K_I^{3.30}$ |

## M4. Crack growth data, stress corrosion

Recommended stress corrosion crack growth data are described in this section. For nuclear applications in Sweden, the recommendations in the latest edition of [M19] shall also be observed. At the time of publication for this edition of the handbook, an evaluation of different crack growth data is being undertaken. The results of which will be presented in [M19], expected during 2018. Generally the stress corrosion crack growth rate is written as

$$\frac{da}{dt} = CK_I^n \text{ mm/s,} \tag{M6}$$

$C$ and $n$ are constants, and $K_I$ is the applied stress intensity factor.

### M4.1 BWR-environment

Stress corrosion crack growth data for stainless steels and nickel base alloys can be found in ref. [M21] and [M22]. These data have been reviewed in ref. [M23], [M24], [M25], [M26] and [M27]. The data are given in Table M13 (austenitic stainless steel in normal water chemistry), Table M14 (austenitic stainless steel in hydrogen water chemistry), Table M15 (Alloy 182 in normal water chemistry), Table M16 (Alloy 182 in hydrogen water chemistry), Table M17 (Alloy 600 in normal water chemistry), Table M18 (Alloy 600 in hydrogen water chemistry), Table M19 (Alloy 82 in normal water chemistry) and Table M20 (Alloy 82 in hydrogen water chemistry).

Table M13. Stress corrosion crack growth rate for stainless steel in normal water chemistry [M21], [M24]

| Environment | $K_I$ [MPa $\sqrt{m}$ ] | d$a$/d$t$ [mm/s] |
|---|---|---|
| BWR | $< 55.5$ | $1.46 \cdot 10^{-12} K_I^{3.0}$ |
| BWR | $\geq 55.5$ | $2.5 \cdot 10^{-7}$ |

Table M14.  Stress corrosion crack growth rate for stainless steel in hydrogen water chemistry [M21]

| Environment | $K_I$ [MPa$\sqrt{m}$] | d$a$/d$t$ [mm/s] |
|---|---|---|
| BWR | > 0 | $7.04 \cdot 10^{-14} K_I^{3.0}$ |

Table M15.  Stress corrosion crack growth rate for Alloy 182 in normal water chemistry [M22], [M25]

| Environment | $K_I$ [MPa$\sqrt{m}$] | d$a$/d$t$ [mm/s] |
|---|---|---|
| BWR | < 30 | $5.1 \cdot 10^{-14} K_I^{4.8}$ |
| BWR | ≥ 30 | $6.28 \cdot 10^{-7}$ |

Table M16.  Stress corrosion crack growth rate for Alloy 182 in hydrogen water chemistry [M22], [M1], [M26]

| Environment | $K_I$ [MPa$\sqrt{m}$] | d$a$/d$t$ [mm/s] |
|---|---|---|
| BWR | < 30 | $2.8 \cdot 10^{-14} K_I^{4.3}$ |
| BWR | ≥ 30 | $6.29 \cdot 10^{-8}$ |

Table M17.  Stress corrosion crack growth rate for Alloy 600 in normal water chemistry [M22], [M27]

| Environment | $K_I$ [MPa$\sqrt{m}$] | d$a$/d$t$ [mm/s] |
|---|---|---|
| BWR | < 30 | $5.0 \cdot 10^{-15} K_I^{5}$ |
| BWR | ≥ 30 | $1.22 \cdot 10^{-7}$ |

Table M18.  Stress corrosion crack growth rate for Alloy 600 in hydrogen water chemistry [M22], [M26]

| Environment | $K_I$ [MPa$\sqrt{m}$] | d$a$/d$t$ [mm/s] |
|---|---|---|
| BWR | < 30 | $4.2 \cdot 10^{-14} K_I^{3.7}$ |
| BWR | ≥ 30 | $1.23 \cdot 10^{-8}$ |

Table M19.  Stress corrosion crack growth rate for Alloy 82 in normal water chemistry [M22], [M25]

| Environment | $K_I$ [MPa$\sqrt{m}$] | d$a$/d$t$ [mm/s] |
|---|---|---|
| BWR | < 30 | $2.0 \cdot 10^{-15} K_I^{5.5}$ |
| BWR | ≥ 30 | $2.66 \cdot 10^{-7}$ |

Table M20.  Stress corrosion crack growth rate for Alloy 82 in hydrogen water chemistry [M22], [M1], [M26]

| Environment | $K_I$ [MPa $\sqrt{m}$] | d$a$/d$t$ [mm/s] |
|---|---|---|
| BWR | < 30 | $6.1 \cdot 10^{-14} K_I^{3.8}$ |
| BWR | ≥ 30 | $2.5 \cdot 10^{-8}$ |

*M4.2  PWR-environment*

For Alloy 182 in PWR-environment the stress corrosion crack growth rate at different temperatures are given in Table M21. For Alloy 600 in PWR-environment the stress corrosion crack growth rate at different temperatures are given in Table M22.

Table M21.  Stress corrosion crack growth rate for Alloy 182 in PWR-environment [M28], [M29]

| Environment / Temperature | $K_I$ [MPa $\sqrt{m}$] | $da/dt$ [mm/s] |
|---|---|---|
| PWR / 290°C | — | — |
| PWR / 320°C | < 27.5 | $3.61 \cdot 10^{-15} K_I^{5.76}$ |
| | ≥ 27.5 | $7.05 \cdot 10^{-7}$ |
| PWR / 345°C | < 26.7 | $1.05 \cdot 10^{-14} K_I^{5.76}$ |
| | ≥ 26.7 | $1.73 \cdot 10^{-6}$ |

Table M22.  Stress corrosion crack growth rate for Alloy 600 in PWR-environment [M30]

| Environment / Temperature | $K_I$ [MPa $\sqrt{m}$] | $da/dt$ [mm/s] |
|---|---|---|
| PWR / 290°C | < 30 | $4.0 \cdot 10^{-19} K_I^{7.5}$ |
| | ≥ 30 | $4.79 \cdot 10^{-8}$ |
| PWR / 320°C | < 30 | $7.0 \cdot 10^{-17} K_I^{6.5}$ |
| | ≥ 30 | $2.8 \cdot 10^{-7}$ |
| PWR / 345°C | < 30 | $1.6 \cdot 10^{-16} K_I^{6.5}$ |
| | ≥ 30 | $6.39 \cdot 10^{-7}$ |

## M5. References

[M1]    —, (2007), ASME Boiler and Pressure Vessel Code, The American Society of Mechanical Engineers, New York, U.S.A.

[M2]    NORRIS, D.M., (1988), "Evaluation of flaws in ferritic piping", Final Report EPRI NP-6045, EPRI Research Institute, U.S.A.

[M3]    ZANG, W., and J. LINDER, (1998), "Fracture toughness and tensile properties for austenitic stainless steels and welds", SAQ/FoU-Report 98/01.

[M4]    SUND, G, (1991), "Fracture toughness of stainless steel", Report No. M-91/26 (in Swedish), Studsvik AB, Studsvik, Sweden.

[M5]    LANDES, J. D., and D. E. McCABE, (1986), "Toughness of Austenitic Stainless Steel Pipe Welds", TopicalReport EPRI NP-4768, EPRI Research Institute, U.S.A.

[M6]    —, (2001), "Standard test method for measurement of fracture toughness", ASTM Standard E1820-01, American Society for Testing and Materials, Philadelphia.

[M7]    Mc DONALD, P., and J. W., SHECKHERD, (1987), "Fracture toughness characterization of thermally aged cast stainless steels", EPRI NP-5439, EPRI Research Institute, U.S.A.

[M8]    HISER, L., (1988), "Tensile and JR-curve characterization of thermally aged cast stainless steels", NUREG/CR-5024, USNRC, Washington D.C., U.S.A.

[M9]    JANSSON, C., (1995), "Degradation of cast stainless steels-a literature survey", SKI Rapport 95:96 (in Swedish), Swedish Nuclear Power Inspectorate, Stockholm, Sweden.

[M10]   HAGGAG, F. M., CORWIN, W. R., and R. K., NANSTAD, (1989), "Effects of irradiation on the fracture properties of stainelss steels weld overlay cladding", Post-SMIRT Conference No 2, Monterey, U.S.A.

[M11]   BASS, R., WINTLE, J., HURST, R. C., and N. TAYLOR, (2001), "NESC-I Project Overview – Final Report", EUR 19051, JRC Petten, European Commission.

[M12]   SATTARI-FAR, I., and M. ANDERSSON, (2006), "Cladding Effects on Structural Integrity of Nuclear Components", SKI Report 2006:23, Swedish Nuclear Power Inspectorate.

[M13]   HAGGAG, F. M., and R. K. NANSTAD, (1997), "Effects of thermal aging and neutron irradiation on the mechanical properties of three-wire stainless steel weld overlay cladding", Report No NUREG/CR-6363, Oak Ridge National Laboratory and U.S. Nuclear Regulatory Commission.

[M14]   YOSHIDA, K., KOJIMA, M., IIDA, M. and I., TAKAHASHI, (1990), "Fracture toughness of weld metals in steel piping for nuclear power plants", *The International Journal of Pressure Vessels and Piping*, Vol. 43, pp. 273-284.

[M15]   BERGENLID, U., (1991), "Fracture toughness of alloy 182 at room temperature", Report No. M-91/129 (in Swedish), Studsvik AB, Studsvik, Sweden.

[M16]   BERGENLID, U., (1991), "Fracture toughness of alloy 182 at 285 °C", Report No. M-91/95 (in Swedish), Studsvik AB, Studsvik, Sweden.

[M17]   ÖBERG, H., (2001), "Fracture mechanical testing of alloy 182", Report DNV 0102, Rev. 010312, The institution of fracture mechanics, Royal Technical School, Sweden.

[M18]   DILLSTRÖM, P., (2002), "Fracture toughness data and JR-curves for Inconel 182", Technical Report 10827200-1 (in Swedish), Rev. 0, Det Norske Veritas AB.

[M19]  BRICKSTAD, B., EKSTRÖM, P., FORSBERG, F. and KJELLIN, D., (2018) "Metodik för analys av skador i mekaniska anordningar i kärntekniska anläggningar, Utredningsrapport SSM2013-3128-2, Swedish Radiation Safety Authority, Stockholm, Sweden (under preparation).

[M20]  JANSSON, C., and U. MORIN, (1995), "Fatigue crack growth in reactor material", MD-02 (in Swedish), Report GEK 87/95, Vattenfall Energisystem AB and Sydkraft Konsult, Sweden.

[M21]  JANSSON, C., (1999), "Stress corrosion growth in BWR environment", MD-01, Rev. 3, Report T-SEK 41/99, SwedPower AB, Sweden.

[M22]  JANSSON, C., (2006), "Materialdatabok MD-01 - Revision 3.1 (2006) Spänningskorrosionstillväxt i BWR-miljö", Rapport T-CKM 06/001, Vattenfall Power Consultant, Sweden.

[M23]  SUND, G., (2000), "Review of MD-01 Rev.3", Report No 102424000-1 (in Swedish), DNV Nuclear Technology, Sweden.

[M24]  RASHID, B., and G. SUND, (2001), "Review of new data points for the plateau of Alloy 182 and 304 in NWC according to MD-01 rev 3", BAR-01-06-28; 17:45, 11143301, Letter 2001-06-28 (in Swedish), DNV Nuclear Technology, Sweden.

[M25]  FISHER, F., (2008), "Inspection report: FRA-All-080227-1", ÅF-TÜV Nord AB, Sweden.

[M26]  TROEDSSON, I., (2012), "Review report: ITO-alla-121128-1", TÜV NORD Sweden, Sweden.

[M27]  —, (2010), "Inspection report: ITO-All-100518-2", ÅF-TÜV Nord AB, Sweden.

[M28]  RASHID, B., and G. SUND, G., (2002), "Review of stress corrosion crack growth rates curves of alloy 182 in PWR environment", BAR-02-04-25; 13:50, 11400701, Letter 2002-04-25 (in Swedish), DNV Nuclear Technology, Sweden.

[M29]  SUND, G., (2002), "Crack growth at 290 °C in PWR-environment", Letter in Swedish at 2002-05-03, DNV Nuclear Technology, Sweden.

[M30]  RASHID, B., and G. SUND, (2002), "Review of stress corrosion crack growth rates curves of alloy 600 in PWR environment", BAR-02-02-14; 18:45, 1136601, Letter 2002-02-14 (in Swedish), DNV Nuclear Technology, Sweden.

[M31]  —, (2015), "Case N-809 Reference Fatigue Crack Growth Rate Curves for Austenitic Stainless Steels in Pressurized Water Reactor  Environments Section XI, Division 1", The American Society of Mechanical Engineers, New York, U.S.A.

[M32]  KIRK, M. T., STEVENS, G. L., ERICKSON, M., and YIN, S., (2011), "A Proposal for the Maximum $K_{IC}$ for use in ASME Code Flaw and Fracture Toughness Evaluations", *ASME PVP*, 2011-57173.

[M33]  SATTARI-FAR, I., (2002), "Fracture Toughness of Ferritic Reactor Steels in the Upper-Shelf Region", DNV Nuclear Technology, Sweden.

[M34]  CHOPRA, O. K., and SHACK, W. J., (2008), "Crack Growth Rates and Fracture Toughness of Irradiated Austenitic Stainless Steels in BWR environments", ANL-06/58, NUREG/CR-6960, U.S. Nuclear Regulatory Commission.

[M35]  CHOPRA, O. K., (2015), "Effects of Thermal Aging and Neutron Irradiation on Crack Growth Rate and Fracture Toughness of Cast Stainless Steels and Austenitic Stainless Steels Welds", ANL-14/10, NUREG/CR-7185, U.S. Nuclear Regulatory Commission.

[M36]  CHOPRA, O. K., (2016), "Estimation of Fracture Toughness of Cast Stainless Steels During Thermal Aging in LWR Systems", NUREG/CR-4513, Rev. 2, U.S. Nuclear Regulatory Commission.

## APPENDIX S.  SAFETY FACTORS FOR NUCLEAR APPLICATIONS

For the choice of safety factors the objective is to retain the safety margins expressed in ASME 2007, Sect. III and XI [S1]. The safety factors are divided into two categories; safety factors against fracture, $SF_K$, and safety factors against plastic collapse, $SF_L$.

### S1.        Safety factors against fracture

$SF_K$ is the safety factor on $K_{cr}$ and corresponds to the safety factor $SF_J$ on $J_{Ic}$. These are related through

$$SF_K = \sqrt{SF_J}. \tag{S1}$$

Table S1 show the safety factors against fracture according to ASME 2007, Sect. XI IWB-3612.

Table S1.  Safety factors against fracture according to ASME 2007, Sect. XI IWB-3612

| Service Level | $SF_K$ |
|:---:|:---:|
| A/B | $\sqrt{10}$ |
| C/D | $\sqrt{2}$ |

### S2.        Safety factors against plastic collapse

$SF_L$ is the safety factor on $L_r$ and is developed with the intent to retain the safety margins expressed in ASME 2007 Sect. III following the methodology [S2] used to derive the safety margins in ASME 2007, Sect XI. More information about the development of this methodology can be found in [S3].

The safety factors are calculated using material data and requires the flow stress, $\sigma_f$, according to ASME 2007 Sect. XI, Appendix C-8200

$$\sigma_f = \frac{\sigma_y^T + \sigma_u^T}{2}, \tag{S2}$$

as well as the design stress intensity, $S_m$, according to ASME 2007 Sect. II. For ferritic materials, $S_m$ can be calculated through

$$S_m = \min\left[ \tfrac{2}{3}\, \sigma_y^{20°C}, \quad \tfrac{1}{3}\, \sigma_u^{20°C}, \quad \tfrac{2}{3}\, \sigma_y^T, \quad \tfrac{1}{3}\, \sigma_u^T \right], \tag{S3}$$

and for austenitic materials it can be calculated through

$$S_m = \min\left[ \tfrac{2}{3}\, \sigma_y^{20°C}, \quad \tfrac{1}{3}\, \sigma_u^{20°C}, \quad 0.9\sigma_y^T, \quad \tfrac{1}{3}\, \sigma_u^T \right]. \tag{S4}$$

For membrane and local bending stresses the safety factor, $SF_L{}^m$, is calculated through

$$SF_L^m = \frac{\sigma_f}{S_m C_p}, \tag{S5}$$

where $C_p$ according to ASME 2007, Sect. III is

$$C_p = \begin{cases} 1.0 & \text{Level A} \\ 1.1 & \text{Level B} \\ 1.5 & \text{Level C} \\ 2.0 & \text{Level D} \end{cases}.$$
(S6)

If the only primary stress is a local membrane stress, $P_L$, the structural factor, $SF_L{}^m$, may be divided by 1.5 for Level A and B load cases in accordance with ASME 2007, Sect III, Figure NB-3221-1.

For global bending stresses the safety factor, $SF_L{}^b$, is calculated through

$$SF_L^b = \max\left[ 1.0, \begin{array}{ll} \dfrac{4}{f_1\pi} \cdot \dfrac{\sigma_f}{S_m} & \text{if} \quad f_1 S_m \le f_2 \sigma_y \\[2mm] \dfrac{4}{f_2\pi} \cdot \dfrac{\sigma_f}{\sigma_y} & \text{if} \quad f_1 S_m > f_2 \sigma_y \end{array} \right],$$
(S7)

where $f_1$ and $f_2$ are safety factors against global bending according to ASME III, Sect III are presented in table S2.

Table S2. Safety factors against global bending according to ASME 2007, Sect III

| Load Level | A | B | C | D |
|---|---|---|---|---|
| $f_1$ | 1.5 | 1.8 | 2.25 | 3.0 |
| $f_2$ | 1.5 | 1.5 | 1.8 | 2.0 |

As there are different safety factors ($SF_L$) for membrane ($SF_L{}^m$) and global bending ($SF_L{}^b$) stresses. When doing a safety assessment, using the procedure in this handbook, an equivalent safety factor ($SF_L$) is introduced

$$SF_L = \frac{L_r^m SF_L^m + L_r^b SF_L^b}{L_r^m + L_r^b},$$
(S8)

where $L_r{}^m$ is the limit load where only membrane stresses are taken into account and $L_r{}^b$ is the limit load where only global bending stresses are taken into account.

## S3. References

[S1]     —, (2007), ASME Boiler and Pressure Vessel Code, The American Society of Mechanical Engineers, New York, U.S.A.

[S2]     CIPOLLA, R. C., SCARTH, D. A., WILKOWSKI, G. M., and V. A. ZILBERSTEIN, (2001), "Technical basis for proposed revision to acceptance criteria for ASME Section XI pipe flaw evaluation", *Proceedings of the 2001 ASME Pressure Vessels & Piping Conference*, Vol. 422, pp. 31-51.

[S3]     VON UNGE, P., (2016), "Säkerhetsvärdering mot plastisk kollaps vid skadetålighetsanalyser", Research Report 2016:35, Swedish Radiation Safety Authority, Stockholm, Sweden. (Available at: http://www.stralsakerhetsmyndigheten.se)

# APPENDIX P. PROBABILISTIC ANALYSIS

Probabilistic calculations can be used as an alternative to the deterministic procedure in order to study safety margins. This is especially useful in cases where the deterministic calculations are close to the safety limits. With probabilistic analyses, it can be studied if sufficiently low probability of failure can be assured.

Probabilistic analysis gives a greater insight into the structural integrity of components than similar deterministic analyses. The analysis allows a direct representation of uncertainties through the use of best-estimate models and distributed inputs. This probabilistic analysis methodology permits determination of the direct impact of uncertainties on the results, which gives the user the ability to determine and possibly refine the specific drivers to the problem.

A probabilistic procedure is included, in the handbook, to calculate two different failure probabilities, $P_F$:

- Probability of failure, defect size given by NDT/NDE.
- Probability of failure, defect not detected by NDT/NDE.


## P1.     Failure probabilities

The procedure [P1-P2] uses two different limit state functions, $g(X)$ ($g_{FAD}(X)$ and $g_{L_r^{max}}(X)$).

$$g_{FAD}(X) = f_{FAD}(X) - K_r(X) \quad , \tag{P1}$$

$$g_{L_r^{max}}(X) = L_r^{max}(X) - L_r(X) \quad . \tag{P2}$$

These limit state functions are based on a simplified R6 failure assessment curve [P3-P4]. To calculate the probability of failure, a multi-dimensional integral has to be evaluated [P1-P2]:

$$P_F = \Pr[g(X) < 0] = \int_{g(X)<0} f_X(x)dx \quad . \tag{P3}$$

The set where the above analysed event is fulfilled, is formulated as $g(X) < 0$, and is called the failure set. The set where $g(X) > 0$ is called the safe set. $f_X(x)$ is a known joint probability density function of the random vector $X$. This integral is very hard (impossible) to evaluate, by numerical integration, if there are many random parameters.

## P2. Parameters

Within the procedure, the following parameters are treated as random parameters:

- Fracture toughness
- Yield strength
- Ultimate tensile strength
- Primary stresses
- Secondary stresses
- Defect size (depth) given by NDT/NDE
- Defect distribution (when a defect is not detected by NDT/NDE)
- POD-curve (when a defect is not detected by NDT/NDE)
- Constants in the fatigue crack growth law
- Constants in the SCC crack growth law

These random parameters are treated as not being correlated with one another. The parameters can follow a normal, lognormal, Weibull or an exponential distribution.

### P2.1 Fracture toughness

The fracture toughness can follow a normal, lognormal or Weibull distribution.

The normal probability density function has the following form:

$$f(K_I) = \frac{1}{\sigma_{K_{Ic}} \cdot \sqrt{2 \cdot \pi}} \exp\left(-\frac{1}{2} \cdot \left[\frac{K_I - \mu_{K_{Ic}}}{\sigma_{K_{Ic}}}\right]^2\right) \quad , \tag{P4}$$

where $\mu_{K_{Ic}}$ (mean) and $\sigma_{K_{Ic}}$ (standard deviation) are input data.

The lognormal probability density function has the following form:

$$f(K_I) = \frac{1}{K_I \cdot \sigma_{LogNor} \cdot \sqrt{2 \cdot \pi}} \exp\left(-\frac{1}{2} \cdot \left[\frac{\ln(K_I) - \mu_{LogNor}}{\sigma_{LogNor}}\right]^2\right) \quad , \tag{P5}$$

where $\mu_{LogNor}$ and $\sigma_{LogNor}$ are the log-normal distribution parameters. $\mu_{K_{Ic}}$ (mean) and $\sigma_{K_{Ic}}$ (standard deviation) are input data and are related to the lognormal distribution parameters as follow:

$$\mu_{LogNor} = \ln\left(\mu_{K_{Ic}}\right) - \frac{1}{2} \cdot \left(\sigma_{LogNor}\right)^2 \quad , \tag{P6}$$

$$\sigma_{LogNor} = \sqrt{\ln\left[1 + \left(\frac{\sigma_{K_{Ic}}}{\mu_{K_{Ic}}}\right)^2\right]} \quad . \tag{P7}$$

The Weibull probability density function has the following form:

$$f(K_I) = \frac{k}{\theta} \cdot \left(\frac{K_I}{\theta}\right)^{k-1} \cdot \exp\left(-\left(\frac{K_I}{\theta}\right)^k\right) \quad , \tag{P8}$$

where $\theta$ (scale) and $k$ (shape) are the Weibull distribution parameters. $\mu_{K_{Ic}}$ (mean) and $\sigma_{K_{Ic}}$ (standard deviation) are input data and are related to the Weibull distribution parameters as follow:

$$\mu_{K_{Ic}} = \frac{\theta}{k} \cdot \Gamma\left(\frac{1}{k}\right) \quad , \tag{P9}$$

$$\sigma_{K_{Ic}} = \sqrt{\frac{\theta^2}{k} \cdot \left[2 \cdot \Gamma\left(\frac{2}{k}\right) - \frac{1}{k} \cdot \Gamma\left(\frac{1}{k}\right)^2\right]} \quad , \tag{P10}$$

where $\Gamma(z)$ is the gamma function, defined by the integral

$$\Gamma(z) = \int_0^\infty t^{z-1} \cdot e^{-t} dt \tag{P11}$$

This non-linear system of equations is solved using a globally convergent method with line search and an approximate Jacobian matrix.

### P2.2 *Yield strength and Ultimate tensile strength*

The Yield strength and the Ultimate tensile strength can follow a normal, lognormal or Weibull distribution. For information regarding input data and distribution parameters, see section P2.1 above.

### P2.3 *Primary stresses / Secondary stresses*

The Primary stresses and the Secondary stresses can follow a normal distribution. For information regarding input data and distribution parameters, see section P2.1 above.

*P2.4*     *Defect size given by NDT/NDE / Defect size distribution*

The defect size given by NDT/NDE or the defect size distribution can follow a normal, lognormal or exponential distribution. For information regarding input data and distribution parameters, using a normal or lognormal distribution, see section P2.1 above.

The exponential probability density function has the following form:

$$f(a) = \lambda \cdot \exp(-\lambda \cdot a) \quad , \tag{P12}$$

where $\lambda$ is the exponential distribution parameter. $\mu_a$ (mean) is input data (equal to the standard deviation, $\sigma_a$, for this distribution) and is related to $\lambda$ as follows:

$$\mu_a = \sigma_a = \frac{1}{\lambda} \quad . \tag{P13}$$

*P2.5*     *POD-curve / Defect not detected by NDT/NDE*

The parameter defect not detected by NDT/NDE can follow a non-constant POD-distribution (POD – Probability Of Detection):

$$POD = F_{POD}\left(\frac{a}{t}\right) = \Phi\left(c_1 + c_2 \ln\left(\frac{a}{t}\right)\right) \quad , \tag{P14}$$

where $\Phi(\ldots)$ is the cumulative distribution function in a standard normal space, $a$ is the defect depth and $t$ is the wall thickness.

*P2.6*     *Constants in the fatigue crack growth law / SCC crack growth law*

The Constants in the fatigue crack growth law and the Constants in the SCC crack growth law can follow a normal distribution. For information regarding input data and distribution parameters, see section P2.1 above.

## P3. Calculation of failure probabilities

As mentioned above, the failure probability integral is very hard to solve using numerical integration. Instead, the following numerical algorithms are included within the procedure [P1-P2]:

- Simple Monte Carlo Simulation (MCS)
- First-Order Reliability Method (FORM)

### P3.1 Simple Monte Carlo Simulation (MCS)

MCS is a simple method that uses the fact that the failure probability integral can be interpreted as a mean value in a stochastic experiment [P6]. An estimate is therefore given by averaging a suitably large number of independent outcomes (simulations) of this experiment.

The basic building block of this sampling is the generation of random numbers from a uniform distribution (between 0 and 1). Simple algorithms "repeats themselves" (already) after approximately $2 \cdot 10^3$ to $2 \cdot 10^9$ simulations and are therefore not suitable to calculate medium to small failure probabilities [P6-P7]. The algorithm chosen repeats itself after approx. $2 \cdot 10^{18}$ simulations [P7]. This algorithm is approximately 20 times slower than the simpler algorithms mentioned above, but it is recommended if one needs more than $1 \cdot 10^8$ simulations.

Once a random number $u$, between 0 and 1, has been generated, it can be used to generate a value of the desired random variable with a given distribution. A common method is the inverse transform method. Using the cumulative distribution function $F_X(x)$, the random variable would then be given as:

$$x = F_X^{-1}(u) \quad .$$
(P15)

To calculate the failure probability, one performs $N$ deterministic simulations and for every simulation checks if the component analysed has failed (i. e. if $g(X) < 0$). The number of failures is $N_F$, and an estimate of the mean probability of failure is:

$$P_{F,MCS} = \frac{N_F}{N} \quad .$$
(P16)

An advantage with MCS, is that it is robust and easy to implement into a computer program, and for a sample size $N \to \infty$, the estimated probability converges to the exact result. Another advantage is that MCS works with any distribution of the random variables and there is no restriction on the limit state functions.

However, MCS is inefficient when calculating failure probabilities, since most of the contribution to $P_F$ is in a limited part of the integration interval.

A simple error estimate (of the probability of failure) can be calculated [P8]:

$$\varepsilon_{MCS} = \sqrt{\frac{1-P_{F,MCS}}{N \cdot P_{F,MCS}}} \cdot \Phi^{-1}\left(\frac{1+\alpha}{2}\right) \quad , \tag{P17}$$

where $\Phi(\dots)$ is the cumulative distribution function in a standard normal space and $\alpha$ is a given confidence level.

*P3.2      Monte Carlo Simulation with Importance Sampling (MCS-IS)*

MCS-IS is an algorithm that concentrates the samples in the most important part of the integration interval. Instead of sampling around the mean values (MCS), one samples around the most probable point of failure (MCS-IS). This point, called MPP, is generally evaluated using information from a FORM / SORM analysis (see section P3.3 below).

*P3.3      First/Second-Order Reliability Method (FORM / SORM)*

FORM / SORM uses a combination of both analytical and approximate methods, when estimating the probability of failure [P6, P9].

First, one transforms all the variables into equivalent normal variables in standard normal space (i. e. with mean = 0 and standard deviation = 1). This means that the original limit state surface $g(x)=0$ then becomes mapped onto the new limit state surface $g_U(u)=0$.

Secondly, one calculates the shortest distance between the origin and the limit state surface (in a transformed standard normal space $U$). The answer is a point on this surface, and it is called the most probable point of failure (MPP), design point or $\beta$-point. The distance between the origin and the MPP is called the reliability index $\beta_{HL}$ (see Figure P1).
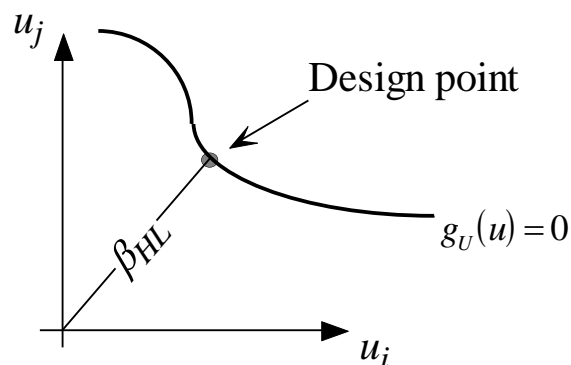


Figure P1.    The definition of design point / MPP and reliability index $\beta_{HL}$.

In general, it requires an appropriate non-linear optimisation algorithm to calculate the most probable point of failure.

One suitable choice to calculate the MPP is the NLPQL-algorithm by Schittkowski [P10]. This algorithm, for example used in the general-purpose probabilistic analysis program PROBAN [P11], was also tested in the development of this procedure [P1]. It gave excellent results for the geometry "a plate with an infinite surface defect", using analytic geometry functions. However, for the other geometries (with tabulated geometry functions), it gave quite slow convergence (or no convergence at all for the geometry "a cylinder with a part circumferential internal surface defect"). Therefore, the NLPQL-algorithm was not chosen for this probabilistic procedure.

In [P9] a linearization of the limit state function is used to calculate the MPP.

$$y_{i+1} = \frac{1}{\left|\nabla g_U(y_i)\right|^2} \cdot \left[\nabla g_U(y_i) \cdot y_i - g_U(y_i)\right] \cdot \nabla g_U(y_i)^T \quad , \tag{P18}$$

where $y_i$ is the current approximation to the MPP and $\nabla g_U(y_i)$ is the gradient of the limit state function. This algorithm, generally called the Rackwitz & Fiessler (R & F) algorithm [P12], is commonly used when evaluating $P_F$, mainly because it is very easy to implement and it converges fast in many cases. However, the R & F algorithm converges extremely slowly in some cases or oscillates about the solution without any convergence at all. Both of these problems occur when $P_F > 0.8$ or when $P_F < 10^{-7}$ (also between these values in some cases). Therefore, the R & F algorithm was not chosen for this probabilistic procedure.

Instead, a modified Rackwitz & Fiessler algorithm [P13-P14] was chosen. It works by "damping" the gradient contribution of the limit state function and this algorithm is very robust and converges quite fast for most cases. In this algorithm one defines a search direction vector $d_i$:

$$d_i = \frac{1}{\left|\nabla g_U(y_i)\right|^2} \cdot \left[\nabla g_U(y_i) \cdot y_i - g_U(y_i)\right] \cdot \nabla g_U(y_i)^T - y_i \quad . \tag{P19}$$

A new approximation to the MPP can then be calculated:

$$y_{i+1} = y_i + s_i \cdot d_i \quad . \tag{P20}$$

The step size $s_i$ as given in [P13] gave quite slow convergence (or no convergence at all for the geometry "a cylinder with a part circumferential internal surface defect"), especially when dealing with the $L_r^{max}$ limit state function in Eq. (P2). Instead a step size $s_i$ was selected as given in [P14] such that the inequality $m(y_i + s_i d_i) < m(y_i)$ holds, where $m(y_i)$ is the merit function:

$$m(y_i) = \frac{1}{2} \cdot |y_i|^2 + c \cdot |g_U(y_i)| \quad , \tag{P21}$$

in which $c$ is a parameter satisfying the condition $c > |y_i| / |\nabla g_U(y_i)|$ at each step $i$. This algorithm is globally convergent, i. e., the sequence is guaranteed to converge to a minimum-distance point on the limit state surface, provided $g_U(u)$ is continuous and differentiable [P14].

Finally, one calculates the failure probability using an approximation of the limit state surface at the most probable point of failure [P6, P9]. Using FORM, the surface is approximated to a hyperplane (a first order / linear approximation). SORM uses a second order / quadratic approximation to a hyperparaboloid (see figure P2.).
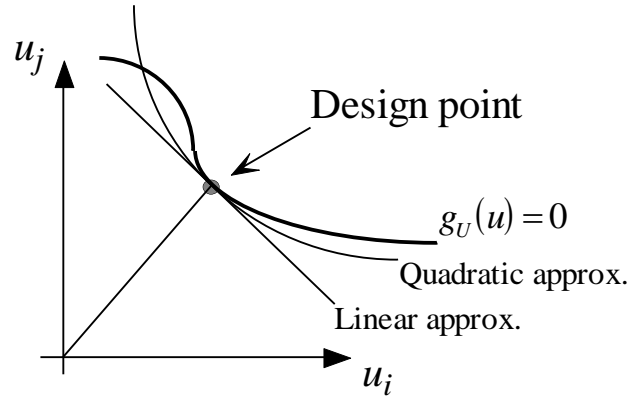


Figure P2.  Schematic difference between a linear and a quadratic approximation of the limit state surface.

The probability of failure is given as [P6, P9]:

$$P_{F,FORM} = \Pr\left[g_{Linear}(u) < 0\right] = \Phi(-\beta_{HL}) \quad , \tag{P22}$$

$$P_{F,SORM} = \Pr\left[g_{Quadratic}(u) < 0\right] \approx \Phi(-\beta_{HL}) \cdot \prod_{i=1}^{N-1} \left(1 - \kappa_i \cdot \beta_{HL}\right)^{-1/2} \quad , \tag{P23}$$

where $\Phi(u)$ is the cumulative distribution function in standard normal space and $\kappa_i$ are the principal curvatures of the limit state surface at the most probable point of failure (MPP).

FORM / SORM are, as regards CPU-time, extremely efficient as compared to MCS. Using the FORM implementation within this procedure, you get quite accurate results for failure probabilities between $10^{-1}$ to $10^{-15}$. A disadvantage is that the random parameters must be continuous, and every limit state function must also be continuous. SORM is not included in the present release of this procedure.

The algorithms presented above are applied when calculating the probability of failure before an inspection. When an inspection has been carried out, there are three levels of information available from the inspection [P15]:

- No detection: This implies that there either does not exist any defect, or that the defect size is less than the detection ability of the inspection method used.
- Detection without any sizing: This implies that a defect has been detected, but the size of the defect has not been sized.
- Detection with sizing: This implies that a defect has been detected and the size of the defect has been measured.

In addition there is a possibility of false identification, which is not included in our model.

Now the following events are defined [P15]:

- The limit state event: $G(t)$   This event is given by the R6-limit state functions defined in section P1. $G(t)$ less than zero implies failure at time $t$.

- The detection event: $D(t_i)$   This event is defined by evaluating the detectable defect size against the actual defect size at time $t_i$. $D(t_i)$ less than zero implies that the defect has been detected at time $t_i$.

Finally, the following failure probabilities are defined [P15]:

- The probability of failure at time $t$, before an inspection is then

$$P_F(t) = \Pr\big[G(t) \le 0\big] \quad . \tag{P24}$$

- The probability of failure at time $t$, after an inspection at time $t_i$ without any defect detection is then $(t > t_i)$

$$P_F(t) = \Pr\big[G(t) \le 0 \,|\, D(t_1) > 0\big] \quad . \tag{P25}$$

- The probability of failure at time $t$, after $N$ multiple inspections without any defect detection is then $(t > t_N > \ldots > t_2 > t_1)$

$$P_F(t) = \Pr\big[G(t) \le 0 \,|\, D(t_1) > 0 \cap D(t_2) > 0 \cap \ldots \cap D(t_N) > 0\big] \quad . \tag{P26}$$

The additional information from the inspection is included in the probability formulation through a conditioning, implying that the failure probability is estimated conditioned on the observed outcome from the inspections that have been carried out. The more available information that is included in the modelling of the failure probability, the more accurately the integrity of the system may be assessed.

In risk based inspection (RBI) studies, our main concern is non-detection of defects. Therefore, we want to evaluate the probability of failure at time $t$, after an inspection at time $t_1$ not resulting in any defect detection. Using Bayes theorem, Eq. (P25) becomes

$$P_F(t) = \frac{\Pr\left[G(t) \leq 0 \cap D(t_1) > 0\right]}{\Pr\left[D(t_1) > 0\right]} \quad . \tag{P27}$$

The limit state event $G(t)$ and the detection event $D(t_1)$ should not be mutually exclusive, since we are interested in events where $\Pr\left[G(t) \leq 0 \cap D(t_1) > 0\right] \neq 0$. If the two events were independent events, we would get the trivial solution $\Pr\left[G(t) \leq 0 \mid D(t_1) > 0\right] = \Pr\left[G(t) \leq 0\right]$. Therefore, the two events must be dependent of each other.

To simplify the calculations, we now assume that the outcome of the detection event is linked to a repair strategy for the component (when a defect is detected, it is assumed that either an effective repair is made or that the defect is kept under close surveillance until the next inspection). Detected defects are then assumed not to contribute to the failure probability. We therefore suggest the following simplification, when calculating the failure probability (the detection event is evaluated at the most probable point of failure).

$$P_F(t) \approx \Pr\left[G(t) \leq 0\right] \cdot \Pr\left[D(t_1) > 0\right] = \Pr\left[G(t) \leq 0\right] \cdot \left(1 - \Pr\left[D(t_1) \leq 0\right]\right) \tag{P28}$$

The assumption above is not valid for a general case, but the resulting error in a RBI study of a reactor pressure vessel is insignificant. This is verified in App. B.

## P4.  Some remarks

No formal sensitivity analysis is done within the procedure [P1-P2]. However, simple sensitivity factors are calculated when using FORM. These sensitivity factors use the most probable point of failure (MPP) in a standard normal space. However, it is possible to estimate partial safety factors, given a target failure probability and characteristic values for the random parameters included in the analysis.

Verification has been carried out, using the probabilistic computer program STAR6 from Nuclear Electric [P16] and the deterministic calculation software ProSACC/ISAAC [P5] from Inspecta. This is presented in App. B. Another important aspect in the development of a new probabilistic flaw evaluation procedure is to compare the behavior against other published procedures and software. Such a benchmark is presented in App. B.

The statistical distribution used for an input parameter has an important impact on the resulting failure probabilities. This is especially true when calculating small failure probabilities. Another important factor is the data used in the probabilistic analysis. Examples on distributions and data to be used are discussed in App. B [P1-P2].

## P5. References

[P1]    DILLSTRÖM, P., (2000), "Probabilistic Safety Evaluation - Development of Procedures with Applications on Components Used in Nuclear Power Plants", SKI Report 00:58, Swedish Nuclear Power Inspectorate.

[P2]    DILLSTRÖM, P., (2000), "ProSINTAP - A probabilistic program implementing the SINTAP assessment procedure", *Engng Fract Mech*, V. 67, pp. 647-668.

[P3]    MILNE, I., AINSWORTH, R. A., DOWLING, A. R., and A. T. STEWART, (1988), "Assessment of the integrity of structures containing defects", *The International Journal of Pressure Vessels and Piping*, Vol. 32, pp. 3-104.

[P4]    —, (2013), "Assessment of the Integrity of Structures Containing Defects", R6 –Revision 4, Up to amendment record No.10, EDF Energy Nuclear Generation Ltd.

[P5]    ISAAC, (2017), User´s Manual, Kiwa Inspecta Technology AB, Stockholm, Sweden.

[P6]    DITLEVSEN, O., and H. O. MADSEN., (1996), "Structural reliability methods", John Wiley & Sons Ltd, Baffins Lane, Chichester, 372p.

[P7]    PRESS, W. H., and S. A. TEUKOLSKY., (1992), "Portable Random Number Generators", *Computers in Physics*, V 6, n 6, pp 522-524.

[P8]    MONTGOMERY, D. C., and G. C. RUNGER., (1994), "Applied Statistics and Probability for Engineers", John Wiley & Sons, Inc, New York, 895p.

[P9]    MADSEN, H. O., KRENK, S., and N. C. LIND., (1986), "Methods of structural safety", Prentice-Hall, Inc., Englewood Cliffs, New Jersey, 403p.

[P10]   SCHITTKOWSKI, K., (1985/6), "NLPQL: A Fortran Subroutine Solving Constrained Nonlinear Programming Problems", *Annals of Operations Research*, V 5, pp 485-500.

[P11]   —, (1996), "SESAM Theory Manual, PROBAN, General Purpose Probabilistic Analysis Program", DNV Software Report No. 96-7017/Rev. 0, Det Norske Veritas, 145p.

[P12]   RACKWITZ, R., and B. FIESSLER., (1978), "Structural Reliability Under Combined Random Load Sequences", *Journal of Computers and Structures*, V 9, pp 489-494.

[P13]   LIU, P-L., and A. DER KIUREGHIAN., (1986), "Optimization Algorithms for Structural Reliability Analysis", Report UCB/SESM-86/09, Department of Civil Engineering, University of California, Berkeley, 37p.

[P14]   DER KIUREGHIAN, A., and T. DAKESSIAN., (1998), "Multiple design points in first and second-order reliability", *Structural Safety*, V 20, pp 37-49.

[P15]   CRAMER, E., and G. SIGURDSSON., (1998-03-30), "RBI Offshore, Probabilistic Modelling", Technical Report 97-3789, Rev. 2, Det Norske Veritas AS.

[P16]   WILSON, R., (1995), "A User`s Guide to the Probabilistic Fracture Mechanics Computer Code: STAR6 - Version 2.2", Memorandum TEM/MEM/0005/95, Nuclear Electric, Engineering Division, 75p.

# APPENDIX B.  BACKGROUND

This appendix gives the background to the current edition of the handbook and its accompanying calculation software ISAAC [B1].


## B1.      Assessment method

The method utilized in this handbook is based on the R6-method first developed at Nuclear Electric plc. [B2]. The fourth revision of the R6-metod contains several options for determination of the safe region in the failure assessment diagram. The Option 1 is a general non-material specific failure assessment. If a more accurate failure assessment diagram is needed either Option 2 can be used where the failure assessment curve is derived from the materials stress-strain curve, or Option 3 where the failure assessment curve is based on complete numerical $J$-integral calculations for different levels of primary load. An approximate Option 2 curve is also included which only requires basic material data and not a complete stress-strain curve. In addition, the R6-method contains recommendations on how stable crack growth shall be considered.

In order to make the procedure safe and easy to use, the procedure has been restricted to the approximate Option 2 of the R6-method [B2].

Ductile materials, e.g. stainless steel base and weld materials, normally show a significant raise of the $J$-resistance curve after initiation. Setting fracture equal to initiation without any consideration of possible stable crack growth is rather strict, especially if an adequate safety margin is used against fracture. A drawback caused by this is that deformation controlled stresses such as thermal transient and weld residual stresses receive an overestimated influence on the fracture assessment since these are not likely to cause unstable crack growth in ductile materials. Therefore, a method where stable crack growth is accounted for is included. The amount of ductile tearing $\Delta a$ must be limited to values where $J$ is still likely to characterize the crack-tip conditions (see section B3 below).


## B2.      Secondary stress

The interaction between secondary and primary stresses on $J$ is in the R6-method [B2] handled by the $\rho$-factor. See Chapter 2.9. $\rho$ is derived by Ainsworth and his original work has been used to derive $\rho$ [B4]. This reduces some of the conservatism in earlier editions of the handbook for low and moderate $L_r$-values. However, $\rho$ is still restricted to non-negative values. One drawback with the deterministic safety evaluation system in earlier editions of the handbook was that it may overestimate the contribution from secondary stresses for ductile materials. Therefore, a new deterministic safety evaluation system has been introduced that gives quantitative recommendation on how to treat secondary stresses for high $L_r$-values in a R6 fracture assessment. This recommendation defines new safety factors against fracture described by $K_I$ and differentiate between $SF_K^{Primary}$ (relating to primary stresses) and $SF_K^{Secondary}$

(relating to secondary stresses). This deterministic safety evaluation system is described in more detail in Chapter B5.

The R6-method prescribes that the elastic stress state is to be used when calculating the stress intensity factor for secondary stresses, $K_{\mathrm{I}}^{\mathrm{s}}$. For high secondary stresses, such as may be induced by thermal transients, the actual $J$-value is overestimated due to plastic relaxation. The problem is further discussed in Ref. [B5], [B6] and [B38]. In the calculation software ISAAC a modified version of the method suggested by Budden [B7] has been built in. The secondary stress intensity factor used to determine $K_{\mathrm{r}}$ according to Eq. (2.9) is then calculated by

$$K_I^s = \max(\sqrt{K_1(a)K_2(a)}, \ \sqrt{K_1(\overline{a})K_2(\overline{a})}) \quad , \tag{B1}$$

where $K_1$ and $K_2$ are stress intensity factors calculated for the elastic and elastic-plastic stress state, respectively. The maximum value of the geometric mean of $K_1$ and $K_2$ calculated for the actual crack size of interest $a$, and the actual crack size with a plastic zone correction according to Irwin

$$\overline{a} = a + \frac{1}{2\pi\beta}\left(\frac{K_{\mathrm{I}}(a)}{\sigma_Y}\right)^2 \quad , \tag{B2}$$

is to replace $K_{\mathrm{I}}^{\mathrm{s}}$ in Eq. (2.9). $\beta$ is set to 1 for plane stress and to 3 for plane strain. In comparison to Ref. [B7], the elastic stress response to the elastic-plastic strain state has been replaced by the elastic stress state. This makes the method somewhat more easy to use and since the load is strain controlled the two stress states should be close to each other. Eq. (B1) is to be considered as an estimate of an effective secondary stress intensity factor that approximates $J$ for high secondary stresses. Numerical evidence exists that the method works well, see Refs. [B5], [B8] and [B9]. Some minor non-conservatism may exist, partly depending on how stresses are categorized as primary or secondary. However, since the method here is used for safety assessment where a safety margin of the order of 1.4 to 3.2 is used against initiation, this can be neglected.

## B3.    Fracture assessment, including stable crack growth

Many materials with high toughness do not fail at a particular value of $J$ [B10]. Rather; these materials display a rising resistance curve, where $J$ increases with crack growth. The traditional measure of fracture toughness, $J_{\mathrm{Ic}}$, is defined near the initiation of stable crack growth. While this initiation toughness provides some information about the fracture behaviour of a ductile material, the entire resistance curve gives a more complete description. The slope of the resistance curve at a given amount of crack extension is indicative of the relative stability of the crack growth; a material with a steep resistance curve is less likely to experience unstable crack propagation. This slope is usually quantified by a dimensionless parameter, tearing modulus,

$$T_R = \frac{E}{\sigma_Y^2} \frac{dJ_R}{da} \quad . \tag{B3}$$

The condition that governs the stability of crack growth is that instability occurs when the driving force is tangent to the resistance curve. It is convenient to express this driving force in terms of an applied tearing modulus,

$$T_{app} = \frac{E}{\sigma_Y^2} \left( \frac{dJ}{da} \right)_{\Delta_{total}} \quad , \tag{B4}$$

where $\Delta_{total}$ is the total displacement of the system. This displacement consists of terms related to applied displacements and to applied forces. However, load control is usually less stable than displacement control. Since the structural stiffness / compliance are unknown in ISAAC [B1], it is therefore assumed that load control is dominating and the non-critical region is defined by (see Figure B1)

$$J = J_R \quad , \tag{B5}$$

$$T_{app} \leq T_R \quad , \tag{B6}$$
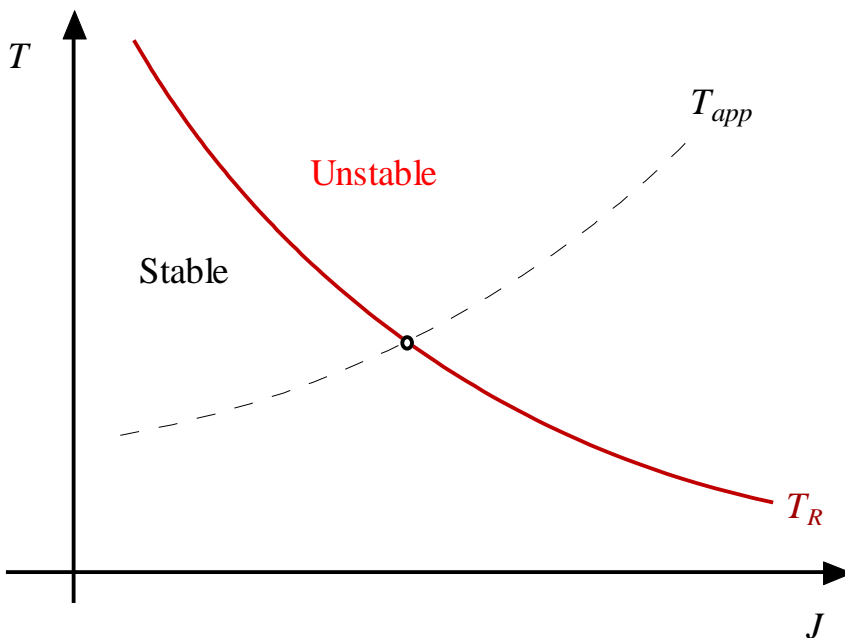


Figure B1.    Schematic stability assessment diagram [B10].

## B4.     Safety assessment

The second edition of the handbook contained a safety assessment system based on partial coefficients. The nominal values of fracture toughness and yield strength were replaced with design quantities according to

$$K_{cr}^d = \frac{K_{cr}}{\gamma_m^k} \quad ,$$
(B7)

$$\sigma_Y^d = \frac{\sigma_Y}{\gamma_m^y} \quad ,$$
(B8)

where $\gamma_m^k$ and $\gamma_m^y$ are so-called partial coefficients. The assessment was then performed with the design quantities instead of the nominal values. The size of the partial coefficients was chosen to give the same overall safety margins against fracture initiation and plastic collapse as applied in ASME Sect. XI and III. For normal and upset conditions, typical values of $\gamma_m^k$ and $\gamma_m^y$ were $\sqrt{10}$ and 1.5, respectively.

In the failure assessment diagram $\gamma_m^k$ and $\gamma_m^y$ move the assessment point $\left(L_r, K_r\right)$ to the right with a factor $\gamma_m^y$ and upwards with a factor $\gamma_m^k$. Since the failure assessment curve drops for higher $L_r$-values a non-uniform safety margin to fracture initiation is obtained depending on the value of $L_r$. This can be further quantified by looking at the criterion for fracture initiation based on the $J$-integral [B11].

$$J = J_{Ic} \quad .$$
(B9)

The R6 failure assessment curve gives the following expressions for $J$ and $J_{Ic}$.

$$J = \frac{(1-v^2)K_I^2}{E} \frac{1}{[f_{R6}(L_r)-\rho]^2} \quad ,$$
(B10)

$$J_{Ic} = \frac{(1-v^2)K_{cr}^2}{E} \quad ,$$
(B11)

where

$f_{R6}$ = R6 approximate Option 2 type failure assessment curve (see Chapter 2.10)  (B12)

With the partial coefficients $\gamma_m^k$ and $\gamma_m^y$ applied, the criterion becomes

$$J = J_{acc} \quad ,$$
(B13)

where, with the same definition of $J$ as above,

$$J_{acc} = \frac{(1-\nu^2)K_{cr}^2}{(\gamma_m^k)^2 E} \frac{[f_{R6}(\gamma_m^y L_r)-\rho]^2}{[f_{R6}(L_r)-\rho]^2} \quad . \tag{B14}$$

The safety margin against fracture initiation is then given by

$$SF = \frac{J_{Ic}}{J_{acc}} = (\gamma_m^k)^2 \frac{[f_{R6}(L_r)-\rho]^2}{[f_{R6}(\gamma_m^y L_r)-\rho]^2} \quad . \tag{B15}$$

The result is shown in Figure B2 for the case $\gamma_m{}^k = \sqrt{10}$, $\gamma_m{}^y = 1.5$ and $\rho = 0$. For low values of $L_r$, the desired safety margin becomes 10 to $J$-controlled initiation as in accordance with the flaw assessment procedure in ASME, Sect. XI, App. A. But for $L_r$-values exceeding 0.6, the margin increases dramatically with a maximum peak of about 90.
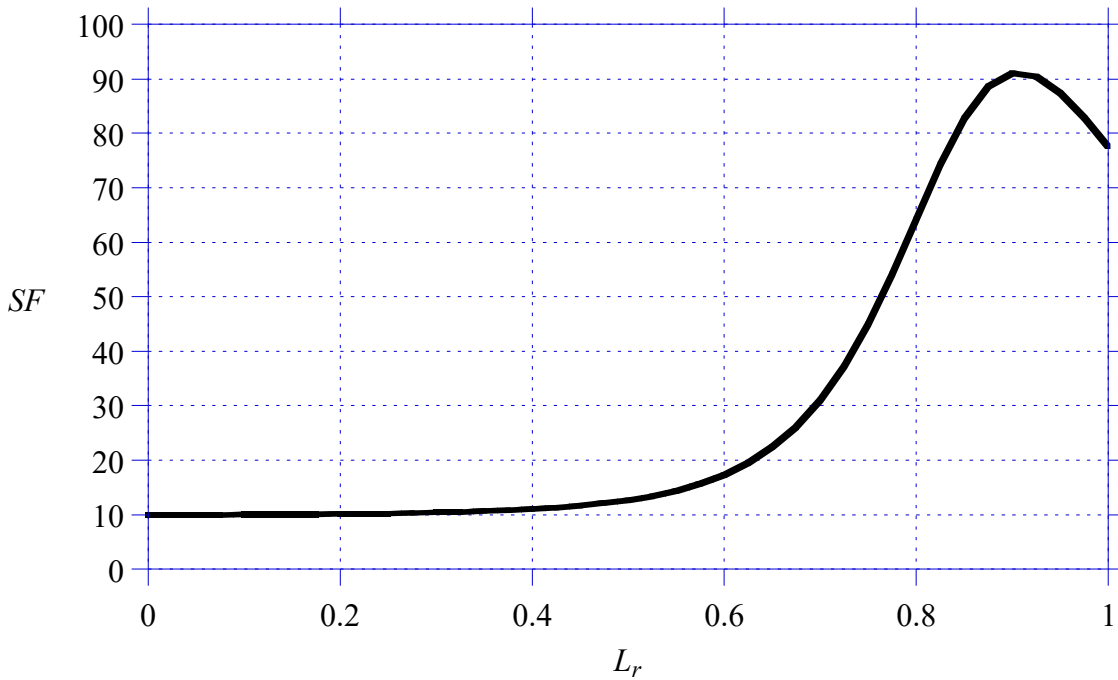


Figure B2.  Increase of safety margin for initiation due to shape of R6 revision 3, Option 1 type failure assessment curve.

The above behavior seemed much too conservative in comparison to the flaw assessment procedure in ASME, Sect. XI, App. A. The presented example corresponds to a maximum safety factor of about 9.5 instead of 3.16 as in ASME, Sect. XI, App. A. For that reason a new safety assessment procedure was developed as described in Ref. [B11] and presented in the third edition of the handbook. The new safety assessment procedure gave a uniform safety margin to fracture initiation.

## B5. New deterministic safety evaluation system

One drawback with the deterministic safety evaluation system above is that it may overestimate the contribution from secondary stresses (i.e. weld residual stresses or stresses due to a thermal transient) for ductile materials. This has to do with the fact that the influence of residual stresses on load carrying capacity is only large at low $L_r$-values. The influence reduces as $L_r$ increases and for larger $L_r$ values there is no effect at all. This has been shown by different experimental [B12] – [B17] and analytical programs [B17], [B37] – [B38].

Due to this, a new deterministic safety evaluation system has been introduced [B38] that gives a quantitative recommendation on how to treat secondary stresses for high $L_r$-values in a R6 fracture assessment. This recommendation defines new safety factors against fracture described by $K_I$ and differentiate between $SF_K^{Primary}$ (relating to primary stresses) and $SF_K^{Secondary}$ (relating to secondary stresses).

As given in Chapter 2, the acceptance criteria is normally defined as,

$$K_r = \frac{K_I^P + K_I^S}{K_{cr}} + \rho / SF_K \leq f_{R6}(L_r) / SF_K \quad , \tag{B16}$$

where $SF_K$ in Eqn. (B16) is the safety factor against fracture described by $K_I$.

In order to use the different safety factors for primary and secondary stresses as well as to differentiate between global secondary stresses and local through-thickness secondary stresses, Eqn (B16) is modified as,

$$K_r = \frac{K_I^P + K_B^S + (K_I^S - K_B^S) * SF_{K,local}^{Secondary} / SF_K}{K_{cr}} + \rho / SF_K \leq f_{R6}(L_r) / SF_K \quad , \tag{B17}$$

where $SF_{K,local}^{Secondary}$ is the safety factor for the local through-thickness secondary stress and $K_B^S$ is the stress intensity factor due to global secondary bending stress.

### B5.1 Estimation of safety factors in the new deterministic safety evaluation system

For a given crack size and load, one can calculate the stress intensity factors ($K_I^P$ and $K_I^S$) and limit load parameter $L_r$. The primary load is then increased until the R6 failure assessment curve is reached such that,

$$\frac{c \cdot K_I^P + K_I^S}{K_{cr}} + \rho = f_{R6}(c \cdot L_r) \quad . \tag{B18}$$

Eqn. (B18) is then used to obtain the load parameter $c$ and the limit load parameter at failure $L_r^*$,

$$L_r^* = c \cdot L_r \quad .$$

$$(B19)$$

The new safety factor for secondary stress is then defined as ($SF_{K,local}^{Secondary} \geq 1$),

$$
\begin{cases}
SF_{K,local}^{Secondary} = SF_K & \text{for } L_r^* \leq 0.80 \\
SF_{K,local}^{Secondary} = SF_K - \left(SF_K - 1\right) \cdot \left(L_r^* - 0.80\right) / \left(1.15 - 0.80\right) & \text{for } 0.80 < L_r^* < 1.15 \\
SF_{K,local}^{Secondary} = 1.0 & \text{for } L_r^* \geq 1.15
\end{cases}
\quad .
$$

$$(B20)$$

## B6. Implementation of the Master Curve in ISAAC

Different options within the Master Curve methodology are implemented in ISAAC [B1] in order to give possibilities for the user to conduct more comprehensive integrity assessment [B39]. It gives the user the possibilities to use 3%, 5% and 50% fracture probability in its analyse. It also gives the possibility to evaluate the fracture toughness $K_{JC}$ from Charpy data ($T_{28J}$ or $T_{41J}$). In addition, the user has the option to make size-correction for the fracture toughness, based on the actual crack configuration. The procedure to use these options in ISAAC is briefly described below.

### B6.1    Determination of Master Curve KJc for 1T-thickness

In ISAAC, the following four options are available to get the Master Curve toughness:

    i)        There is a valid $T_0$ value from fracture toughness testing on the actual material.

    ii)      There is valid value on $T_{28J}$ from Charpy impact testing on the actual material.

    iii)    There is valid value on $T_{41J}$ from Charpy impact testing on the actual material.

    iv)    There is a valid $K_{IC}$ value from fracture toughness testing on the actual material.

The user should give the relevant value to the parameter of this option ($T_0$ or $T_{28J}$ or $T_{41J}$ or $K_{IC}$) and the actual temperature for which the program will compute $K_{JC}$. In addition, one should select which fracture probability (3% or 5% or 50%) is intended for the ISAAC analysis. There is also the option to adjust the $K_{JC}$ value for the crack front length. This option is described in the next section. The program will compute the relevant fracture toughness $K_{JC}$ and the possibility to have a plot on the results. The user also gets information on different Master curves, the range of application window for the actual material, the input or evaluated $T_0$ value, and the fracture toughness for the actual temperature ($T_{act}$). If the given $T_{act}$ is outside the application window, the fracture toughness assessment based on Master Curve is not valid, and the user gets a warning on that.

### B6.2    Correction for crack front size

Within ISAAC, there is the possibility to adjust the $K_{JC}$ value for the crack front length. If the component is clad, the cladding thickness should be given as input in the material box. If there is no cladding, the value of the cladding thickness should be given as zero. Corrections for different crack configurations are considered in the program. It is assumed that the size-correction due to crack-front-length (*cfl*) is

valid for crack front length between 25-100 mm. It implies that no benefits on fracture toughness increase due to short cracks (*cfl* < 25 mm) are accounted for in the program. For *cfl* >100 mm, it is assumed that *cfl* =100 mm. Equation (B21) gives the fracture toughness values corrected for the crack-front-length.

$$K_{JC}^{cfl} = 20 + \left[ K_{JC}^{1T} - 20 \right] \left( \frac{25}{cfl} \right)^{1/4} \tag{B21}$$

The values of *cfl* for different crack geometries are obtained from the following procedure.

Size correction for through-thickness cracks:

$$cfl = 2t \qquad\qquad \text{For components without cladding}$$
$$cfl = 2t - 2t_{clad} \qquad \text{For components with cladding}$$

   If $cfl > 100$ mm, it is considered that $cfl = 100$ mm.

   If $cfl < 25$ mm, it is considered that $cfl = 25$ mm.

Here, *t* is the thickness of the component and $t_{clad}$ the thickness of cladding.

Size correction for finite surface cracks:

$$cfl = \frac{\pi}{2} \left[ 3(a+c) - \sqrt{10ac + 3(a^2 + c^2)} \right] \qquad\qquad \text{For components without cladding}$$

$$cfl = \frac{\pi}{2} \left[ 3(a+c) - \sqrt{10ac + 3(a^2 + c^2)} \right] - 2t_{clad} \quad \text{For components with cladding}$$

   If $cfl > 100$ mm, it is considered that $cfl = 100$ mm.

   If $cfl < 25$ mm, it is considered that $cfl = 25$ mm.

Here, *a* is crack depth, *c* half of the crack length and $t_{clad}$ the thickness of cladding. The size correction for components with cladding is approximately corrected for the cladding thickness (this correction may be coarse for cracks only slightly deeper than the cladding thickness but is good for deep cracks compared to the cladding thickness).

Size correction for embedded cracks:

$$cfl = \pi \left[ 3(a+c) - \sqrt{10ac + 3(a^2 + c^2)} \right]$$

   If $cfl > 100$ mm, it is considered that $cfl = 100$ mm.

   If $cfl < 25$ mm, it is considered that $cfl = 25$ mm.

Here, *a* is crack depth and *c* half of the crack length. It is assumed that the crack does not include any cladding.

Size correction for infinite cracks:

For long extended (infinite) surface cracks in plates and cylinders (internal and external), the *cfl* is assumed to be 100 mm.

*B6.3    Lower and upper tolerance bounds for the estimated fracture toughness*

The Master Curve is defined as the median (50% probability) toughness for the 1T (25 mm thick) specimen over the transition range for the material. Based on fitting to test results, the shape of the Master Curve for the 1T specimen is described for 50% fracture probability by Eqn. (B22):

$$K_{Jc(50\%)} = 30 + 70 \exp\left[0.019\left(T - T_0\right)\right].$$
(B22)

With the $T_0$ value, the master curve function in Eq. (B22) is fully determined, and then the lower and upper tolerance bounds of the master curve can be calculated using the following equation [B40]:

$$K_{Jc(0.xx)} = 20 + \left[\ln\left(\frac{1}{1 - 0.xx}\right)\right]^{1/4}\left\{11 + 77\exp\left[0.019\left(T - T_0\right)\right]\right\},$$
(B23)

where 0.*xx* represents the selected cumulative probability level; for example, 0.*xx* = 0.95 implies a 95% confidence of survival to that $K_{Jc}$ level at the temperature $T$. Based on Eq. (B23), different tolerance bounds for the toughness distribution can be constructed as needed.

The lower-bound 3% and 5% probability curves and the upper-bound 95% probability curve are then given by the following expressions:

$$K_{Jc(3\%)} = 24.6 + 32.2 \exp\left[0.019\left(T - T_0\right)\right],$$
(B24)

$$K_{Jc(5\%)} = 25.2 + 36.6 \exp\left[0.019\left(T - T_0\right)\right],$$
(B25)

$$K_{Jc(95\%)} = 34.5 + 101.3 \exp\left[0.019\left(T - T_0\right)\right].$$
(B26)

Where, $K_{Jc}$ is in MPa$\sqrt{m}$ and $T$ and $T_0$ in °C (an example, using $T_0$ = -5 °C, is given in Figure B3).
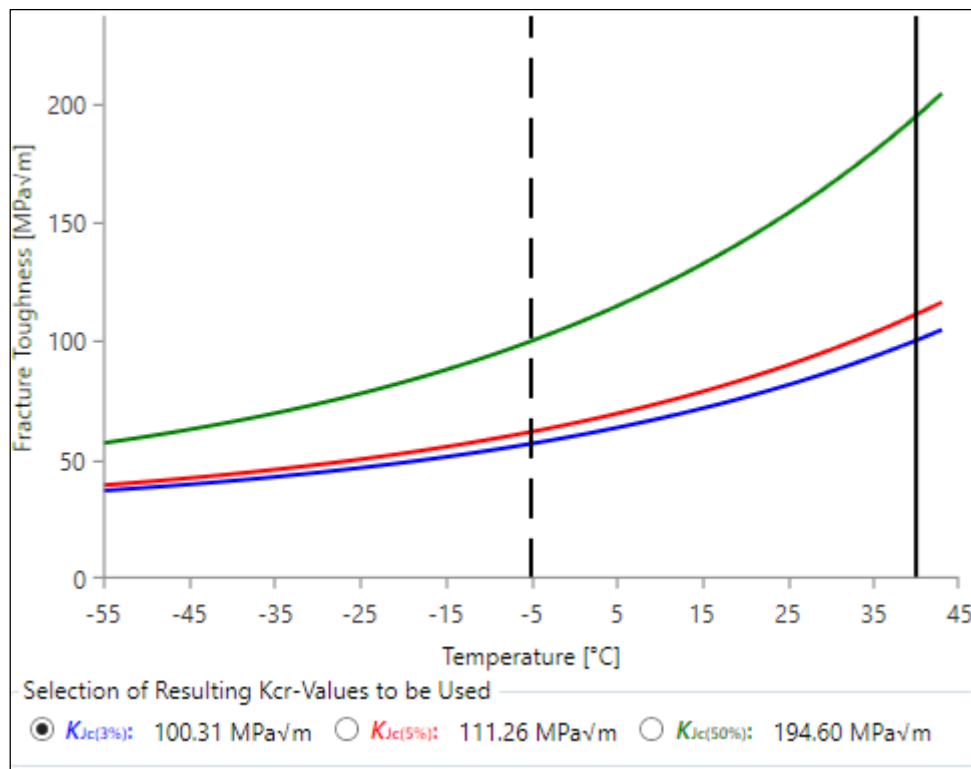
Figure B3.   ISAAC [B1] Master Curve fracture toughness evaluations based on a given $T_0$ value ($T_0 =$ -5 °C in this example).

## B7.   Fit of stress distribution for stress intensity factor calculation

Beginning with the third edition of the handbook, stress intensity factor solutions are included for a polynomial stress distribution through the thickness up to the order of 5. A problem then arises how the actual stress distribution is fitted to a polynomial to estimate $K_I$ as accurate as possible. Depending on type of situation, the following alternatives are suggested:

a)   For a smooth continuous stress distribution, the actual stress distribution over the extension of the crack is least-square fitted to a polynomial with an order within the range available. The order of the polynomial that gives the agreement with the actual stress is chosen.

b)   For a discontinuous stress distribution such as may arise if dissimilar materials through the thickness are present, an accurate least-square polynomial fit may not be possible since the order of the polynomial is restricted. Instead a linearization is recommended where the linear stress distribution is given the same resulting normal force and moment as the actual stress distribution over the extension of the crack.

The calculation software ISAAC assists the user to select the best alternative. The program displays a graph where the actual and fitted stress distributions are shown. By testing different alternatives and looking at the outcome on the graph the user can find out which alternative to select. When in doubt the fitting procedure that gives the most conservative result in the assessment should be used.

# B8. Probabilistic analysis

A probabilistic procedure is described in Appendix P. Results for applying the procedure has been verified, using the probabilistic software STAR6 from Nuclear Electric [B18] and the deterministic software ProSACC [B41] (the predecessor to ISAAC [B1]). This is presented in section B8.1. Another important aspect in the development of a new probabilistic flaw evaluation procedure is to compare the behavior against other published procedures and software. Such a benchmark is presented in section B8.2.

The statistical distribution used for an input parameter has an important impact on the resulting failure probabilities. This is especially true when calculating small failure probabilities. Another important factor is the data used in the probabilistic analysis. Examples on distributions and data to be used are discussed in section B8.3 [B20] – [B21].

## B8.1   Verification

The procedure has been verified using three different verification procedures.

- Firstly, a general verification was made [B20] – [B21] and presented in section B8.1.1.
- Secondly, a specific verification, using input data relevant to risk based inspection studies of a reactor pressure vessel, was made and presented in section B8.1.2.
- Finally, a verification of the assumptions for the POD-model was made and presented in section B8.1.3.

## B8.1.1   General verification of the procedure

### Deterministic verification
To check the deterministic parts a comparison was made against the software ProSACC [B41]. ProSACC contains several options and for this validation a fracture assessment procedure based on the R6-method was used. All comparisons showed good agreement.

### Verification with normally distributed parameters
To check the probabilistic parts of the procedure, a comparison was made against the computer program STAR6 from Nuclear Electric [B18]. First a verification using normally distributed parameters was made.

Two different cases were investigated:
- $P_F$ as a function of primary membrane stress, using two different values of standard deviation for the dominating parameter sizing probability.
- $P_F$ as a function of standard deviation for the dominating parameter sizing probability, using two different values of primary membrane stress.

### Probability of failure as a function of primary membrane stress
The following data was used for this verification:

- Probability of failure, defect size given by NDT/NDE was analyzed, using the following algorithms:
  - First-Order Reliability Method (FORM).
  - Simple Monte Carlo Simulation (MCS).
  - Monte Carlo Simulation with Importance Sampling (MCS-IS).
- The STAR6 geometry "extended edge defect in a plate under tension" was chosen (thickness t = 103 mm).
- Fracture toughness, mean = 200 MPa $\sqrt{m}$ and standard deviation = 10 MPa $\sqrt{m}$ [B20].
- Yield strength, mean = 350 MPa and standard deviation = 30 MPa [B20].
- Ultimate tensile strength, mean = 500 MPa and standard deviation = 30 MPa [B20].
- Defect size given by NDT/NDE, for two different NDE procedures [B22]. The data given is from component 1 in [B22]:
  - An advanced NDE procedure, mean = 26.0 mm and standard deviation = 6.5 mm.
  - A bad NDE procedure, mean = 30.2 mm and standard deviation = 18.1 mm.

In Figure B4, one can find the result using an advanced NDE procedure.
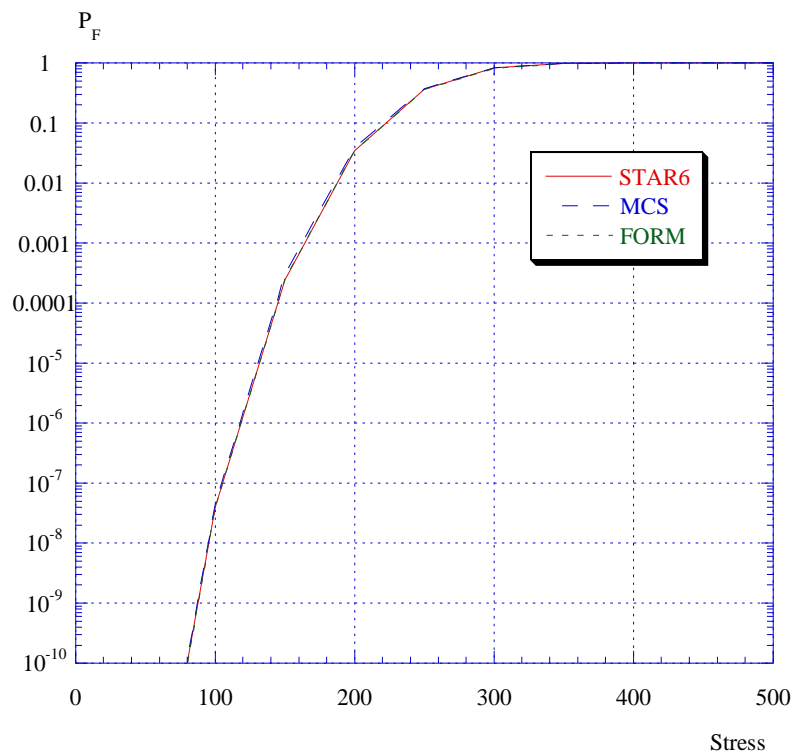


Figure B4.    Probability of failure as a function of primary membrane stress, using an advanced NDE procedure.

For both cases (the result using a bad NDE procedure is not shown), there were an excellent agreement between this procedure and STAR6.

*Probability of failure as a function of sizing standard deviation*

The main data used were the same as in the example above. The difference was that this time one calculated the probability of failure as a function of standard deviation for the dominating parameter sizing probability, using two different values of primary membrane stress (150 and 200 MPa). The results can be found in Figure B5 below.
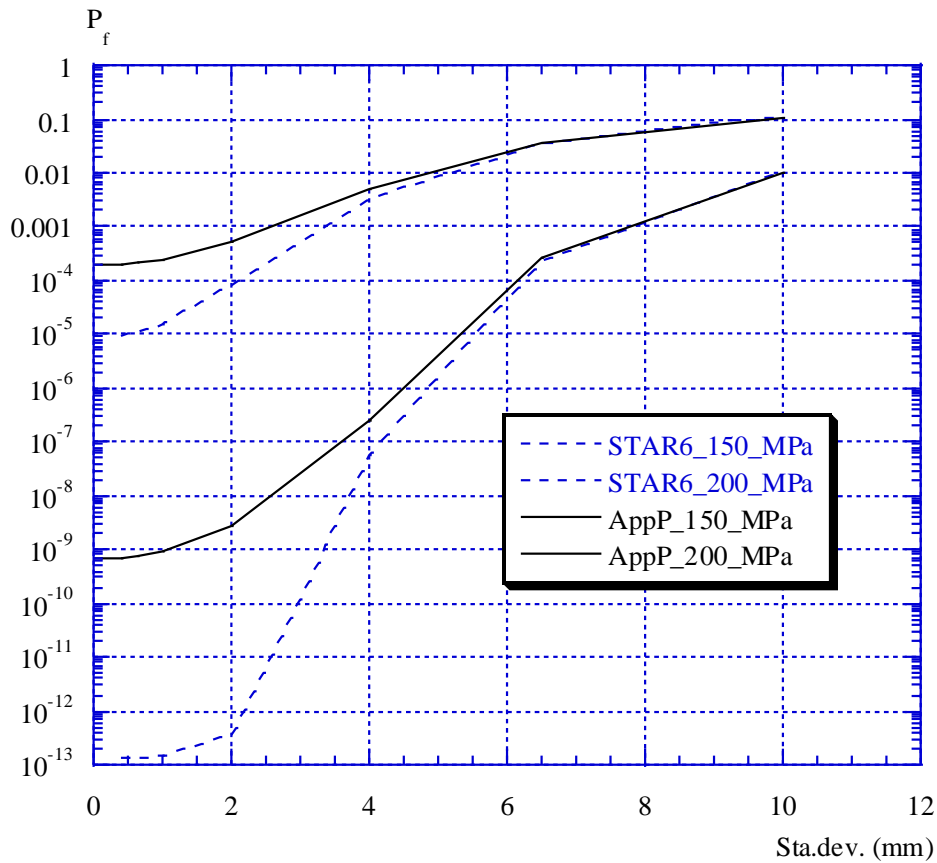


Figure B5.   Probability of failure as a function of standard deviation for the dominating parameter sizing probability, using two different values of primary membrane stress.

As shown in Figure B5, the agreement between this procedure (see App. P) and STAR6 is very bad for small values of sizing standard deviation. After investigating this difference, it was shown that the results from this procedure were correct, and that the algorithms used in STAR6 were not intended to work for a general problem, when the standard deviation is either "small" or "large".

195

The main data used were the same as above. The difference was that this time one calculated the probability of failure using an exponential sizing probability (with two different mean values). The results can be found in Figure B6 below.
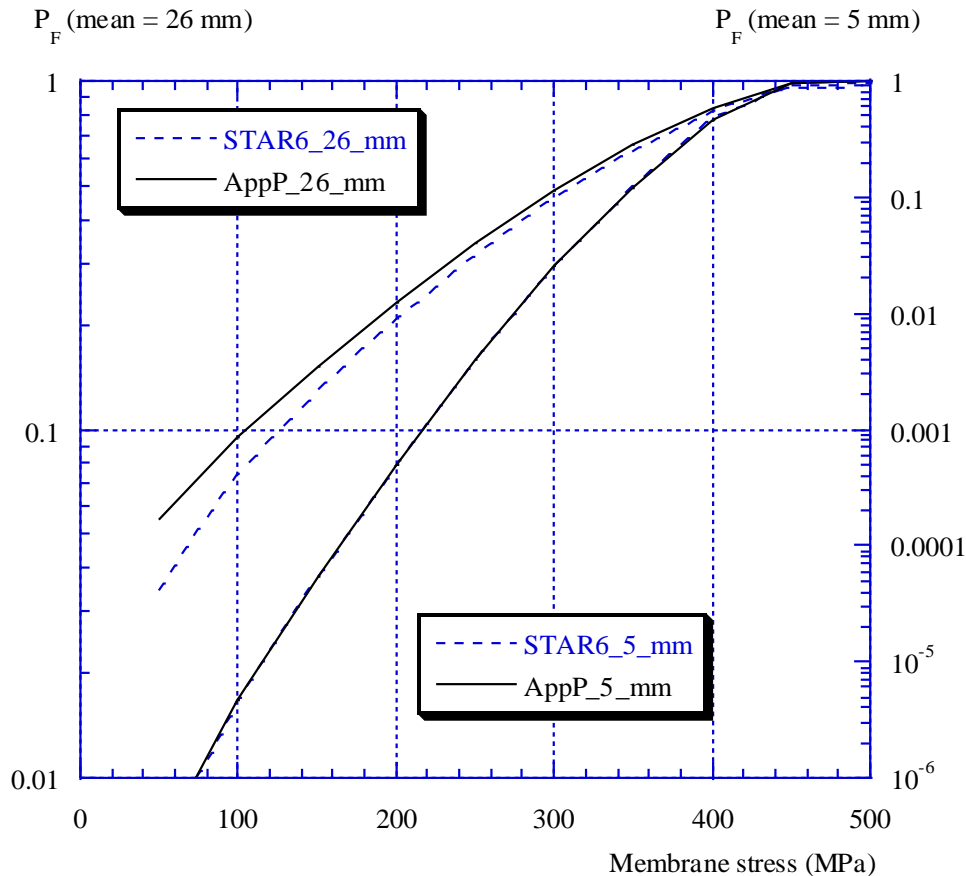


Figure B6.    Probability of failure using an exponential sizing probability, with two different mean values.

As shown in Figure B6, the agreement between this procedure (see App. P) and STAR6 is quite bad for the case with a large mean value (and also a large standard deviation). After investigating this difference, it was shown that the results from this procedure were correct, and that the algorithms used in STAR6 were not intended to work for a general problem, when the standard deviation is either "small" or "large".

The main data used was the same as above. The difference was that this time one calculated the probability of failure as a function of the applied secondary membrane stress (using a constant primary membrane stress equal to 100 MPa). The results can be found in Figure B7 below.
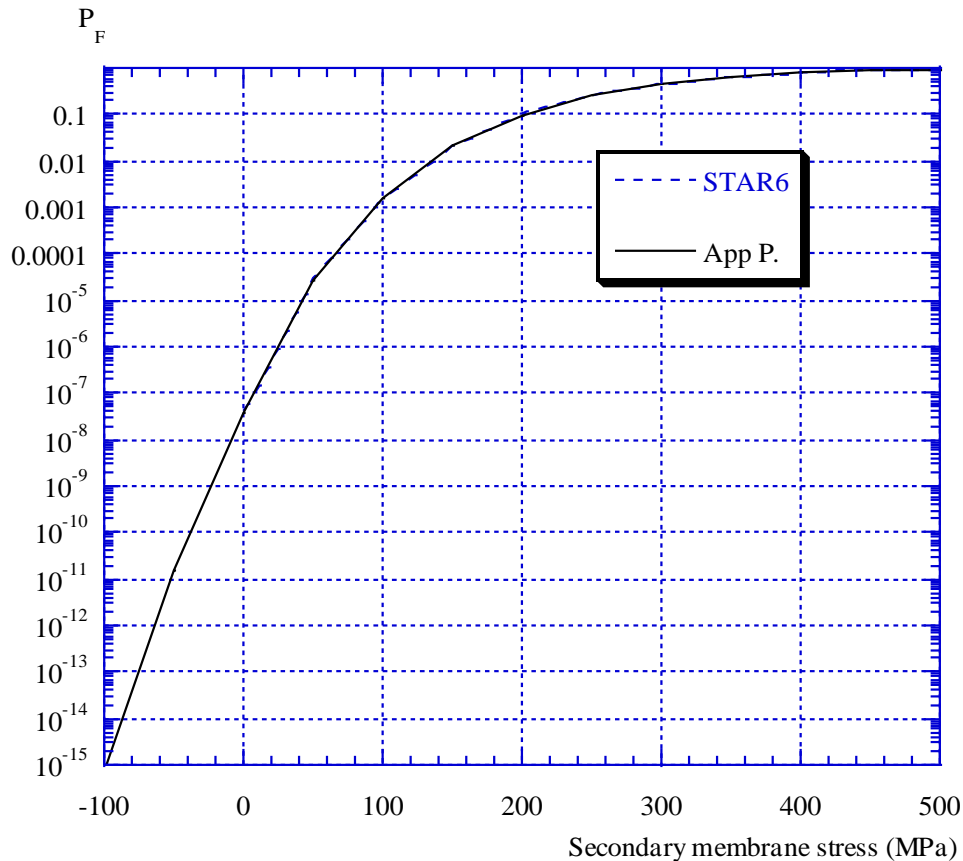


Figure B7.    Probability of failure as a function of applied secondary membrane stress.

As shown in Figure B7, the agreement between this procedure (see App. P) and STAR6 is excellent in this case, using a simple $\rho$ definition for the verification exercise only.

### B8.1.2    Verification using input data relevant to RBI studies of a reactor pressure vessel

The verification in section B8.1.1 showed that the results from this procedure, in general, are very accurate. A specific verification, using input data relevant to risk based inspection studies of a reactor pressure vessel, is also presented below.

In this verification a comparison of the results using FORM (an approximate method) and MCS (an exact method, when using sufficient number of simulations) is made. The reason for this verification is that in the RBI studies of different RPV`s, only FORM were used. The weld W1111 from the Ringhals 1 RPV was chosen (Weld ID = RW1111_1_F1) [B23], using an exponential defect depth distribution and with no in-service inspection event taken into account (when calculating the probability of failure). The results are summarised in Table B1, using different mean values of defect depth $\mu_a$.

Table B1. Verification using input data relevant to RBI studies of a reactor pressure vessel

| $\mu_a$ [mm] | $P_F$ (FORM) | $P_F$ (MCS, $N = 10^5$) | $P_F$ (MCS, $N = 10^7$) |
|---|---|---|---|
| 5.0 | $4.29 \cdot 10^{-8}$ | 0.0 | 0.0 |
| 6.3 | $1.37 \cdot 10^{-6}$ | 0.0 | $1.80 \cdot 10^{-6}$ |
| 7.5 | $1.17 \cdot 10^{-5}$ | $1.00 \cdot 10^{-5}$ | $1.20 \cdot 10^{-5}$ |
| 10.0 | $1.96 \cdot 10^{-4}$ | $1.90 \cdot 10^{-4}$ | $2.02 \cdot 10^{-4}$ |
| 12.5 | $1.07 \cdot 10^{-3}$ | $0.91 \cdot 10^{-3}$ | $1.12 \cdot 10^{-3}$ |
| 15.0 | $3.33 \cdot 10^{-3}$ | $3.29 \cdot 10^{-3}$ | $3.37 \cdot 10^{-3}$ |
| 17.5 | $7.50 \cdot 10^{-3}$ | $7.84 \cdot 10^{-3}$ | $7.51 \cdot 10^{-3}$ |
| 20.0 | $1.38 \cdot 10^{-2}$ | $1.42 \cdot 10^{-2}$ | $1.38 \cdot 10^{-2}$ |

As shown in table B1, the agreement between FORM and MCS is excellent when a sufficiently large number of simulations are used. $P_F$ (MCS) = 0.0 indicates that more simulations are needed to get an accurate estimate of the failure probability.

### B8.1.3   *Verification of the assumptions for the POD-model in the procedure*

To simplify the calculation of the probability of failure when a defect is not detected by NDT/NDE (using FORM) a simplified expression (see Eq. (P28)) is used instead of Eq. (P27). How this influences the resulting failure probabilities is shown in Figure B8 to Figure B10. The POD-data is taken from section B8.3.4, and the analysis using Eq. (P28) is done by Monte Carlo simulation.

The following data was used for this verification:
- An exponential defect depth distribution was chosen (mean = 6.3 mm).
- POD-data from three different UT procedures was used (Low effectiveness UT, Good practice UT and Advanced UT).

In Figure B8 to Figure B10 the probability of failure before an inspection (*i. e.* no inspection) are given on the x-axis and the probability of failure after an inspection not resulting in any defect detection are given on the y-axis.

The resulting most probable point of failure, with respect to crack depth, was between 1 mm and 80 mm (this extended range covered most of the practical cases in the RBI study [B23]).
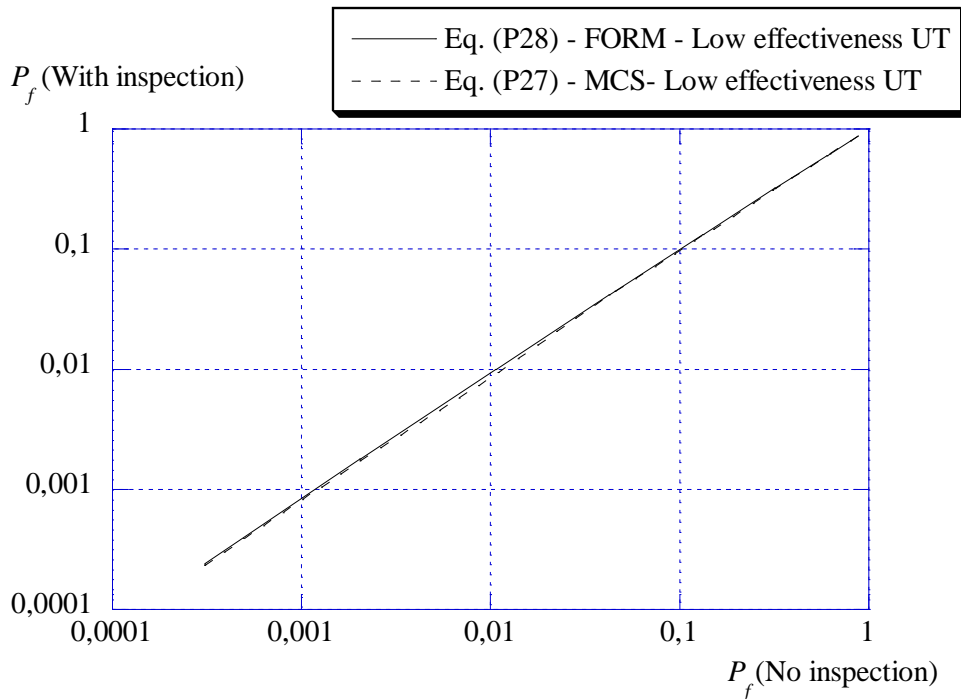
Figure B8.    Probability of failure, using different assumptions in the analysis and using a low effectiveness UT procedure.

As can be seen in Figure B8, there is almost no difference between the results using the two methods to calculate the probability of failure. This has to do with the fact that that there is no real benefit from using a low effectiveness UT procedure.
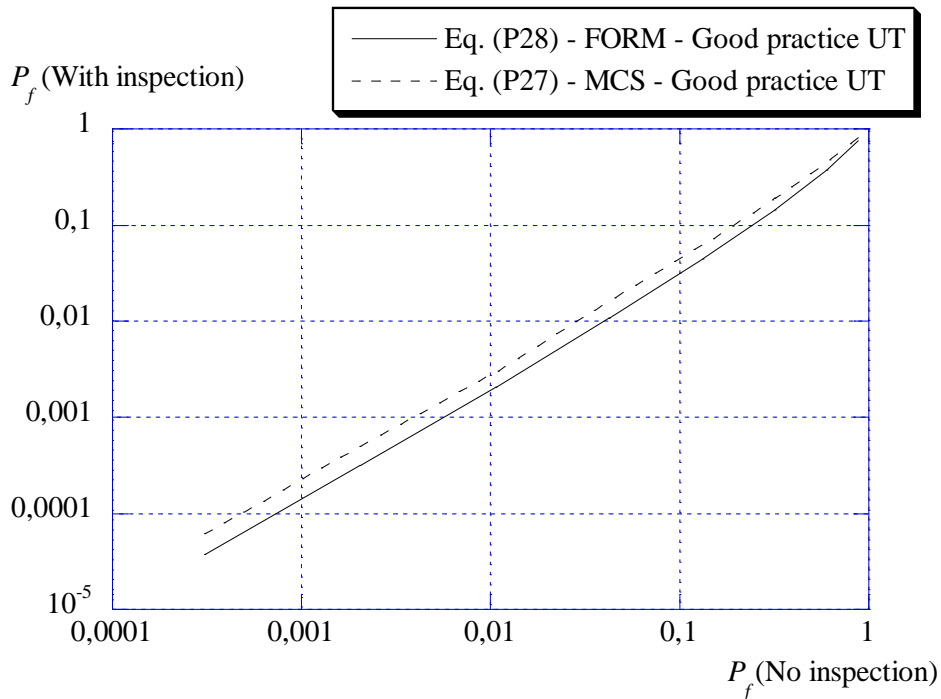


Figure B9.    Probability of failure, using different assumptions in the analysis and using a good practice UT procedure.

As can be seen in Figure B9, there is a small difference between the results using the two methods to calculate the probability of failure (using a good practice UT procedure). This difference, however, is consistent for all cases in a RBI study and should therefore be of no importance when comparing failure probabilities for different regions (welds) in a reactor pressure vessel.
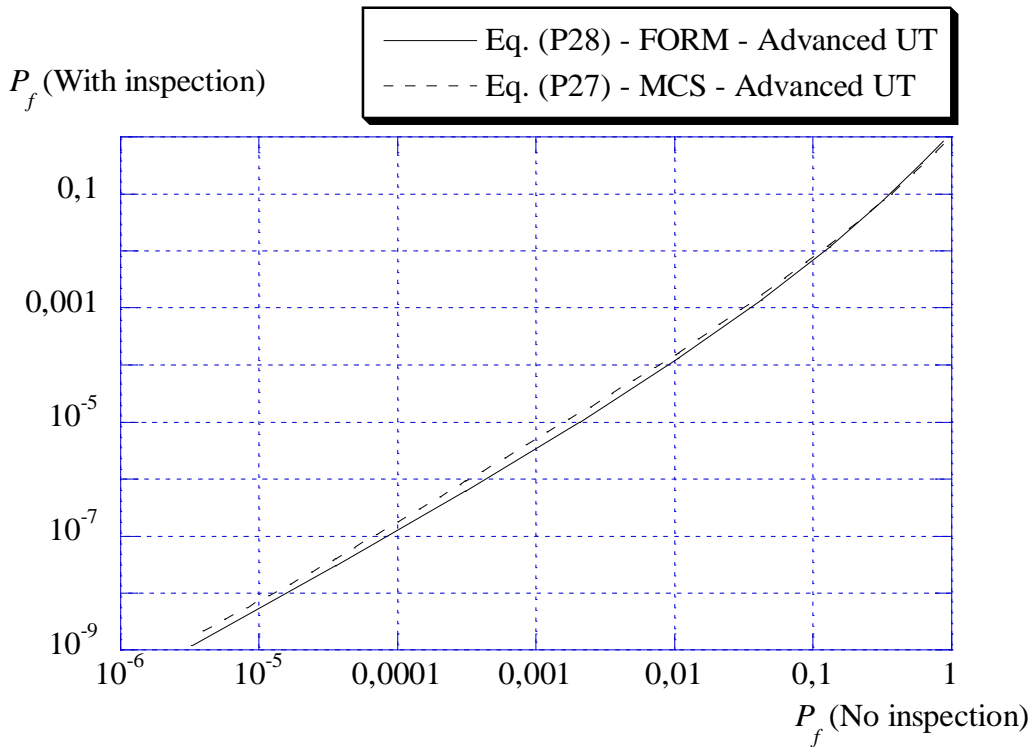


Figure B10.  Probability of failure, using different assumptions in the analysis and using an advanced UT procedure.

As can be seen in Figure B10, there is almost no difference between the results using the two methods to calculate the probability of failure (when using an advanced UT procedure).

This verification (as presented in Figure B8 to Figure B10) shows that the error in using a simplified POD model is insignificant when used to compare different regions (welds) in a reactor pressure vessel.

B8.2     *Benchmarking probabilistic procedures and software*

One important aspect in the development of a new probabilistic flaw evaluation procedure is to compare the behavior against other published procedures and software. The objective of such a benchmark study could be to:

- Review probabilistic procedures and associated software in terms of main features, capabilities and limitations.
- Benchmark probabilistic procedures and associated software by performing a comprehensive sensitivity study and compare the results.
- Investigate the reasons for differences in results from the benchmark study and identify strengths and weaknesses of the probabilistic procedures and associated software.

This procedure has been included in a benchmark study within the Fifth Framework of the European Atomic Energy Community [B24]. The title of the project was "Nuclear Risk-Based Inspection Methodology for passive components (NURBIM)". Also this procedure was part of an OECD benchmark study called "PROSIR - Probabilistic Structural Integrity of a PWR Reactor Pressure Vessel" [B25].

*B8.3      Distribution and data to be used in a probabilistic analysis*

The statistical distribution used for an input parameter has an important impact on the resulting failure probabilities. This is especially true when calculating small failure probabilities. Another important factor is the data used in the probabilistic analysis. Examples on distributions and data to be used are discussed below [B20] – [B21].

*B8.3.1      Fracture toughness*

The process of crack growth depends on the microstructural conditions in the crack tip vicinity. These are to some extent of random nature. Depending on the particular mechanism of crack growth, the random element is more or less apparent. Thus for instance we can be expecting that crack growth due to cleavage exhibit a prominently random character. This is also found in experimentation. Ductile crack growth on the other hand is of a more deterministic nature. The difference is due to the fact that cleavage fracture depends on the conditions in very small region around a single point while the ductile process will depend more on the average properties.

The normal, lognormal and Weibull distributions are most often used to describe the variations in fracture toughness [B3], [B20] – [B21], [B26] – [B27]. The fracture toughness data employed should, whenever possible, be for the actual material being considered. A disadvantage of the use of a normal distribution is that the algorithms used in MCS and FORM/SORM, may result in negative values of fracture toughness. Both the lognormal and Weibull distributions have the correct property that only non-negative values are permitted and are therefore more suitable distributions to be used for fracture toughness. The choice of distribution is then determined by whichever provides the better fit to experimental data. Where some uncertainty exists, a sensitivity analysis is recommended [B3], [B20] – [B21], [B26].

However, fairly little information is available for the random distribution of fracture toughness and related properties. In the lower shelf and transition region Wallin [B28], [B29] and others have argued for the use of Weibull type distributions. In the wholly ductile temperature region a Weibull distribution is not appropriate. The results in [B30] instead suggest a lognormal distribution. Wallin [B29] indicates that a normal distribution provides a good fit to experimental $J_R$-data.

If no experimental data is available, the following data may be used [B26], [B29], [B31]:

- In the lower shelf and transition region: $\sigma_{K_{Ic}} \approx 0,2 \cdot \mu_{K_{Ic}} - 0,3 \cdot \mu_{K_{Ic}}$

- In the wholly ductile temperature region: $\sigma_{K_{Ic}} \approx 0,05 \cdot \mu_{K_{Ic}} - 0,1 \cdot \mu_{K_{Ic}}$

- In the wholly ductile temperature region (using correlated Charpy data):
$$\sigma_{K_{Ic}} < 0,1 \cdot \mu_{K_{Ic}}$$

The distributions for fracture toughness (i. e. the normal, lognormal and Weibull distributions), are also most often used to characterise the yield strength and ultimate tensile strength [B20] – [B21], [B26].

The yield limit of a material can for instance be regarded as the sum of the yield limit of many grains and it is thus reasonable to assume the macroscopic limit to be normally distributed. Using an extensive data set from the English Health and Safety Executive materials database, to fit the yield strength to normal, lognormal and Weibull distributions, it was found that the lognormal distribution gave the best fit to most of the cases considered [B32]. With the data given, a typical standard deviation of 28 MPa could be evaluated [B21].

If only measured mean values for yield strength ($\mu_{\sigma_Y}$) and ultimate tensile strength ($\mu_{\sigma_U}$) are available, the following standard deviation values may be used [B29]:

- Yield strength: $\sigma_{\sigma_Y} = 0{,}03 \cdot \mu_{\sigma_Y}$

- Ultimate tensile strength: $\sigma_{\sigma_U} = 0{,}05 \cdot \mu_{\sigma_U}$

If only standardized minimum values for yield strength ($R_e$) and ultimate tensile strength ($R_m$) are available, the following data may be used [B29]:

- Yield strength: $\mu_{\sigma_Y} = R_e + 70$ MPa and $\sigma_{\sigma_Y} = 30$ MPa

- Ultimate tensile strength: $\mu_{\sigma_U} = R_m + 70$ MPa and $\sigma_{\sigma_U} = 30$ MPa

*B8.3.3 Defect size given by NDT/NDE*

NDE data generally results from the application of an inspection procedure based on several techniques, on the skill of the operator, on decision steps such as recording or not, geometric indication or not, false call or not. The size of a recorded defect is usually established by the operator, often not following rigorous reasoning that could be documented. The NDE data used by the structural integrity engineer will always be the result of a complex combination of various information and decisions taken during the process of generating that information [B22]. Most studies has then come to the conclusion that it is very common that small defects are overestimated in size and large defects are underestimated in size [B32] – [B33].

The distribution most often used is the normal distribution, which could be applied for analyses where a single defect is either known or postulated to exist in a weld [B3], [B32].

It is impossible to give general recommendations on data to be used for a specific case. However, in table B2 below, some typical sizing error values from [B22] are summarized.

Table B2. Typical values of defect sizing error (UT = Ultrasonic testing) [B22]

| Component | Material | NDE procedure | Sizing error ($\sigma_a$) |
|---|---|---|---|
| Plate $t > 75$ mm $\mu_a = 0.4 \cdot t$ | Ferritic steel | Advanced UT | 5 mm |
| | | Good practice UT | 12 mm |
| | | Low effectiveness UT | 15 mm |
| Piping ($D > 250$ mm) 30 mm $< t < 75$ mm $\mu_a = 0.4 \cdot t$ | Ferritic steel | Advanced UT | 5 mm |
| | | Good practice UT | 15 mm |
| | | Low effectiveness UT | 15 mm |
| Piping ($D > 250$ mm) 10 mm $< t < 30$ mm $\mu_a = 0.4 \cdot t$ | Ferritic steel | Advanced UT | 3 mm |
| | | Good practice UT | 5 mm |
| | | Low effectiveness UT | 10 mm |
| Piping ($D < 250$ mm) 5 mm $< t < 30$ mm $\mu_a = 0.4 \cdot t$ | Ferritic steel | Advanced UT | 3 mm |
| | | Good practice UT | 5 mm |
| | | Low effectiveness UT | 10 mm |
| Piping ($D > 250$ mm) $t > 30$ mm $\mu_a = 0.4 \cdot t$ | Wrought austenitic steel | Advanced UT | 5 mm |
| | | Good practice UT | 5 mm |
| | | Low effectiveness UT | 7 mm |
| Piping ($D < 250$ mm) $t < 30$ mm $\mu_a = 0.4 \cdot t$ | Wrought austenitic steel | Advanced UT | 2 mm |
| | | Good practice UT | 3 mm |
| | | Low effectiveness UT | 5 mm |

*B8.3.4    Defect not detected by NDT/NDE*

As no NDT device is able to detect all defects in the structural weld, there is always a possibility that a defect will remain in the component following inspection and repair. The probability of this occurring depends on many parameters, such as fabrication techniques, NDT methods and requirements, reliability of the methods and the operators etc. [B20] – [B21], [B32]. The probability of not detecting a defect will of course decrease as the defect size is increased and it will be near unity for very small defects, whereas it approaches zero with increase in crack size (using a sufficiently advanced procedure).

It is quite difficult to give general recommendations on data to be used for a specific case. However, in table B3 below, some typical detection probability values from the European SINTAP project [B22] are summarized.

Table B3. Typical values of detection probability (using different defect depths) [B22].

| Component | Material | NDE procedure | Detection probability | | | |
|---|---|---|---|---|---|---|
| | | | $a = 0.05 \cdot t$ | $a = 0.1 \cdot t$ | $a = 0.4 \cdot t$ | $a = 1.0 \cdot t$ |
| Plate $t > 75$ mm | Ferritic steel | Advanced UT | 0.5 | 0.95 | 1.0 | 1.0 |
| | | Good practice UT | 0.5 | 0.7 | 0.8 | 0.95 |
| | | Low effectiveness UT | 0.0 | 0.1 | 0.25 | 0.4 |
| Piping ($D > 250$ mm) 30 mm $< t <$ 75 mm | Ferritic steel | Advanced UT | 0.8 | 0.95 | 1.0 | 1.0 |
| | | Good practice UT | 0.8 | 0.9 | 1.0 | 1.0 |
| | | Low effectiveness UT | 0.0 | 0.2 | 0.4 | 0.6 |
| Piping ($D > 250$ mm) 10 mm $< t <$ 30 mm | Ferritic steel | Advanced UT | 0.7 | 0.95 | 1.0 | 1.0 |
| | | Good practice UT | 0.6 | 0.9 | 1.0 | 1.0 |
| | | Low effectiveness UT | 0.0 | 0.4 | 0.6 | 0.8 |
| Piping ($D < 250$ mm) 5 mm $< t <$ 30 mm | Ferritic steel | Advanced UT | 0.5 | 0.9 | 1.0 | 1.0 |
| | | Good practice UT | 0.4 | 0.8 | 0.95 | 1.0 |
| | | Low effectiveness UT | 0.0 | 0.3 | 0.5 | 0.8 |
| Piping ($D > 250$ mm) $t > 30$ mm | Wrought austenitic steel | Advanced UT | 0.5 | 0.9 | 1.0 | 1.0 |
| | | Good practice UT | 0.6 | 0.8 | 0.9 | 0.95 |
| | | Low effectiveness UT | 0.1 | 0.2 | 0.4 | 0.8 |
| Piping ($D < 250$ mm) $t < 30$ mm | Wrought austenitic steel | Advanced UT | 0.3 | 0.95 | 1.0 | 1.0 |
| | | Good practice UT | 0.0 | 0.7 | 0.95 | 1.0 |
| | | Low effectiveness UT | 0.0 | 0.5 | 0.7 | 0.8 |

As an example a POD-curve (distribution) for "Low effectiveness UT" corresponding to the lower bound performance among all teams that were evaluated in a program to assess inspection efficiency for piping [B34] is shown in Figure B11 (using Eq. (P14) with $c_1 = 0.240$ and $c_2 = 1.485$). The POD-curve of "Good practice UT" corresponding to that of a team with over average performance ($c_1 = 1.526$ and $c_2 = 0.533$), and a POD-curve of the "Advanced UT" corresponding to the performance that could be achieved with improved procedures [B34] ($c_1 = 3.630$ and $c_2 = 1.106$) are also shown in Figure B10. For qualified inspection procedures used in Sweden, the POD-curve is assumed to correspond to the curve for a "Good practice UT".
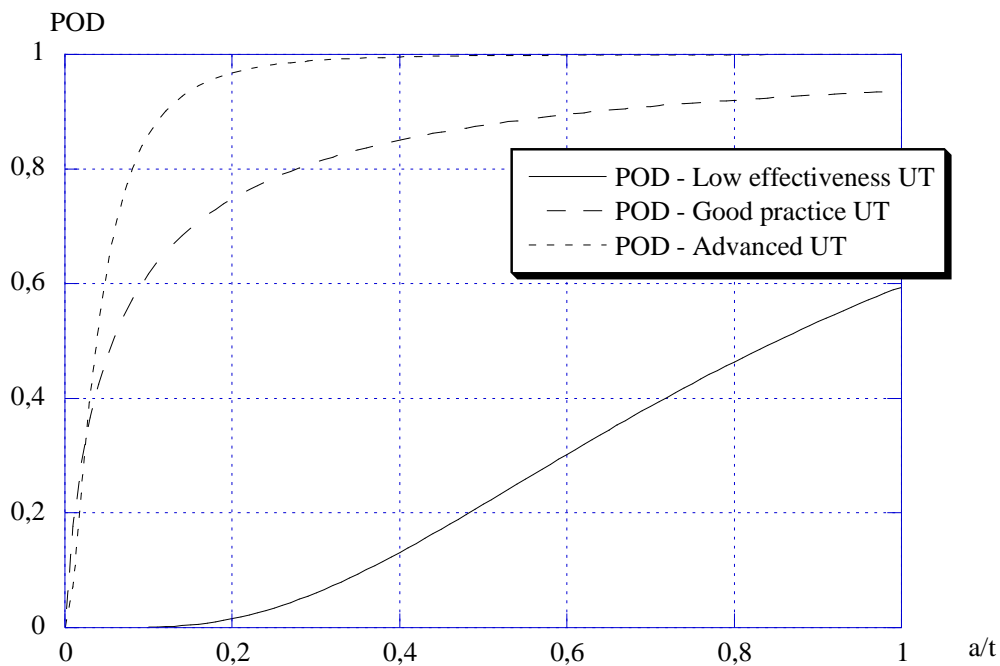
Figure B11. The probability of detection for different qualities of the inspection equipment and procedures, as a function of crack depth *a* relative to section thickness *t*.

The detection probability for thick plates (> 75 mm) of ferritic steel were assessed within the project SINTAP (table B3) [B22], and the curve for "Good practice UT" in Figure B11 is a good approximation of the POD for these thick ferritic plates.

### B8.3.5    *Defect distribution*

Defect depth distributions are quite difficult to estimate reliably for any given application. This is because very few defects of significance have been observed by NDE of plain welds in pressure vessels or critical structural components. Therefore, whenever possible, sensitivity studies should be performed as part of an assessment to investigate the dependency on the assumed defect distribution [B3].

The defect depth distributions most often used are the lognormal, Weibull and exponential distributions [B3], [B26], [B32]. The so-called Marshall distribution, was earlier used within the nuclear industry, and is a particular case of the exponential distribution.

A more suitable defect distribution for thick-section butt welds has been developed to eliminate some of the anomalies in using the Marshall distribution for these welds (this distribution is based on ultrasonic data acquired in the early 1970s). Using modern ultrasonic and destructive inspection techniques shows a significantly higher probability of defects of depths less than ~10 mm and lower probability of larger defects [B35] (see Figure B12). Using an expert system [B36] to model different factors that influence the likelihood and size of defects mainly comes to the same conclusion (an example is shown in Figure B13).
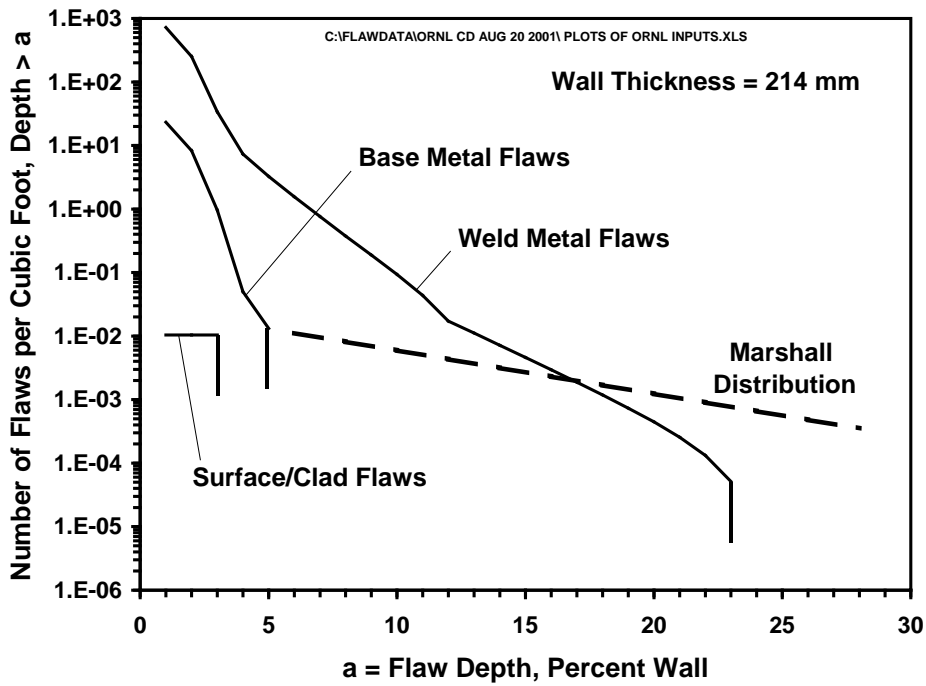
Figure B12. Example of new data on defects compared with the Marshall distribution [B35].
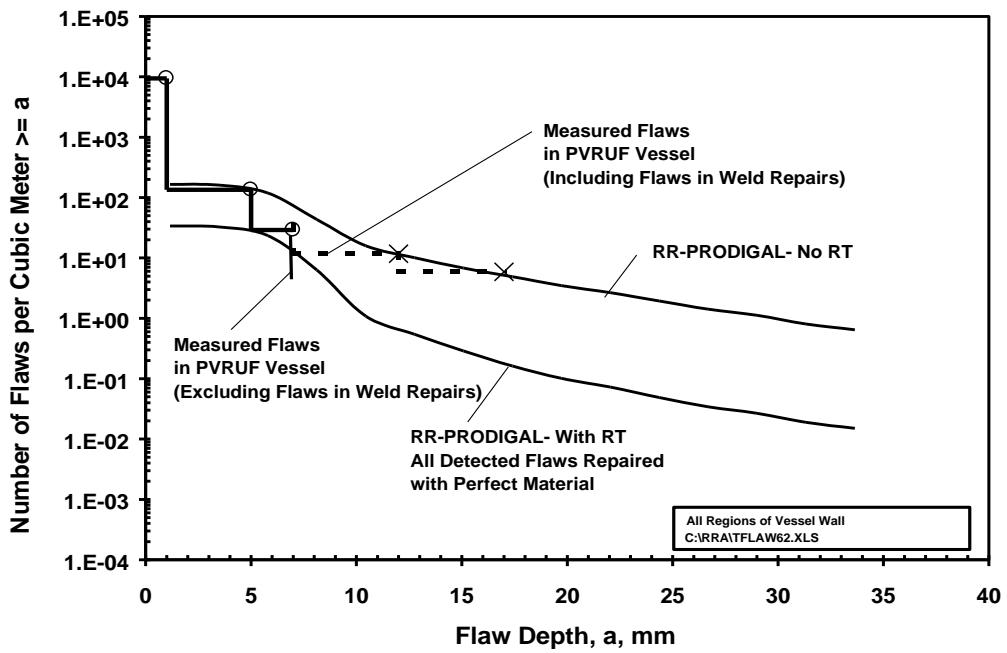


Figure B13. Comparison between measured defect data and resulting defect distribution using the expert system RR-PRODIGAL [B35] – [B36].

206

## B9.    ISAAC

The procedure described in this handbook including calculation of crack growth due to fatigue and stress corrosion has been implemented in a Windows based software named ISAAC [B1]. ISAAC also contains options for assessment of cracks according to the 2007 edition of the ASME Boiler and Pressure Vessel Code, Section XI. Appendices A, and C for assessment of cracks in ferritic pressure vessels, austenitic piping and ferritic piping, respectively. Please contact Kiwa Inspecta Technology AB for more information.

### B10.    References

[B1]   ISAAC, (2017), User´s Manual, Kiwa Inspecta Technology AB, Stockholm, Sweden.

[B2]   MILNE, I., AINSWORTH, R. A., DOWLING, A. R., and A. T. STEWART, (1988), "Assessment of the integrity of structures containing defects", *The International Journal of Pressure Vessels and Piping*, Vol. 32, pp. 3-104.

[B3]   —, (2015), "Assessment of the Integrity of Structures Containing Defects", R6 –Revision 4, Up to amendment record No.11, EDF Energy Nuclear Generation Ltd.

[B4]   AINSWORTH, R. A., (1986), "The treatment of thermal and residual stresses in fracture assessments", *Engineering Fracture Mechanics*, Vol. 24, pp. 65-76.

[B5]   BERGMAN, M., (1996), "Fracture mechanics analysis for secondary stresses - Part 1", SA/FoU-Report 94/03 (in Swedish), SAQ Kontroll AB, Stockholm, Sweden.

[B6]   DELFIN, P., SATTARI-FAR, I., and B. BRICKSTAD, (1997), "Effect of thermal and weld-induced residual stresses on the *J*-integral and CTOD in elastic-plastic fracture analyses", SAQ/FoU-Report 97/02, SAQ Kontroll AB.

[B7]   BUDDEN, P., (1989), "Fracture assessments of combined thermal and mechanical loads using uncracked body stress analysis", CEGB Report RD/B/6158/R89, Central Electricity Generating Board, Berkley, U.K.

[B8]   SATTARI-FAR, I., (1986), "Constraint effects on behaviour of surface cracks in cladded reactor pressure vessels subjected to PTS transient", *The International Journal of Pressure Vessels and Piping*, Vol. 67, pp. 185-197.

[B9]   HALLBÄCK, N., and F. NILSSON, (1992), "Fracture assessments for secondary loads", *Fatigue & Fracture of Engineering Materials and Structures*, Vol. 15, No. 2, pp. 173-186.

[B10]  ANDERSON, T.L., (1995), "Fracture Mechanics – Fundamentals and Applications", CRC Press, Second edition, Boca Raton, USA, 688p.

[B11]  BRICKSTAD, B., and M. BERGMAN, (1996), "Development of safety factors to be used for evaluation of cracked nuclear components", SAQ/FoU-Report 96/07, SAQ Kontroll AB, Stockholm, Sweden.

[B12]  SHARPLES, J. K., SANDERSON, D. J., BOWDLER, B. R., WIGHTMAN, A. P. and R. A. AINSWORTH, (1995), "Experimental programme to assess the effect of residual stresses on fracture behaviour", *Proceedings of the 1995 ASME Pressure Vessels & Piping Conference*, V. 437, pp. 539-551.

[B13]  SHARPLES, J.K. and L. GARDNER, (1996), "Ductile tearing tests of 316 stainless steel wide plates containing weldments", *Int. Jour of Pres. Ves. & Piping*, Vol. 65, pp. 353-363.

[B14]  MOHR, M.C., MICHALERIS, P. and M.T. KIRK, (1997), "An improved treatment of residual stresses in flaw assessment of pipes and pressure vessels fabricated from ferritic steels", *Proceedings of the 1997 ASME Pressure Vessels & Piping Conference*, Vol. 359.

[B15]  Mirzaee_Sisan, A., Truman, C. E., Smith, D.J. and Smith, M.C. (2007) "Interaction of residual stress with mechanical loading in a ferritic steel", Eng. Fract. Mech. Vol. 74, pp. 2864-2880.

[B16]  Mirzaee_Sisan, A., Truman, C. E., Smith, D.J. and Smith, M.C. (2008) "Interaction of residual stress with mechanical loading in an austenitic stainless steel", Fatigue. Fract. Engng. Mater. Struct. Vol. 31, pp. 223-233.

[B17]  BOLINDER, T., and I. SATTARI-FAR, (2011), "Experimental evaluation of influence from residual stresses on crack initiation and ductile crack growth at high primary loads", Research Report 2011:19, Swedish Radiation Safety Authority, Stockholm, Sweden. (Available at: http://www.stralsakerhetsmyndigheten.se)

[B18]    WILSON, R., (1995), "A User`s Guide to the Probabilistic Fracture Mechanics Computer Code: STAR6 - Version 2.2", Memorandum TEM/MEM/0005/95, Nuclear Electric, Engineering Division, 75p.

[B19]    BERGMAN, M., (1996), "User`s manual SACC version 4.0", SAQ/FoU-Report 96/09, SAQ Kontroll AB, 9p.

[B20]    DILLSTRÖM, P., (2000), "Probabilistic Safety Evaluation - Development of Procedures with Applications on Components Used in Nuclear Power Plants", SKi Report 00:58, Swedish Nuclear Power Inspectorate.

[B21]    DILLSTRÖM, P., (2000), "ProSINTAP - A probabilistic program implementing the SINTAP assessment procedure", *Engng Fract Mech*, V. 67, pp. 647-668.

[B22]    CRUTZEN, S., FRANK, F., FABBRI, L., LEMAITRE, P., SCHNEIDER, Q., and W. VISSER, (1999), "Compilation of NDE effectiveness data", SINTAP Task 3.4 Final Report, JRC - IAM, Petten, 77p.

[B23]    GUNNARS, J., ANDERSSON, P., DILLSTRÖM, P. and G. SUND., (2002), "Risk based ranking of inspection sites for the reactor pressure vessels of Barsebäck 2, Oskarshamn 2 and Ringhals 1", Technical Reports 10393500-3/4/7, Rev. 0/1, Det Norske Veritas AB.

[B24]    BRICKSTAD, B., CHAPMAN, O.J.V., SCHIMPFKE, T., SCHULTZ, H., and A. MUHAMMED., (2003), "WP-4, Review and benchmarking of SRMs and associated softwares. Final Report", Draft Report No. NURBIM D4, Det Norske Veritas AB and O.J.V. Consultancy.

[B25]    DILLSTRÖM, P., (2015), "PROSIR - Probabilistic Structural Integrity of a PWR Reactor Pressure Vessel", Research Report 2015:09, Swedish Radiation Safety Authority, Stockholm, Sweden. (Available at: http://www.stralsakerhetsmyndigheten.se)

[B26]    BULLOUGH, R., GREEN, V. R., TOMKINS, B., WILSON, R., and J. B. WINTLE., (1999), "A review of methods and applications of reliability analysis for structural integrity assessment of UK nuclear plant", *International Journal of Pressure Vessel and Piping*, V 76, pp 909-919.

[B27]    DILLSTRÖM, P., NILSSON, F., BRICKSTAD, B., and M. BERGMAN, (1993), "Probabilistic Fracture Mechanics Analysis of a Nuclear Pressure Vessel for Allocation of In-Service Inspection", *International Journal of Pressure Vessel & Piping*, V 54, pp 435-463.

[B28]    WALLIN, K., (1984), "The scatter in $K_{Ic}$ -results", *Engineering Fracture Mechanics*, V 19, pp 1085-1093.

[B29]    WALLIN, K., (1998), "Probabilistisk säkerhetsvärdering PROPSE - Materialparametrar", Rapport VALC444, VTT Tillverkningsteknik, 20p.

[B30]    NILSSON, F., and B. ÖSTENSSON, (1978), "$J_{Ic}$-testing of A-533 B – statistical evaluation of some different testing techniques", *Engineering Fracture Mechanics*, V 10, pp 223-232.

[B31]    WALLIN, K., (2001), "Low cost J-R-curve estimation based on CVN upper shelf energy", *Fatigue and Fracture of Engineering Materials and Structures*, V. 24, pp 537-550.

[B32]    BURDEKIN, F. M., and W. HAMOUR, (1998), "SINTAP, Contribution to Task 3.5, Safety Factors and Risk", UMIST, 25p.

[B33]    SKÅNBERG, L., (1994), "Kvalificering av OFP-system", SKi Rapport 94:25, Statens kärnkraftinspektion, 45p.

[B34]    BRICKSTAD, B., (2000), "The Use of Risk Based Methods for Establishing ISI-Priorities for Piping Components at Oskarshamn 1 Nuclear Power Station", SAQ/FoU-Report 99/05, SAQ Kontroll AB / Det Norske Veritas.

[B35]    JACKSON, D. A., ABRAMSON, L., DOCTOR, S. R., SIMONEN, F., and G. SCHUSTER, (2001), "Development of Generalized Flaw Distribution as Input to the Re-Evaluation of the

Technical Basis for US Pressurized Thermal Shock Regulation for PWRs", *Presented at the NDE/Structural Integrity Conference – Seville, Spain –November 14-16, 2001*, United States Nuclear Regulatory Commission.

[B36]   CHAPMAN, O.J.V., and F. A. SIMONEN, (1998), "RR-PRODIGAL – Model for Estimating the Probabilities of Defects in Reactor Pressure Vessel Welds", NUREG/CR-5505, United States Nuclear Regulatory Commission.

[B37]   LEI, Y., O'DOWD, N.P. AND G.A. WEBSTER, (2000), "Fracture mechanics of a crack in a residual stress field", *Int. Jour of Fracture*, Vol. 106, pp. 195-216.

[B38]   DILLSTRÖM, P., ANDERSSON, M., SATTARI-FAR, I., and W. ZANG, (2009), "Analysis Strategy for Fracture Assessment of Defects in Ductile Materials", Research Report 2009:27, Swedish Radiation Safety Authority, Stockholm, Sweden. (Available at: http://www.stralsakerhetsmyndigheten.se)

[B39]   VON FEILITZEN, C., and I. SATTARI-FAR, (2012), "Implementation of the Master Curve method in ProSACC", Research Report 2012:07, Swedish Radiation Safety Authority, Stockholm, Sweden. (Available at: http://www.stralsakerhetsmyndigheten.se)

[B40]   KIRK, M., ERICKSON, M., SERVER, W., STEVENS, G., and R. CIPOLLA, (2014), "Assessment of Fracture Toughness Models for Ferritic Steels Used in Section XI of the ASME Code Relative to Current Data-Based Models", *Proceedings of the 2014 ASME Pressure Vessels & Piping Division Conference, July 20-24, Anaheim, CA, USA*.

[B41]   ProSACC, (2016), User's Manual, Inspecta Technology AB, Stockholm, Sweden.

## APPENDIX X.  EXAMPLE PROBLEM

A defect has been discovered in a plate, see Fig X1. The plate is assumed to be a component in a nuclear power plant and made of ferritic steel.
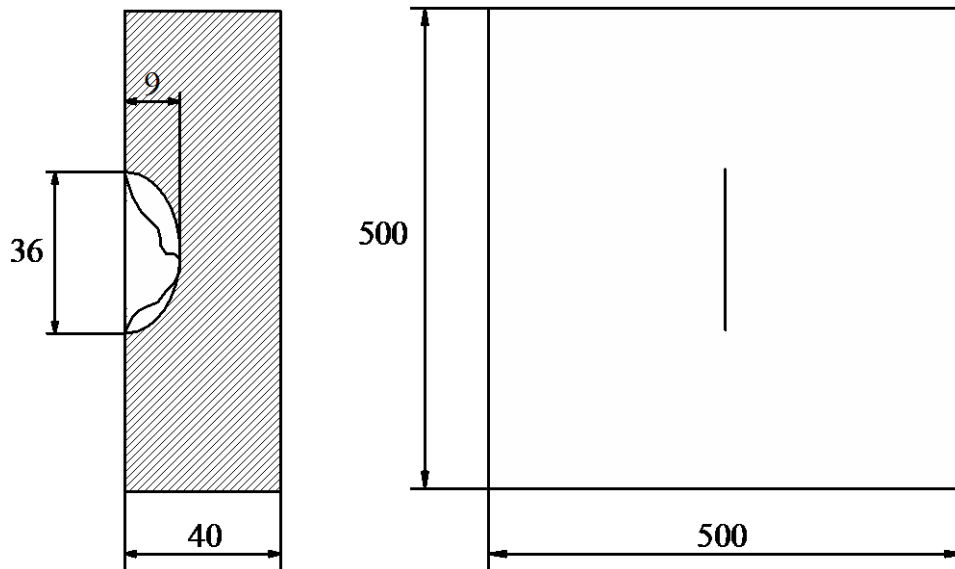


Figure X1.  Plate with a defect (unit mm).

The material has the following measured properties at 20 and 150 °C.

$R_{p0.2}(20\ °C) = 300$ MPa, $\qquad$ $R_m(20\ °C) = 490$ MPa,

$R_{p0.2}(150\ °C) = 280$ MPa, $\qquad$ $R_m(150\ °C) = 490$ MPa,

$K_{Ic}(150\ °C) = 160$ MPa$\sqrt{m}$, $\qquad$ $E(150\ °C) = 200$ GPa.

The plate is loaded by a tensile load due to dead weight and a thermal gradient. A stress analysis reveals that the nominal stress is 100 MPa due to dead weight and that the thermal gradient affects the plate with a bending stress of 180 MPa. The bending stress is tensile on the cracked side of the plate. The stresses act perpendicularly to the crack plane.

Perform a defect assessment to decide whether the crack can be accepted or not if the load event is categorised as normal. For reasons of simplicity, the temperature can be considered as constant and equal to 150 °C in the assessment.

# X1. Solution

The defect assessment is performed according to the procedure described in Chapter 2 of this handbook.

## X1.1 *Characterization of defect*
According to Appendix A, the defect is characterized as a semi-elliptical surface crack with depth $a = 9$ mm and length $l = 36$ mm.

## X1.2 *Choice of geometry*
A plate with a finite surface crack is selected, see Fig. G1.1. The thickness of the plate is 40 mm.

## X1.3 *Determination of the stress state*
The primary stress state consists of a membrane stress $\sigma_m^p = 100$ MPa due to dead weight, and the secondary stress state of a bending stress $\sigma_b^s = 180$ MPa due to the thermal gradient.

## X1.4 *Determination of material data*
According to Chapter 2.5 the yield strength $\sigma_Y$, the ultimate tensile strength $\sigma_U$ and the critical stress intensity factor $K_{cr}$ must be determined. This is done by setting $\sigma_Y = R_{p0.2}$, $\sigma_U = R_m$ and $K_{cr} = K_{Ic}$. Thus

$\sigma_Y(20\ °C) = 300$ MPa, $\qquad\qquad$ $\sigma_U(20\ °C) = 490$ MPa,

$\sigma_Y(150\ °C) = 280$ MPa, $\qquad\qquad$ $\sigma_U(150\ °C) = 490$ MPa,

$K_{cr}(150\ °C) = 160$ MPa$\sqrt{\text{m}}$, $\qquad$ $E(150\ °C) = 200$ GPa.

## X1.5 *Calculation of possible crack growth*
No crack growth mechanisms need to be considered in this case.

## X1.6 *Calculation of $K_I^p$ and $K_I^s$*

The stress intensity factors $K_I^p$ and $K_I^s$ are calculated according to Appendix K, Eqs. (K1) and (K2). The primary and secondary stress are expressed according to Eq. (K2).

$$\sigma^p = 100 = \sigma_0^p,$$

$$\sigma^s = 180\left(1 - \frac{2u}{t}\right) = 180 - 360\frac{u}{t} = 180 - 360\frac{u}{a}\frac{a}{t} = 180 - 81\frac{u}{a} = \sigma_0^s + \sigma_1^s\frac{u}{a}$$

Hence $\sigma_0^p = 100$ MPa, $\sigma_0^s = 180$ MPa and $\sigma_1^s = -81$ MPa. All other stress components are zero. With $a/t = 9/40 = 0.225$ and $a/l = 9/36 = 0.25$, linear interpolation in Tables K1 and K2 gives the required geometry functions.

$$f_0^A = 0.908, \qquad f_1^A = 0.578,$$

$$f_0^B = 0.735, \qquad f_1^B = 0.122,$$

$K_I^p$ and $K_I^s$ at the deepest point of the crack (point A) become

$$\left(K_I^p\right)^A = \sqrt{\pi a}\left(\sigma_0^p f_0^A\right) = \sqrt{\pi \cdot 0.009}(100 \cdot 0.908) = 15.27 \text{ MPa}\sqrt{m},$$

$$(K_I^s)^A = \sqrt{\pi a}(\sigma_0^s f_0^A + \sigma_1^s f_1^A) = \sqrt{\pi \cdot 0.009}(180 \cdot 0.908 - 81 \cdot 0.578) = 19.62 \text{ MPa}\sqrt{m}.$$

$K_I^p$ and $K_I^s$ at the intersection of the crack with the free surface (point B) become

$$\left(K_I^p\right)^B = \sqrt{\pi a}\left(\sigma_0^p f_0^B\right) = \sqrt{\pi \cdot 0.009}(100 \cdot 0.735) = 12.35 \text{ MPa}\sqrt{m},$$

$$(K_I^s)^B = \sqrt{\pi a}(\sigma_0^s f_0^B + \sigma_1^s f_1^B) = \sqrt{\pi \cdot 0.009}(180 \cdot 0.735 - 81 \cdot 0.122) = 20.57 \text{ MPa}\sqrt{m},$$

*X1.7 Calculation of $L_r$*

$L_r$ is calculated according to Appendix L, Eqs. (L1) - (L3). Eq. (L2) gives

$$\zeta = \frac{al}{t(l+2t)} = \frac{9 \cdot 36}{40 \cdot (36 + 2 \cdot 40)} = 0.0698 \quad .$$

Since the primary stress state in this case only consists of a membrane stress, $L_r$ becomes

$$L_r = \frac{\sqrt{(1-\zeta)^{3.14}\left(\sigma_m^p\right)^2}}{(1-\zeta)^2 \sigma_Y} = \frac{\sqrt{(1-0.0698)^{3.14} \cdot 100^2}}{(1-0.0698)^2 \cdot 280} = 0.368 \quad .$$

*X1.8 Calculation of $K_r$*

$K_r$ is calculated according to Chapter 2.9. In the deepest point of the crack (point A) we obtain

$$\chi^A = \frac{(K_I^s)^A L_r}{\left(K_I^p\right)^A} = \frac{19.62 \cdot 0.368}{15.27} = 0.473,$$

which according to [2.8] is calculated to $\rho = 0.040$. Hence,

$$K_r^A = \frac{\left(K_I^p\right)^A + (K_I^s)^A}{K_{cr}} + \rho^A = \frac{15.27 + 19.62}{160} + 0.040 = 0.258.$$

Similarly we obtain at the intersection of the crack with the free surface (point B),

$$\chi^B = \frac{(K_I^s)^B L_r}{\left(K_I^p\right)^B} = \frac{20.57 \cdot 0.368}{12.35} = 0.613,$$

213

$$\rho = 0.045,$$

$$K_r^B = \frac{\left(K_I^p\right)^B + \left(K_I^s\right)^B}{K_{cr}} + \rho^B = \frac{12.35 + 20.57}{160} + 0.045 = 0.251.$$

The maximum value of $K_r$ is used in the assessment and is obtained at the deepest point of the crack (point A).

*X1.9        Fracture assessment*

The fracture assessment is described in Chapter 2.10. The non-critical region in the failure assessment diagram for materials with continuous yielding is defined by

$$K_r \leq f_{R6}(L_r) = f_2^{cy}(L_r) = \begin{cases} \dfrac{0.3 + 0.7e^{-\mu L_r^6}}{\sqrt{1 + 0.5L_r^2}} & L_r \leq 1, \\[2mm] f_2^{cy}(1)L_r^{\frac{N_{R6}-1}{2N_{R6}}} & 1 < L_r < L_r^{max}, \end{cases}$$

and

$$L_r \leq L_r^{max},$$

where

$$\mu = \min\left(\frac{0.001E}{\sigma_Y}; 0.6\right) = \min\left(\frac{0.001 \cdot 200 \cdot 10^3}{280}; 0.6\right) = 0.6,$$

and

$$N_{R6} = 0.3\left[1 - \frac{\sigma_Y}{\sigma_U}\right] = 0.1286.$$

Since the component is nuclear and made of a ferritic material without a yield plateau ($R_{p0.2}$ has been measured instead of $R_{eL}$), $L_r^{max}$ is given by

$$L_r^{max} = \frac{\sigma_f}{\sigma_Y} = \left\{\sigma_f = \frac{\sigma_Y + \sigma_U}{2} = \frac{280 + 490}{2} = 385\right\} = \frac{385}{280} = 1.375.$$

The point $(L_r, K_r) = (0.368, 0.258)$ is plotted in the failure assessment diagram. See Fig. X2.
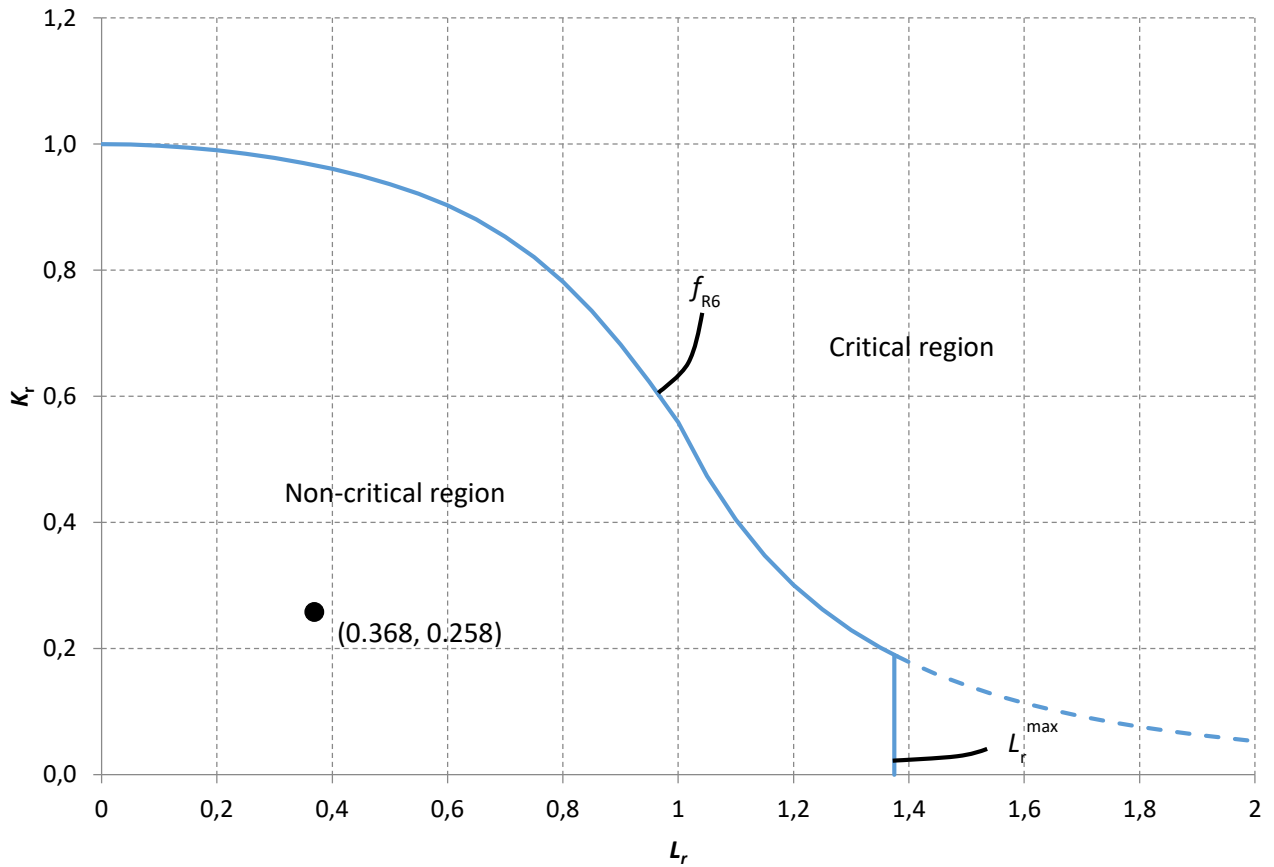
Figure X2.  Fracture assessment.

The point is situated within the non-critical region in the failure assessment diagram. Thus fracture is not to be expected. However, the defect may still not be acceptable with respect to required safety demands to continue operation without repair or replacement of the component. This is investigated in the safety assessment.

*X1.10        Safety assessment*

The safety assessment is described in Chapter 2.11. The acceptable region in the failure assessment diagram is defined by

$$K_r^{acc} = \frac{K_I^p + K_I^s}{K_{cr}} + \frac{\rho}{\sqrt{SF_J}} \leq \frac{f_{R6}(L_r)}{\sqrt{SF_J}},$$

$$L_r \leq \frac{L_r^{max}}{SF_L} \quad .$$

Recommended values for the safety factors $SF_J$ and $SF_L$ are found in Appendix S. For a ferritic steel component under a normal load event, $SF_J = 10$. Hence the maximum value of $K_r^{acc}$ (i.e. at the deepest point of the crack) becomes

$$K_r^{acc} = \frac{15.27 + 19.62}{160} + \frac{0.040}{\sqrt{10}} = 0.231.$$

For a ferritic material $SF_L$ is calculated using through

$$SF_L = SF_L^m = \frac{\sigma_f}{S_m C_p},$$

where

$$S_m = \min\left(\frac{2}{3}\,\sigma_Y^{20°C};\ \frac{1}{3}\,\sigma_U^{20°C};\ \frac{2}{3}\,\sigma_Y^{150°C};\ \frac{1}{3}\,\sigma_U^{150°C}\right)$$
$$= \min\left(\frac{2}{3}\,300;\ \frac{1}{3}\,490;\ \frac{2}{3}\,280;\ \frac{1}{3}\,490\right) = 163.3,$$

and

$$C_p = 1.0.$$

This results in

$$SF_L^m = \frac{385}{163.3 \cdot 1.0} = 2.36.$$

The point $(L_r, K_r) = (0.368, 0.231)$ is plotted in the failure assessment diagram where also the acceptable region has been drawn. See Fig. X3.
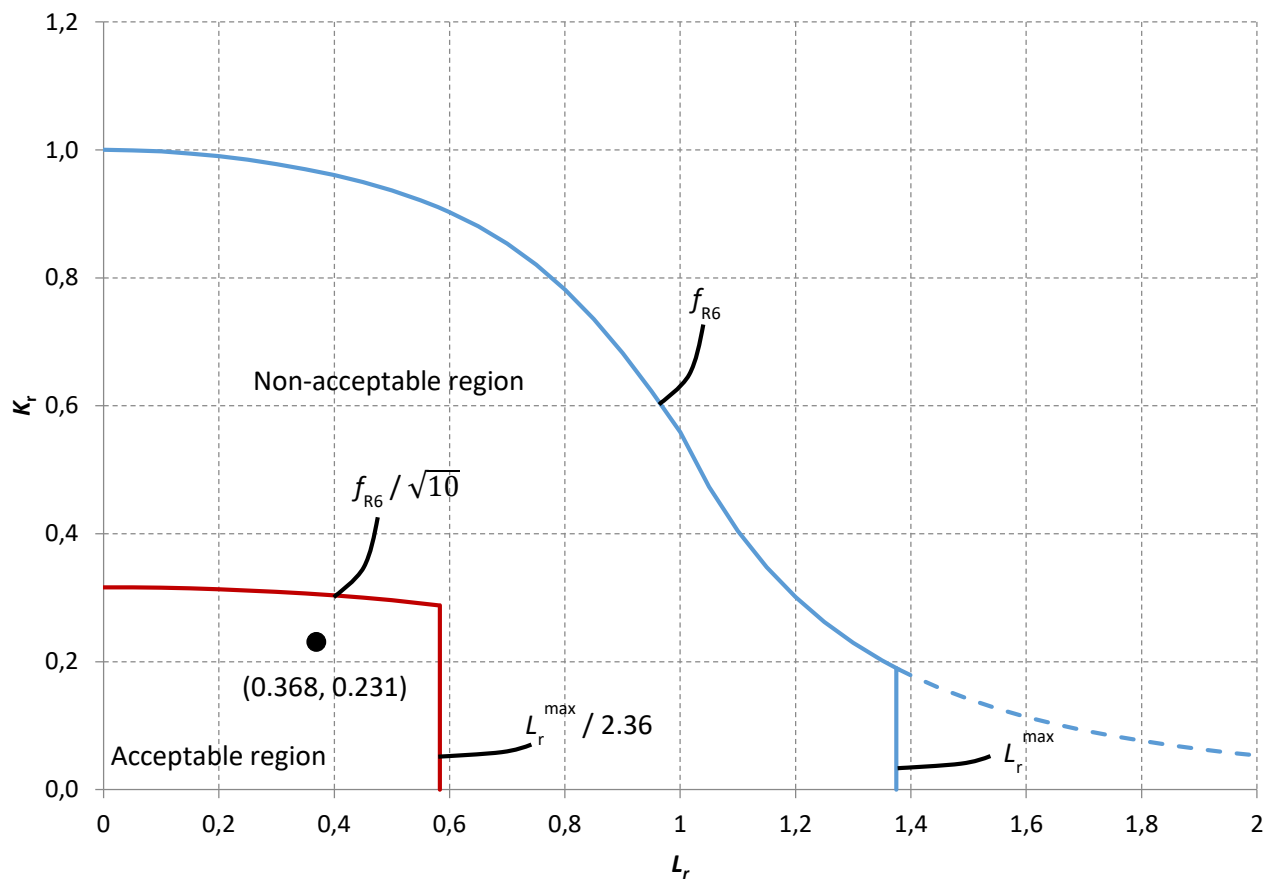
Figure X3.  Safety assessment.

The point is situated within the acceptable region of the failure assessment diagram. Hence the defect is acceptable with respect to required safety demands and operation may continue without repair or replacement of the component.

The acceptable crack size can be obtained by gradually increasing the crack size and repeating the above calculations until the assessment point coincides with the line that limits the acceptable region in Fig. X3. By doing this for a fixed crack aspect ratio of $l \, / \, a = 4$, an acceptable crack depth of 16.5 mm is obtained.

2018:18

The Swedish Radiation Safety Authority has a comprehensive responsibility to ensure that society is safe from the effects of radiation. The Authority works to achieve radiation safety in a number of areas: nuclear power, medical care as well as commercial products and services. The Authority also works to achieve protection from natural radiation and to increase the level of radiation safety internationally.

The Swedish Radiation Safety Authority works proactively and preventively to protect people and the environment from the harmful effects of radiation, now and in the future. The Authority issues regulations and supervises compliance, while also supporting research, providing training and information, and issuing advice. Often, activities involving radiation require licences issued by the Authority. The Swedish Radiation Safety Authority maintains emergency preparedness around the clock with the aim of limiting the aftermath of radiation accidents and the unintentional spreading of radioactive substances. The Authority participates in international co-operation in order to promote radiation safety and finances projects aiming to raise the level of radiation safety in certain Eastern European countries.

The Authority reports to the Ministry of the Environment and has around 300 employees with competencies in the fields of engineering, natural and behavioural sciences, law, economics and communications. We have received quality, environmental and working environment certification.